LMSC-HREC TR D496975

LDV MEASUREMENTS OF B-747 WAKE VORTEX CHARACTERISTICS

M. R. Brashears

A. D. Zalay

January 1977

Final Report

Document is available to the public through the
National Technical Information Service,
Springfield, Virginia 22151.

Prepared for

U. S. DEPARTMENT OF TRANSPORTATION
TRANSPORTATION SYSTEMS CENTER
KENDALL SQUARE, CAMBRIDGE, MA 02142

NOTICE

This document is disseminated under the sponsorship of the Department of Transportation in the interest of information exchange. The United States Government assumes no liability for its contents or use thereof. Use of trade names of manufacturers in this report does not consitute an official endorsement of such products or manufacturers, either expressed or implied by Lockheed Missiles & Space Company, Inc., or any agency of the United States Government.

TECHNICAL REPORT STANDARD TITLE PAGE

1. Report No.	2. Government Accession No.	3. Recipient's Catalog No.

4. Title and Subtitle	5. Report Date
LDV MEASUREMENTS OF B-747 WAKE VORTEX CHARACTERISTICS	January 1977
	6. Performing Organization Code

7. Author(s)	8. Performing Organization Report No.
M. R. Brashears, A. D. Zalay*	LMSC-HREC TR D496975

9. Performing Organization Name and Address	10. Work Unit No.
Lockheed Missiles & Space Company, Inc. Huntsville Research & Engineering Center 4800 Bradford Drive Huntsville, AL 35807	11. Contract or Grant No. DOT-TSC-1145
	13. Type of Report and Period Covered
12. Sponsoring Agency Name and Address Department of Transportation Federal Aviation Administration Systems Research and Development Service Washington DC 20590	Final Report Nov. 1975 – Jan. 1977
	14. Sponsoring Agency Code FA-605/705

15. Supplementary Notes

*Under Contract to: Department of Transportation
Transportation Systems Center, Kendall Square
Cambridge, MA 02142

16. Abstract

In order to determine the behavior of the wake vortices of a B-747 at low altitudes and to measure the vortex decay process behind the B-747 as a function of altitude above ground, flap and spoiler settings and different flight configurations; a B-747 aircraft flew 54 passes at low level over a ground-based laser Doppler velocimeter (LDV) system and other sensors. From the LDV measurements, the location and velocity distribution of the wake vortices and the general vortex roll-up, transport and decay trends were obtained. Results of the study indicated that the deployment of spoilers and flaps enhanced the decay of the vortex peak tangential velocity in the near wake while aircraft altitude glide slope, and landing gear deployment has little effect. The report discusses the LDV wake vortex measurements including the instrumentation used, the experimental test sequence, and the results of the wake measurements in terms of the vortex roll-up, transport and decay trends, and a comparison of the wake vortex characteristics for different configurations.

17. Key Words	18. Distribution Statement
Aircraft Wakes Wake Vortices Laser Doppler Velocimetry Trailing Vortex	Unlimited

19. Security Classif. (of this report)	20. Security Classif. (of this page)	21. No. of Pages	22. Price
Unclassified	Unclassified		

Form DOT F 1700.7 (8-69)

FOREWORD

This final report presents the results of work performed by the Lockheed Missiles & Space Company, Inc., Huntsville Research & Engineering Center, under Contract DOT-TSC-1145 for the Department of Transportation, Transportation Systems Center, Cambridge, Massachussetts. The period of performance for this study was from November 1975 through January 1977. Lockheed-Huntsville personnel contributing to this effort were C. E. Craven, B. B. Edwards, J. L. Jetton, A. J. Jordan, M. C. Krause, T. R. Lawrence, and K. R. Shrider.

The authors are especially greatful to Dr. J. N. Hallock, TSC Contracting Officer's Technical Monitor, for his technical contributions and able assistance during the performance of this contract. A special thanks is also extended to the NASA-MSFC Optics Branch for making the NASA LDV filter bank and signal processor available for this study and to J. W. Bilbro and H. B. Jeffreys at NASA-MSFC and to Bill Keenum, Earl Lucas and Rick Bynum at CSC for processing the high-speed filter bank measurements.

CONTENTS

1. INTRODUCTION

Wake vortex, transport and decay parameters near the ground are important factors in determining safe aircraft separation distances for terminal areas. For an operational Wake Vortex Avoidance System (WVAS) a knowledge of the location and intensity of wake vortices near the terminal area is necessary to determine the minimum-delay safe spacings. Under light crosswind conditions, a wake vortex can remain in the approach corridor, and the minimum aircraft separation distance is dictated primarily by the wake decay process near the ground. Therefore, an important consideration in determining safe aircraft separations is the decay of the wake vortex near the ground. While numerous vortex decay theories have been proposed, there are little full-scale experimental data available for comparison. Experimental vortex decay data near the ground are also lacking for aerodynamic wake minimization concepts where variations in aircraft geometry are used to tailor the wake vortex flow. Flight tests by NASA have shown that certain flap and spoiler settings can reduce the imposed rolling moments on following aircraft (in the near wake); however, wake vortex measurements near the ground for full-scale aircraft with different wake minimization concepts are needed. Thus, for both wake vortex avoidance and wake vortex minimization techniques, a knowledge of the vortex rollup, transport, and decay characteristics near the ground is important.

In order to determine the behavior of aircraft wake vortices at low altitudes a flight test program was conducted by DOT/NASA. The primary goal of the test program was to measure the wake vortex decay process behind a conventional jumbo jet as a function of altitude above ground, flap and spoiler settings, and different flight configurations. To isolate the influence of aircraft and flight parameters on the wake decay process, the flight tests were conducted at the Rosamond Dry Lake test area in California during the

early morning hours when calm atmospheric conditions prevailed. The Rosamond wake decay measurements were sought as an input to the WVAS predictive model to quantify the effect of burst, link and viscous decay parameters on the wake vortex dissipation process. The wake decay measurements were also sought for demonstrating the effectiveness of recently developed vortex minimization concepts. In addition to the wake decay measurements, the flight tests were also focused on measuring the wake vortex rollup and transport phenomena in ground plane proximity.

The Rosamond flight tests involved airborne and ground-based meteorological sensors, an acoustic Doppler system, a mobile laser Doppler velocimeter, and flow visualization using smoke and balloons. In this report the measurements obtained with the laser Doppler velocimeter system are discussed including: (1) the initial downwash field; (2) the lateral and horizontal transport of the coherent wake vortex; and (3) the decay of the vortex flow in terms of the time history of the circulation, peak tangential velocity, and the diffusion of the viscous core radius. While the application of laser Doppler velocimeter techniques for the study of wake vortex flows is not novel, this is the first time, to our knowledge, that the details of the vortex formation, and decay process have been recorded for a full-scale aircraft using a laser Doppler system. In addition to providing detailed wake measurements for comparison with available theoretical and empirical models, the results show the influence of changes in flap, spoiler, and landing gear settings on the wake characteristics.

The report discusses the LDV wake vortex measurements including the instrumentation used, the experimental test sequence, and the results of the wake measurements in terms of the vortex rollup, transport and decay trends, and a comparison of the wake vortex decay characteristics for different configurations. A brief discussion of the LDV wind measurements is given followed by the overall conclusions and recommendations.

2. INSTRUMENTATION

The wake vortex and atmospheric wind measurements were carried out by means of a scanning laser Doppler velocimeter system contained in mobile van unit. Preliminary processing of the data was carried out with a SEL computer aboard the van. Reduction and analysis of the vortex and wind signatures were carried out by off-line processing software using a Univac 1108 and a PDP11 computer. A description of the instrumentation and the data processing methods for the Rosamond tests is given in terms of the LDV system configuration and the data processing techniques used.

2.1 LDV SYSTEM

The Lockheed-Huntsville laser Doppler velocimeter was used to obtain wake vortex measurements during the Rosamond flight tests. A photograph of the van-mounted LDV system is given in Fig. 1. The wake velocity measurements were accomplished as follows: (1) the wake generated by the aircraft was scanned by the CO_2 laser; (2) the radiation backscattered from the aerosol in the wake was collected; (3) the radiation was photomixed with a portion of the transmitted beam on a photodetector; and (4) the intensity and Doppler shift frequency of the signal were displayed.

The difference in frequency between the transmitted and backscattered signal generated at the photodetector, the Doppler shift frequency, is a measure of the aerosol line-of-sight velocity within the laser focal volume

$$\left|\overline{V}\right| = \frac{\lambda \, \Delta f}{2 \cos \gamma} \qquad (1)$$

where $\left|\overline{V}\right|$ is the velocity in the region being sensed, λ is the laser radiation wavelength (10.6 μm), Δf is the Doppler shift, and γ is the angle subtended by

Fig. 1 - Lockheed LDV System Monitoring Wake Vortex Generated by a B-747 Aircraft at the Rosamond California, Test Site

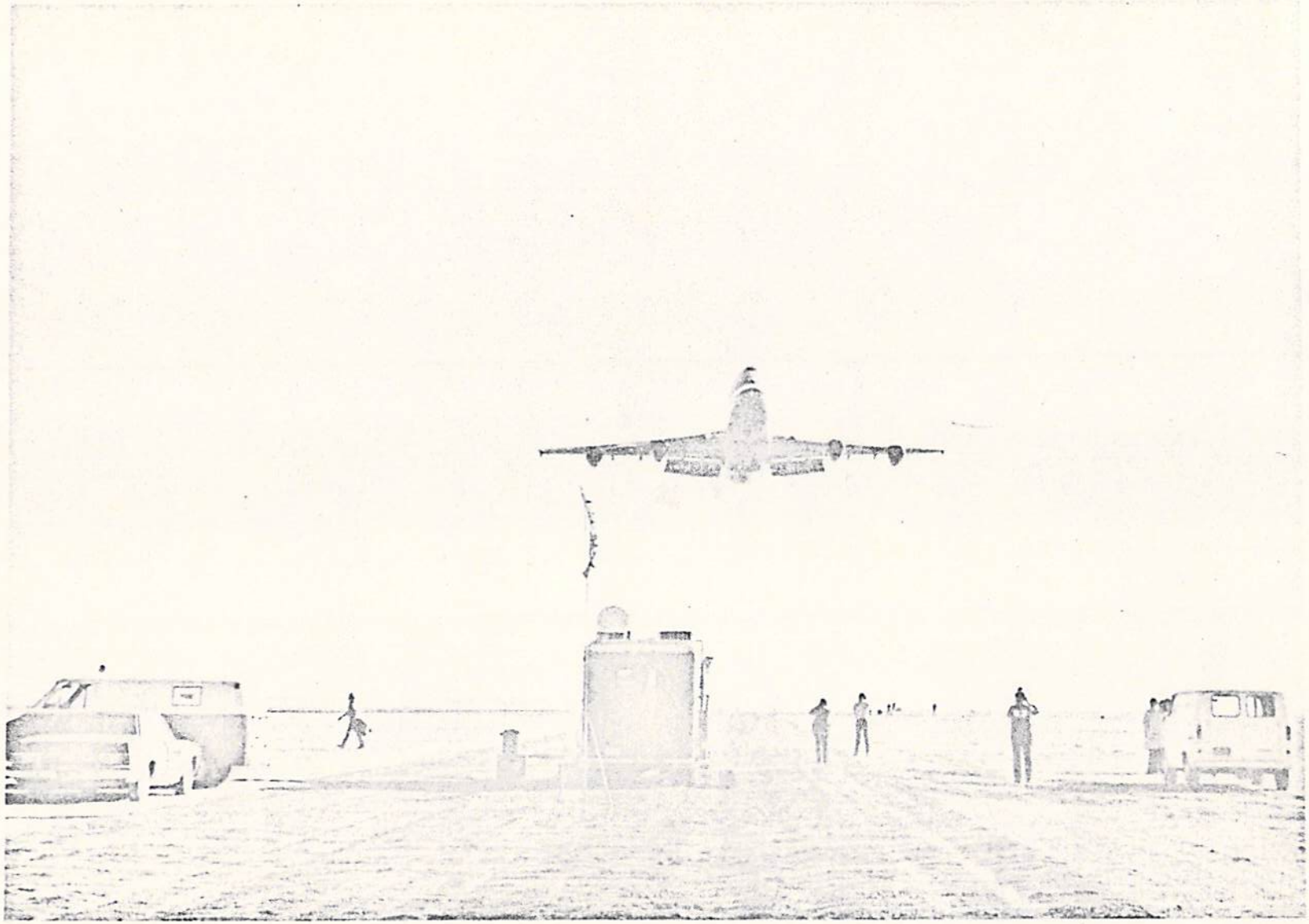

the velocity vector and the optic system line of sight. From Eq. (1) it is noted that the Doppler shift is a direct and absolute measure of aerosol velocity and a frequency shift of 188 kHz corresponds to a 1 m/sec line-of-sight velocity.

A sketch of the optical and electronic equipment for measuring the intensity and frequency spectrum of the coherent backscatter from the focal volume is shown in Fig. 2 and described in more detail in Refs. 1, 2 and 3. Photographs of the optical and electronic equipment for measuring the aerosol backscatter are shown in Figs. 3, 4 and 5.

The Lockheed LDV system used in the Rosamond wake vortex tests monitors the velocity of ambient atmospheric particulate matter within its instantaneous sensing volume. The pertinent operating characteristics of the LDV are summarized as follows:

Performance

1. Velocity Measurement Threshold: 0.5 m/sec
2. Velocity Range: 0.5 to 28 m/sec

Sample Rate

1. Low Data Rate: 70 Hz
2. High Data Rate: 500 Hz (using the NASA filter bank processor)

Spatial Resolution

1. Range Accuracy: $\pm$0.4 m at 30 m, $\pm$ 44 m at 300 m
2. Elevation Angle Accuracy: $\pm$0.25 deg

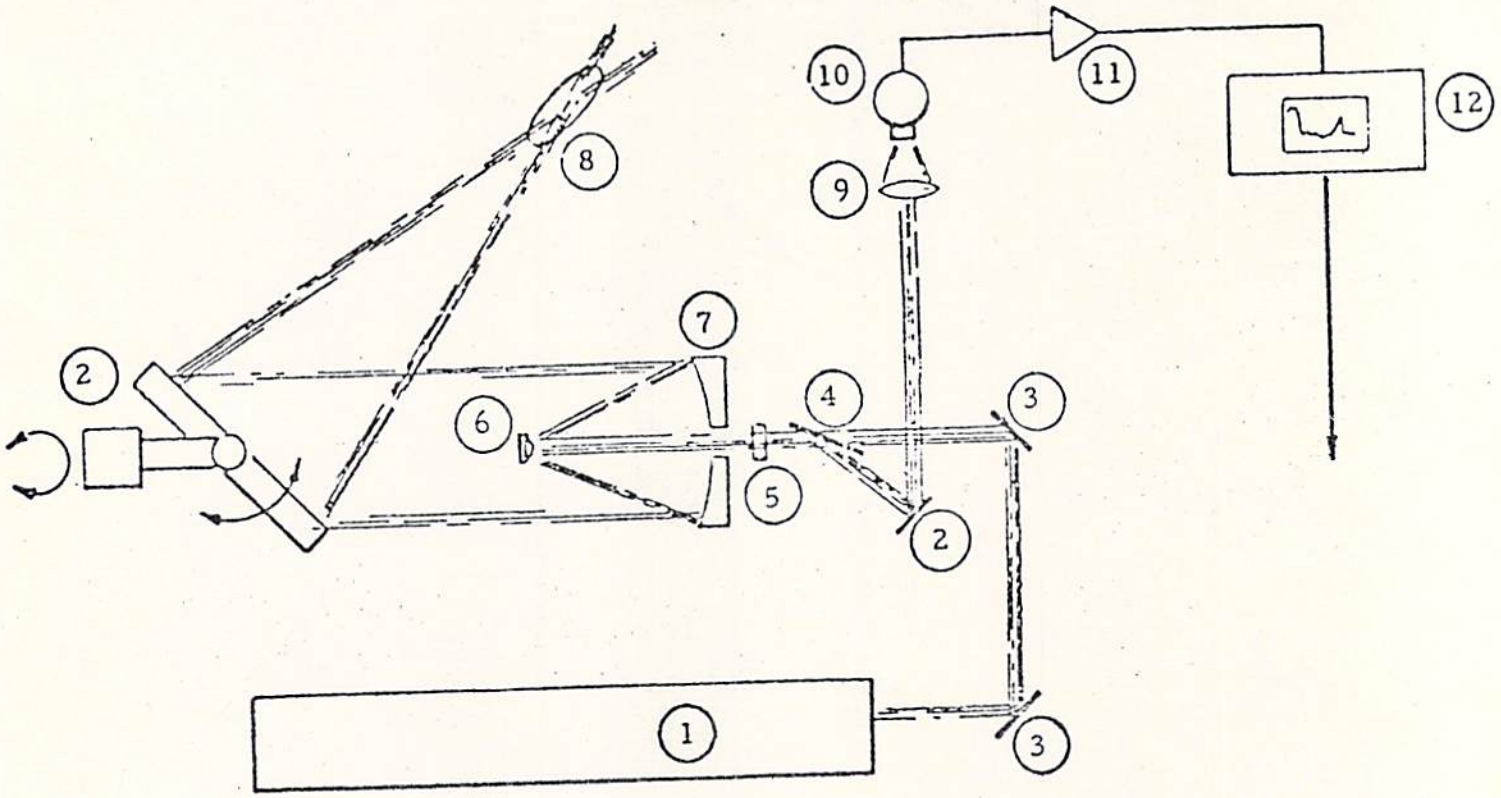

1. CO_2 Laser
2. Mirror
3. Mirror
4. Brewster Window
5. Quarter Wave Plate
6. Secondary Mirror
7. Primary Mirror
8. Focal Volume
9. Lens
10. Photodetector
11. Preamplifier
12. Spectrum Analyzer

Fig. 2 - Component Configuration of the Lockheed LDV

Fig. 3 - View Through Side Window of LDV Depicting Scanning Optics (Note reflection of telescope primary mirror in beam directing mirror)

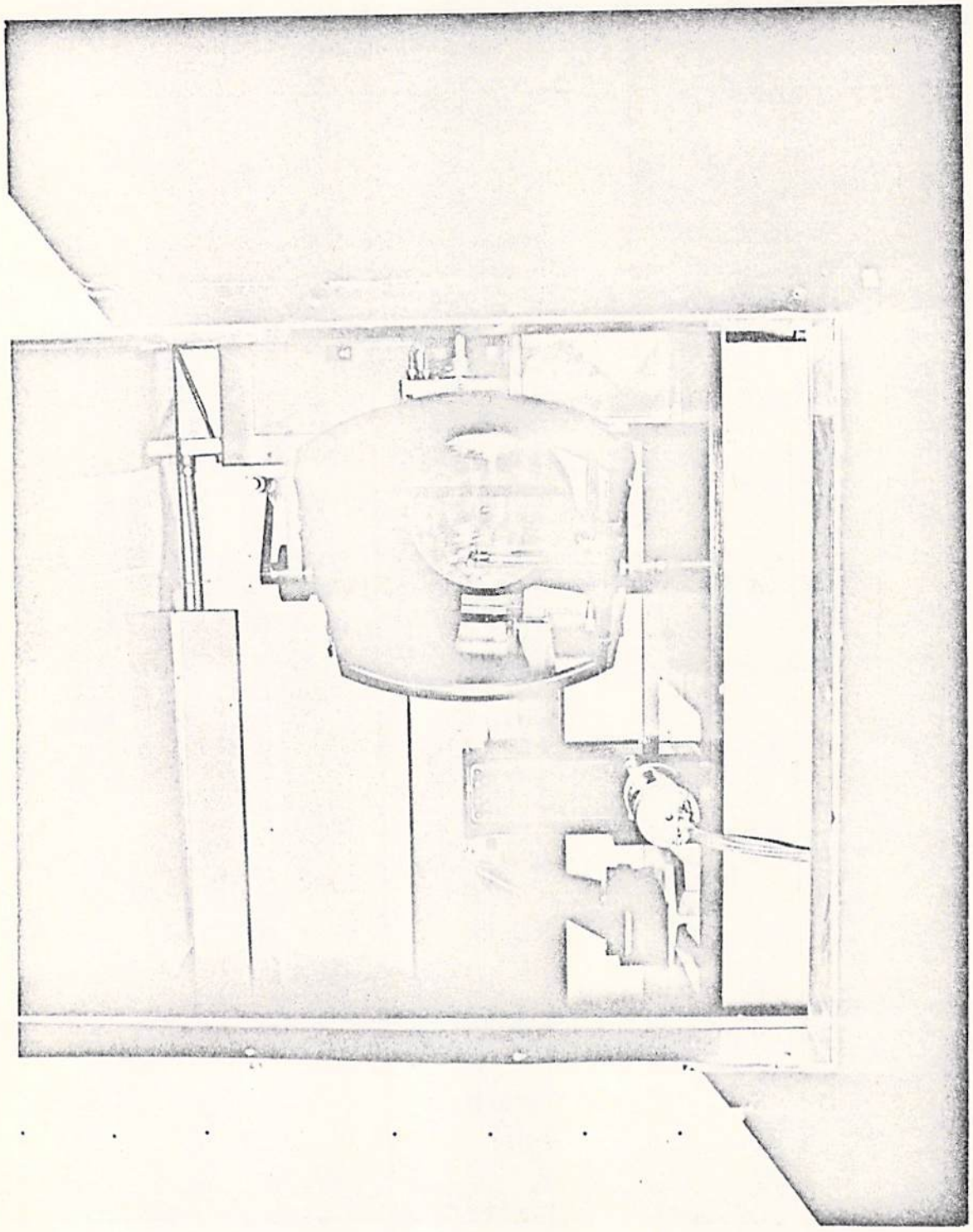

Fig. 4 - Interior View of LDV Van Looking Forward (Depicted in foreground is elevation scanning mirror on left and laser on right. Teleprinter in right rear.)

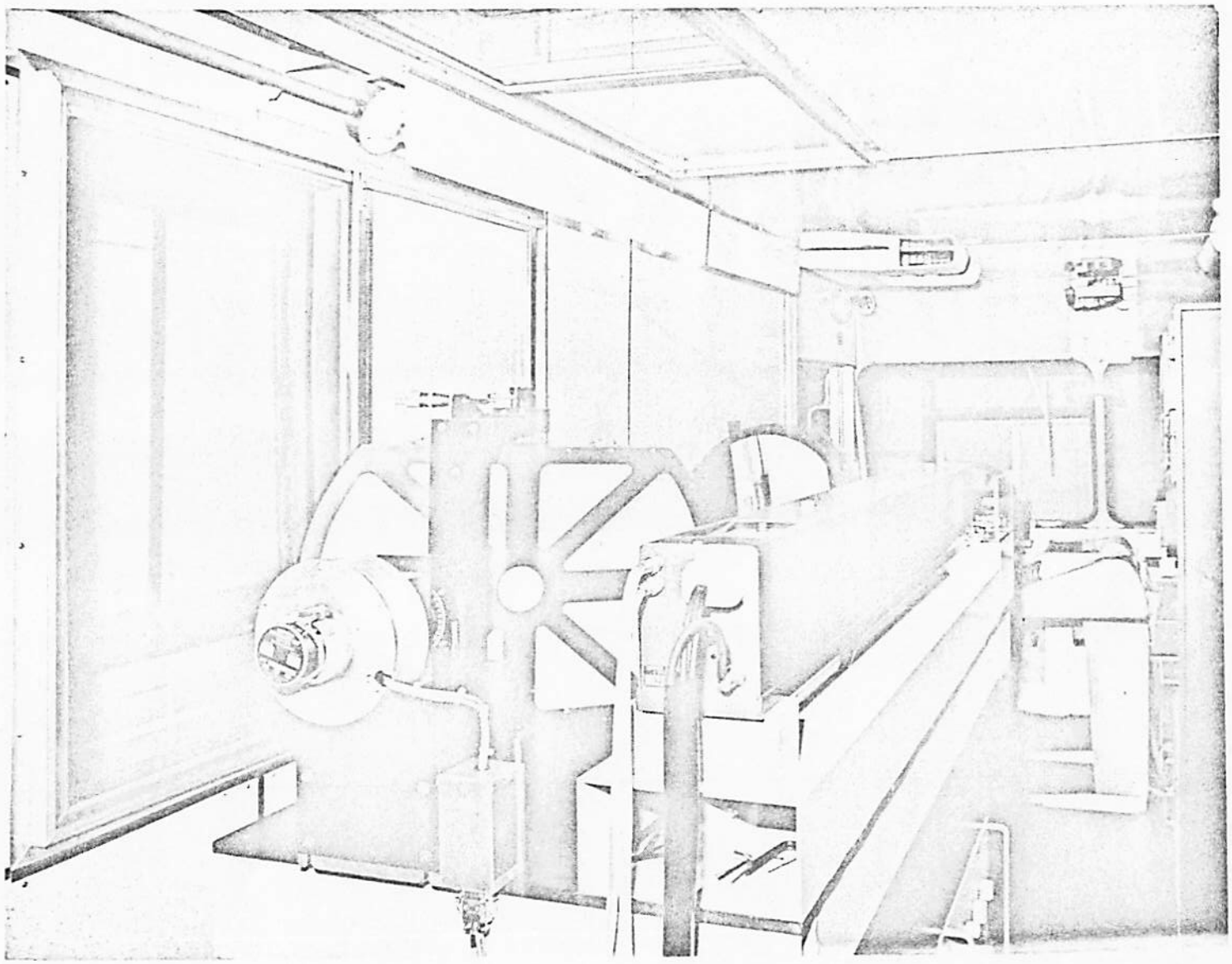

Fig. 5 - Interior View of LDV Van (Display and scanner controls in first rack, computer in second rack, digital tape unit aft and optics package on right.)

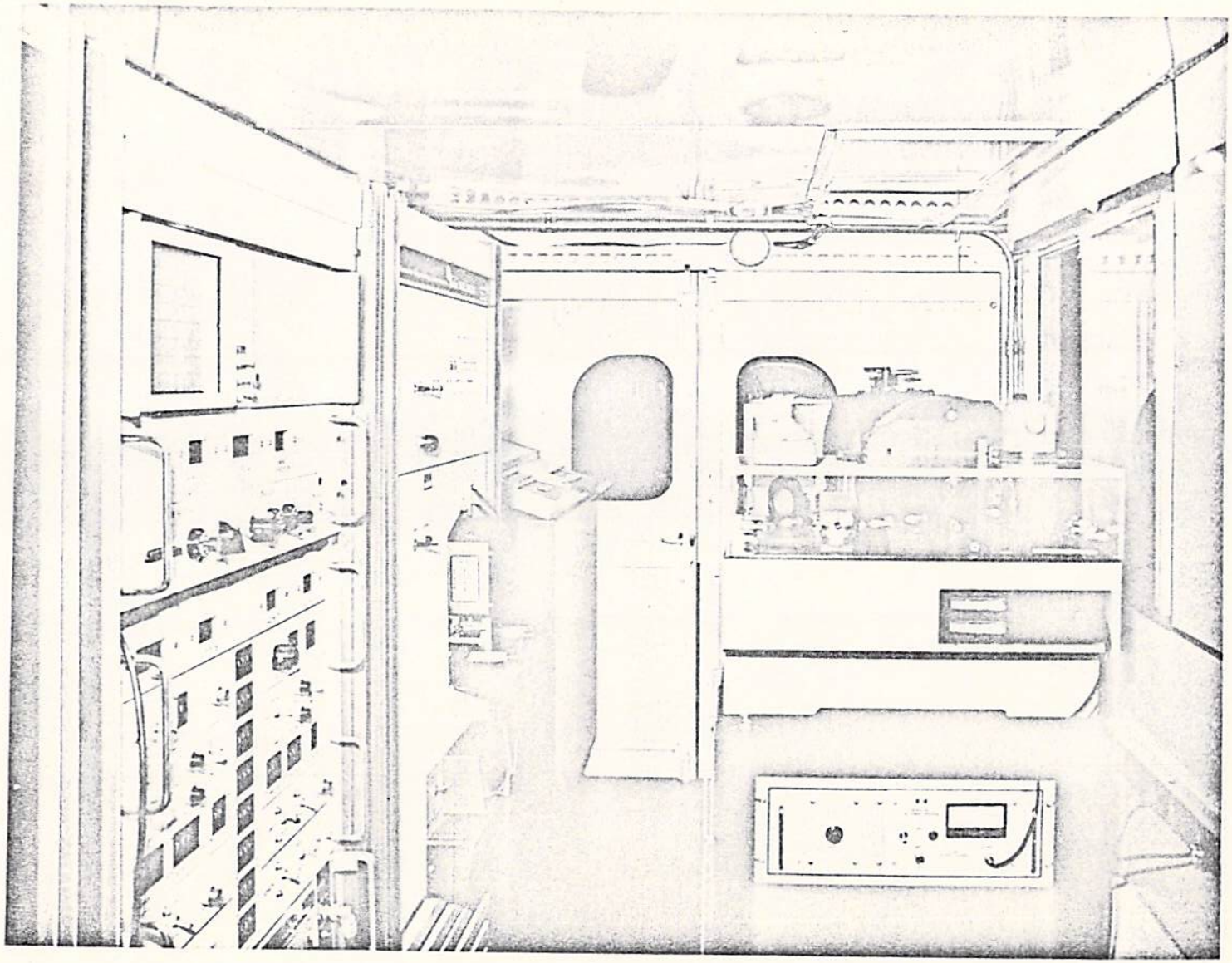

Scan Modes

1. Range or Line Scan
2. Elevation
3. Altitude
4. Azimuth
5. Horizontal Wind Velocity
6. Vertical Wind Velocity
7. Wind Direction
8. Line-of-Sight Velocity

The characteristic output signal from the LDV system is an intensity versus frequency spectrum illustrated in Fig. 6. The output parameters V_{pk} and V_{ms} are indicative of the velocities in the LDV focal volume corresponding to the fastest particle (or particles) above the amplitude threshold and the particle (or particles) having the highest backscatter, respectively. The bandwidth, N, is a measure of the range of particle velocities in the focal volume. Intensity and velocity thresholds are applied to the signal, as shown, to eliminate noise and to improve the resolution of the system. For example, in the vortex tracking mode the frequency threshold of the LDV is set high to filter out the low frequency signal associated with the ambient wind.

The velocity resolution of the LDV is determined by the signal-to-noise ratio characteristics of the system as well as the atmospheric aerosol particle size distribution. During the Rosamond tests, no difficulty was encountered detecting the high velocity regions, as high as 28 m/sec, associated with the wake vortex phenomena. The very low ambient wind velocities, on the order of 1-2 m/sec, were also detected by the LDV at Rosamond which were above the system's velocity threshold of 0.5 m/sec.

The spatial resolution of the LDV is determined by the size of the laser beam sensing volume where the beam is focused. The extent of the laser Doppler system sensing volume is a function of range which is shown in the following table ($\Delta r = 9.84 \times 10^{-4}$ (m^{-1}) R^2) obtained from calibration measurements (Ref. 4).

V_{pk} = Velocity of highest channel above amplitude threshold

V_{ms} = Velocity of the channel having the peak signal

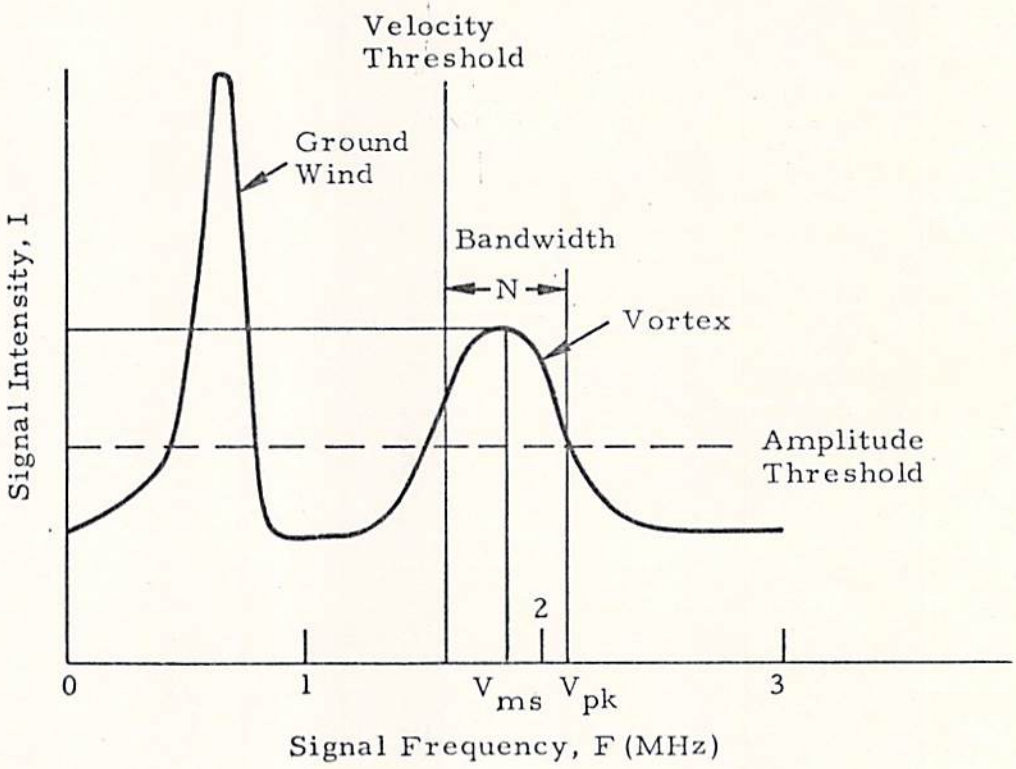

Fig. 6 - Definition of Laser Doppler Velocimeter Output Signature

Range to Focus, R(m)	Sensing Volume Length (Half Power Value), Δr (m)
76	5.68
100	9.84
152	22.73

For example, if the LDV system is tracking wake vortices at a range of 60 m, a needle-shaped volume of the vortex 3.54 m long and 4 mm in diameter is sampled. During the Rosamond tests the typical vortex range was 60 m so that the spatial resolution due to the spreading of the focal volume was 3.54 m.

In addition to the finite focal volume, the sampling rate of the LDV plays an important role in determining the overall resolution of the system. During the Rosamond tests, measurements were obtained at two data rates, at 70 and 500 Hz. The lower data rate was achieved with a scanning spectrum analyzer and the higher data rate was achieved with a filter bank provided by NASA-MSFC. Since the spatial resolution of the flow is a function of the selected data rate and scan mode, the resolution must be considered separately for each type of operation: the arc scan, finger scan, and LDV modes.

2.1.1 Arc Scan Mode of Operation

In the arc scan mode the LDV interrogates the vortex wake at a fixed range along an arc normal to the aircraft flight path. As shown in Fig. 7 the sensing volume is moved between two elevation limits (the typical cone angle is $2\alpha = 30$ deg) at a fixed rate (the typical scan rate is 0.5 Hz) while the vortex drifts past the scanned arc. Thus, the arc scan measurements indicate the spanwise downwash distribution in the wake of the aircraft provided the vortex range is sufficiently close to the selected scan range.

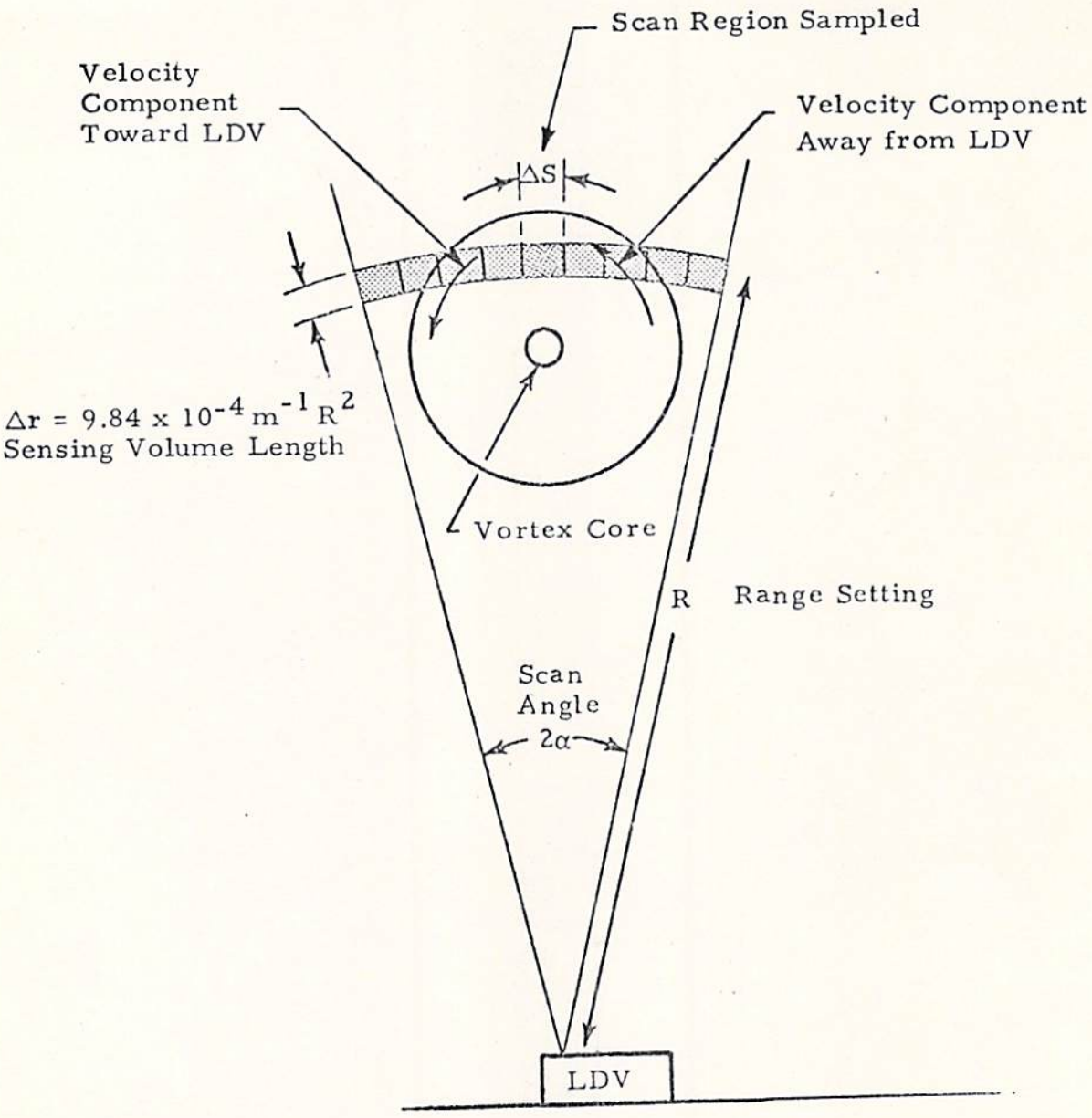

Fig. 7 - Geometry for Arc Scanning for Rosamond Wake Vortex Tests

During one arc scan of the vortex wake, the vortex velocity field is sampled at discrete evenly space intervals along the arc as shown in Fig. 7. The separation between successive sample points, ΔS, based on the sampling rate f, range R, and cone angle 2α is given by

$$\frac{\Delta S}{R} = \frac{2\pi}{360^{o}} \frac{2\alpha/\text{sec}}{f}$$

where 2α/sec is the elevation angle scan rate at a frequency of 0.5 Hz. For a typical arc scan wake vortex measurement at Rosamond f = 500 and 70 Hz, R = 60 m and 2α = 30 deg so that the wake vortex flow field is sampled every 0.06 and 0.4 m at the high and slow data rates, respectively. Since the range of vortex core diameters measured for a B-747 aircraft is 0.3 to 2 m based on tower fly-bys (Ref. 5), the sampling rate of the LDV system is sufficient to obtain several cuts through the vortex core along the arc (or essentially in the spanwise direction), particularly at the high data rate.

The drift of the wake vortex affects the resolution of the vortex measurements in the vertical direction. During a single scan frame, the vortex is translated by an amount depending on the cross-wind velocity and on the mutual induction of the complete vortex field. Since the tests were conducted during the early morning hours, cross winds were generally negligible and the primary motion of the wake vortex was in the downward direction. Assuming a typical vortex descent rate of 2 m/sec, and a typical scan rate of 0.5 Hz, this implies that a spanwise traverse of the wake vortex is taken every 2 m in the vertical plane in the arc scan mode. Based on these values, it is noted that the LDV arc scan technique can observe the detailed characteristics of the wake vortex phenomena which are larger in extent than 0.06 and 2 m in the horizontal and vertically directions, respectively.

2.1.2 Finger Scan Mode of Operation

During the Rosamond flight tests 56% of the LDV wake vortex measurements were conducted using the finger scan mode. In the finger scan mode both the range and elevation of the laser beam were varied simultaneously and

linearly with time producing a multiple lobe scan pattern with the laser beam as shown in Fig. 8. The settings and sampling rates for the finger scan mode are given in Appendix A.

The distance between sample points for the finger scan mode is higher than for the previous arc scan mode. From Appendix A, it is noted that the typical range scan excursion for the finger scan mode is 105 m and the normal range rate is 3.5 Hz. It follows that the beam scan velocity is 735 m/sec. Because the velocity measurements were sampled every 2 and 14.3 milliseconds at the low and high data rates, the wake vortex flow field is measured at every 1.5 and 10.5 m increment in range, respectively. Thus, the finger scan mode can interrogate a large cross-sectional area rapidly and this is ideal for vortex tracking. In addition, the LDV finger scan measurements contain essential information regarding the wake vortex phenomena.

The characteristic line-of-sight velocity as a function of range and elevation angle during one finger scan sweep is shown in Fig. 8. A pair of double-peak patterns is noted in the line-of-sight velocity profile as a function of elevation angle. The maximum velocities occur at the elevation angles where the line-of-sight is tangent to the viscous core radius of the vortex. Thus, the mean elevation angle of the local maxima in the V_{pk} vs θ curve yields the elevation angle of the wake vortex, $\theta_{vortex} = (\theta_1 + \theta_2)/2$. Similarly, the difference between the two elevation angles is a measure of the vortex viscous core radius, $r_{vortex\ 1} = R_1 \left| \tan \frac{\theta_1 - \theta_2}{2} \right|$. The peak tangential velocity and core circulation of the vortex is given by $V_{pk\ vortex\ 1} = (V_{pk\ \theta_1} + V_{pk\ \theta_2})/2$ and $\Gamma_{vortex\ 1} = 2\pi R_{vortex\ 1} V_{pk\ vortex\ 1}$ assuming circular symmetry. The peak line-of-sight velocity at the two edges of the vortex, $V_{pk\ \theta_1}$ and $V_{pk\ \theta_2}$ are not necessarily equal due to a velocity contribution by the other vortex and the ambient winds. The range of the vortex, R_1, is given by the local maximum in the line-of-sight velocity versus range profile shown in the bottom of Fig. 8 and is not affected by the ambient winds. Based on the characteristic LDV signature observed for one scan, it is noted

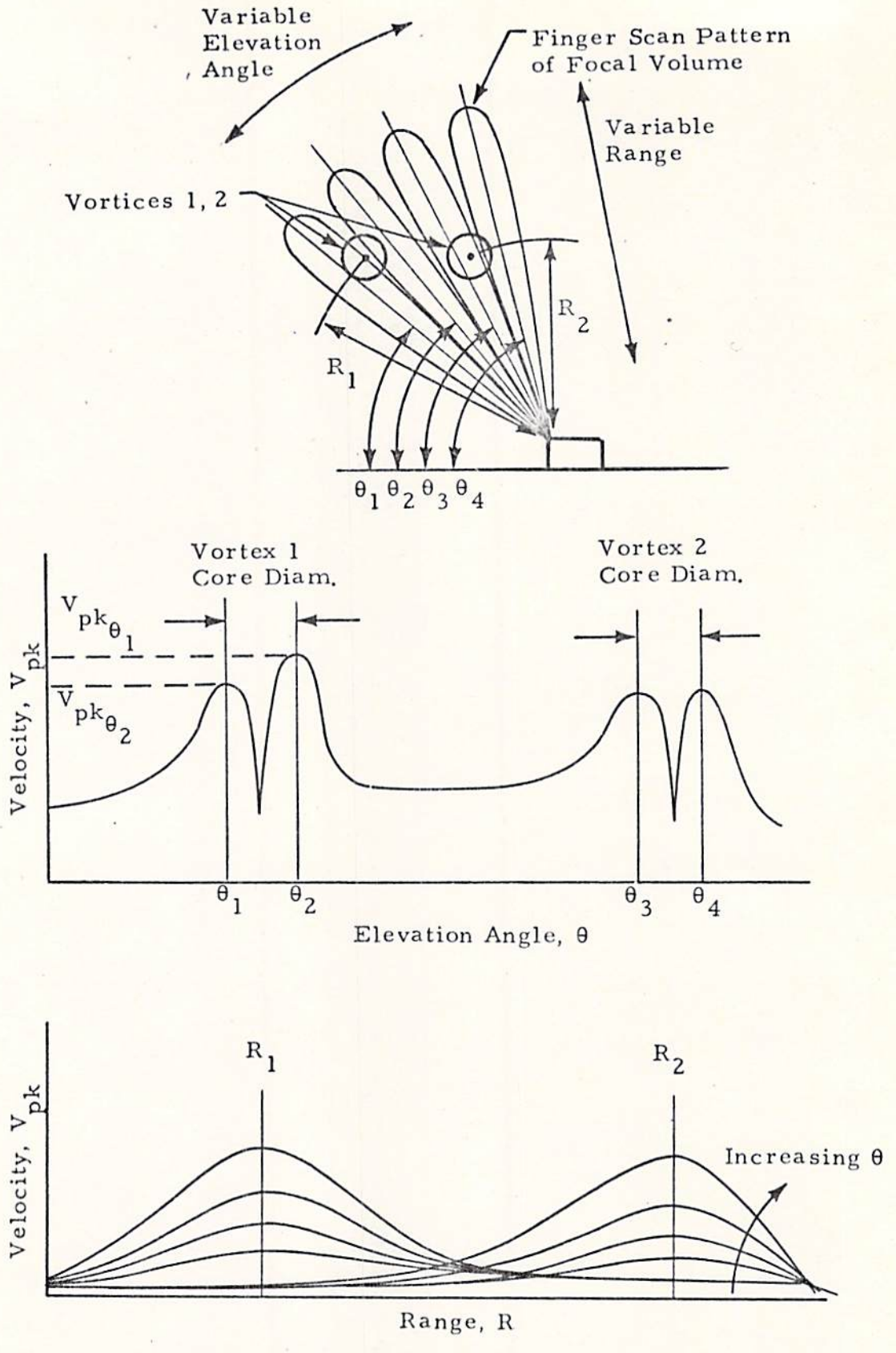

Fig. 8 - Characteristic LDV Velocity Profile Observed During One Finger Scan Sweep

that several successive finger scans contain the essential decay history of the wake vortices provided that at least two sample points are obtained for each vortex, one upwash and one downwash measurement, where the line-of-sight is tangent to the viscous core and the mean vortex range is within the LDV focal volume.

2.2 DATA PROCESSING

The output from the LDV system consisting of the coherent backscatter intensity versus frequency from the focal volume as well as the location of the focal volume in space was processed to yield the aircraft downwash field and the wake vortex characteristics. Reduction and analysis of the LDV measurements were carried out as follows: (1) the low-speed signal was digitized and stored on magnetic tape by the onboard SEL computer and subsequently processed off-line on a Univac 1108 computer, and (2) the high-speed data were both digitized and processed off-line on a Univac 1108 computer and the vortex tracks computed on a PDP 11 computer. A flow chart of the data processing sequence used for the Rosamond wake decay study is shown in Fig. 9. The software system for processing the low-speed and high-speed LDV data is described in more detail in Refs. 4 and 6, respectively.

The high-speed processor utilized the raw range and elevation signal while the low-speed processor utilized the raw range and commanded elevation signal to determine the location of the LDV focal volume. As a result, the velocity versus elevation angle measurements obtained with the high-speed processor showd scatter due to the specified ± 0.25 degree elevation angle resolution. In addition, noise was present in the elevation angle versus time distribution from the high-speed data characterized by a square wave with a frequency of $\sim$ 14 Hz and an amplitude of 0.7 deg. This was believed to be a symptom of a processing or decode problem. The normal scatter in the elevation angle was not noticeable at the low data rate but the low-speed data did show a finite lag in the scan pattern. A time lag of approximately 0.3 seconds, and a corresponding lag in the position of the LDV focal volume depending on the selected scan rate was

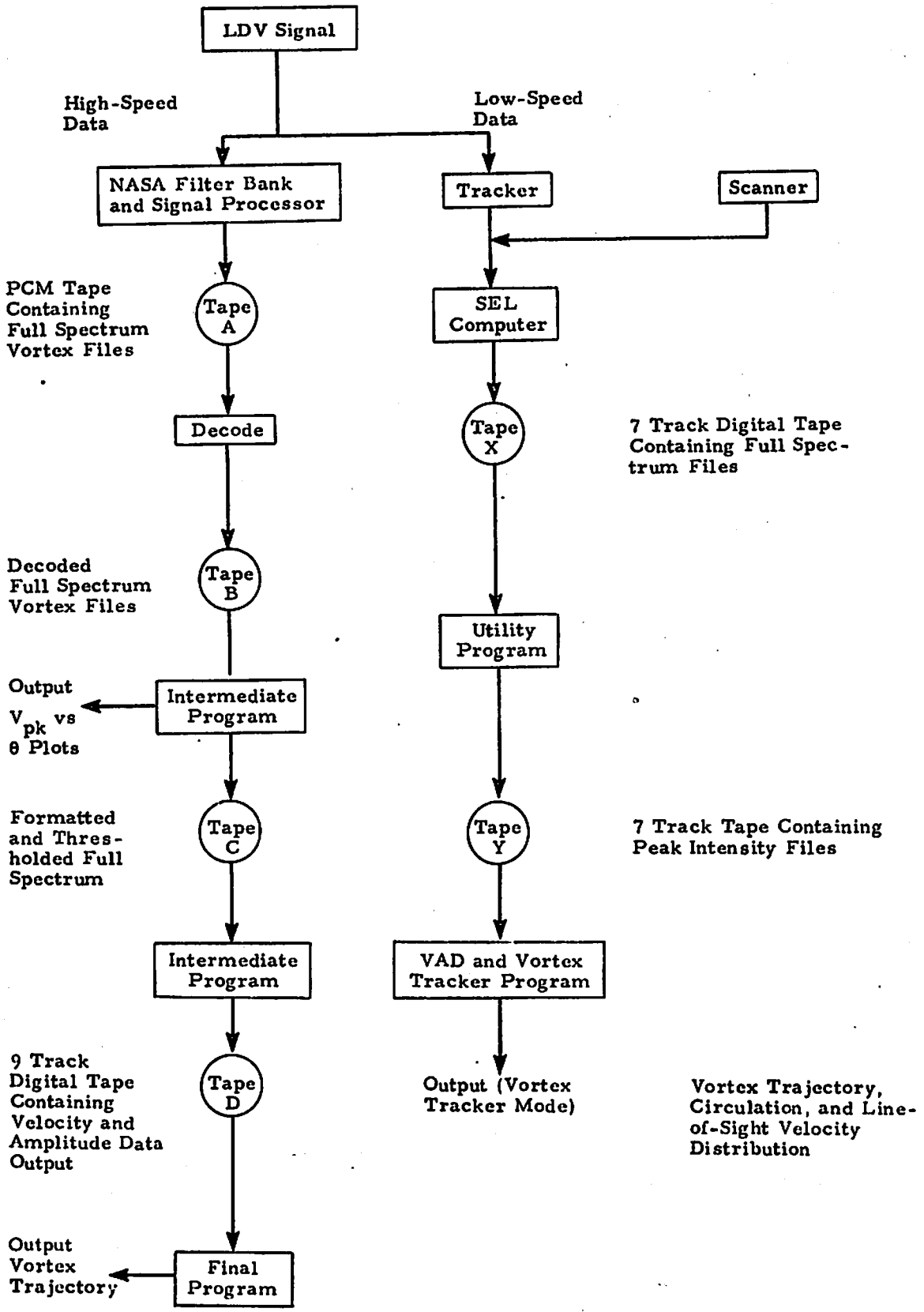

Fig. 9 - Flow Chart of Data Processing Sequence Carried Out for the Rosamond Wake Decay Measurements

observed. The lag in the system resulted from the difference between commanded versus actual angular position of the scanning mirror.

The manner in which the wake vortex measurements were processed from both the high-speed and low-speed data is summarized as follows. The frequencies and amplitudes associated with the laser Doppler signal were sampled at fixed intervals. The spectrum was recorded if it was above the frequency and amplitude threshold settings (Fig. 6). The amplitude and frequency threshold settings for the Rosamond tests are given in the log sheets in Appendix A. From the array of recorded frequency and intensity points, the line-of-sight velocity field was computed and the vortex parameters including location and velocity distribution were determined.

To compute the wake vortex transport and decay characteristics from the low-speed line-of-sight velocity distributions, the Rosamond measurements were analyzed using the "VAD and Vortex Track Program" described in Ref. 5. Based on previous experience with the program, the following parameters were selected for the analysis of the Rosamond data:

INTVEL = 2	Flag INTVEL = 1 Velocity oriented vortex determination INTVEL = 2 Intensity oriented vortex determination
NPSUF = 4	Sufficient number of points to determine vortex position
APERCT = 0.1	Fraction of the maximum peak velocity or intensity points
BPERCT = 0.1	Fraction of points within the correlation wake where Q is at least APERCT fraction of the maximum Q (Q is velocity or intensity as determined by INTVEL)
CPERCT = 0.5	Fraction of number of points in correlation circle used for determining vortex 1 required for determination of vortex 2
RPERCT = 0.3	Fraction of aircraft wing span used for correlation radius
EPERCT = 2.0	Fraction of correlation radius from vortex 1 for excluding initial point of vortex 2
NOISEF = 0	Noise floor
ADJI = 0.0	Intensity adjustment (Fraction of noise floor added to total intensity)

A sample output from the VAD and Vortex Track Program is presented in Appendix B. The intermediate sorting parameters used in determining the location of the vortex core region are also given in the printouts along with "scatter plots" indicating the line-of-sight velocity distributions. From the typical line-of-sight velocity distribution illustrated in Appendix B, the time history of the vortex wake was determined for many of the flybys.

In parallel with the low-speed data acquisition and processing, the LDV signal was also fed into the high-speed NASA-MSFC data processing system as illustrated in Fig. 9. The high-speed data processing technique is similar to the low-speed technique described earlier, and is described in detail in Ref. 6. A sample output from the NASA-MSFC LDV data processing routines is shown in Appendix C including the listing of the raw line-of-sight velocity profile, the plot of V_{pk} versis elevation angle, and plots of the vortex trajectory.

3. DESCRIPTION OF EXPERIMENTAL TESTS

A two-day test sequence was carried out to determine the wake vortex characteristics of a B-747 aircraft as a function of spoiler, flap and landing gear settings, altitude above ground, and glideslope. The test consisted of 54 low level passes during the early morning hours over the LDV system deployed at Rosamond Dry Lake near Edwards AFB, California, on 2-3 December 1975. Key elements of the experimental tests included the flight test program and the operation of the LDV remote sensor system.

3.1 FLIGHT TEST PROGRAM

The aircraft used for the tests was a Boeing 747-123 aircraft. A plan view of the aircraft showing the details of the flap and spoiler configurations is presented in Fig. 10.

Aircraft configuration varied from run to run, with dominant emphasis on as close to a normal landing configuration as operating conditions would allow. The clean configuration was also studied, and special flap and spoiler configurations were investigated for vortex alleviation effectiveness. The Boeing 747 flew at 30 to 250 m above the ground level of 700 m MSL. Runs were made in level flight as well as in descending and climbing flight. Descents were at about 250 m/min. A lift coefficient of approximately 1.4 was used for all flaps-down runs.

Of the 54 runs, 35 (or about 65%) were made with the inboard flaps lowered 30 deg and the outboard flaps lowered 30 deg (denoted 30/30); eight (approximately 15%) with 10/10 flaps and 5 (approximately 9%) with flaps retracted. The remaining six runs had the inboard flaps lowered 30 deg and the outboard flaps lowered 1 deg, to test the effects of this configuration

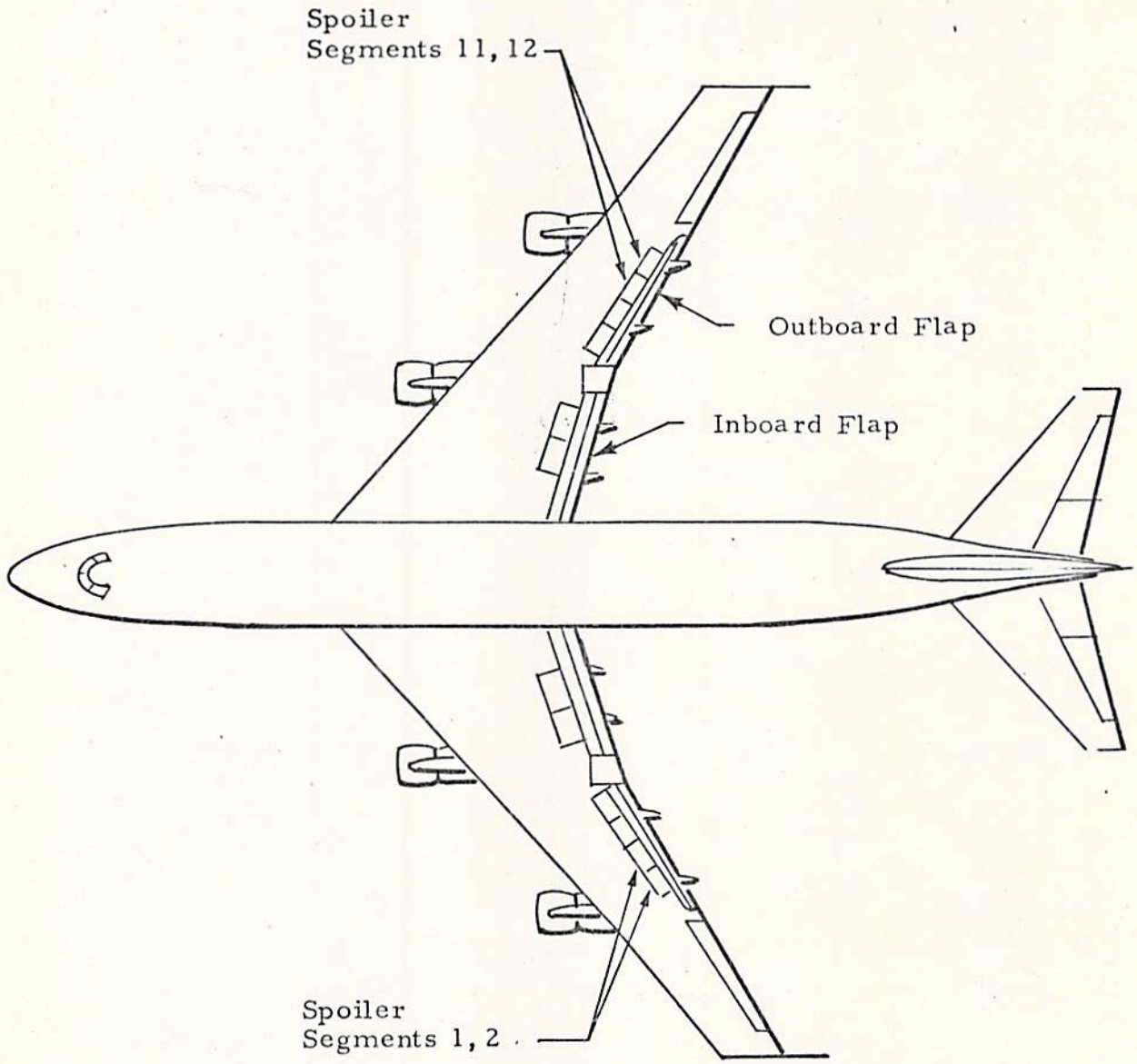

Fig. 10 - Spoiler and Flap Arrangement on B-747 Aircraft

on vortex alleviation. For each flap setting, runs were conducted with the gear down or retracted and some had spoilers deployed (the extension angle was always 41 deg) in addition to the flap. A summary of the aircraft altitude, speed, weight, and flap, landing gear and spoiler settings for each of the fly-bys is given in Table 1.

3.2 OPERATION OF LDV REMOTE SENSOR

The LDV system was set up and calibrated at the Rosamond test site prior to conducting the actual wake surveys. A discussion of the calibration procedure and the conduct of the wake vortex surveys is summarized below.

3.2.1 Calibration

During the set-up process, the optical bench was leveled with the external van jacks using a bubble level for reference (estimated accuracy of $\pm$0.5 deg). For the second day of the tests, the scanner was offset 45 deg using a tri-square for reference (estimated accuracy of $\pm$0.5 deg). Prior to the actual wake surveys, the elevation and azimuth angle readouts from the LDV were calibrated. The calibration involved pointing the optical system at the sun and comparing the observed elevation and azimuth angle readouts with those given in the ephemeris. The results indicated that a -3 deg and $\pm$139 deg correction should be applied to the raw elevation and azimuth readouts from the LDV, respectively.

During the Rosamond tests the range resolution and signal-to-noise ratio characteristics of the LDV were not recalibrated. The range and signal-to-noise ratio calibrations taken a few months earlier and documented in Ref. 4 were assumed to be representative of the systems overall performance.

3.2.2 Wake Surveys

During the Rosamond wake decay tests, a total of 53 aircraft fly-bys were recorded with the LDV system (flyby 36 was lost due to a loss in CPU power). The test conditions and the LDV scan, range, and elevation settings

Table 1

SUMMARY OF B-747 FLIGHT PARAMETERS

Flyby No.	Altitude (m AGL)	IAS (knots)	Weight (kg/1000)	Flaps (degrees)	Spoilers Deployed	Thrust (EPR)	Gear
1	66	146	255	30/30	0	1.25	Down
2	62	146	252	30/30	0	1.21	Down
3	68	145	250	30/30	0	1.25	Down
4	65	145	249	30/30	0	1.22	Down
5	122	144	248	30/30	0	1.22	Down
6	122	144	247	30/30	0	1.23	Down
7	244	143	245	30/30	0	1.23	Down
8	244	143	244	30/30	0	1.20	Down
9	61	143	236	30/30	1,2,11,12	1.26	Down
10	122	143	235	30/30	1,2,11,12	1.26	Down
11	183	142	234	30/30	1,2,11,12	1.25	Down
12	244	142	232	30/30	1,2,11,12	1.25	Down
13	64	142	230	30/30	1,2,11,12	1.24	Down
14	65	138	228	30/30	1,2,11.12	1.20	Down
15	61	138	227	30/30	1,2,11,12	1.20	Down
16	61	138	226	30/30	1,2,11,12	1.18	Down
17	30	141	222	30/1	0	1.19	Down
18	37	141	218	30/1	0	1.18	Down
19	38	141	216	30/1	0	1.18	Up
20	67	139	215	30/1	0	1.18	Down
21	64	139	213	30/1	0	1.16	Up
22	91	139	212	30/1	0	1.23	Down
23	122	148	260	30/30	0	1.24	Down
24	122	220	259	0/0	0	1.03	Up
25	122	147	258	30/30	0	1.24	Down
26	122	215	256	0/0	0	1.06	Up
27	67 (LDG)	146	255	30/30	0	1.20	Down
28	66	146	254	30/30	0	1.20	Down
29	72 (LDG)	146	252	30/30	0	1.14	Down
30	66	145	251	30/30	0	1.24	Down
31	107 (TO)	156	243	10/10	0	1.38	Up
32	65	156	242	10/10	0	1.11	Up
33	57 (TO)	156	241	10/10	0	1.36	Up
34	59	143	240	10/10	0	1.15	Up
35	63	142	239	30/30	0	1.20	Down
36	68	142	238	30/30	0	1.20	Up
37	67	141	237	30/30	0	1.21	Down
38	61	141	236	30/30	0	1.22	Up
39	47 (TO)	151	230	10/10	1,2,11,12	1.36	Up
40	46 (TO)	151	228	10/10	0	1.36	Up
41	48 (TO)	150	227	10/10	1,2,11,12	1.36	Up
42	54 (TO)	150	226	10/10	0	1.40	Up
43	61	138	225	30/30	0	1.24	Down
44	63 (LDG)	138	224	30/30	0	1.12	Down
45	50 (LDG)	138	223	30/30	0	1.16	Down
46	37	137	222	30/30	0	1.24	Down
47	91	135	215	30/30	0	1.15	Down
48	91	135	214	30/30	1,2,11,12	1.20	Down
49	37	134	213	30/30	1,2,11,12	1.20	Down
50	91 (LDG)	134	210	30/30	0	1.11	Down
51	122	200	209	0/0	0	1.11	Down
52	122	200	208	0/0	0	1.03	Up
53	122	133	207	30/30	0	1.22	Down
54	122	200	206	30/30	0	1.05	Up

LDG: Aircraft descending along imaginary glideslope.

TO: Aircraft ascending as in actual takeoff.

for the Rosamond tests are summarized in the external log sheets given in Appendix A while a list of the flight parameters is given in Table 1. Primarily those flybys have been processed from the wake measurements where flow visualization and photographic data were available for comparison with the LDV measurements.

In order to maximize the amount of data collected regarding wake vortex trajectories, velocity profiles, and decay rates, the LDV was operated in different scan modes including: (1) arc scan and, (2) finger scan configurations. The wake vortex surveys were conducted in the following manner.

On the first test day the LDV was located directly under the flight path (Fig. 11) and scanned arcs in a plane perpendicular to the flight path (Fig. 12) with a complete scan every two seconds. Scans were at a fixed range until the vortex passed through the scan arc, at which time the sensor range was lowered and remained fixed again until the vortex descended through the new range. The objective of the overhead arc scan measurements was the measurement of the initial downwash field and the wake vortex rollup process.

On the second test day the LDV was moved 60 m north of the flight path (Fig. 11) and scanned simultaneously in elevation and range (finger-scan mode) at a frequency of 0.2 Hz, and 2 – 2.5 Hz, respectively. The objective of the finger scan measurements was to track the location of the vortex pair and to observe the vortex decay rates. The coordinated variations in range and elevation settings for the finger scan mode were selected on the basis of the observed aircraft wake vortex parameters. In addition, during the last sorties the azimuth angle was changed during the run at 90 and 180 deg angles to scan both down the vortex (axially) and to follow the vortex drift away from the LDV.

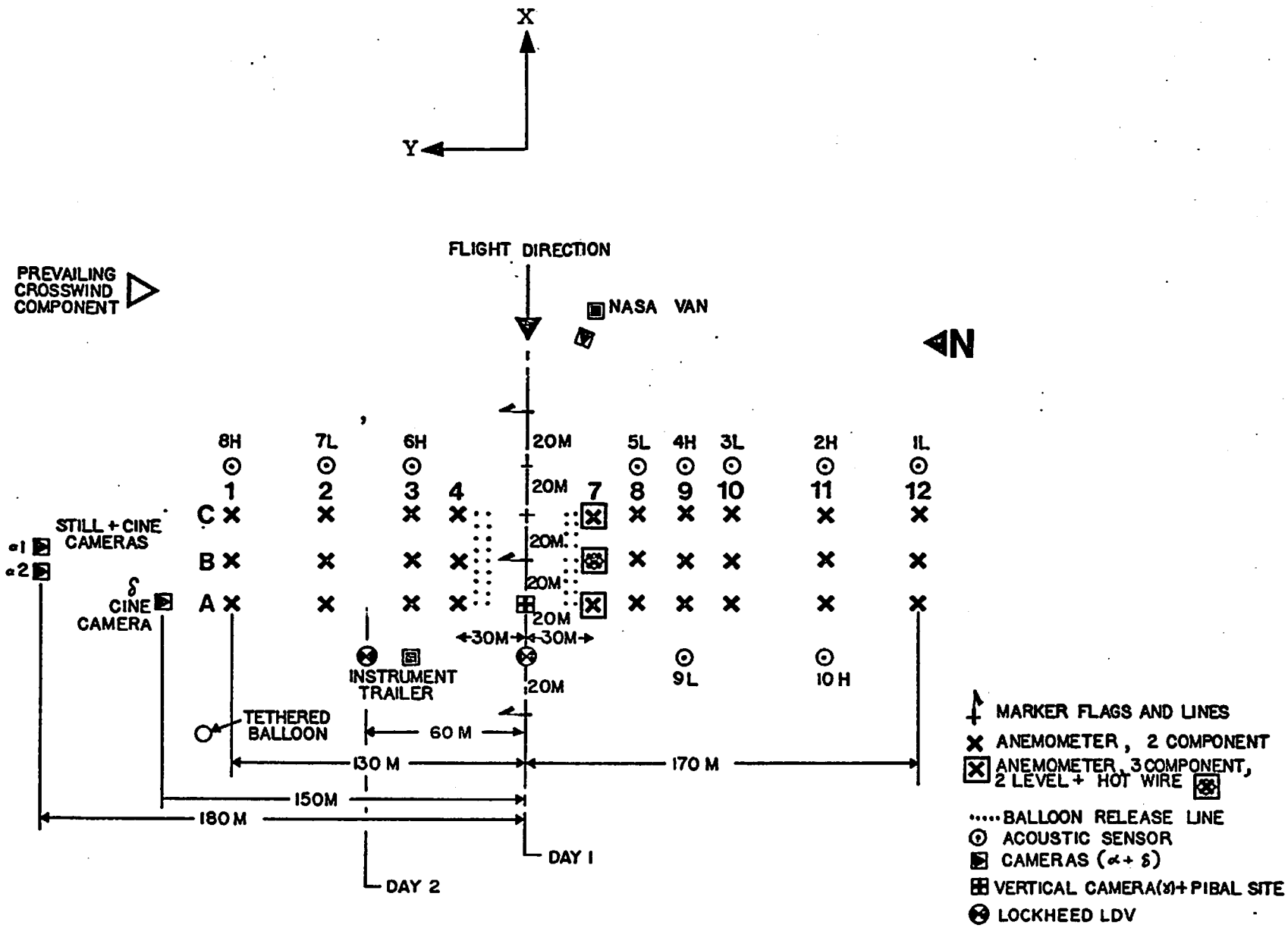

Fig. 11 - Location of Lockheed LDV During the Rosamond Wake Vortex Measurements

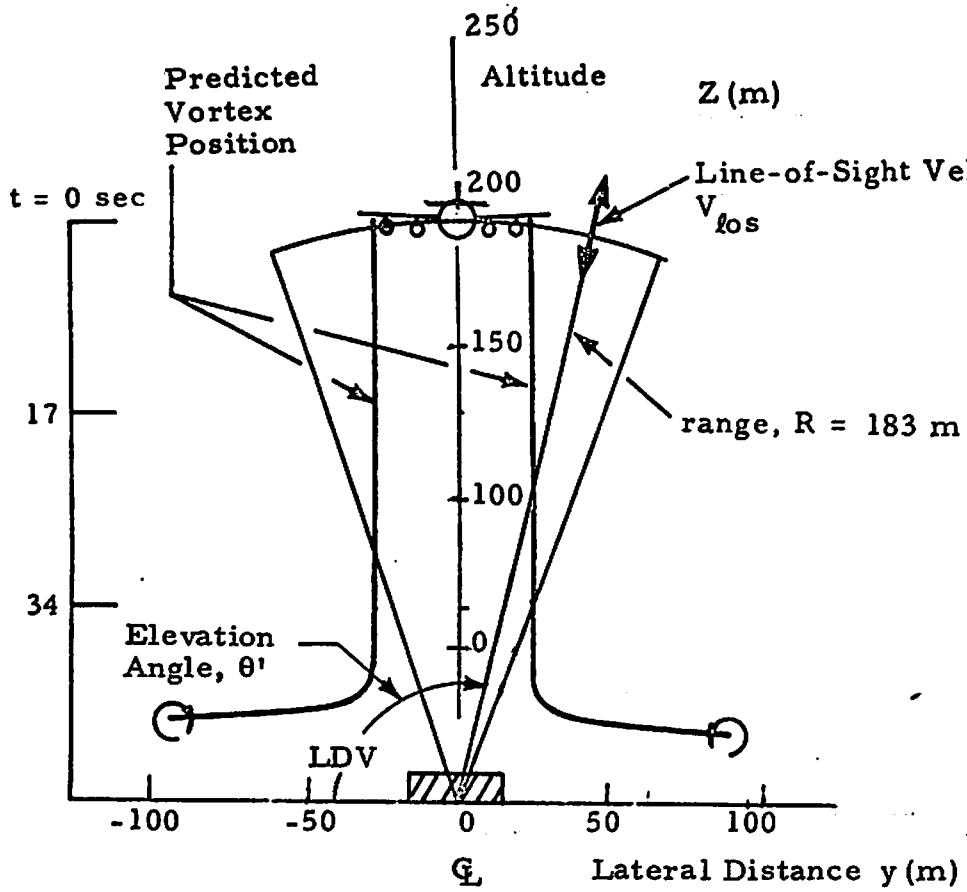

Fig. 12 - Overhead Arc Scan Configuration Illustrated for Rosamond Flyby 11

4. RESULTS OF WAKE VORTEX MEASUREMENTS

The LDV measurements obtained during the Rosamond tests have been analyzed to determine the dominant characteristics of the B-747 wake. In the following discussion the observed wake vortex characteristics are described including the vortex rollup, vortex transport and vortex decay parameters.

4.1 VORTEX ROLLUP

To determine the vortex rollup parameters, the downwash field behind the B-747 aircraft was measured with the LDV operated in a constant range arc scan mode. In the typical arc scan configuration, illustrated earlier in Fig. 13, the line-of-sight velocity component observed by the LDV was essentially a measure of the spanwise downwash distribution in the aircraft near-wake. Thus, from the LDV line-of-sight velocity distribution in the near wake the downwash and vortex formation and rollup characteristics were determined.

4.1.1 Initial Spanwise Downwash Distribution

The magnitude of the peak line-of-sight velocity distribution, $|V_{pk}|$ (m/sec), from the high speed data is shown as a function of lateral distance, y (m), in Figs. 13 through 16 for flybys 8, 11, 12 and 13, respectively, over the time interval t = 0 to 8 sec. Each scan is defined as the period between two successive elevation angle reversals and is approximately 1 sec in duration. Occasionally, some overlapping occurs between successive scans due to limitations in the processing software. Therefore successive scans shown in Figs. 13 through 16 do not always have the same starting and ending limits and, as a result, the lateral scales can be different. The direction and mid-time of each scan is indicated in the figures. The lateral distance, y, was computed directly from the raw range, R, and raw elevation angle

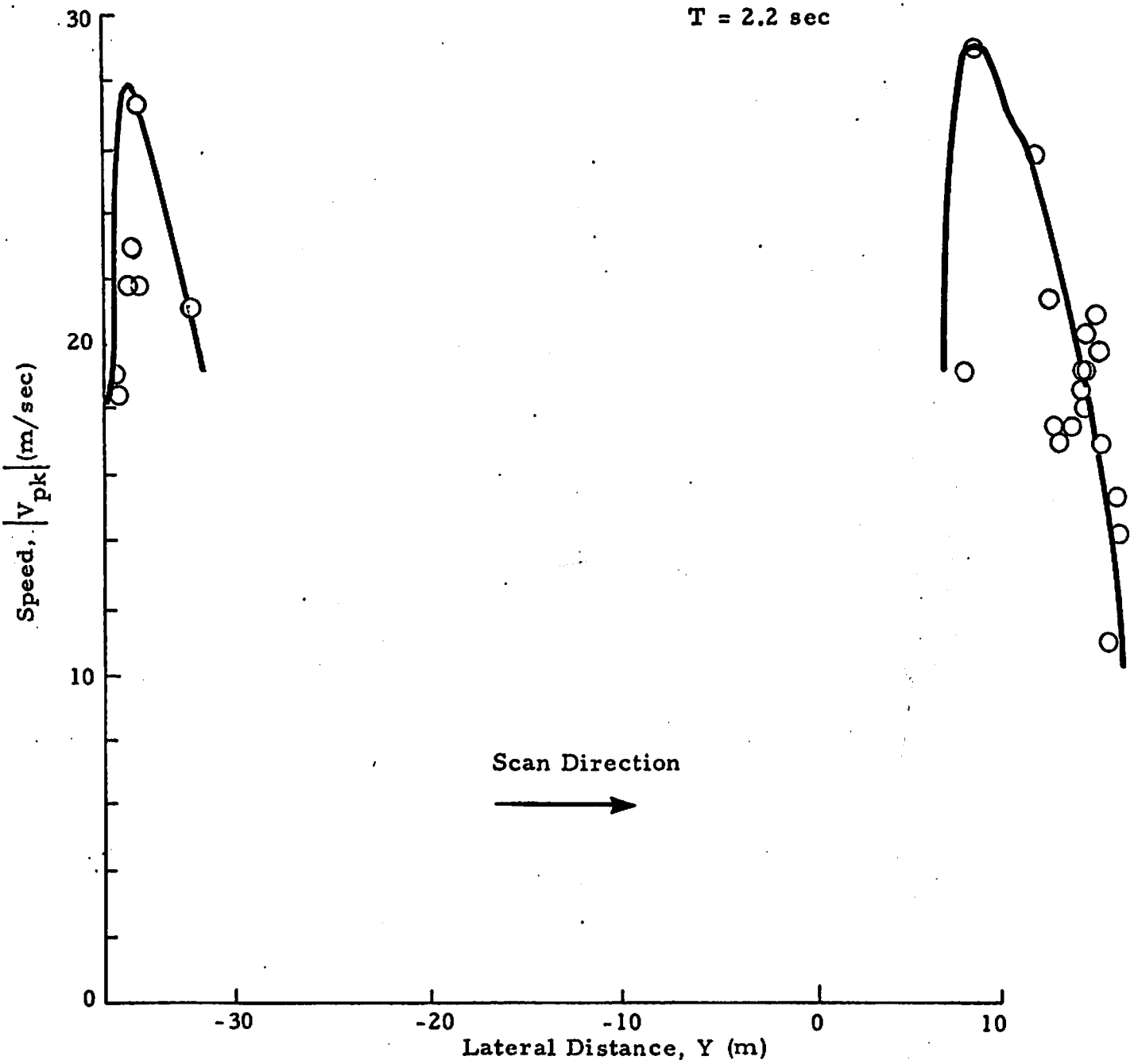

Fig. 13 - $|V_{pk}|$ as a Function of Lateral Distance for Rosamond B-747 Flyby 8

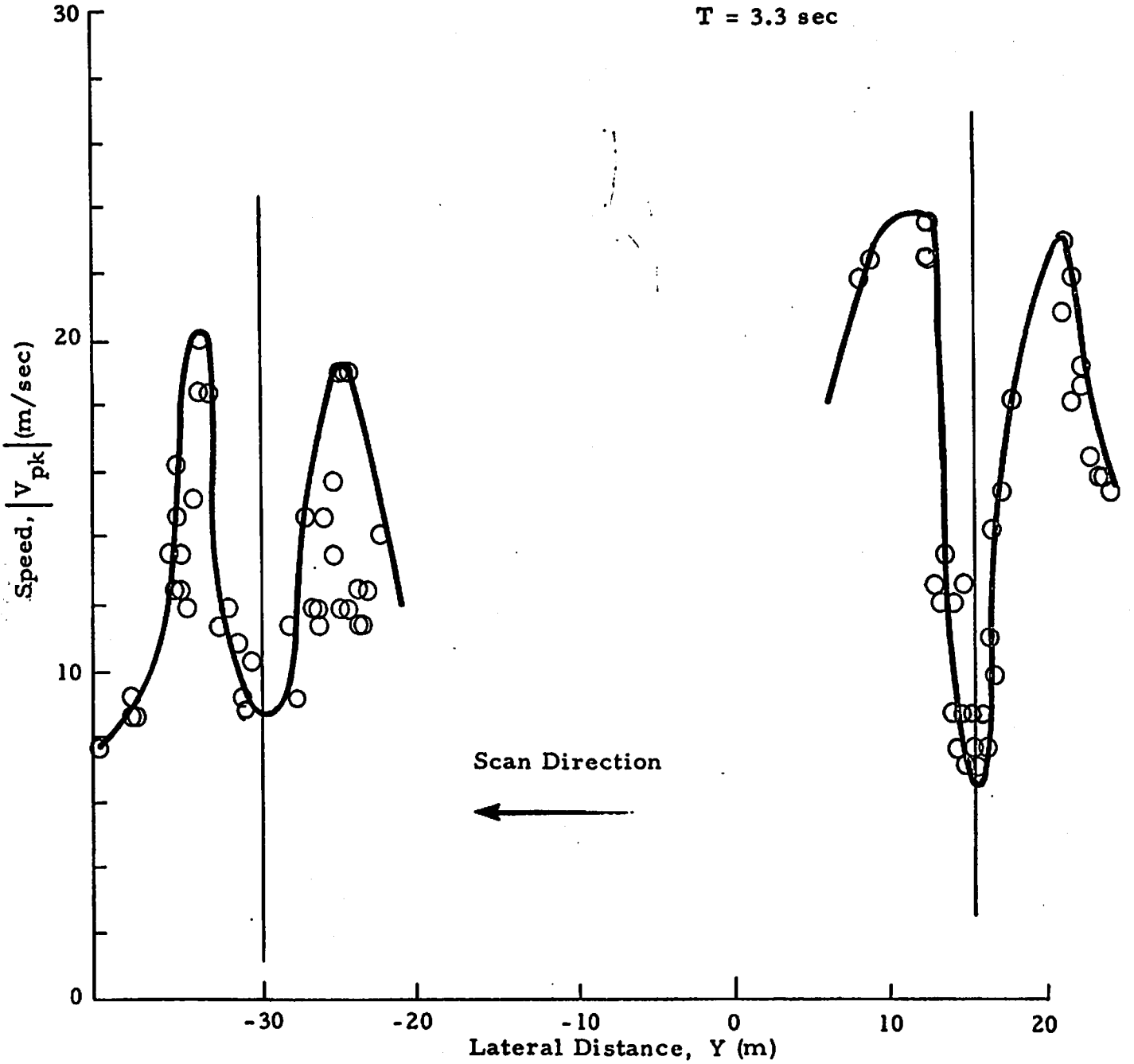

Fig.13 (Continued)

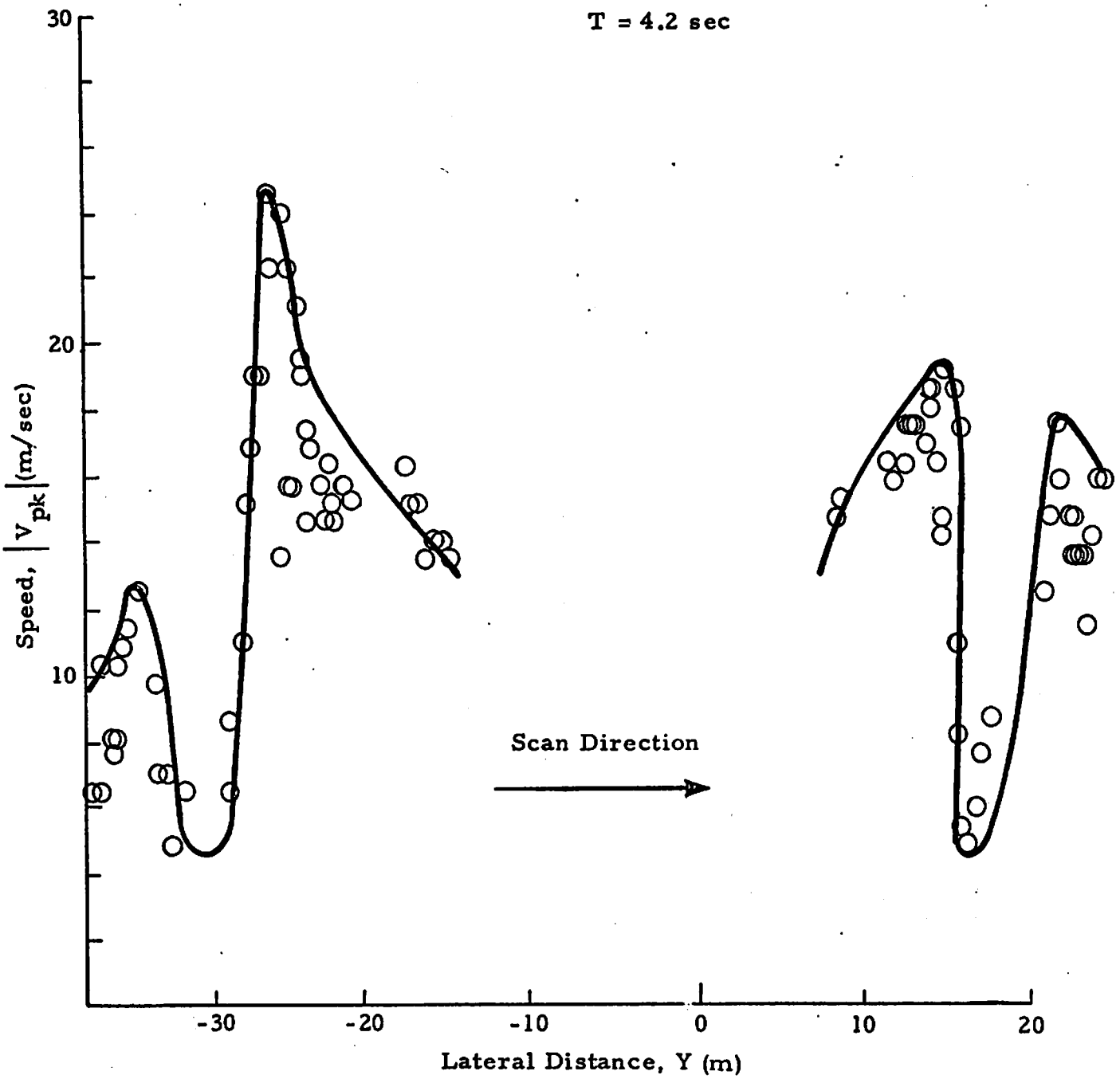

Fig. 13 (Continued)

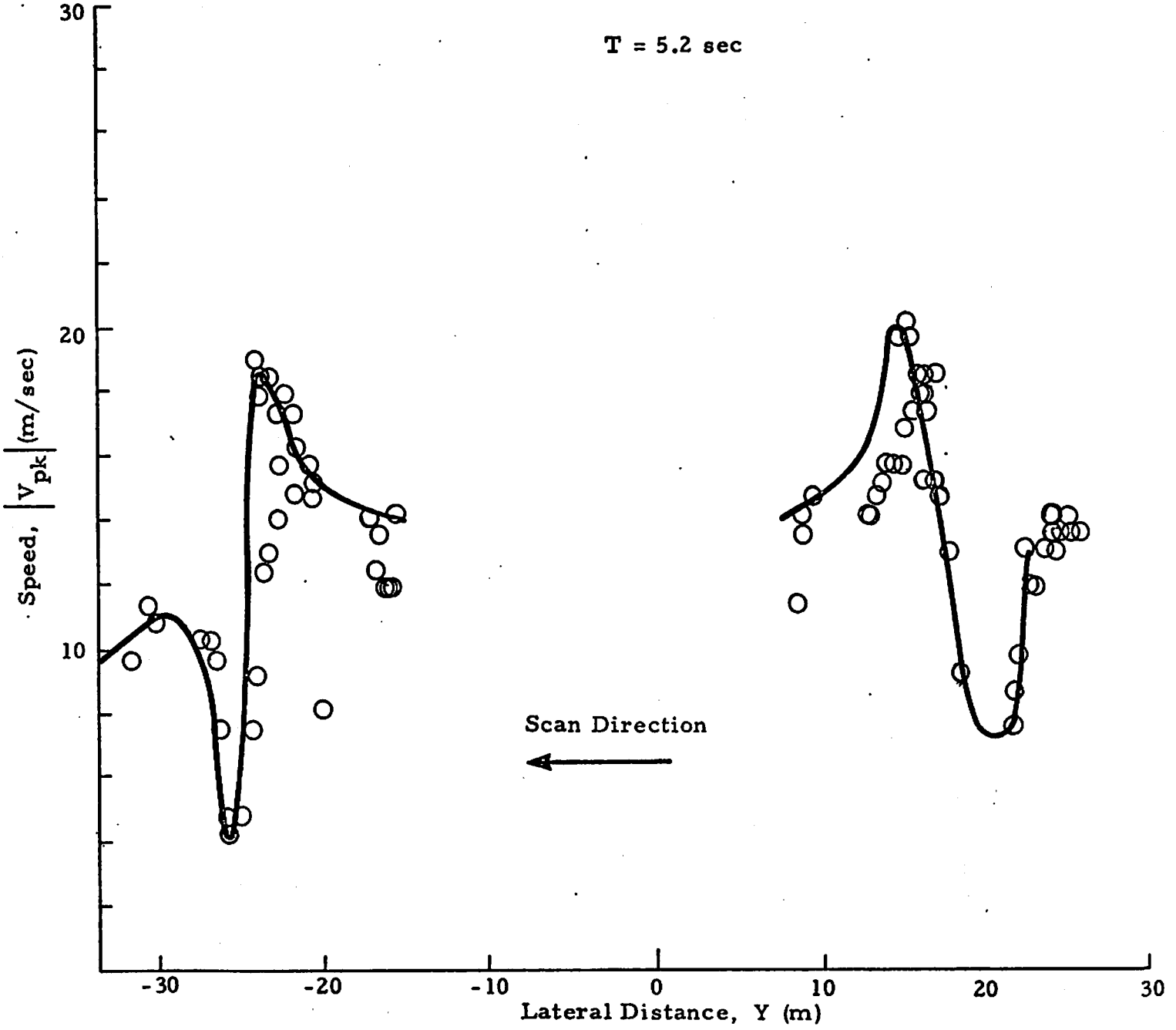

Fig. 13 (Continued)

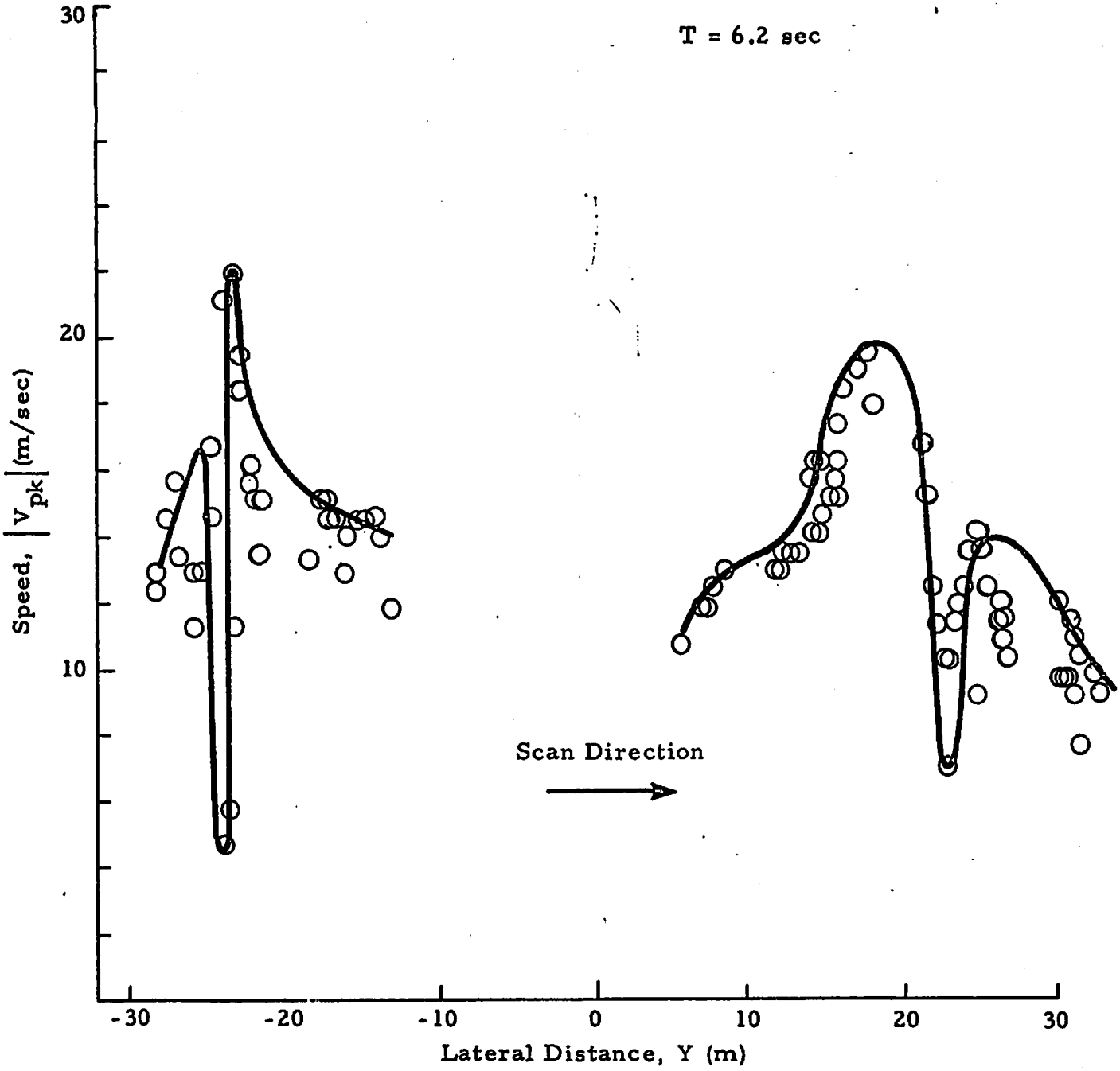

Fig. 13 (Continued)

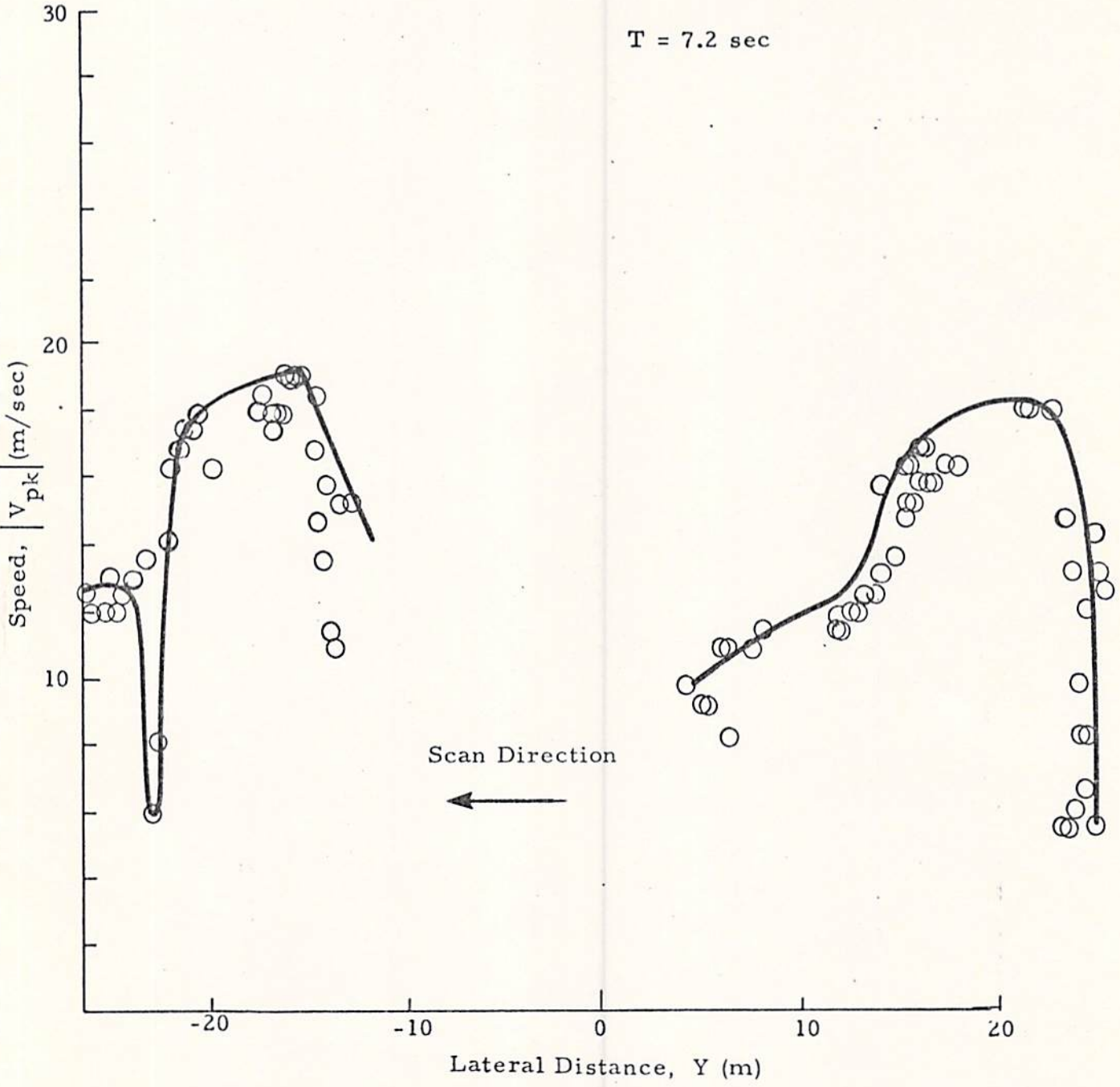

Fig. 13 (Continued)

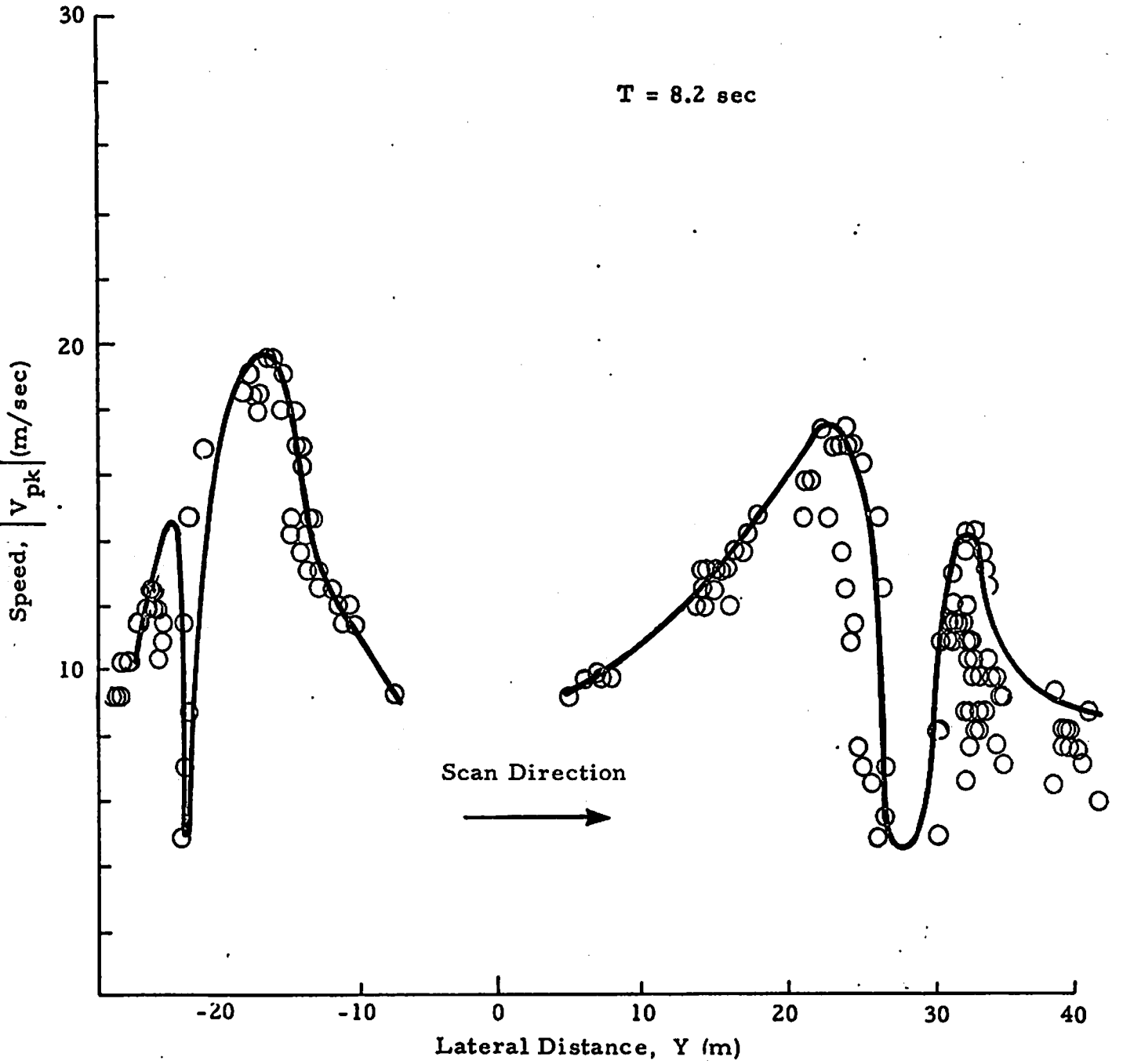

Fig. 13 (Concluded)

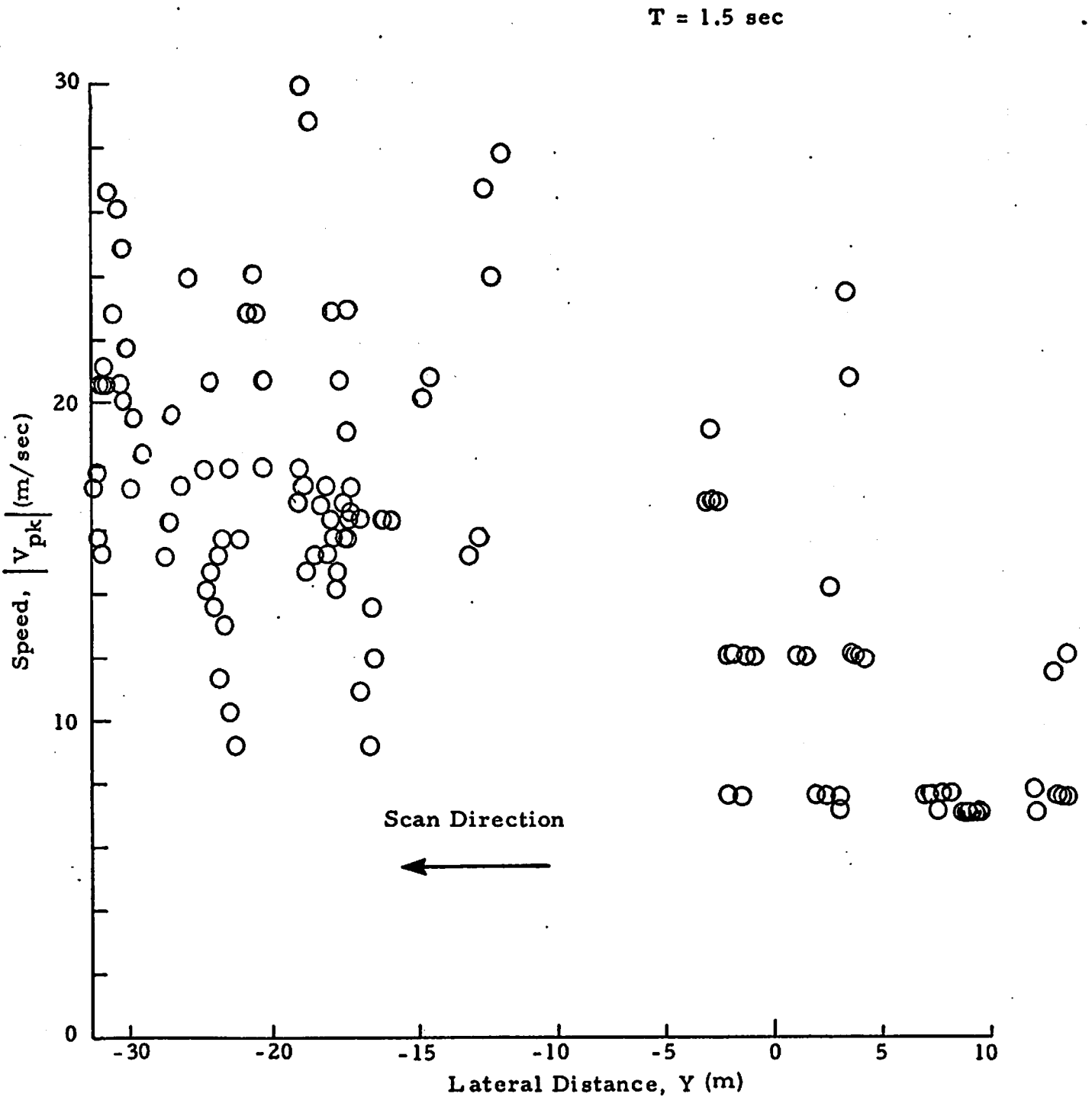

Fig.14 - $|V_{pk}|$ as a Function of Lateral Distance for Rosamond B-747 Flyby 11

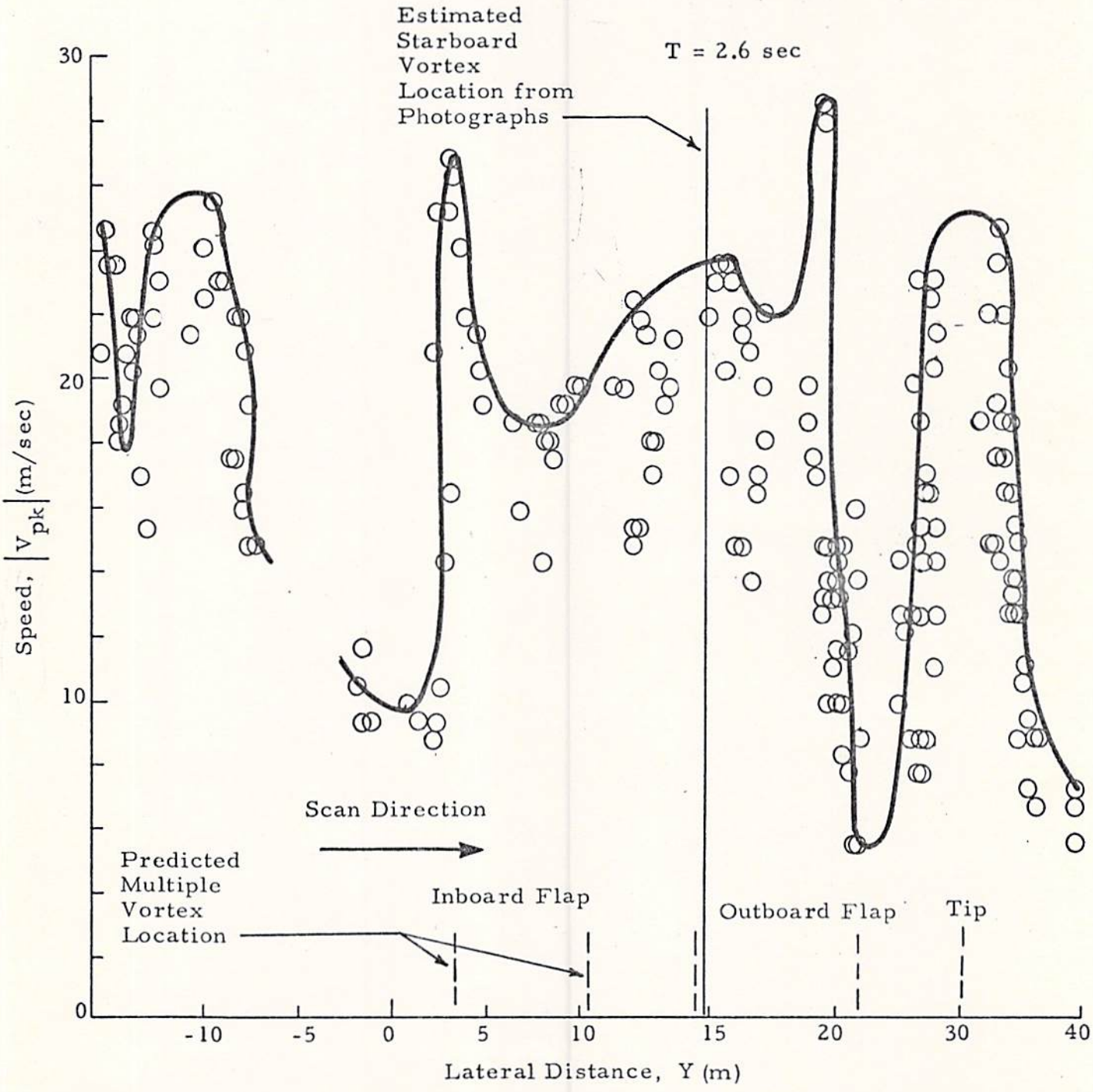

Fig. 14 (Continued)

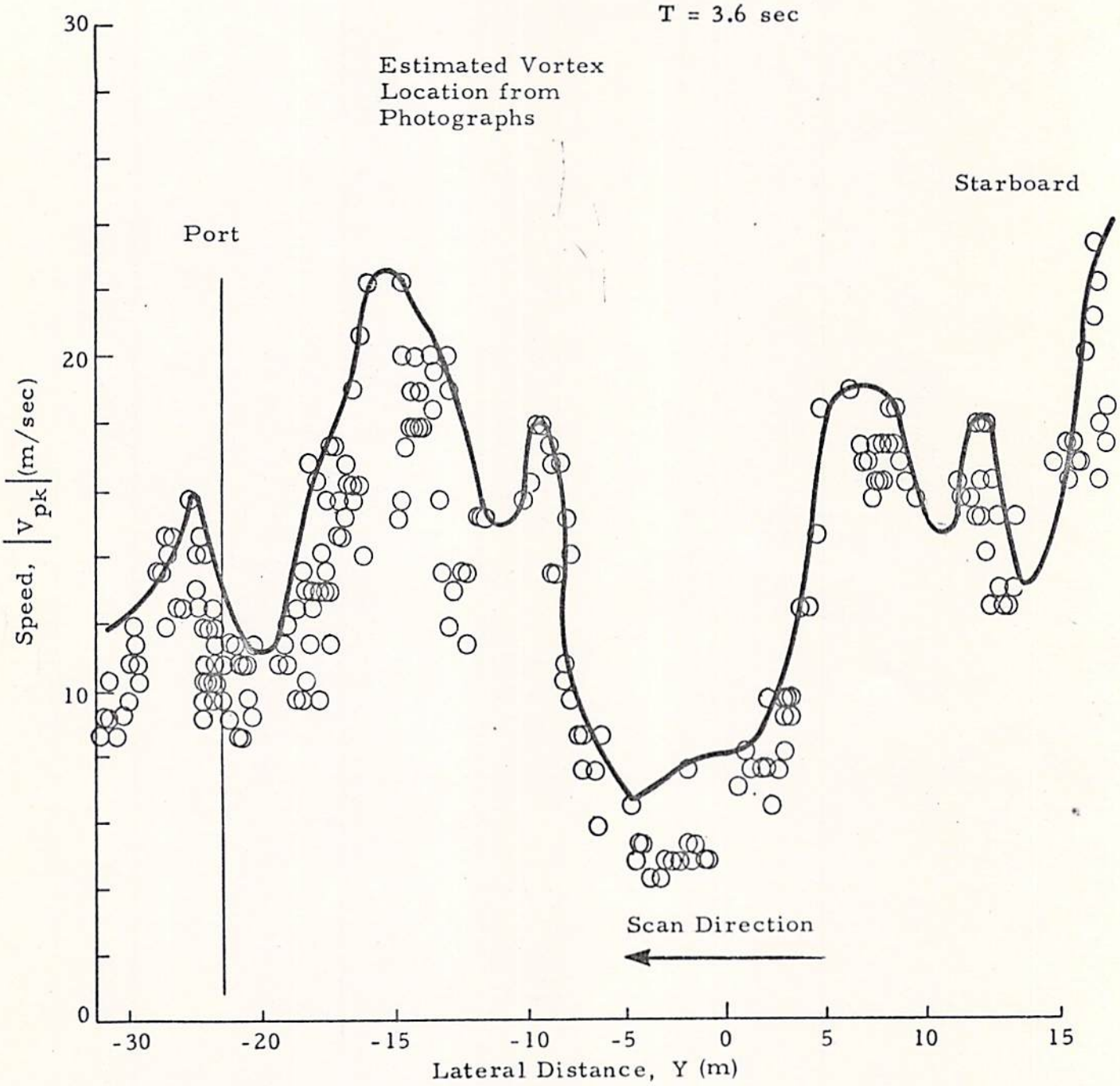

Fig. 14 (Continued)

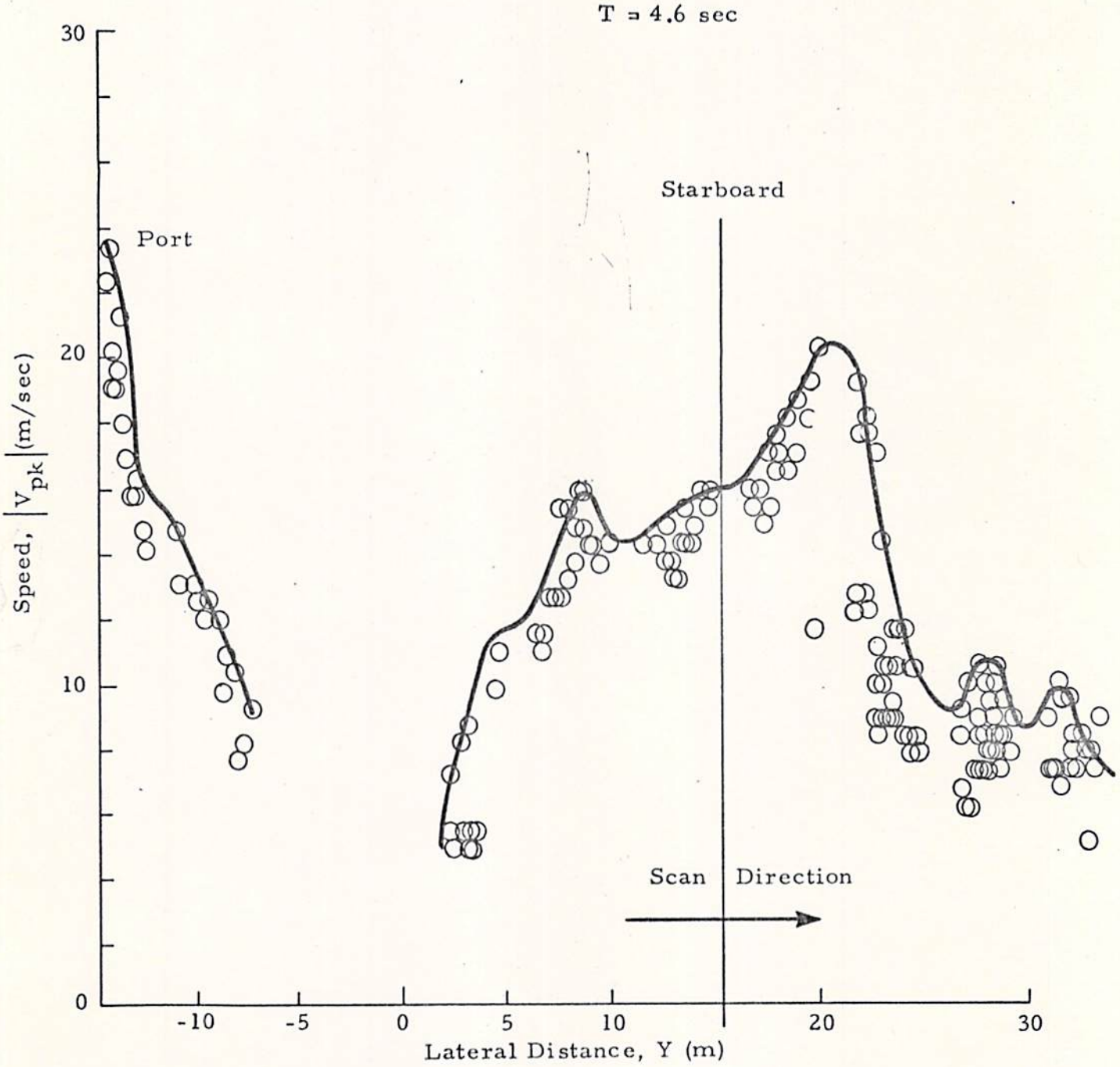

Fig. 14 (Continued)

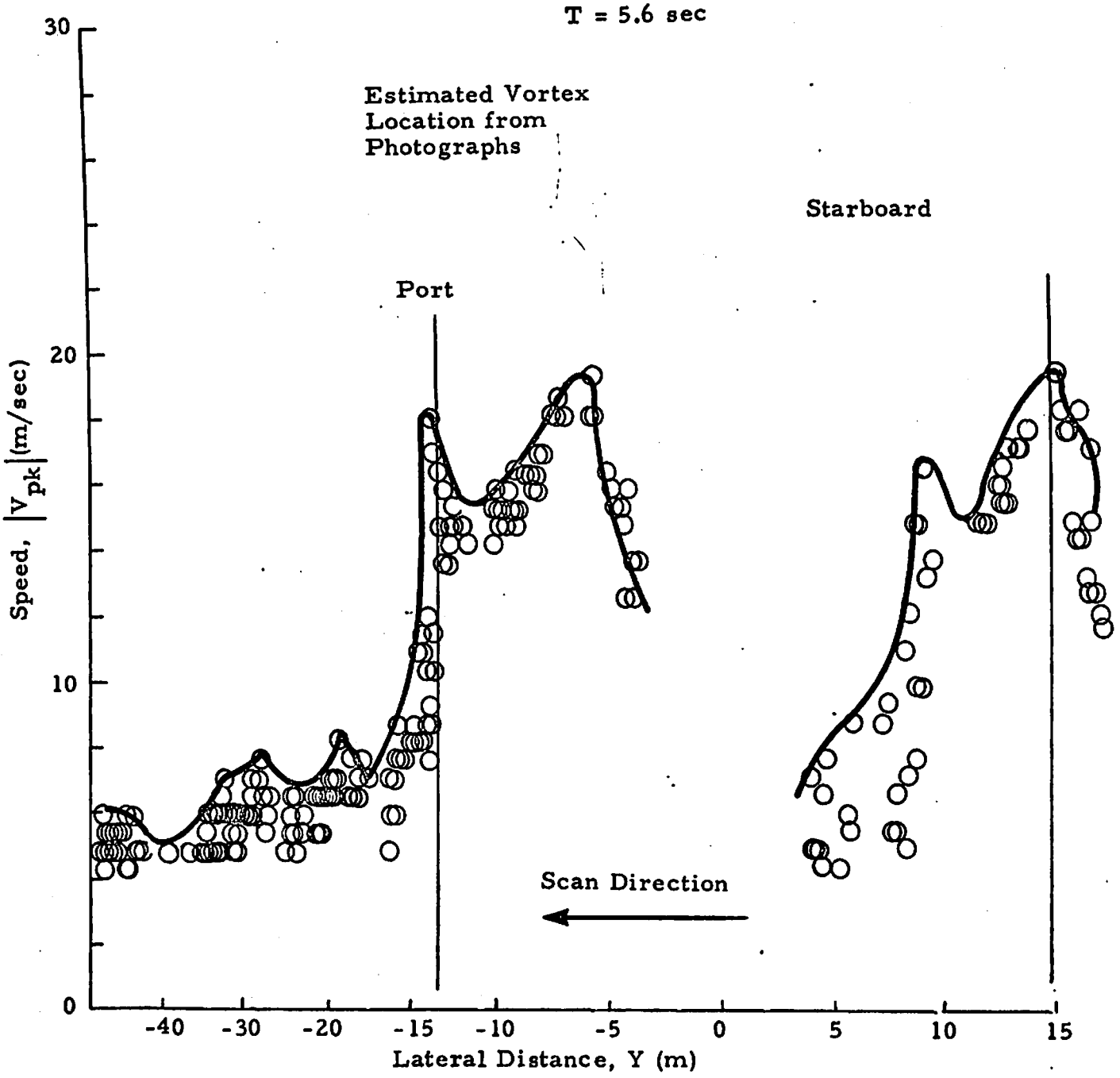

Fig. 14 (Continued)

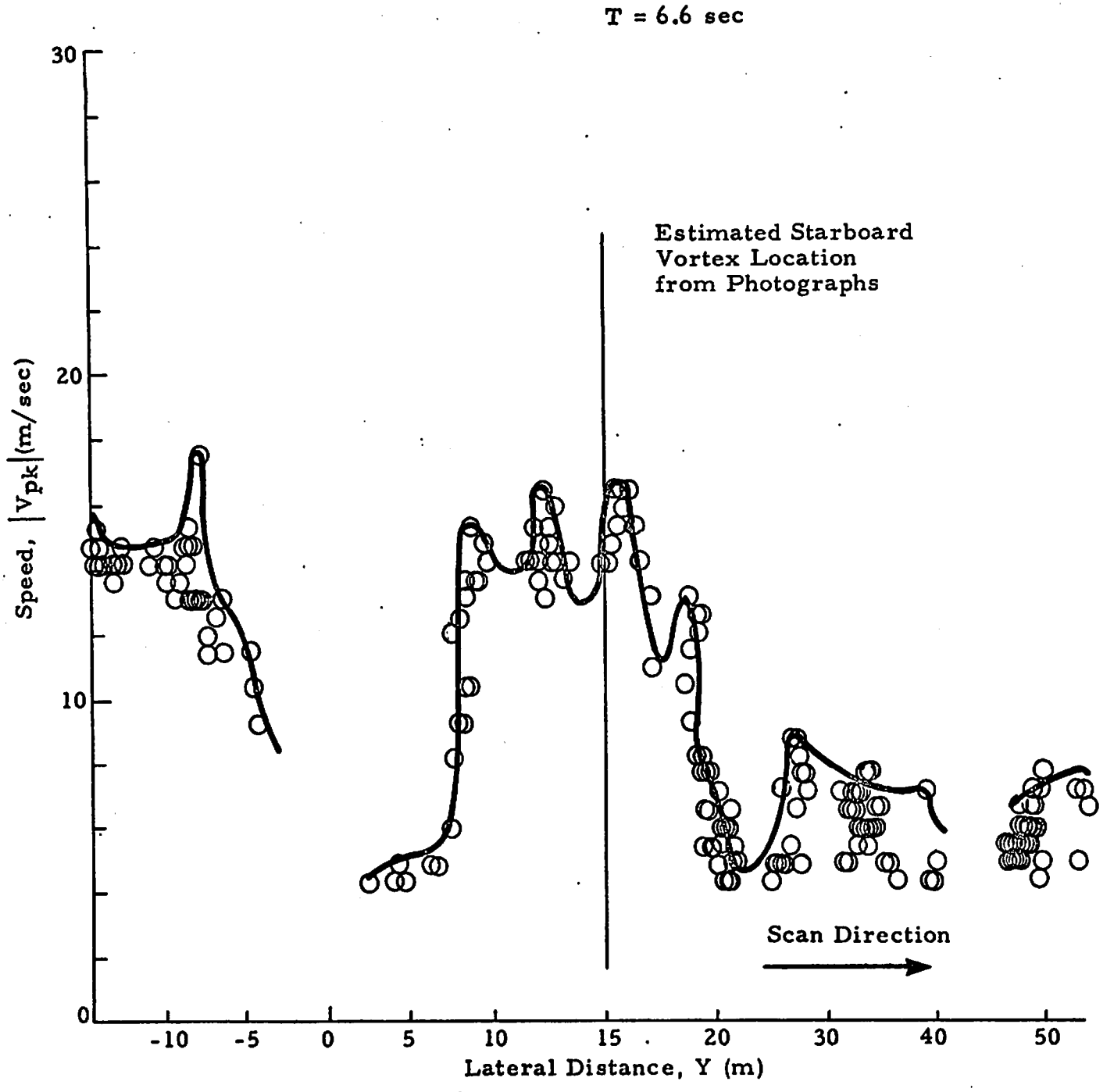

Fig. 14 (Continued)

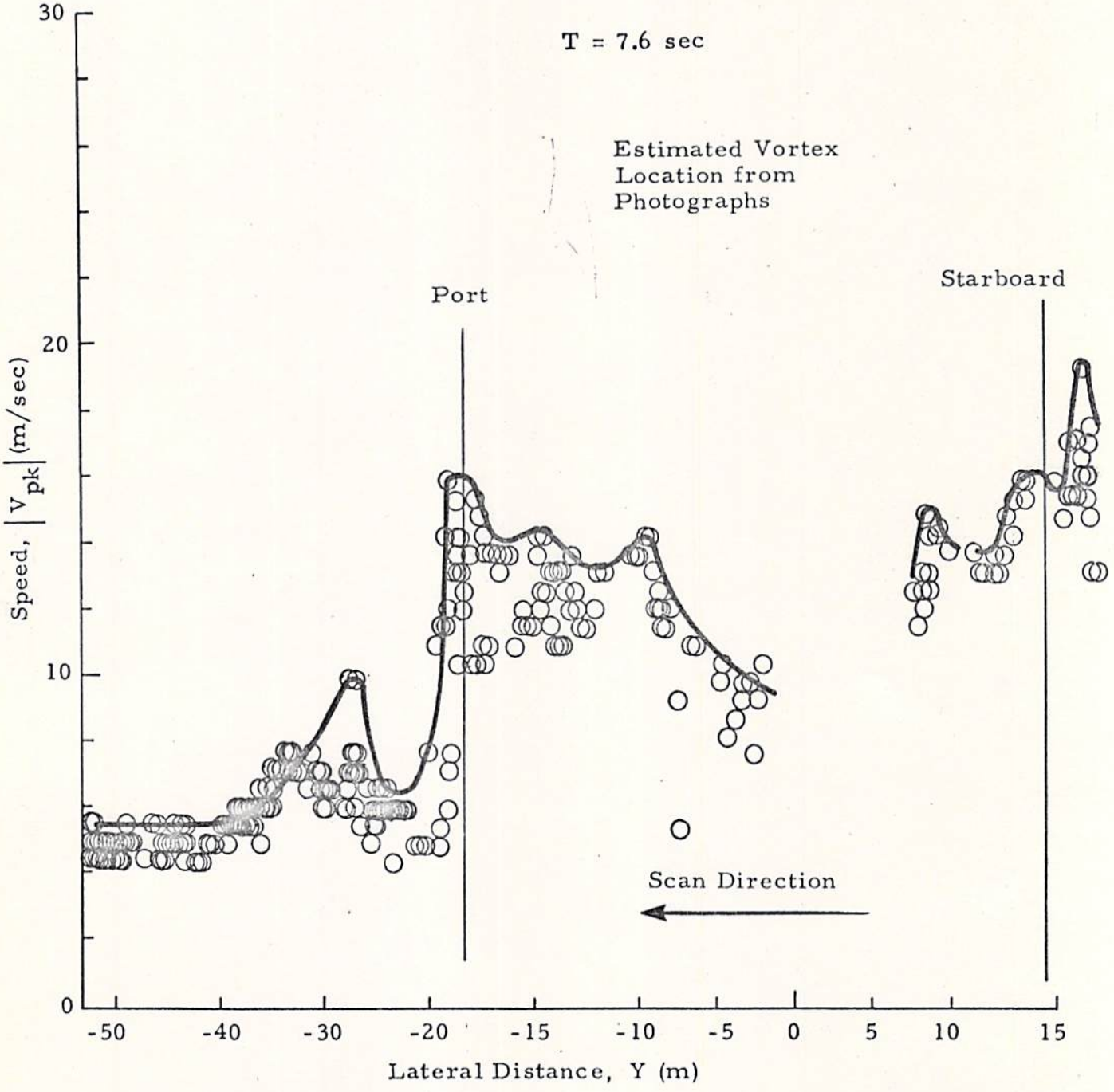

Fig. 14 (Continued)

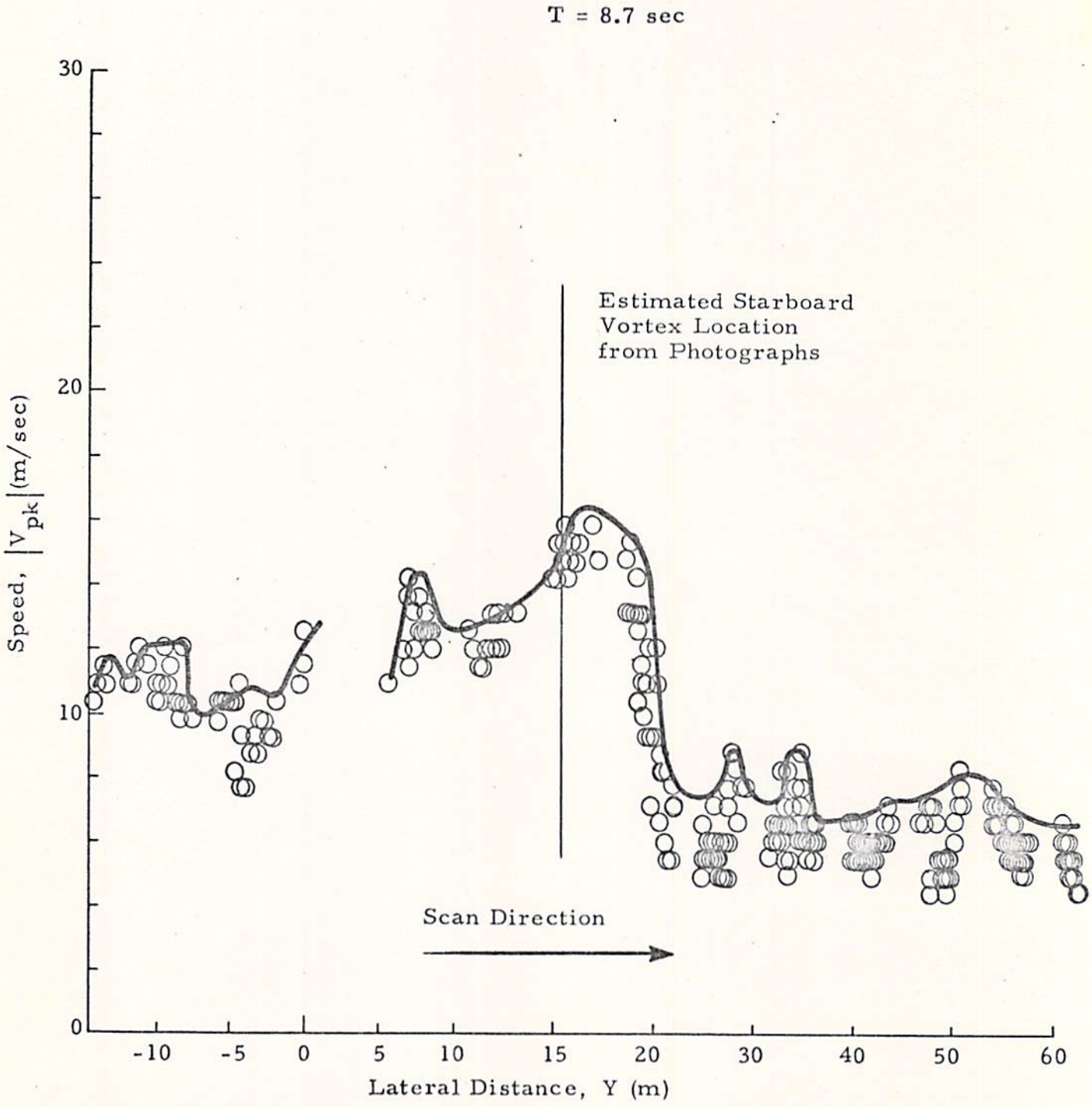

Fig. 14 (Continued)

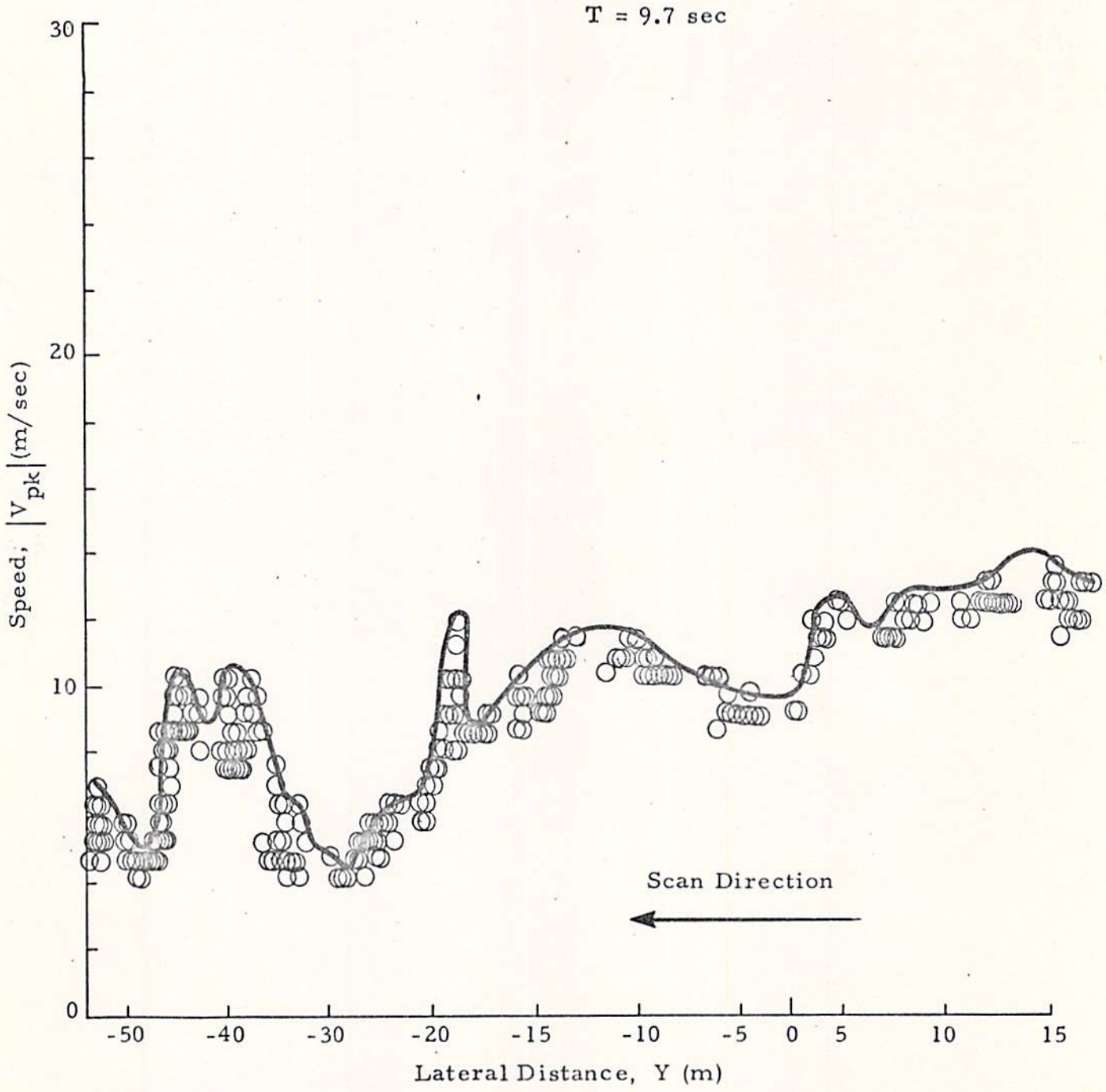

Fig. 14 (Concluded)

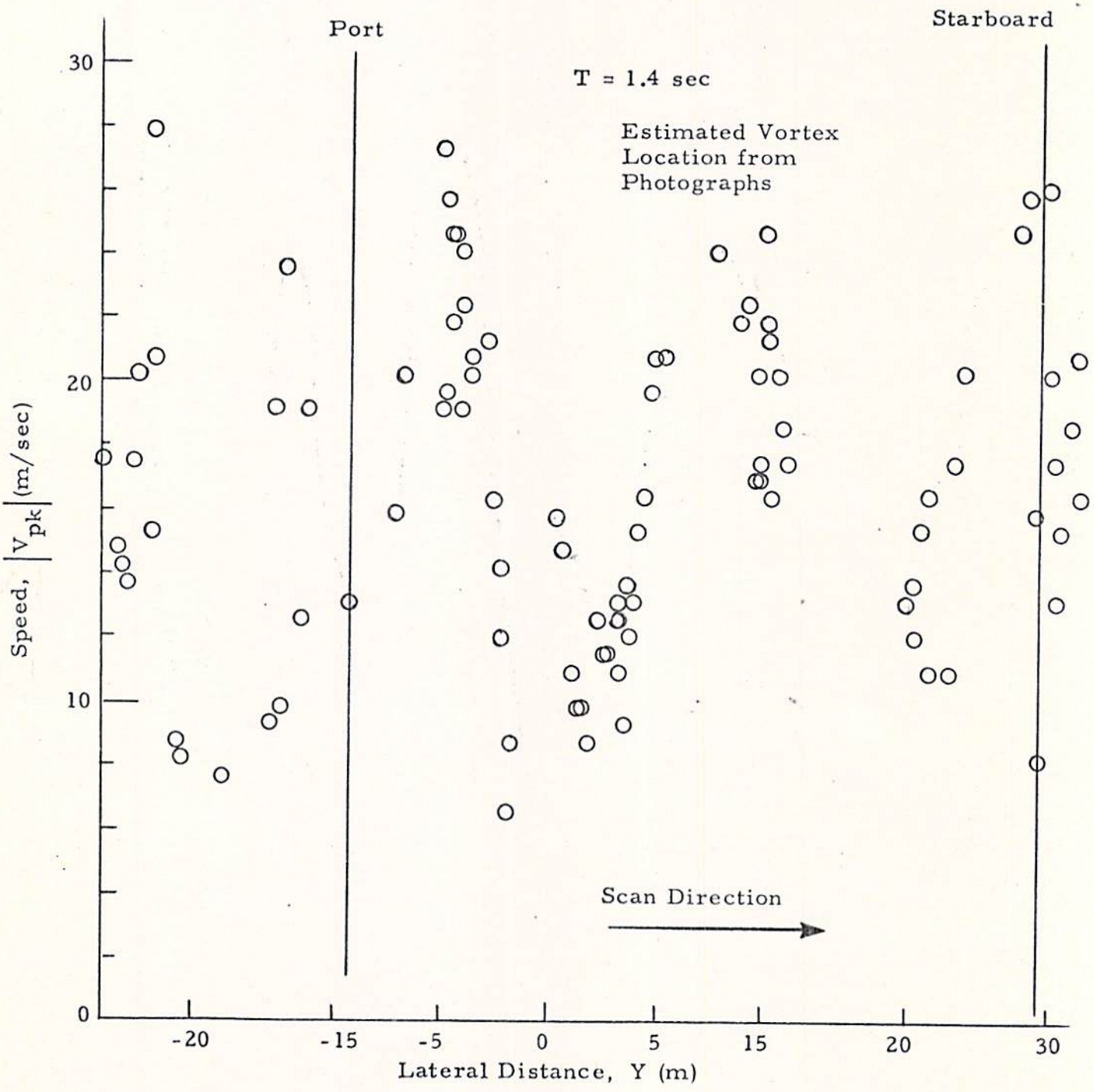

Fig. 15 - $|V_{pk}|$ as a Function of Lateral Distance for Rosamond B-747 Flyby 12

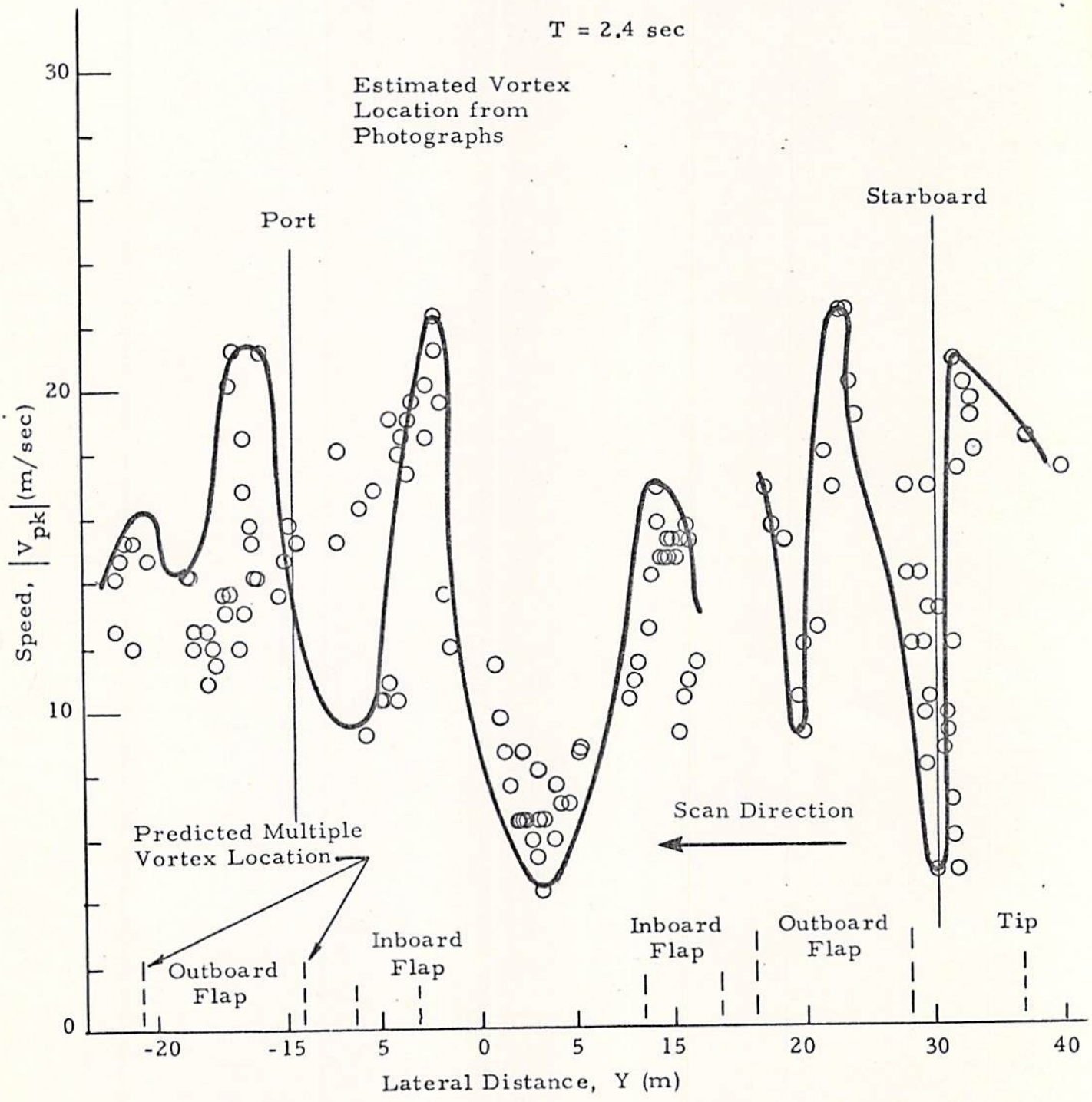

Fig. 15 (Continued)

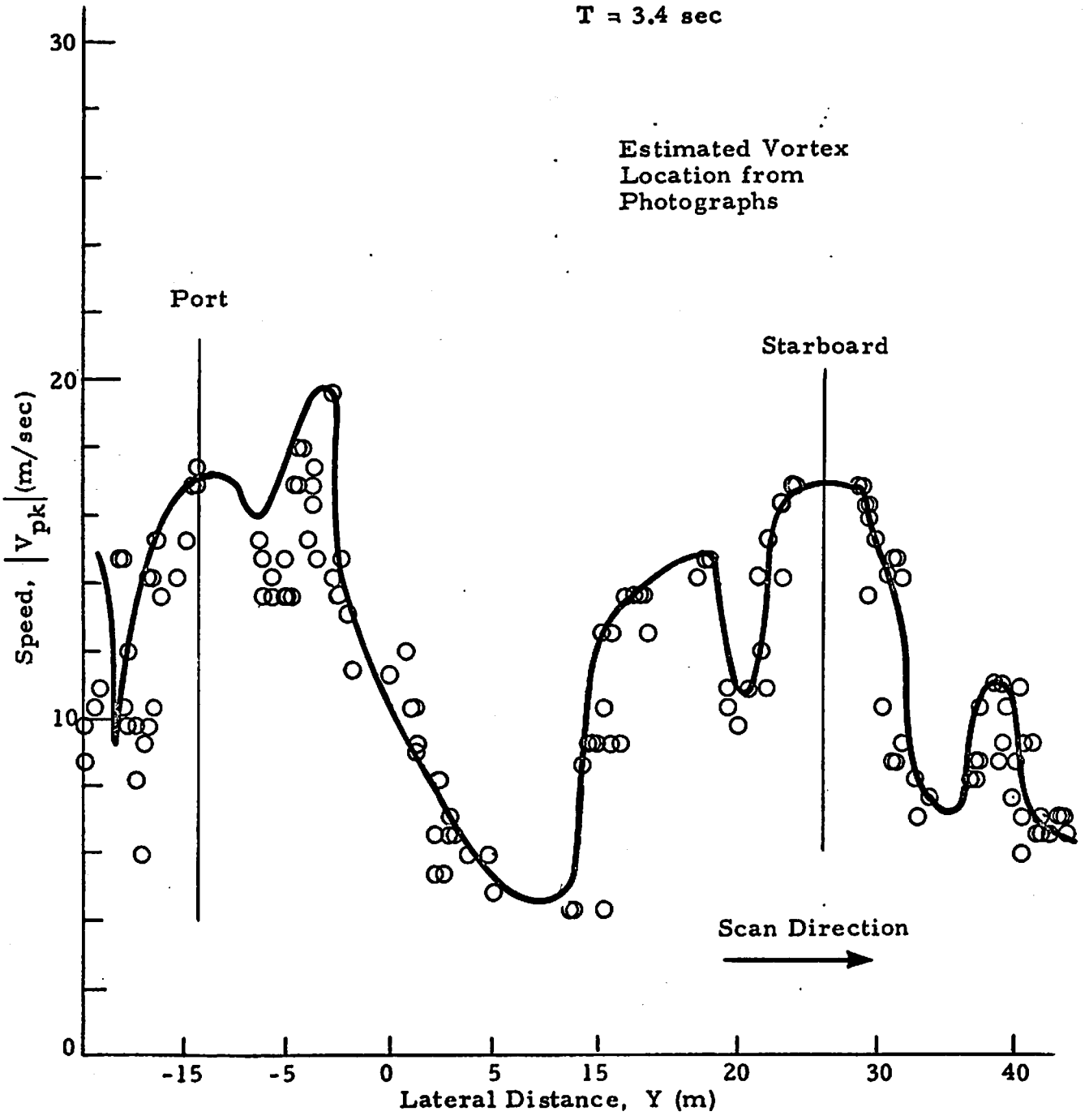

Fig. 15 (Continued)

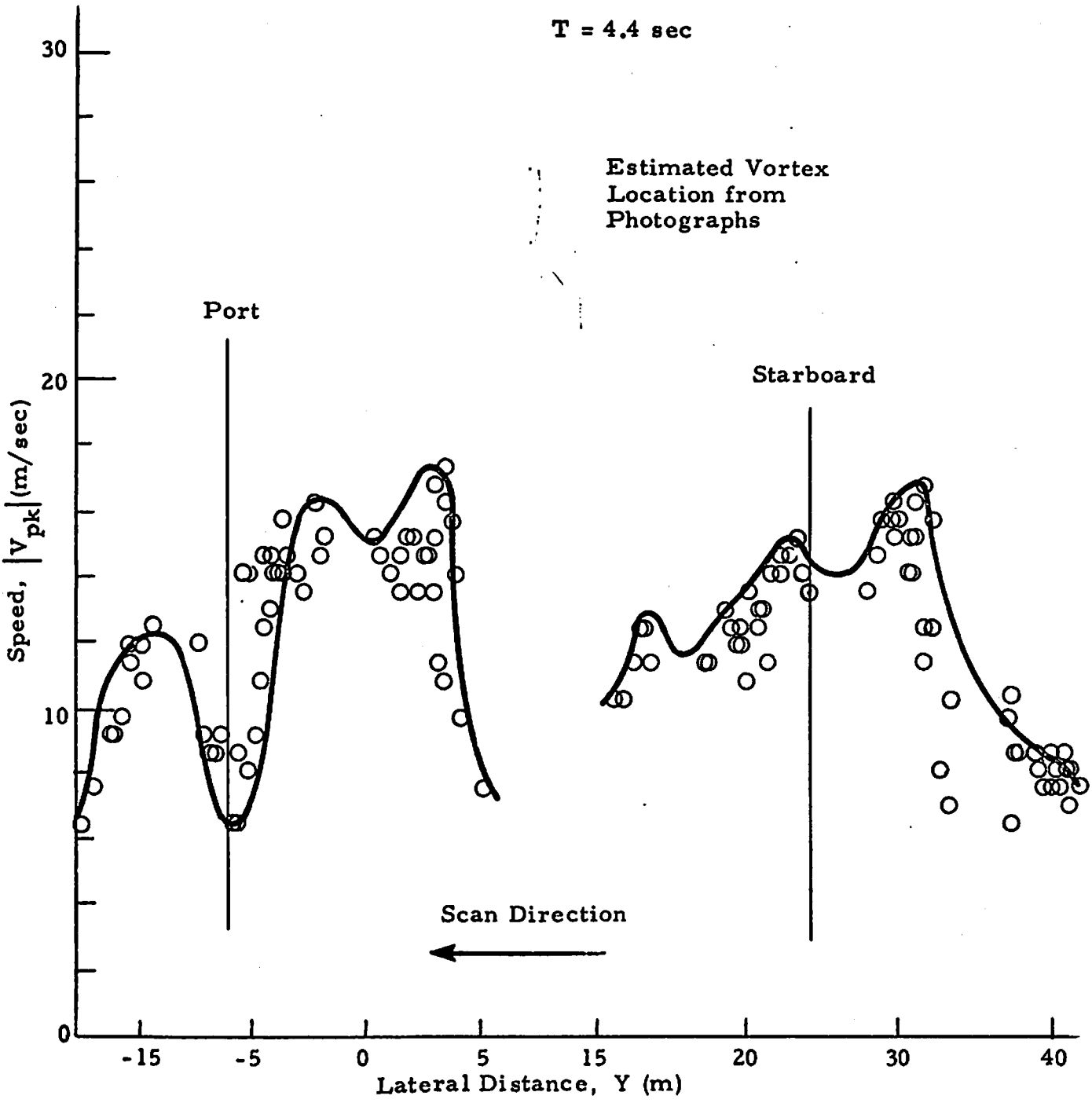

Fig. 15 (Continued)

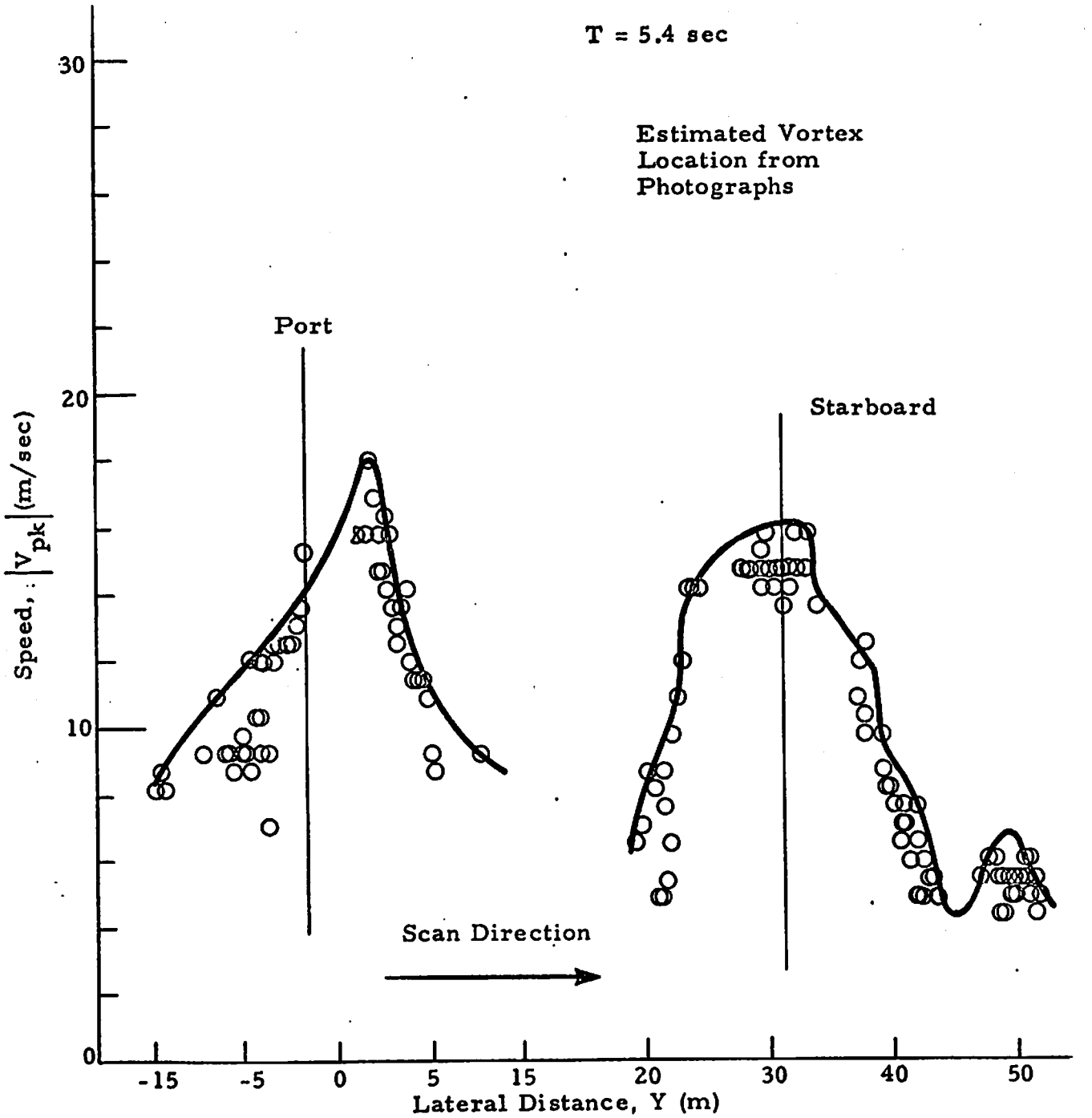

Fig. 15 (Continued)

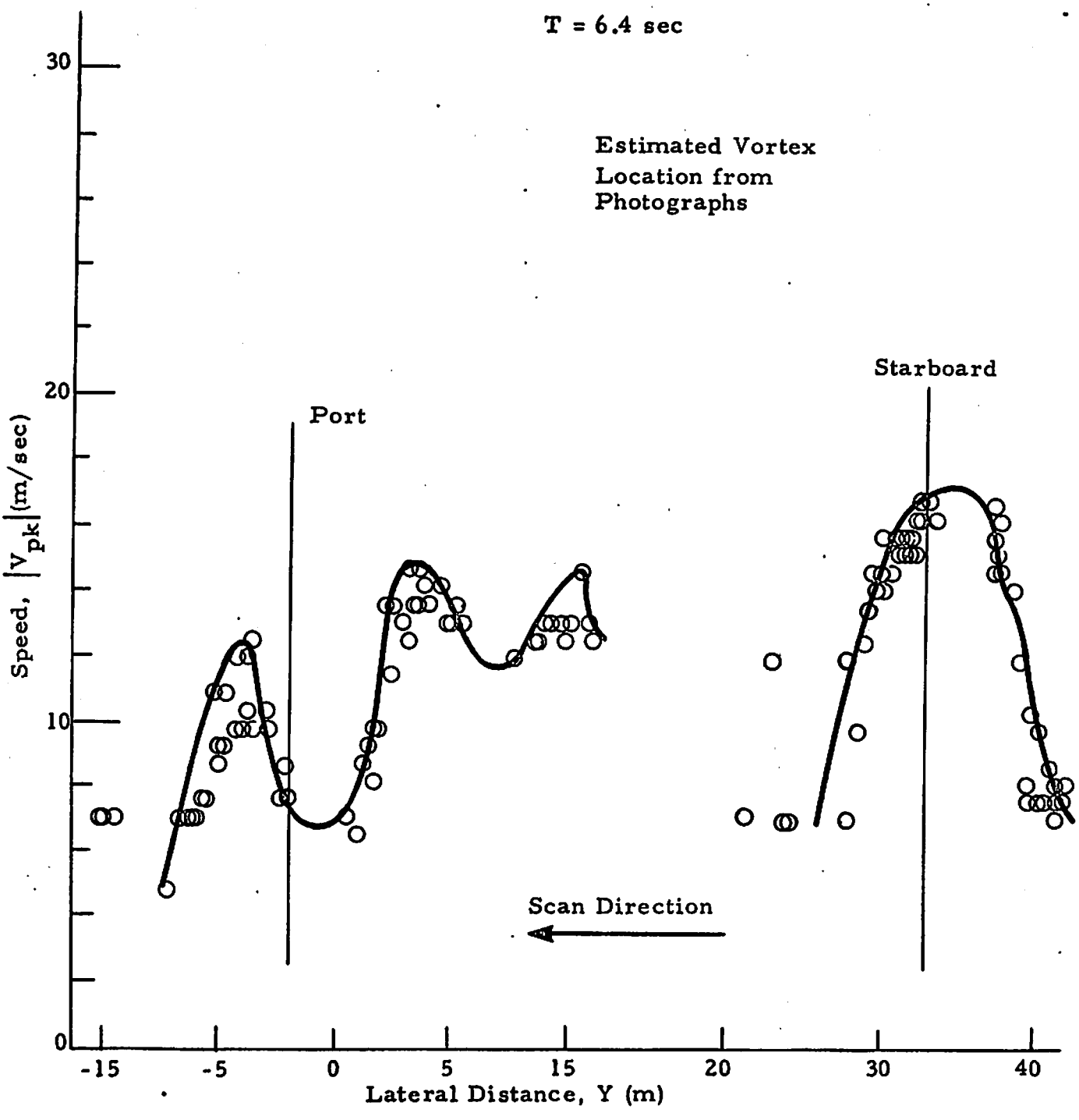

Fig. 15 (Continued)

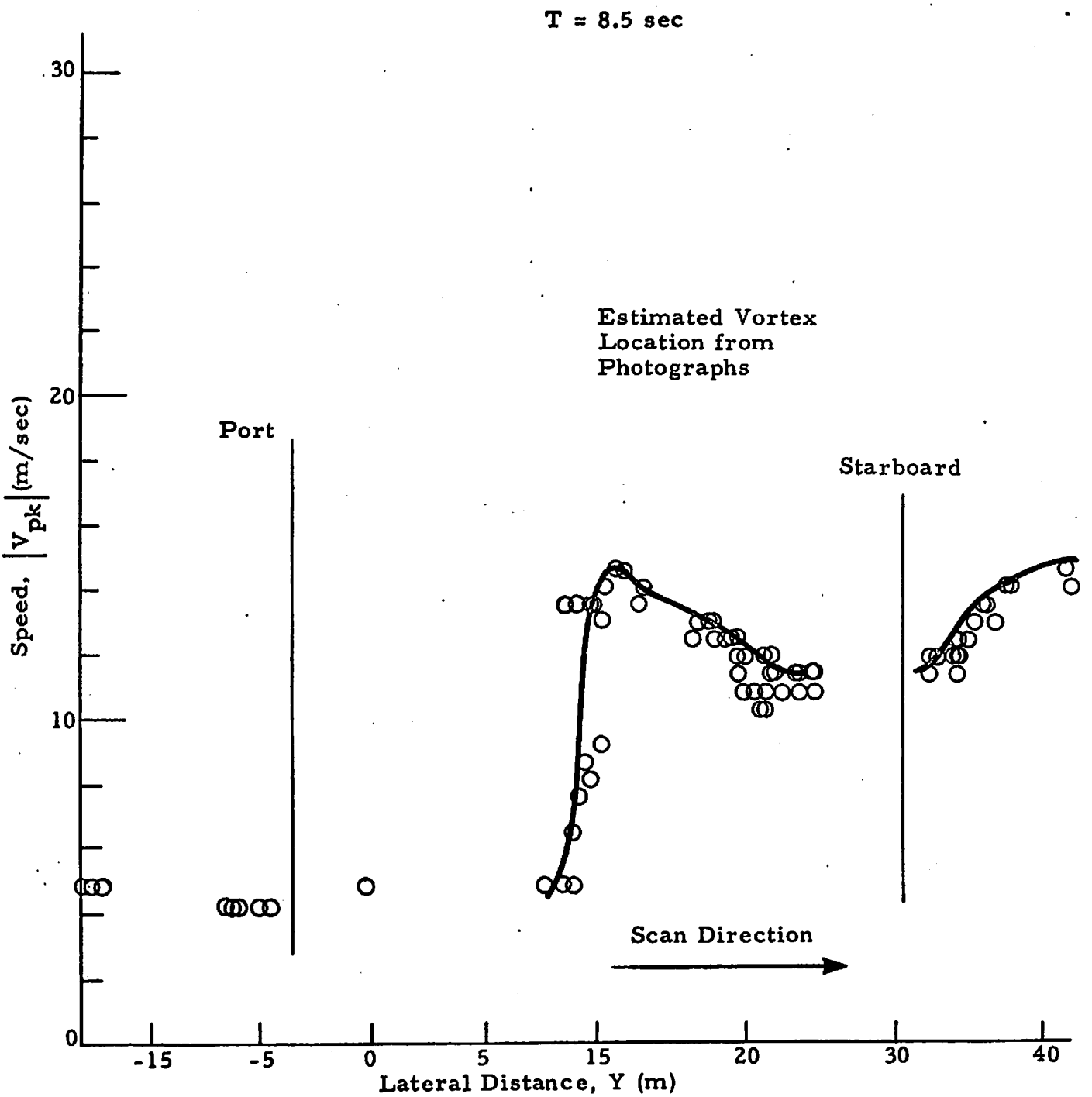

Fig. 15 (Concluded)

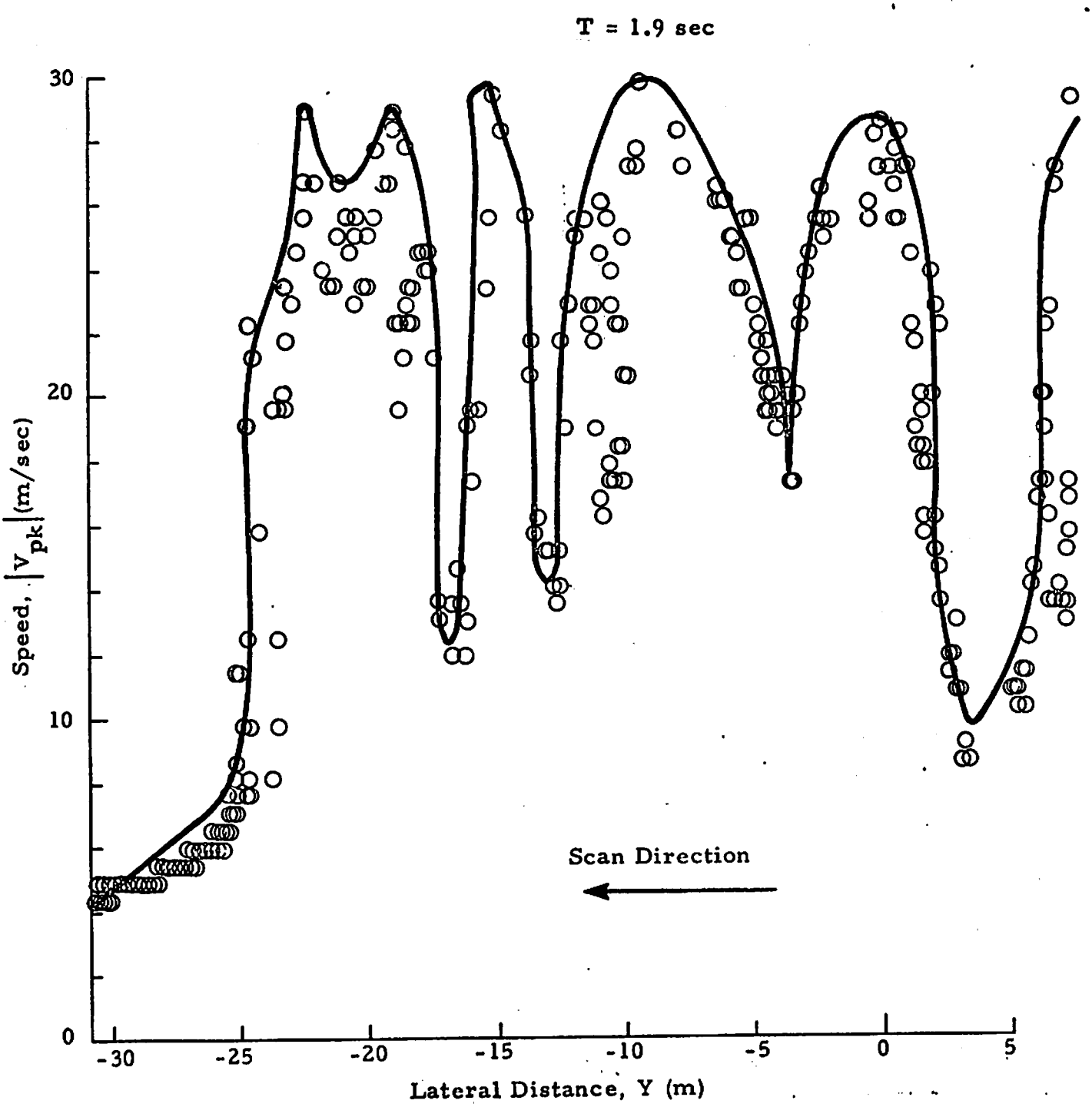

Fig. 16 - $|V_{pk}|$ as a Function of Lateral Distance for Rosamond B-747 Flyby 13

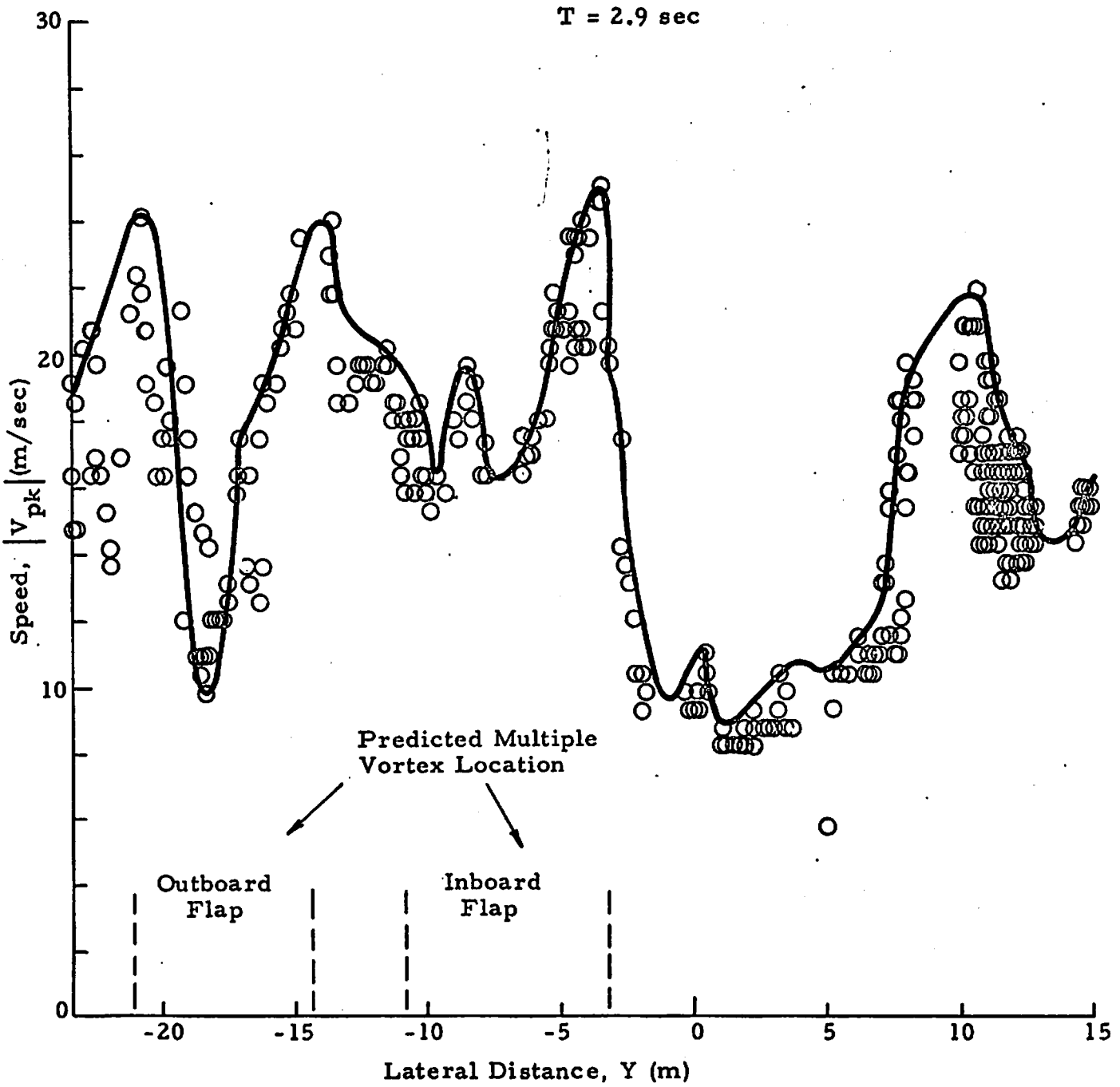

Fig. 16 (Continued)

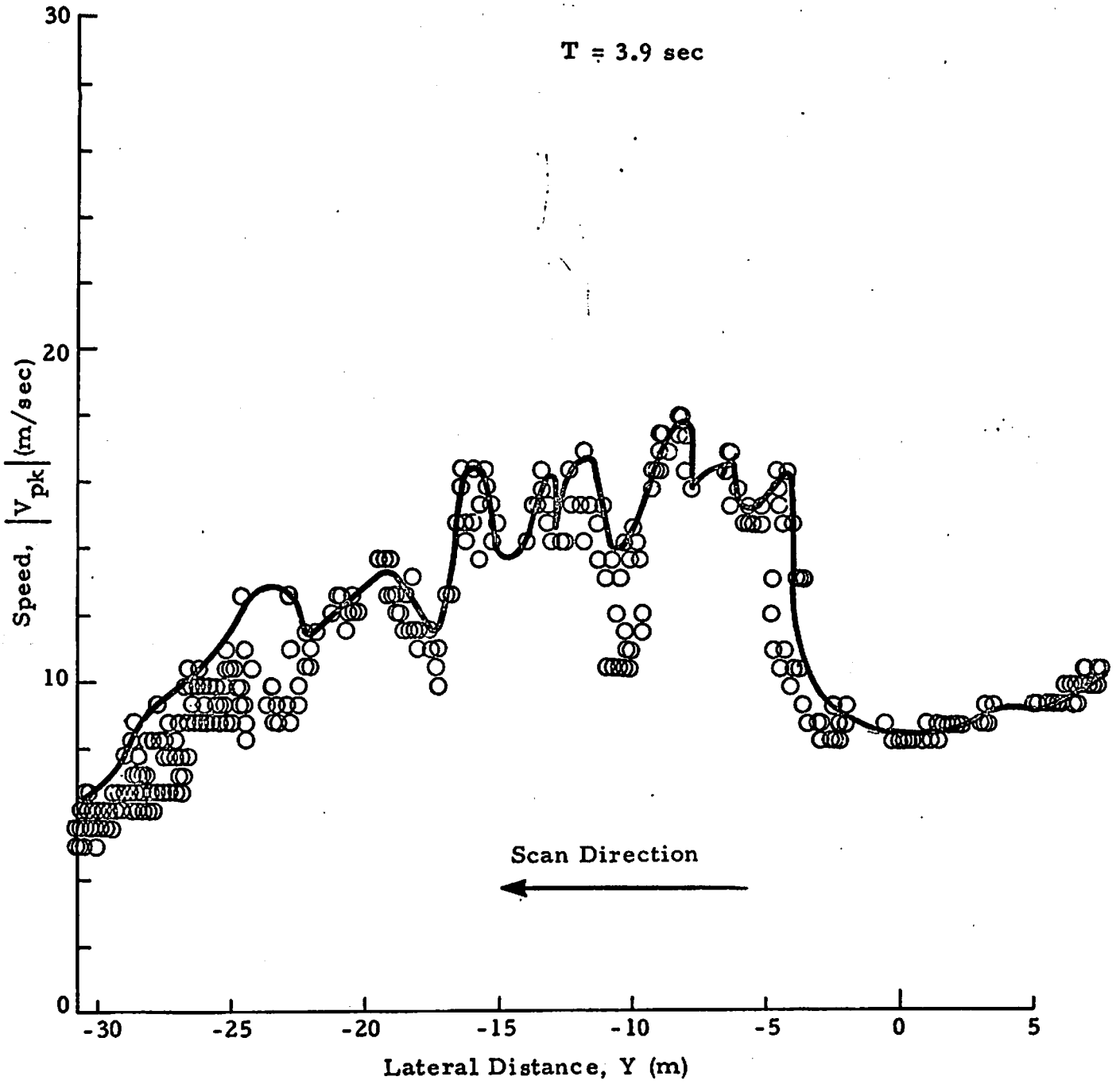

Fig. 16 (Continued)

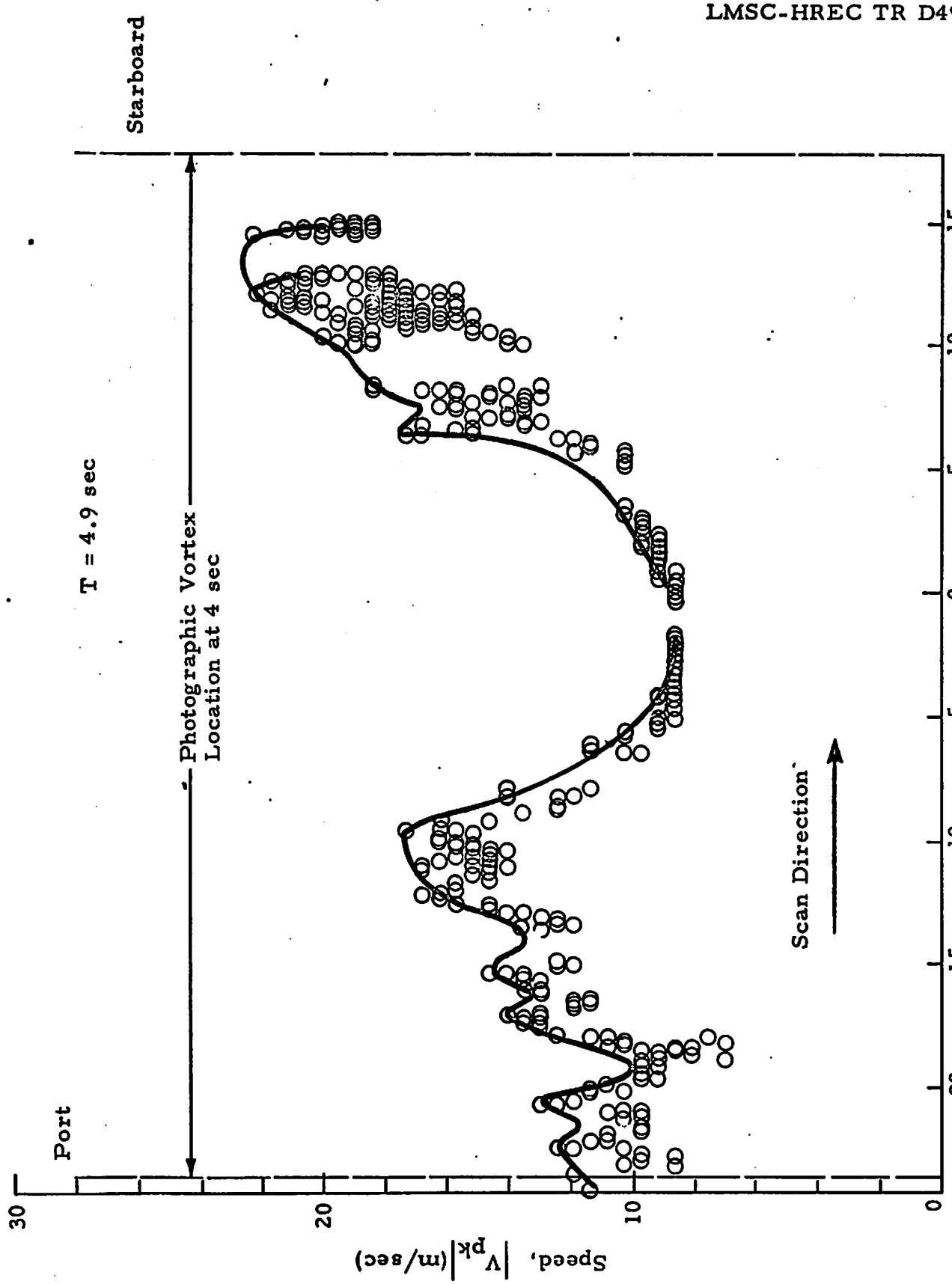

Fig. 16 (Continued)

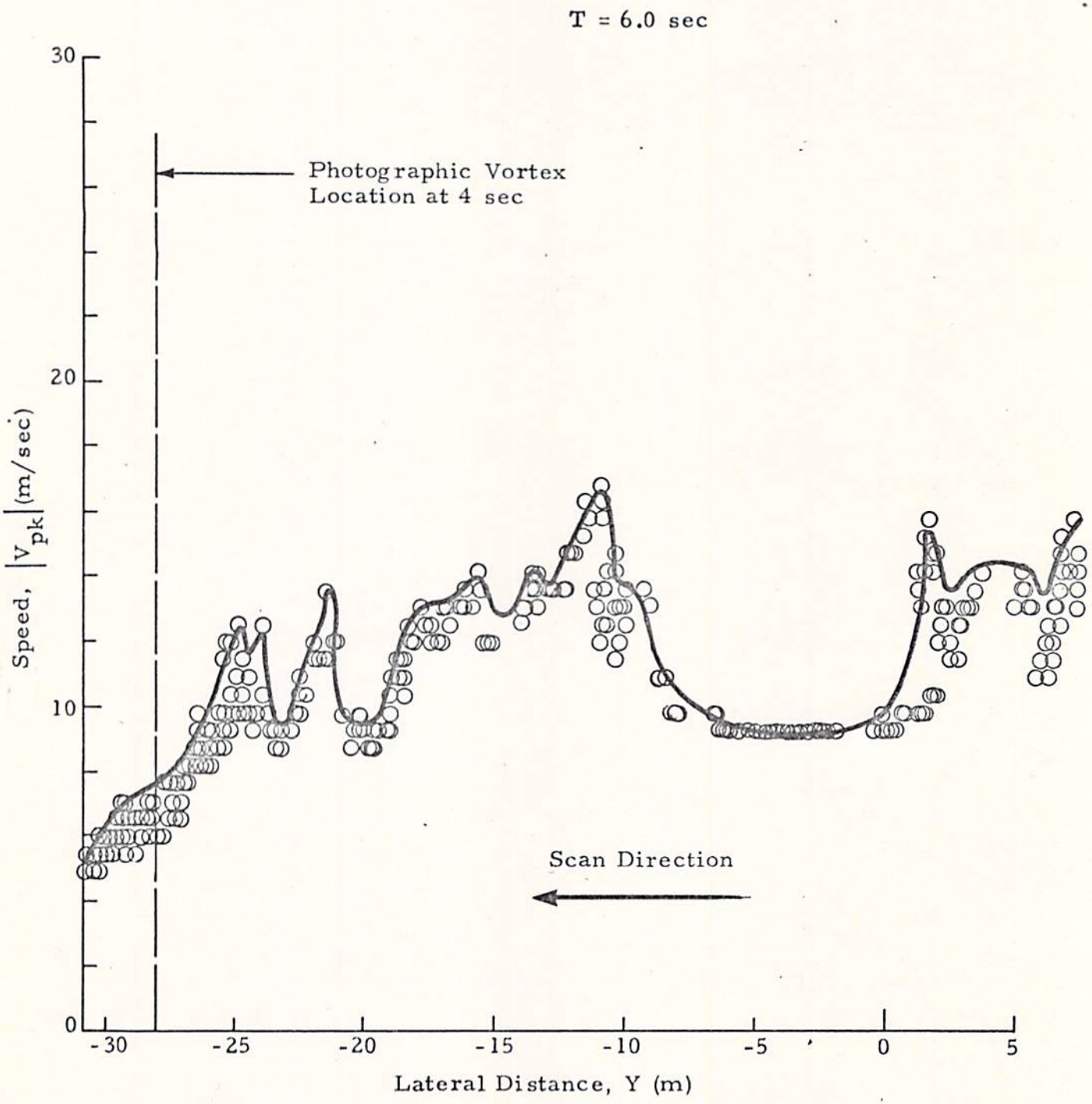

Fig. 16 (Continued)

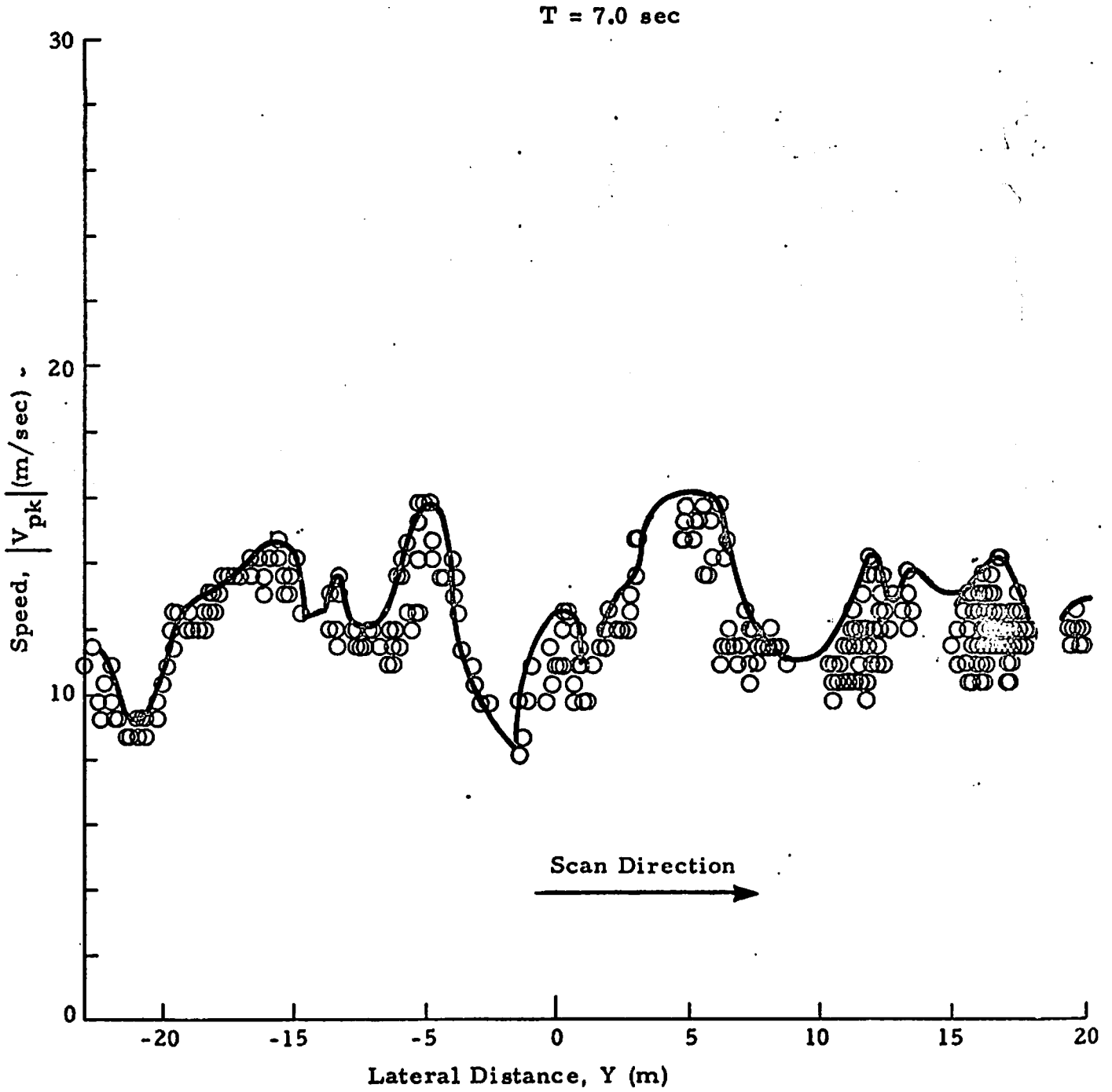

Fig. 16 (Continued)

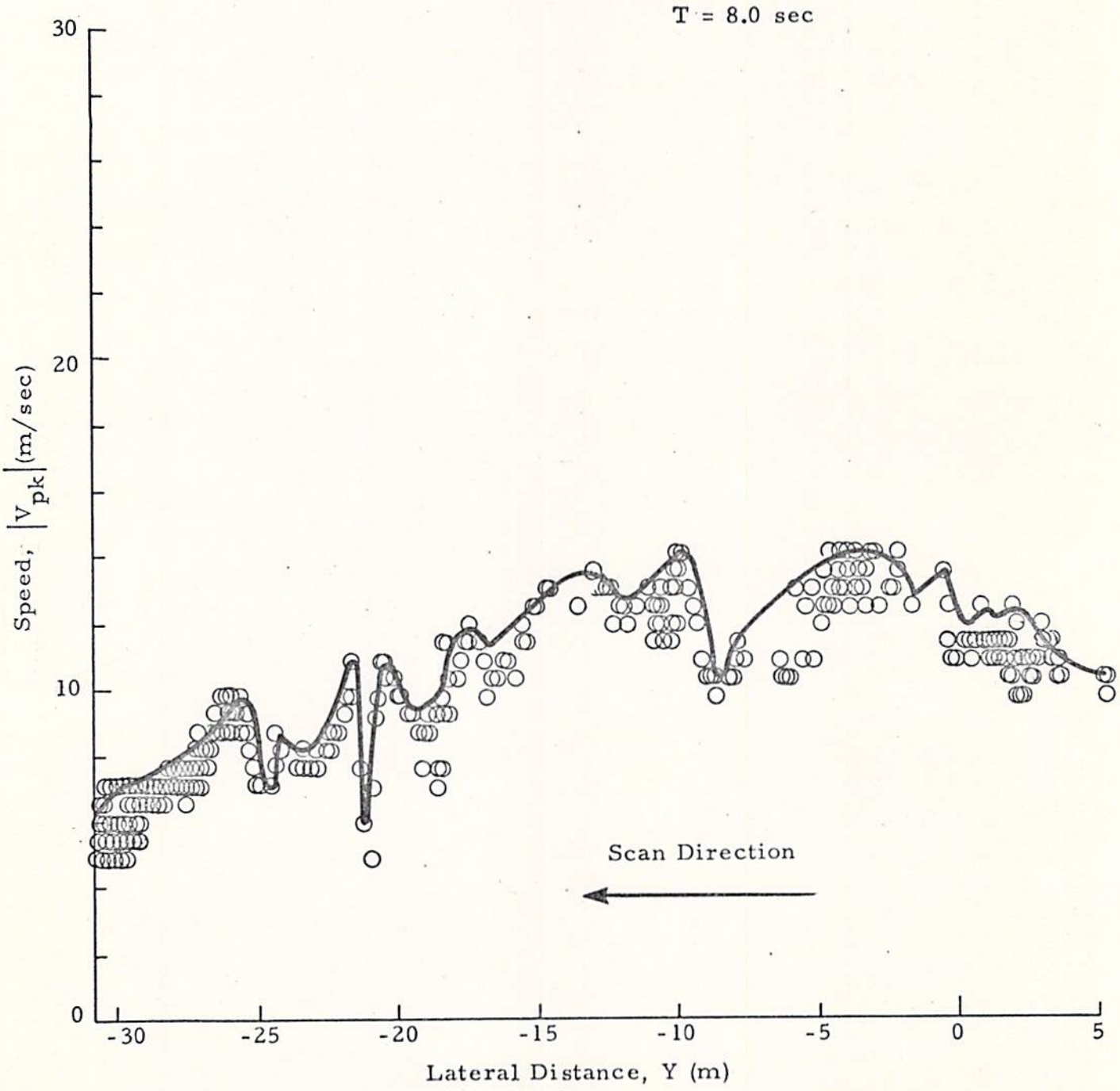

Fig. 16 (Concluded)

measurements, θ, where $y = -R \cos\theta$. This resulted in a nonlinear lateral scale at extended distances from the flight path centerline.

To illustrate the maximum downwash or upwash velocities in the aircraft nearwake, the highest values of V_{pk} occurring over one degree increments were faired by a smooth curve. The solid lines in the plots represent a faired curve through the highest LDV measurements given by the circles. Since the arc scan measurements were made at an initial range equal or to somewhat less than the airplane height, and since the maximum descent rate of the trailing vortices was on the order of 2 m/sec, the wake vortex remained essentially in the focal volume of the LDV system over the time period of 0 to 8 sec. Thus, the solid lines shown in Figs 13 through 16 are indicative of the peak velocities observed with the LDV system in the aircraft near wake.

Available measurements of vortex lateral position obtained from a triangulation of simultaneous photographs or estimated from overhead photographs are also shown in Figs. 13, 14 and 15.

The spanwise downwash distribution for flyby 8, the 0-spoiler configuration, shows a well defined double-peak signature in most of the plots shown in Fig. 13 which is suggestive of a coherent vortex. For example, the Fig. 13 at t = 2.2 sec two high-velocity peaks are observed separated by a spacing of 0.76 wingspans. The lack of signature in the inboard regions may be attributed to the lack of high velocities or aerosols near the flight path centerline. The two high-velocity peaks become more well defined at later times (t = 3.3 to 8.2 sec) showing a double-peak signature characteristic of the rotational velocity profile of a viscous vortex. The lateral separation and the maximum velocity for the two double-peak signatures does not change significantly over this time range.

In contrast to the coherent wake structure observed earlier for the 0-spoiler configuration (Fig. 13), the downwash field for flybys 11, 12 and 13 where the two outer spoilers were deployed shows a broad high velocity region composed of narrower closely spaced peaks. This is suggestive of multiple

vortices and an incomplete vortex rollup phase. These measurements indicate that the deployment of spoilers has a marked effect on the near wake strucuture tending to retard the early formation of a coherent trailing vortex pair. Analysis of the downwash field shown in Figs. 13 through 16 has been carried out to determine the basic characteristics of single and multiple vortices such as location, circulation strength, and the radial velocity distribution.

4.1.2 Vortex Pair Characteristics

For the 0-spoiler configuration, the spanwise downwash distribution in the wake shows a well defined double-peak signature (Fig. 13). A double-peak signature is predicted theoretically when a vortex pair is interrogated in the arc-scan mode. For example, the theoretical line-of-sight velocity distribution for Rosamond flyby 11 at $t \sim 2$ sec assuming a fully rolled-up vortex pair is shown in Fig. 17. The magnitude of the line-of-sight velocity generated by a distribution of N line vortices with LDV located at the origin is given by

$$\left|V_{\ell os}\right| = \frac{1}{2\pi} \sum_{n=1}^{N} \Gamma_n \frac{\left[(Y_n - Y_o) X_o + (X_o - X_n) Y_o\right]}{\left[(X_o - X_n)^2 + (Y_o - Y_n)^2\right] \left[X_n^2 + Y_n^2\right]^{1/2}}$$

where (X_o, Y_o) is the location of the centroid of the focal volume and (X_n, Y_n) and Γ_n are the coordinate and circulation strength of the n^{th} vortex.

In Fig. 17, the computed line-of-sight velocity distribution is shown for a pair of line vortices with spacing $b' = Kb = 41.8$ m and circulation strength $\Gamma = U_\infty \bar{c}\, C_L/2K = 606\ m^2/sec$ where the spanwise loading coefficient, wingspan, flight velocity, mean chord, and lift coefficient are taken to be $K = 0.7$, $b = 59.7$ m, $U_\infty = 72.5$ m/sec, $\bar{c} = 8.3$ m, $C_L = 1.41$. The vortex pair was assumed to be located at an altitude of 180 m and the selected arc scan range was 183 m. The computed line-of-sight velocity distribution for the vortex pair shows the characteristic double peak signatures noted earlier in the LDV measurements. The magnitude of the peak velocity is determined by the

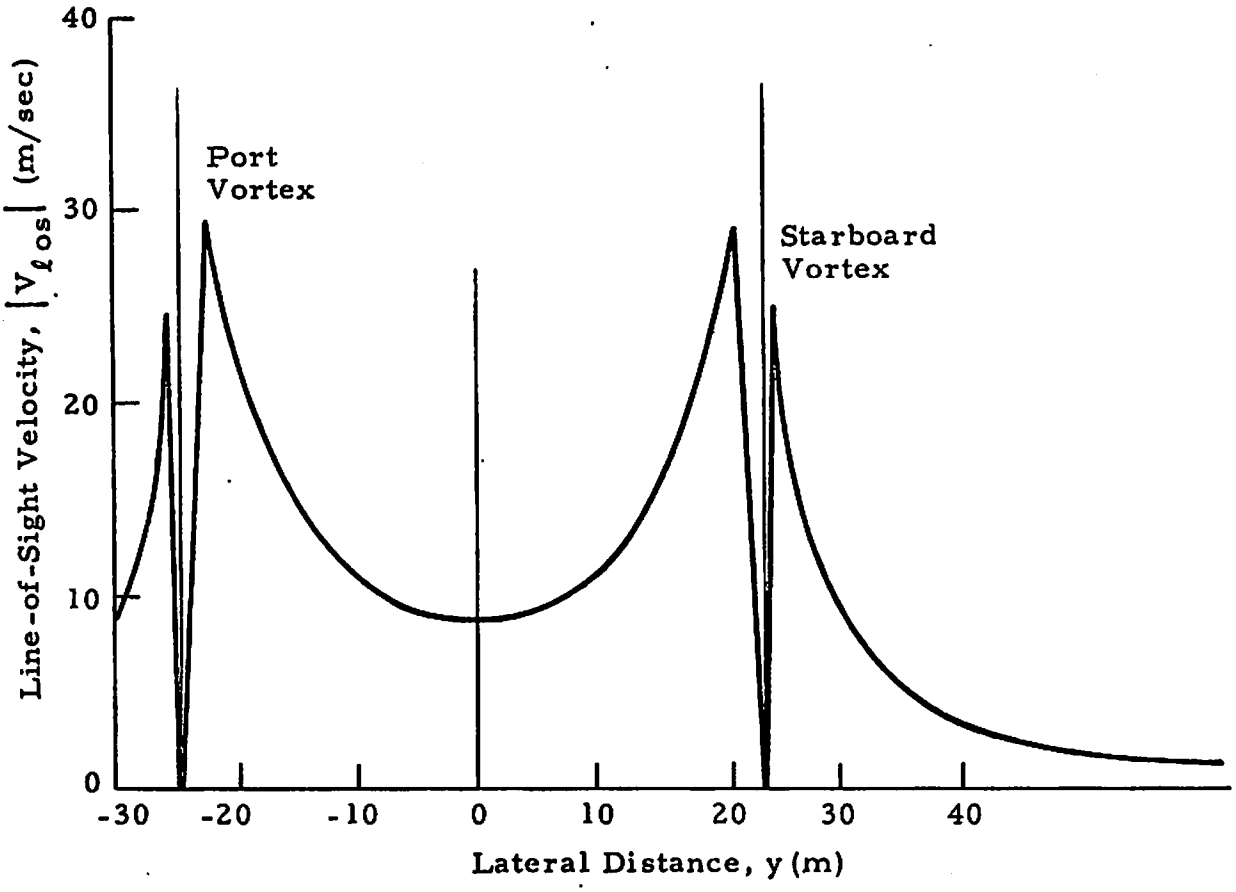

Fig. 17 - Theoretical Line-of-Sight Velocity for Rosamond B-747 Flyby 11 at t ~ 2 sec, Assuming a Fully Rolled-Up Vortex Pair

separation distance between the vortex pair and the scan arc. The slight asymmetry in the double peaks results from the velocity contribution of the adjoining vortex, the scan geometry and the decrease in the contribution of the vortex rotational velocity along the line of sight at extended lateral distances from the centerline.

Note the two double-peak patterns in the V_{los} distribution in Fig. 17 at $y = \pm 23$ m which correspond to the approximate location of the two vortices. As the vortex pair is traversed by the arc-scan pattern the peak tangential velocity, resolved about the line of sight, is observed giving rise to the closely spaced double peaks. When the vortex center is intersected exactly by the arc scan, the location of the peaks is a measure of the vortex position, the magnitude of the peaks is indicative of the peak tangential velocity in the core, and the lateral separation between the peaks is a measure of the vortex core diameter. If the vortex is below (or above) the arc scan, as shown in the sample simulation in Fig. 17, the vortex position is bounded by the lateral location of the two peaks, the magnitude of the two peaks is less than the peak tangential velocity, and the lateral separation between the two peaks is a function of the separation distance between the vortex and the scan arc.

The predicted line-of-sight velocity distribution shown in Fig. 17 agrees with the trends shown by the 0-spoiler flyby (Fig. 13) while the 1, 2, 11 and 12 spoiler flybys (Figs. 14 to 16) are noticeably different. Since the LDV signature for flyby 8 is suggestive of a coherent vortex pair, it is useful to make a more detailed analysis of this case. From the seven scans shown in Fig. 13 the earliest scan showing the two double peak signatures was selected ($t = 3.3$ sec); the minimum points were used to determine the lateral position of the port vortex (vortex altitude was assumed to be the scan range $R = 240$ m), and the peak velocity points observed by the LDV for the port vortex were plotted as a function of radius about the vortex center in Fig. 18. For comparison, the theoretical velocity profiles for a potential line vortex and a turbulent viscous vortex are also shown in Fig. 18 matched to the experimentally measured core circulation and core velocity.

LDV Measurements of Port Vortex, Flyby 8

Time = 3.3 sec

Core Radius = 4.5 m

Circulation = 565 m^2/sec

○ Starboard Scan

□ Port Scan

Theory

——— Hoffman & Joubert Model (Ref. 8)

— — — 1/r Field for Line Vortex with Circulation Γ = 565 m^2/sec

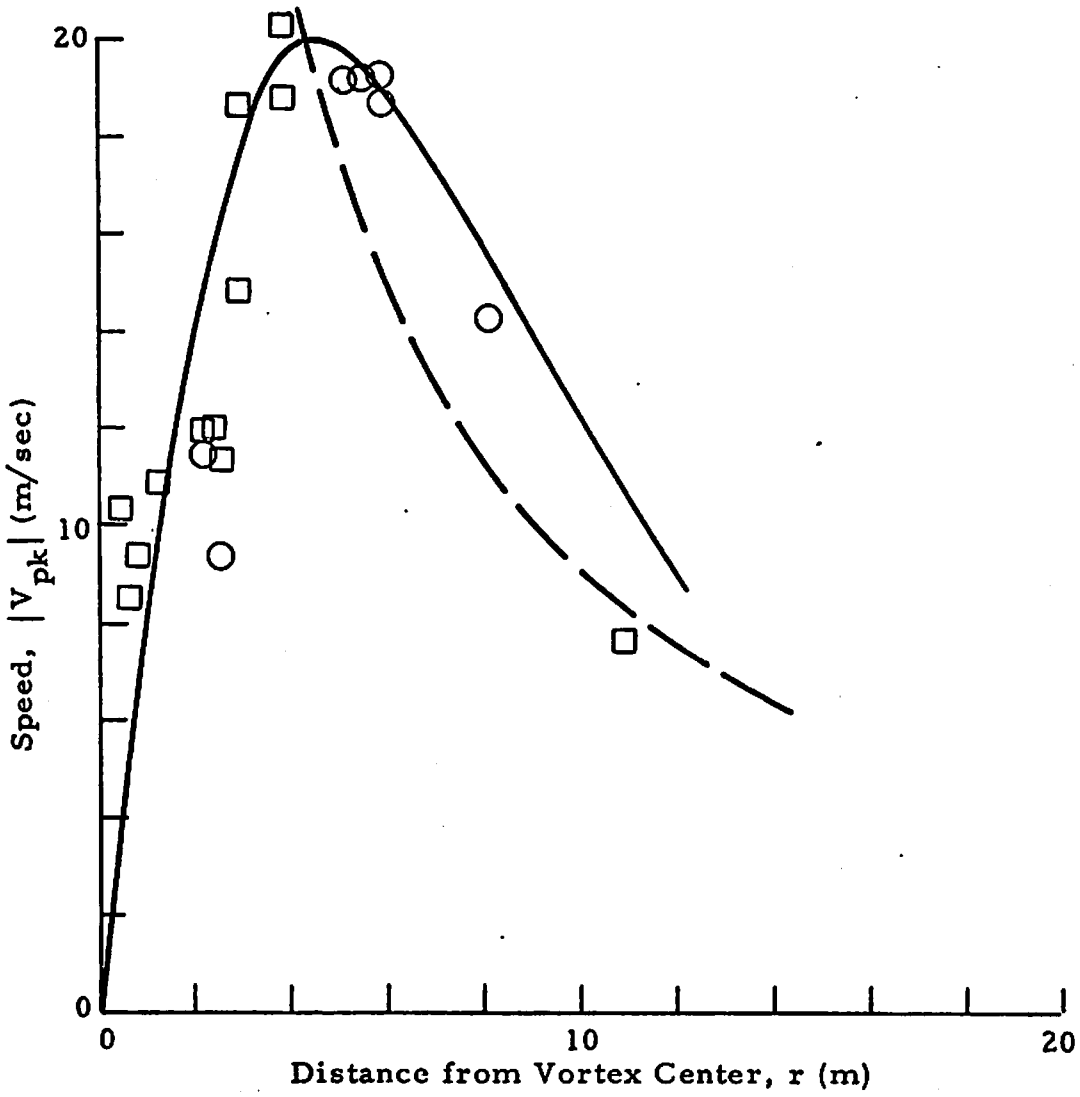

Fig. 18 - Wake Vortex Velocity Distribution with 0 Spoilers

The results in Fig. 18 indicate that the velocity distribution observed with the LDV is in general agreement with the theoretical model of Hoffman and Joubert near the core region of the vortex. In the outer flow region the experimental velocity distribution decreases more rapidly than the theoretical logarithmic circulation model and approaches the 1/r profile. However, sufficient scatter exists in the LDV data points to make a detailed comparison difficult,and agreement with other theoretical models is possible.

The circulation distribution derived from the vortex velocity distribution is shown in Fig. 19. Note that essentially all of the circulation is contained within the viscous core region of radius r_c = 4.5 m and of circulation Γ_c = 565 m^2/sec. This suggests that the vortex rollup process is complete for the 0-spoiler configuration at t = 3.3 sec. In comparison, the predicted vortex circulation strength for this flyby is $\Gamma = \frac{1}{2} U_\infty \bar{c} C_L/K$ = 565 m^2/sec where the flight velocity, mean wing chord, lift coefficient and spanwise loading coefficient are given by U_∞ = 73.6 m/sec, $\bar{c}$ = 8.3 m, C_L = 1.41, K = 0.762. The value of K was selected on the basis of the observed separation between the vortex pair. The circulation distribution predicted from the turbulent viscous vortex model using the observed core parameters is also shown in Fig. 19 where

$$\Gamma = \Gamma_c \, 1.83 \, (r/r_c)^2$$

$$\Gamma = \Gamma_c \left[1 + 2.14 \log_{10} (r/r_c) \right]$$

in the inner and outer core regions, respectively.

4.1.3 Multiple Vortex Characteristics

The spanwise downwash distributions for the 1, 2, 11 and 12 spoiler configurations (Figs. 14 to 16) showed multiple closely spaced peaks which did not resemble the velocity distribution predicted for a coherent trailing vortex pair (Fig. 17). Since the multiple high-velocity peaks in the near-wake downwash field are found in multiple vortex wakes; and the 1, 2, 11 and 12 spoiler configurations (flybys 11, 12 and 13) have been analyzed to identify possible multiple vortex characteristics.

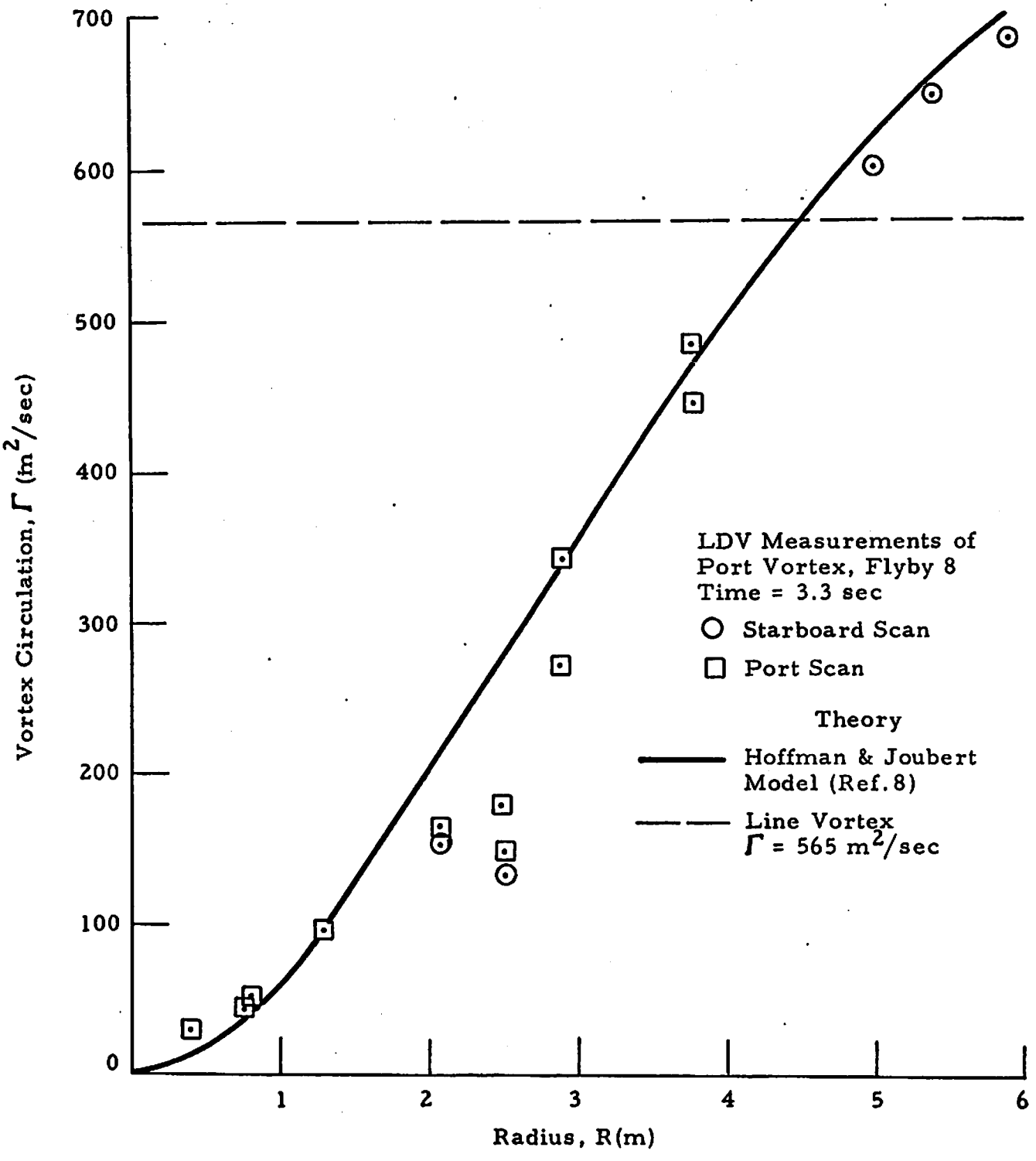

Fig. 19 - Circulation as a Function of Radius for 0 Spoiler Flight Configuration

The predicted line-of-sight velocity distribution for a B-747 aircraft assuming the multiple vortices are shed from the inboard and outboard flaps and wing tips is presented in Fig. 20. The strength and lateral spacing of the multiple vortices given on the top of Fig. 20 were calculated from the modified Betz rollup technique (Ref. 9) and the altitude of the vortices was 180 m and the arc scan range was 183 m. From the velocity distribution shown in Fig. 20 it is noted that the multiple vortices generate multiple peaks of varying magnitudes with the zero points occuring near the vortex locations. Assuming the LDV arc scan intersects the centers of the multiple vortices, the spacing and magnitudes of the multiple peaks can be used to deduce the location, strength, and peak velocity of the wake vortices.

As an example, consider the velocity profile shown in Fig. 14. Note that for the 1.5-sec plot high velocities are recorded but the peaks are scattered and it is difficult to distinguish the location of the multiple vortices suggested in Fig. 20. At 2.6 sec the multiple peaks in Fig. 14 are more ordered and resemble the line-of-sight velocity distribution predicted by the multiple vortex model. For example, the starboard vortex occupies a broad region spanning from approximately 3 to 40 meters from the centerline and the zero points occur at $y \sim 0$, 10, 15, 22 and 30 meters at $t = 2.6$ sec in Fig. 14. The superimposed predicted multiple vortex locations are at $y = 3$, 10.4, 14, 21.3 and 29.6 m (Fig. 20). Thus, the broad multiple peak regions in flyby 11 contain to some extent the multiple vortex peaks predicted from theory. A similar trend can be noted for the other 1, 2, 11 and 12 spoiler cases. In Fig. 15 at $t = 2.4$ sec, the zero points on the starboard side are located at $y \sim 0$, 17, 25 and 32 m and in Fig. 18 at $t = 2.9$ sec, the zero points on the port side occur at $y \sim 0$, 5, 10 and 18 m. Comparing all three 1, 2, 11 and 12 spoiler runs, it is observed that minimums occur in the downwash velocity profile repeatedly for lateral spacings of $y \sim 0$, 10, 15 and 25 m from the wake centerline.

These results suggest that three or four merged vortices are present in the near wake for each semispan. A more detailed analysis of the LDV measurements may establish the strength and core radius of these vortices.

Γ_1 = 62.3 m^2/sec, Γ_2 = 433.5 m^2/sec, Γ_3 = -158.4 m^2/sec, Γ_4 = 298 m^2/sec, Γ_5 = -16.2 m^2/sec
Γ_6 = -62.3 m^2/sec, Γ_7 = -433.5 m^2/sec, Γ_8 = 158.4 m^2/sec, Γ_9 = -298 m^2/sec, Γ_{10} = 16.2 m^2/sec
y_1 = 29.6 m, x_1 = 180 m, y_2 = 21.3 m, x_2 = 180 m, y_3 = 14 m, x_3 = 180 m, y_4 = 10.4 m, x_4 = 180 m,
y_5 = 3 m, x_5 = 180 m, y_6 = -29.6 m, x_6 = 180 m, y_7 = -21.3 m, x_7 = 180 m, y_8 = -14 m, x_8 = 180 m,
y_9 = -10.4 m, x_9 = 180 m, y_{10} = -3 m, x_{10} = 180 m
(Subscripts 1-5 Starboard Vortices, 6-10 Port Vortices)

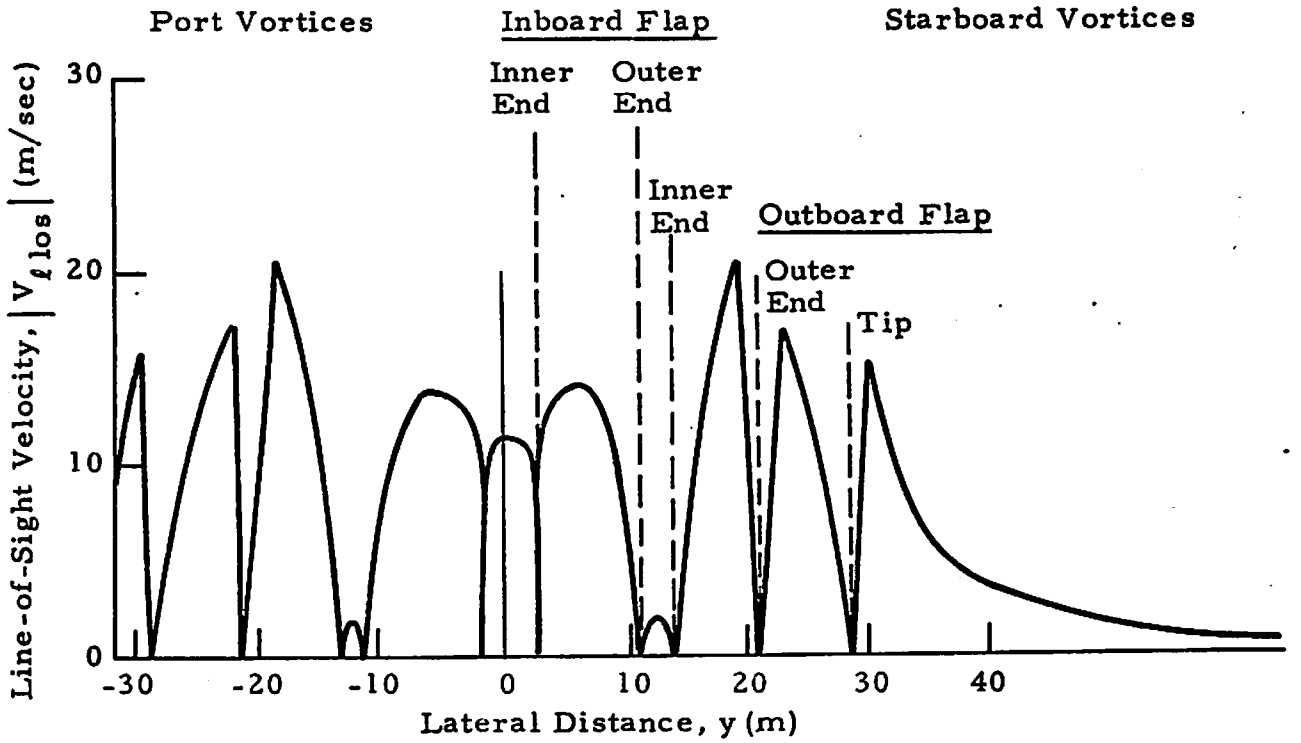

Fig. 20 - Predicted Line-of-Sight Velocity for Rosamond B-747 Flyby 11 at t ~ 2 sec, Assuming Multiple Wake Vortices

However, the LDV measurements have shown that multiple vortices exist in the near wake of the B-747 aircraft when spoilers are deployed whereas a coherent rolled-up trailing vortex pair exists in the near wake for 0 spoilers.

4.2 VORTEX TRANSPORT

The line-of-sight velocity measurements obtained by the LDV in the wake of the B-747 aircraft in the finger-scan mode have been processed to yield the altitude and lateral position of the vortices and have been compared with photographic, acoustic and theoretical wake vortex trajectories. The following analysis of the vortex transport characteristic includes the early near-wake flow as well as the subsequent far-wake transport process.

4.2.1 Near-Wake Vortex Tracks

From the Rosamond wake measurements, those flybys where photographic measurements of the near-wake trajectory were available for comparison with the LDV tracks have been selected. The near wake was assumed to be the region within 20 spans downstream of the aircraft, $x/b \leq 20$.

The lateral versus horizontal wake vortex location 5 to 10 sec after aircraft passage is shown in Figs. 21 and 22. The LDV and photographic measurements indicate that the center of the wake vortex pair is located at approximately 80% semispan and descends at ~ 1.5 m/sec over the 4 to 10 sec interval. However, as much as a 15% scatter in the vortex lateral location and 50% scatter in the descent rate can be noted in the initial vortex trajectories which may be associated with uncertainties in the airplane location or may be due to the different flight configurations. The photographic measurements shown in Figs. 21 and 22 are in general agreement with the LDV trends.

4.2.2 Far Wake Vortex Tracks

The line-of-sight velocity measurements obtained with the LDV system in the finger-scan mode have been processed with the VAD and Vortex Track Program and the I_{pk} program to determine the far-wake vortex trajectories.

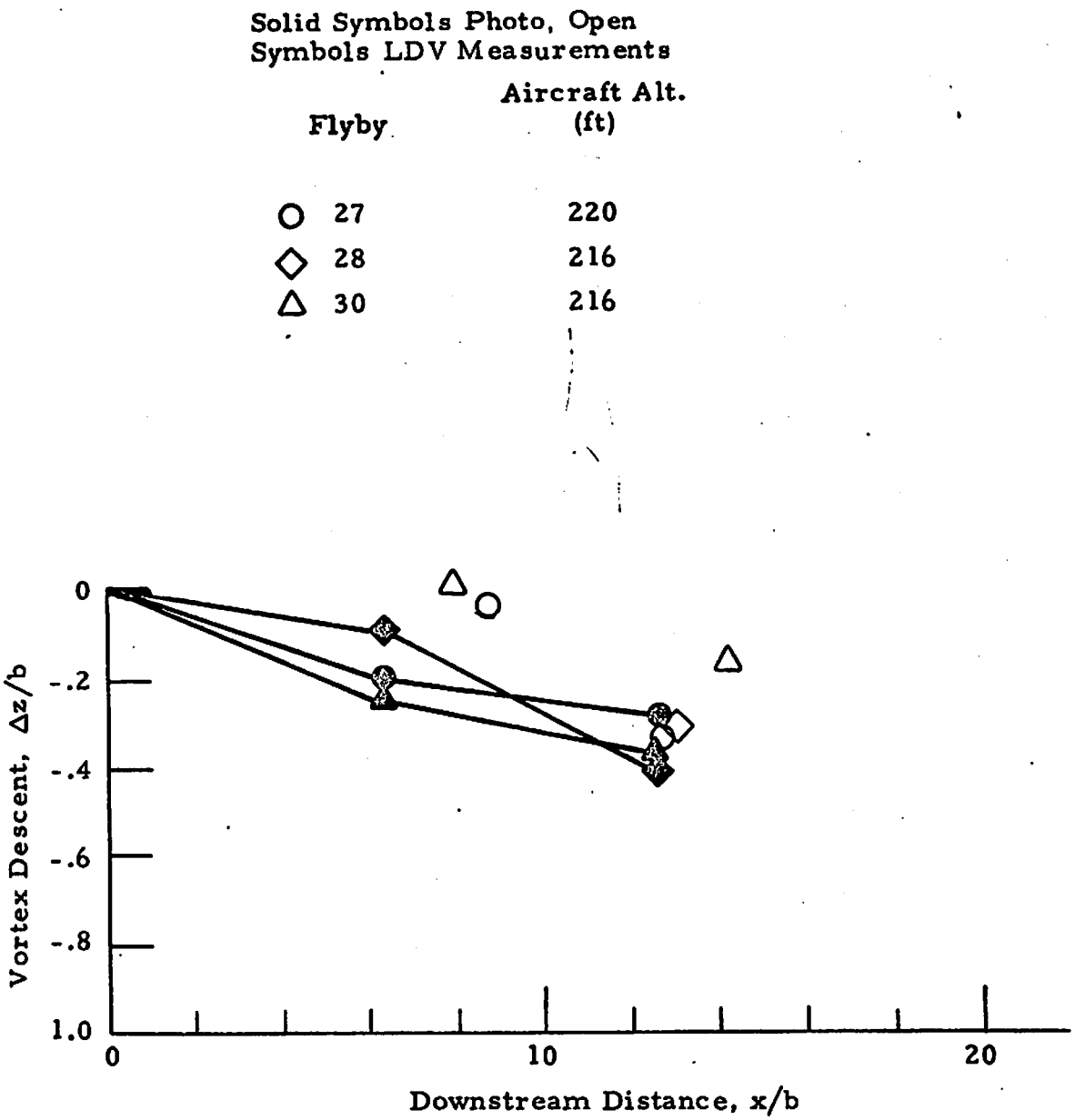

Fig. 21 - Vortex Descent as a Function of Downstream Distance for Flybys with 30/30 Flaps, O Spoilers

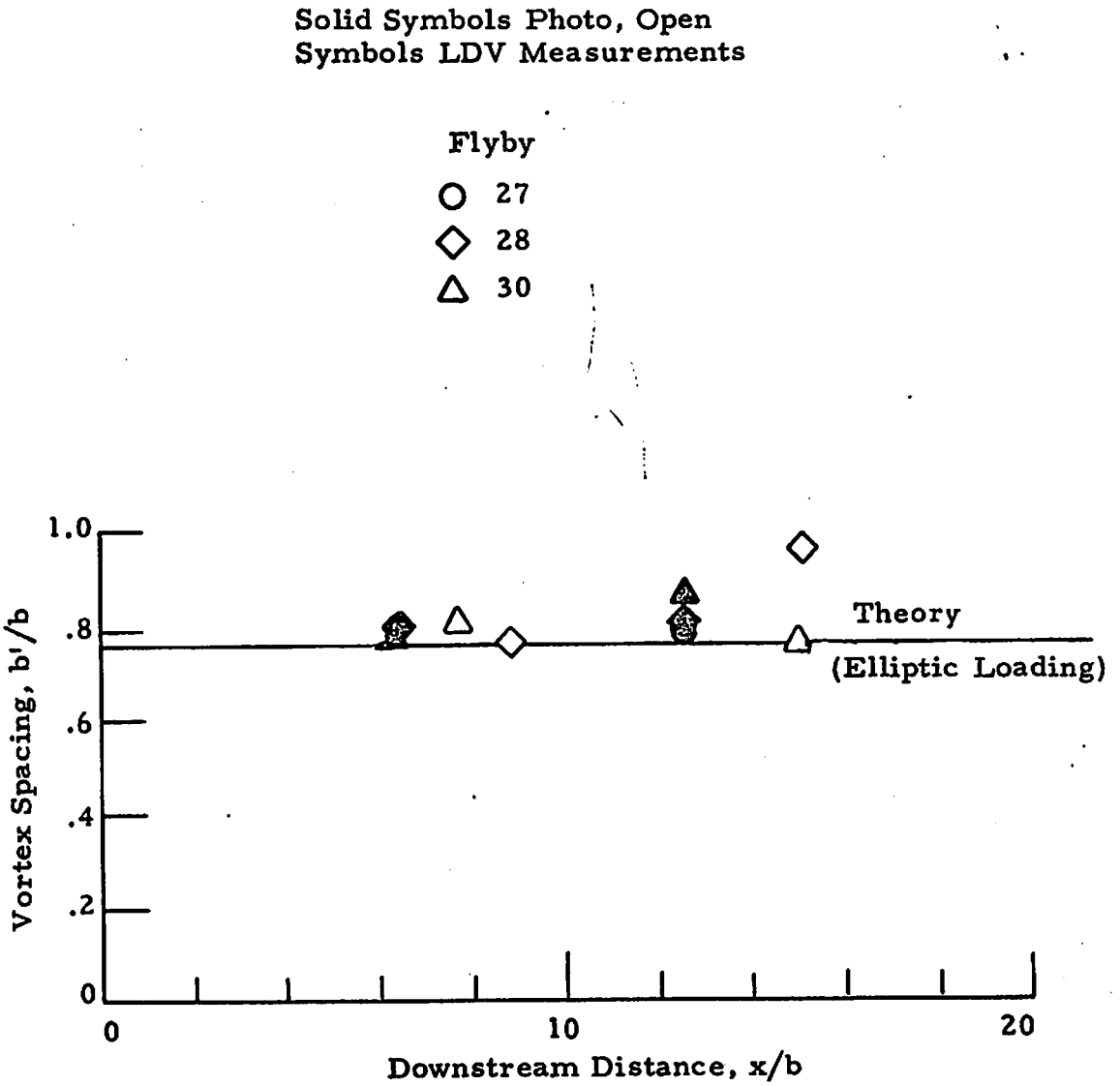

Fig. 22 - Vortex Spacing as a Function of Downstream Distance for Flybys with 30/30 Flaps, O Spoilers

The regions of the maximum backscatter intensity were used to locate the vortex core region. The wake vortex tracks from the Rosamond tests include the results from the low-speed data and high-speed data.

4.2.2.1 Low-Speed Data

The wake vortex trajectories from the low-speed LDV measurements are presented in Appendix D. The circles, triangles and diamond symbols represent the port, starboard and undefined vortex, respectively. For each flyby, the predicted wake vortex trajectory assuming zero crosswind is shown by the solid lines. The vortex tracks were computed from the predicted model described in Ref. 10 for a circulation strength of $\Gamma = 662\ m^2/sec$ and an initial vortex spacing of $b' = 41.8$ m. Available photographic and acoustic measurements also appear on the plots, the solid circles and triangles representing the former and the x's the latter measurements. The dashed line is a smooth curve drawn through the photographic vortex tracks.

From the wake vortex trajectories presented in Appendix D, the following wake transport characteristics can be noted:

1. The wake vortex descends nearly vertically with very little horizontal motion.
2. The initial descent rate over the period 0 through 20 sec after aircraft passage is in general agreement with the predictive model.
3. The wake descent diminshes after 20 sec and the vortex tends to remain at a constant altitude in ground effect.

In addition to the above trends, some scatter is noted in the location of the vortices. Since both the photographic and LDV tracks show the vortex wandering in lateral position and altitude, particularly at late times, this is believed to be the effect of random atmospheric winds and gusts. However, in some cases a large scatter is noted in the LDV vortex tracks which is not seen in the corresponding photographic measurements. This has been investigated using the high-speed data since accurate determination of the vortex position

is a prerequisite in determining other relevant parameters such as the decay of the vortex rotational velocity and circulation strength.

4.2.2.2 High-Speed Data

The wake vortex tracks computed from the high-speed LDV data using the I_{pk} algorithm are given in Appendix E for flybys 27, 28, 44, 47, 48 and 49. The vertical and lateral vortex trajectories computed from the high-speed data show the same trends as the low-speed tracks discussed earlier.

Comparison of the high-speed wake vortex measurements with the observed photographic vortex position is shown in the V_{pk} versus elevation angle curves in Figs. 23 and 24. With the exception of any dominant low velocity spikes, the solid line in the plots connects the maximum values of V_{pk} observed by the LDV in the finger scan mode for one scan between the two elevation angle limits (i.e., it represents the maximum value of V_{pk} for many finger-scan lobes). Since the LDV is scanned rapidly in range (3.5 Hz) and slowly in elevation angle (0.2 Hz), the peaks in the V_{pk} versus elevation-angle curves indicate the elevation angle at which the maximum line-of-sight velocity is observed by the LDV system. Thus, when a vortex is interrogated by the LDV system, two maxima occur in the V_{pk} versus elevation angle at those angles where the line-of-sight is tangent to the vortex core and a minimum occurs at the mid-elevation angle, or in other words, a double-peak signature results. The low velocity spike bounded by the high velocity peaks marks the vortex core and here the minimum V_{pk} points are connected. For a number of LDV measurements this double-peak signature can be clearly recognized; for example at t = 6.6, 9.0 and 14.1 sec for flyby 23 (Fig. 27) and at t = 4.2 and 14.2 sec for flyby 28 (Fig. 24). In addition, the elevation angle at which these double-peak patterns occur is ofter within a few degrees of the vortex elevation angle measured photographically.

While the photographic and LDV measurements agree well for some scans, in terms of the location of the vortex signature, for other scans the scatter in elevation angle is as high as 6 deg (Fig. 24 t = 5, 9 sec). It is

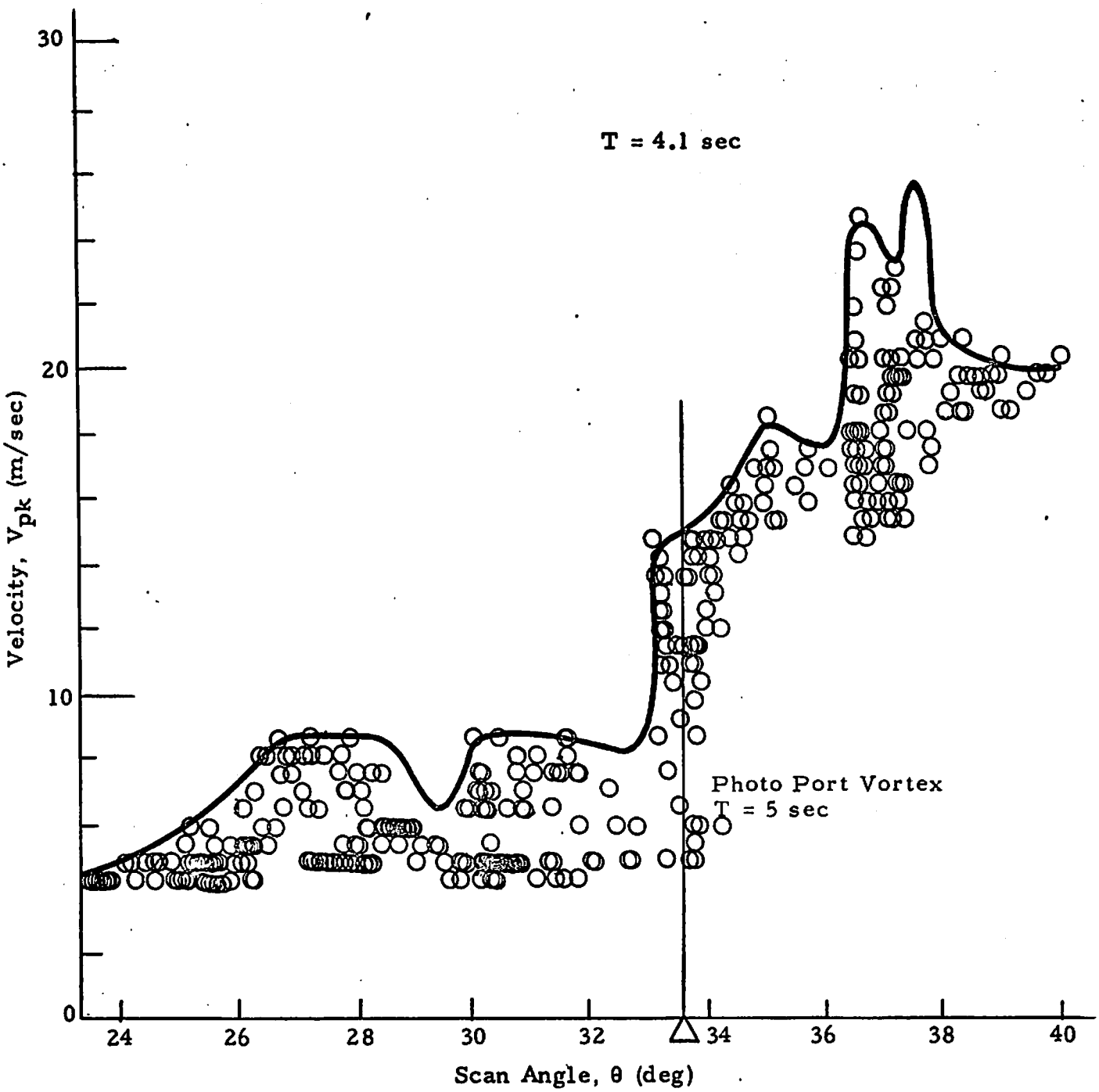

Fig. 23 - Comparison of Photographic and LDV Measurements for Rosamond B-747 Flyby 27

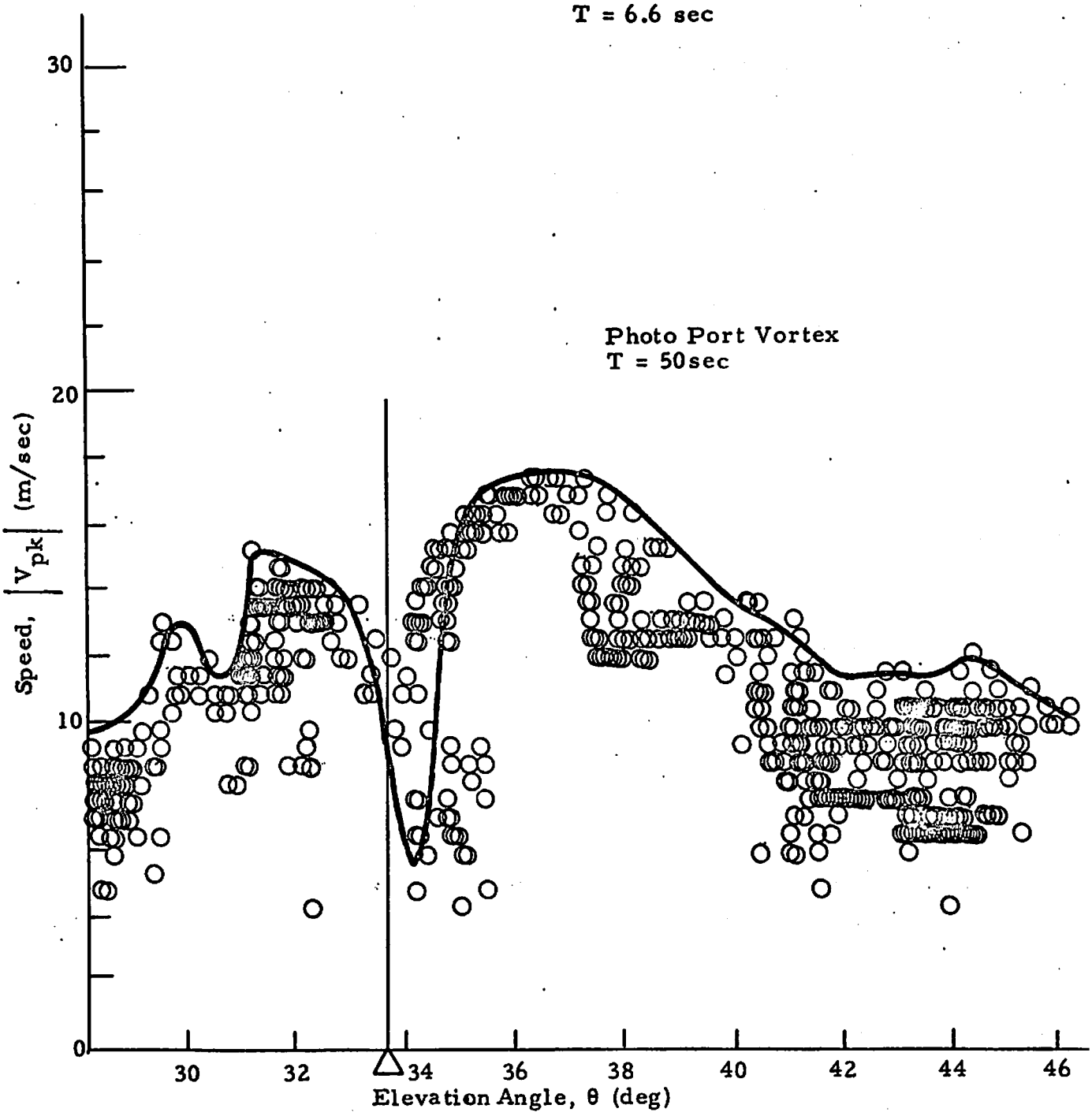

Fig. 23 (Continued)

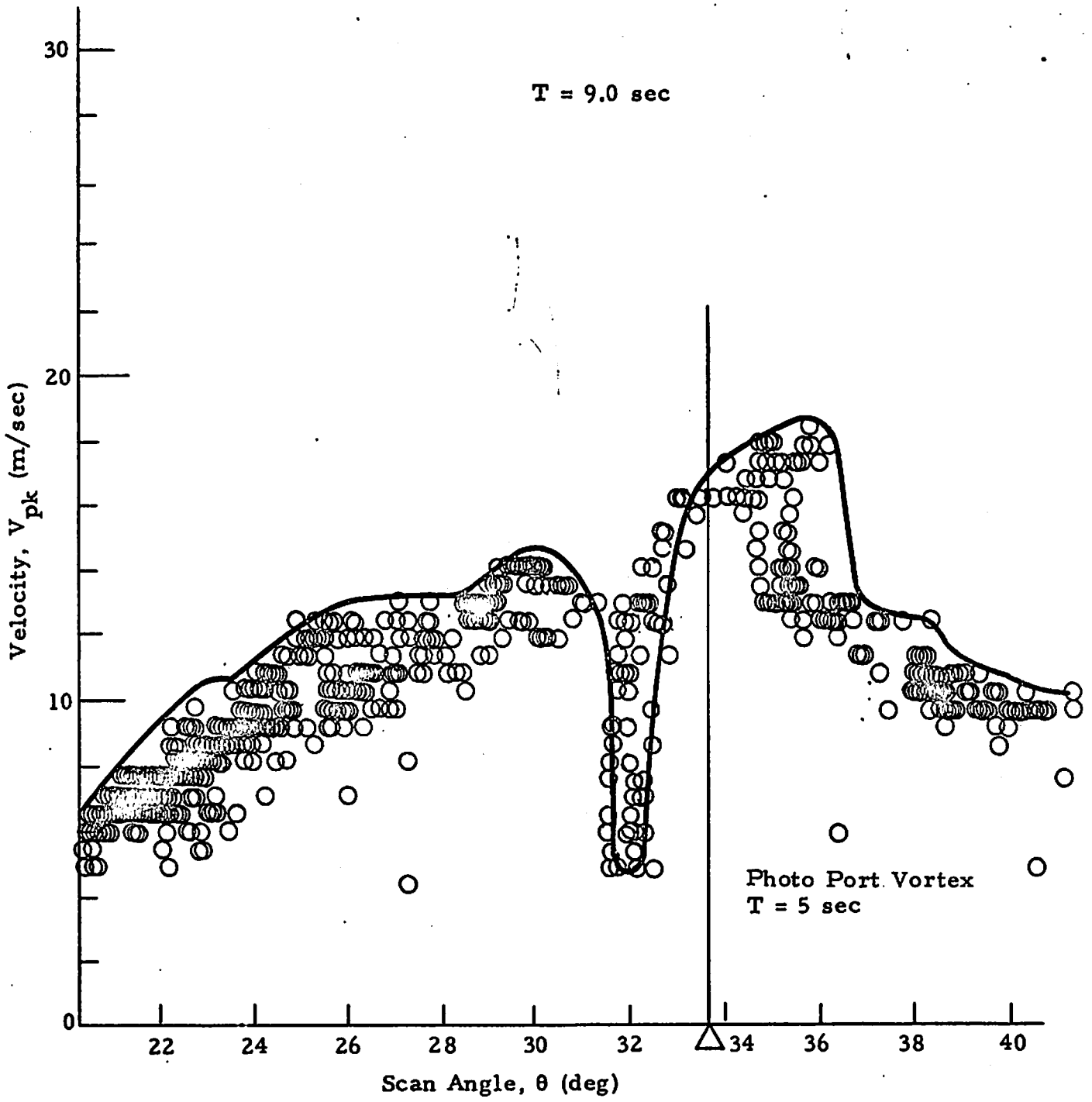

Fig. 23 (Continued)

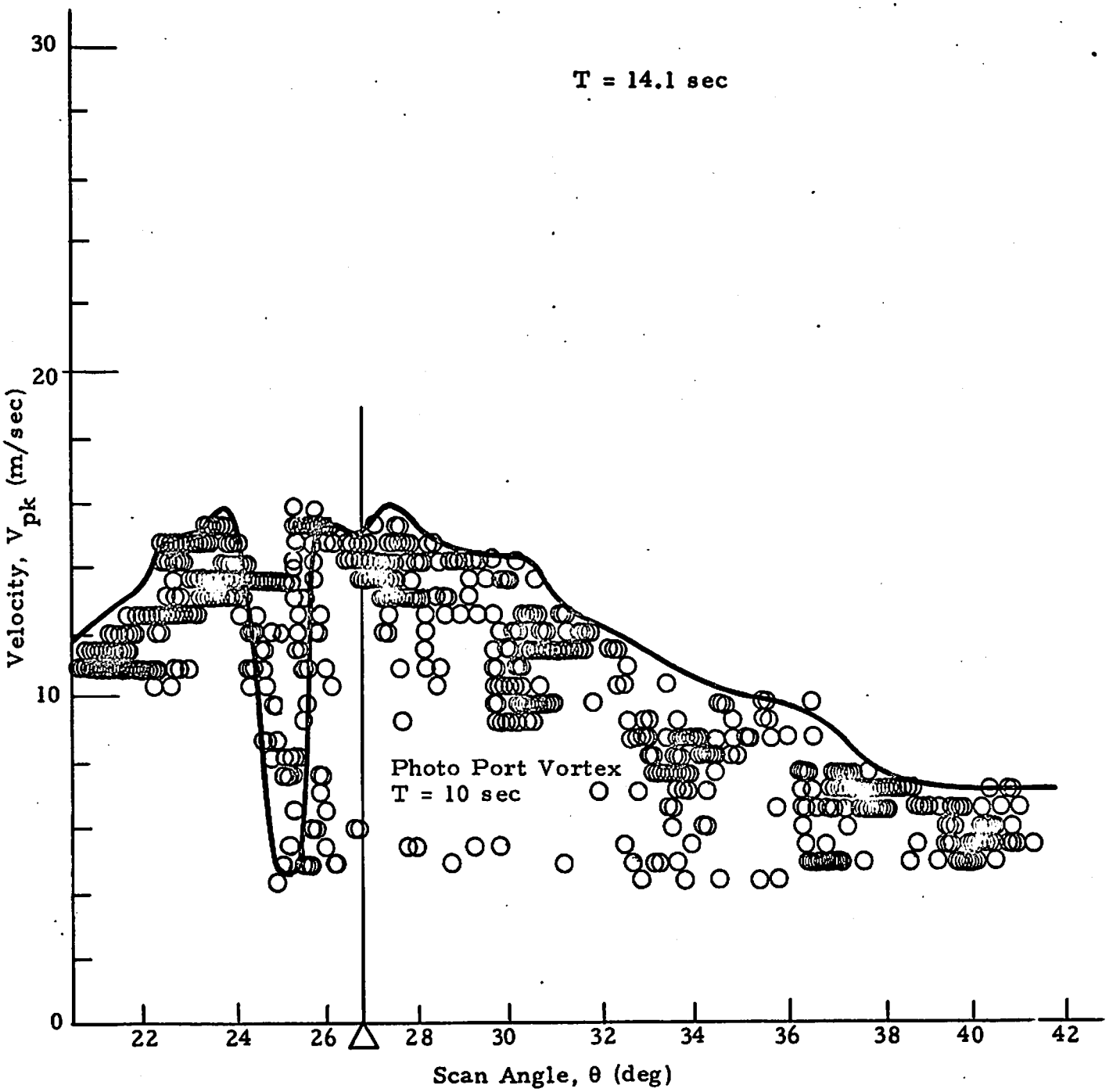

Fig.23 (Concluded)

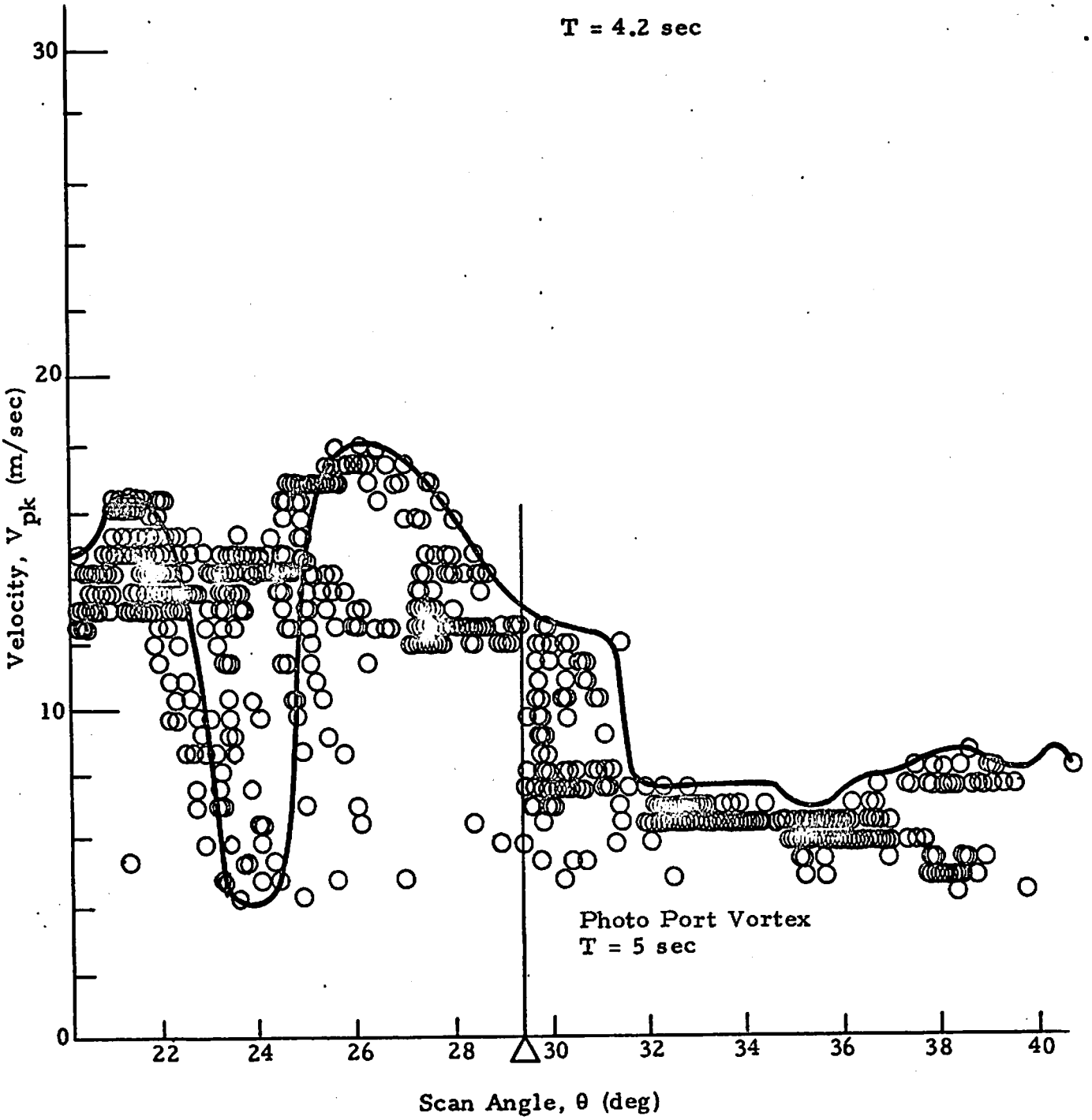

Fig. 24 - Comparison of Photographic and LDV Measurements for Rosamond B-747 Flyby 28

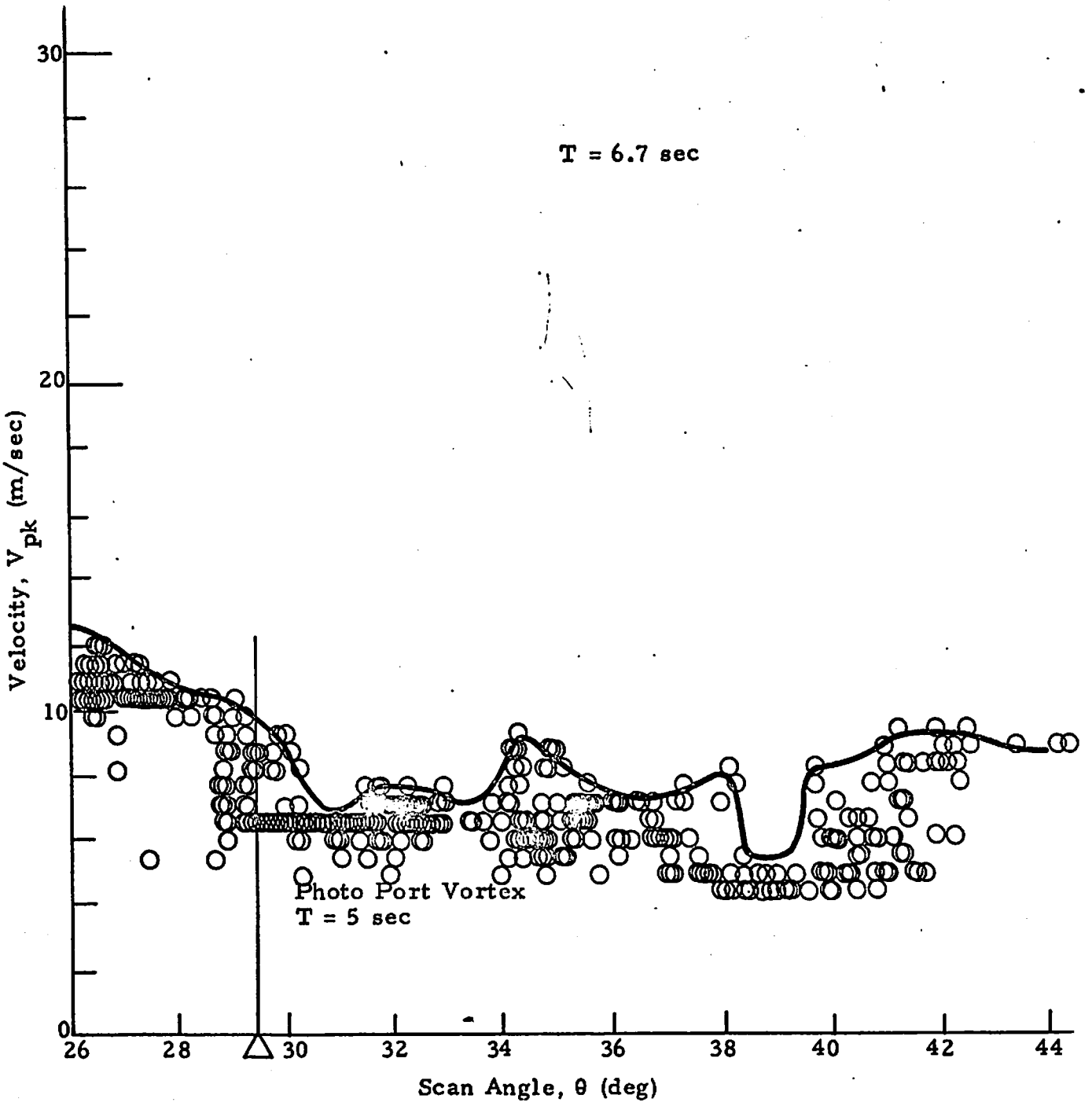

Fig. 24 (Continued)

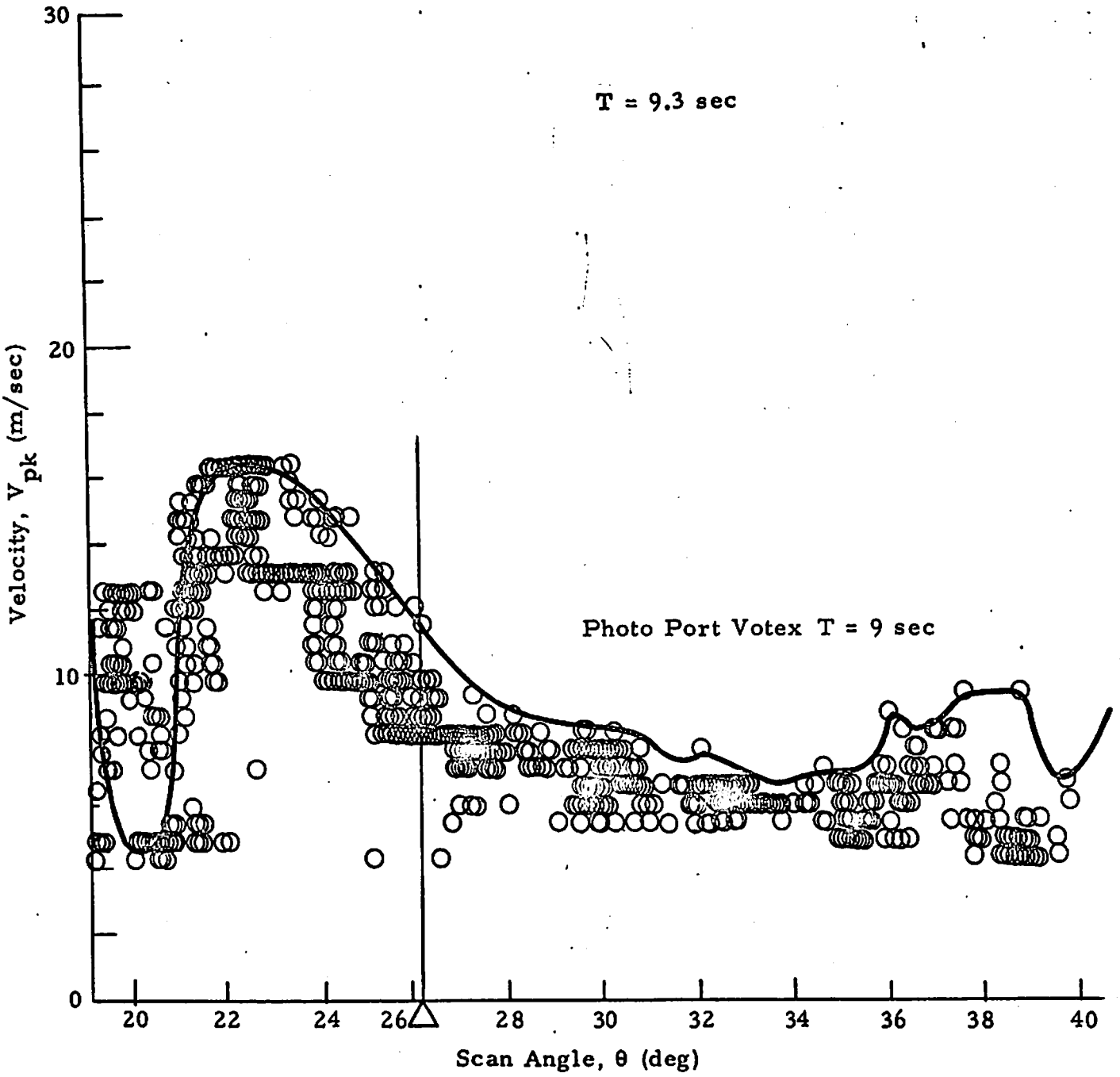

Fig. 24 (Continued)

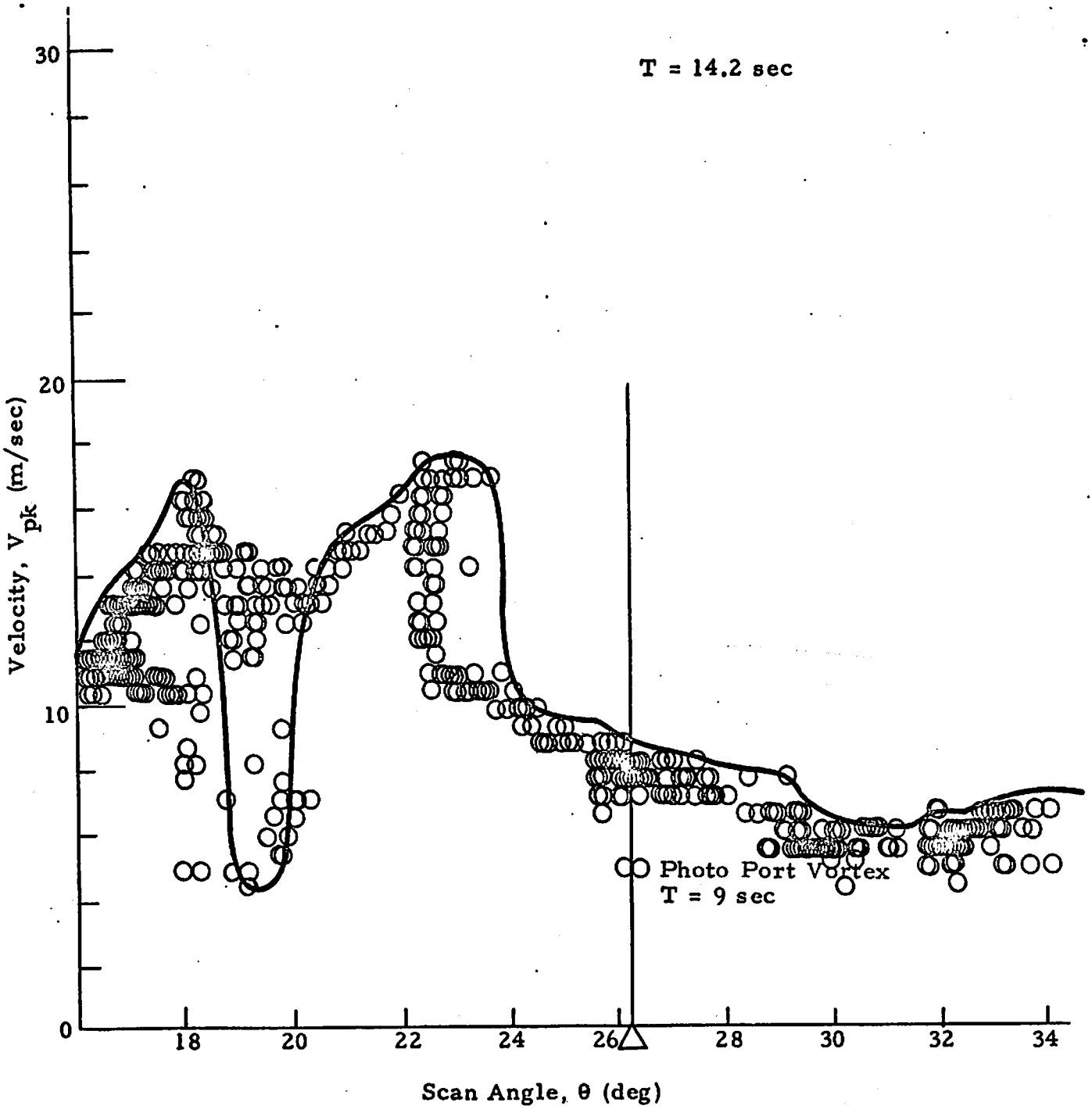

Fig. 24 (Concluded)

possible that the core diameter of the vortex is small and the scan pattern misses the peak-tangential velocity regions. It is also possible that the photographic measurements may be subjected to some errors or that the smoke does not mark the exact vortex location accurately. Lastly, the error may be a result of anomalies in the determination and processing of the LDV elevation angle.

4.3 VORTEX DECAY

Information regarding the decay of wake vortices such as the time history of the peak tangential velocity, circulation and viscous core radius is contained in the line-of-sight velocity distributions measured by the LDV system. In the following discussion, the decay of the peak tangential velocity, the circulation decay and the core radius time history of the wake vortex are presented.

4.3.1 Decay of Vortex Rotational Velocity

To determine the decay of the wake vortex rotational velocity from the LDV line-of-sight velocity distributions, two basic methods were used to pick out the maximum tangential velocity of the vortex:

1. Selection of the maximum value of V_{pk} (or V_{ms}) occuring during each scan between minimum and maximum elevation settings.
2. Selection of the maximum value of V_{pk} occuring within ± 3 deg of the known elevation angle of the vortex.

For both techniques, the maximum value of V_{pk} is a good measure of the peak tangential velocity of the vortex if the LDV line-of-sight is tangent at some point with the circular core region of the vortex and the vortex range falls within the focal volume. However, in the first approach the V_{pk} time history becomes meaningless if the vortex drifts out of the scan area. To eliminate this uncertainty, in the second approach other information, i.e., photographic vortex position, is used to establish the approximate location of the vortices.

These regions are then searched for the maximum V_{pk} values which are associated with the vortex phenomena.

The V_{pk} and V_{ms} time histories determined using the first technique are shown in Appendix F. A bandwidth criteron of $N \geq 2$ was used in analysis to filter out random high frequency noise i.e., at least two of the 100 frequency bins had to be activated for the data to be used. A sample of the results, presented in Fig. 25, indicates that the wake vortex rotational velocity is nearly constant approximately 50 spans downstream of the aircraft followed by 1/time decay. Some scatter which may be associated with the uncertainty in vortex location may be noted in the velocity decay curve.

Using the photographic vortex tracks to determine the approximate vortex location (the second technique above), the V_{pk} time history has been recomputed for flybys 27 and 28 and is presented in Figs. 26 and 27. The results shown in Figs. 26 and 27 also indicate a nearly constant vortex tangential velocity within 50 spans downstream of the aircraft. Less scatter occurs in V_{pk} versus time plots when the photographic tracks are used to establish the vortex center. Unfortunately, photographic measurements were not available at late times to establish the final vortex decay process.

4.3.2 Core Radius Time History

The vortex core radius was determined from the observed variations in V_{pk} with range and elevation angle according to the technique discussed earlier in Section 2.1.2. The computed vortex core radius time history for flybys 27, 28 and 44 is given in Figs. 28, 29 and 30. Photographic vortex tracks were compared with LDV V_{pk} distributions to compute the core radius time history in Figs. 28, and 29, while the predicted vortex tracks were used to compute the core radius time history in Fig. 30. The laser Doppler velocimeter wake vortex measurements show that the vortex core radius is approximately constant in the aircraft near wake. The observed core radius ranges from 1 to 4 m, and the mean core radius is approximately 2 m.

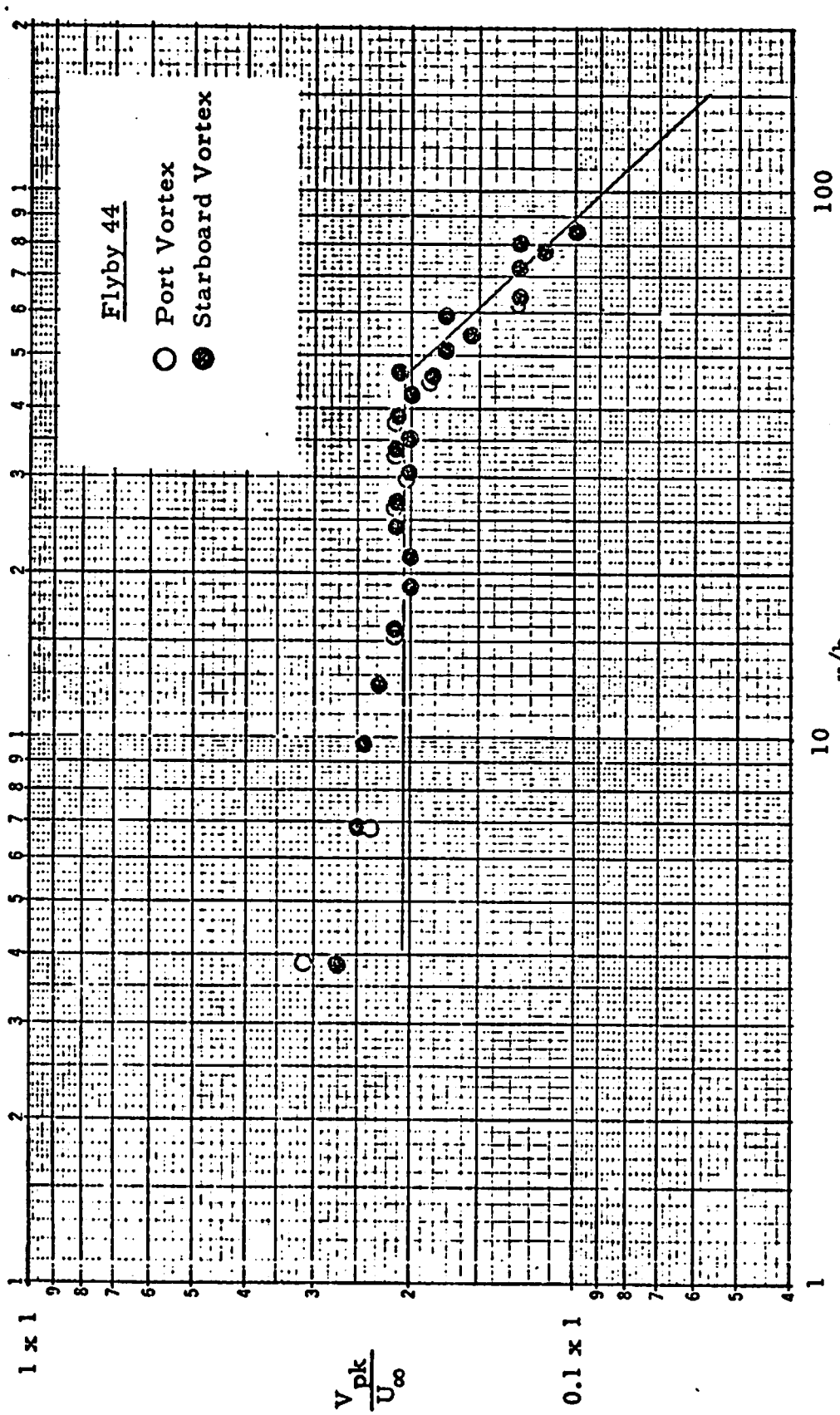

Fig. 25 - Decay of Wake Vortex Rotational Velocity for Flyby 44

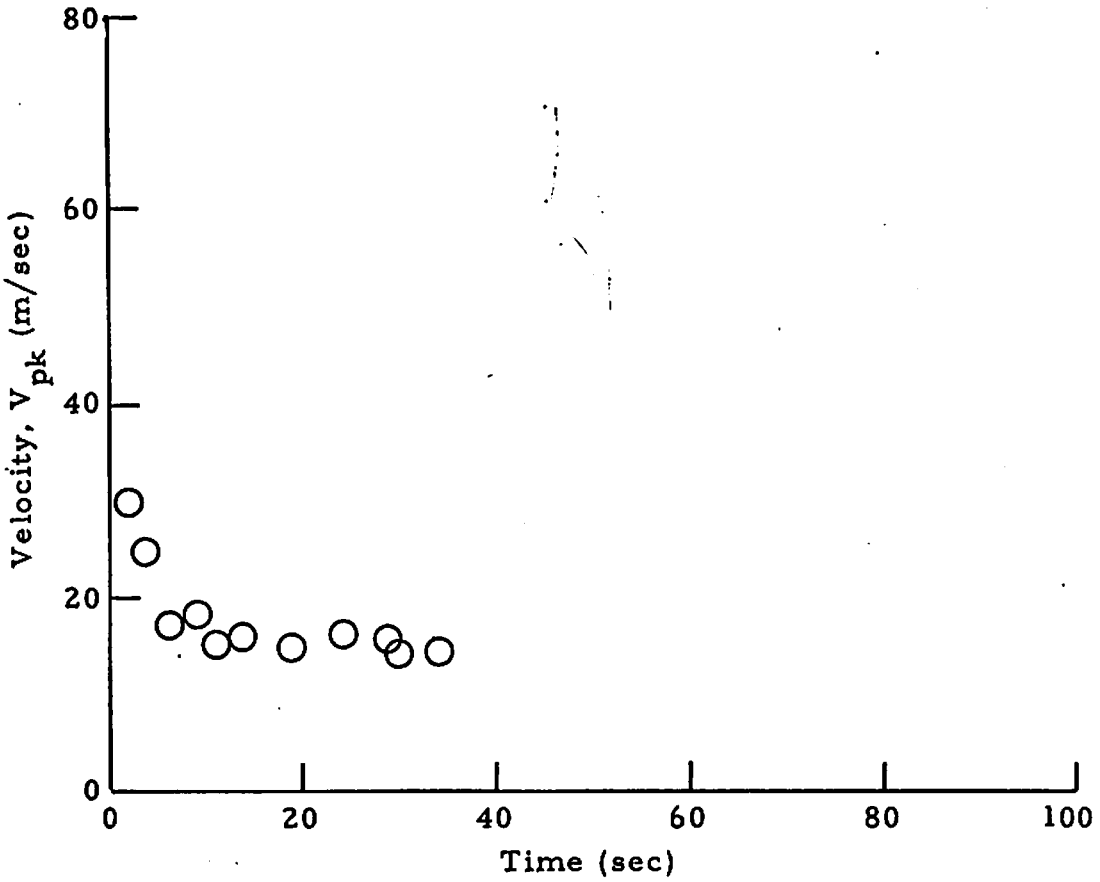

Fig. 26 - V_{pk} as a Function of Time for Flyby 27 Using Photographic Tracks to Locate the Vortex Center

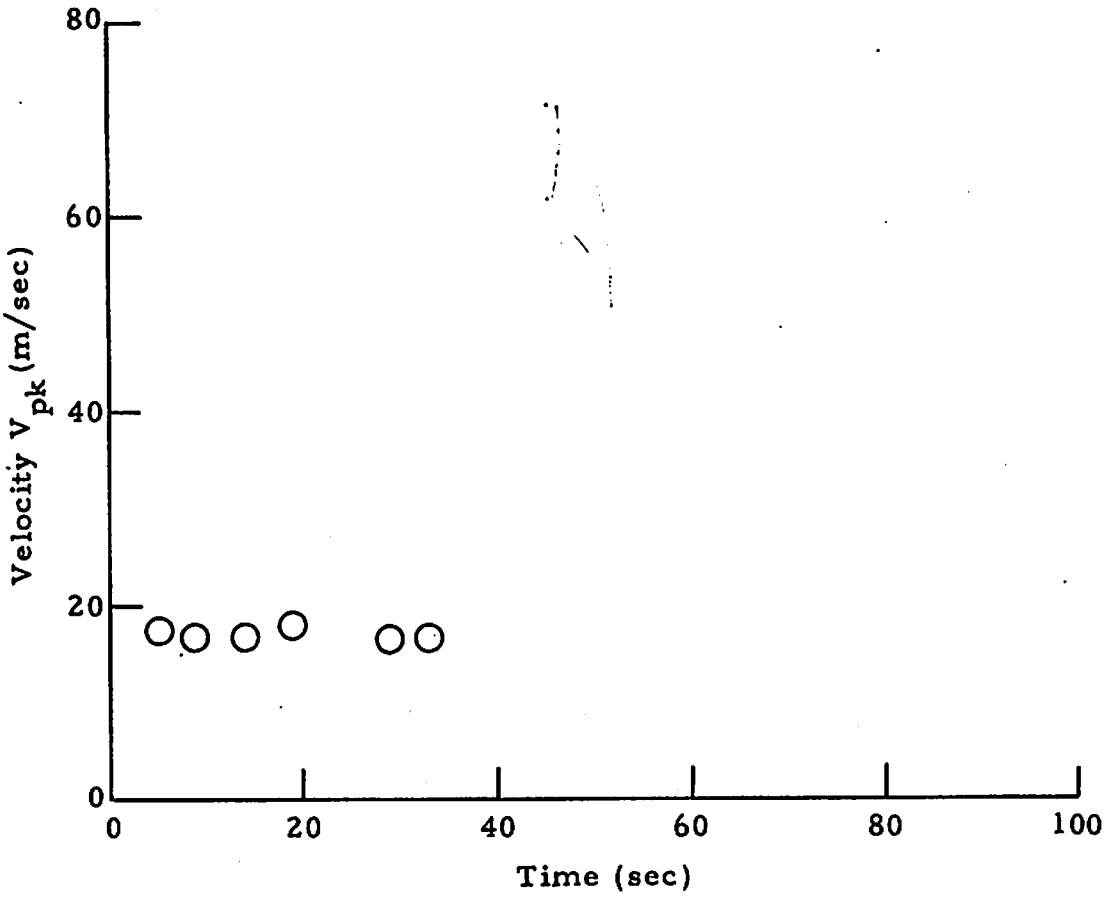

Fig. 27 - V_{pk} as a Function of Time for Flyby 28 Using Photographic Tracks to Locate the Vortex Center

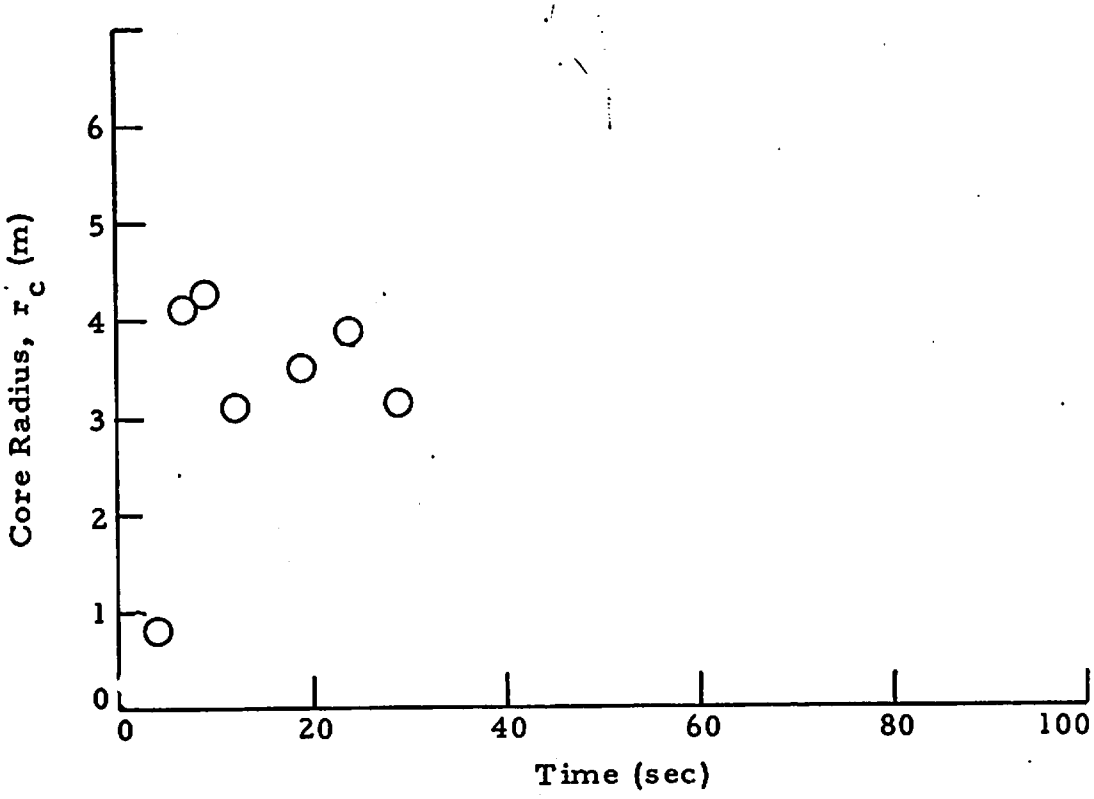

Fig. 28 - Vortex Core Radius as a Function of Time for Flyby 27

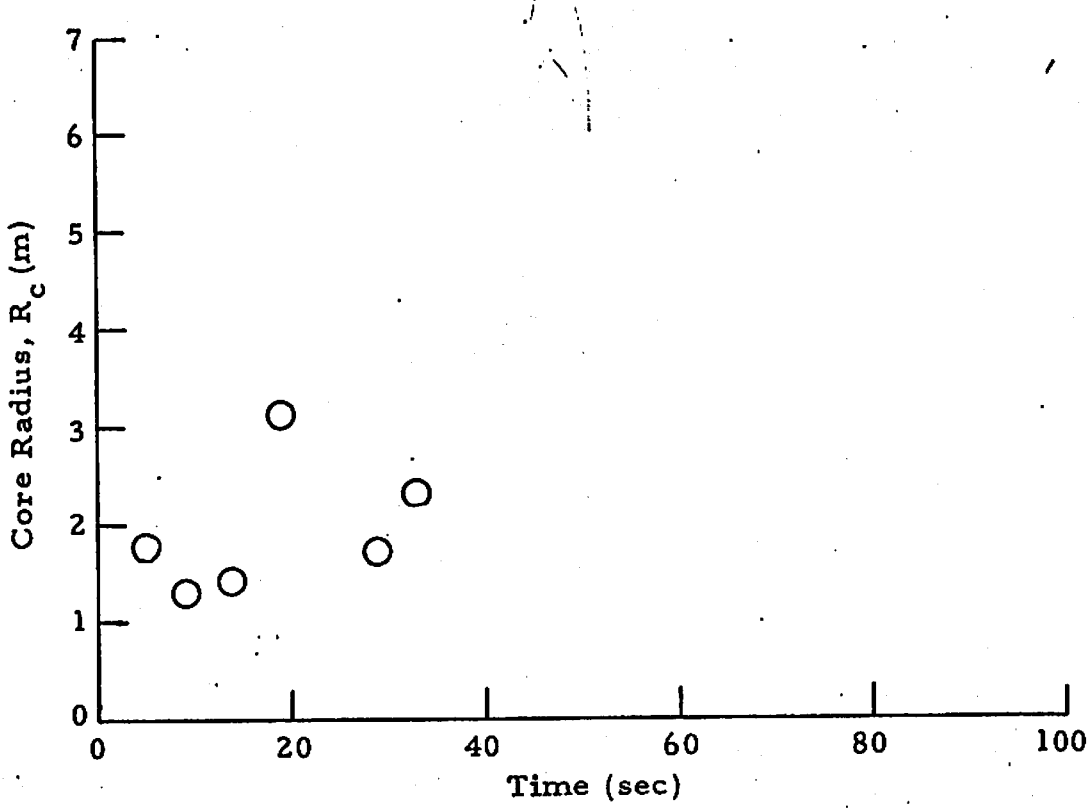

Fig. 29 - Vortex Core Radius as a Function of Time for Flyby 28

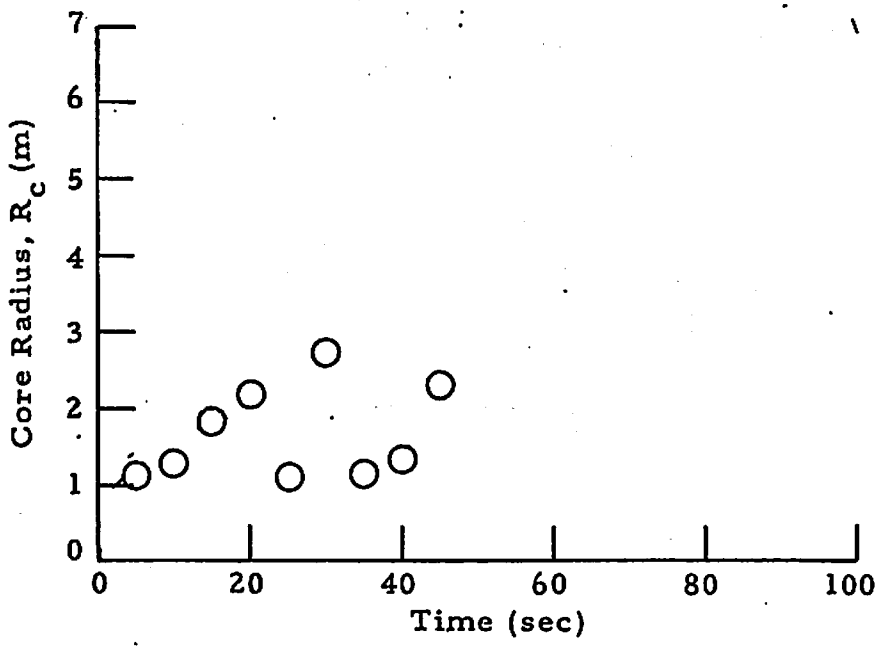

Fig. 30 - Vortex Core Radius as a Function of Time for Flyby 44

4.3.3 Circulation Decay

The circulation time history was computed from the observed LDV line-of-sight velocity distribution using: (1) the vortex tracks from the low-speed data, and (2) the photographic tracks to determine the vortex location. In the first technique, the circulation was determined from the average moment of the line-of-sight velocity components within a correlation radius of the computed vortex center. In the second technique, the circulation was computed from the moment of the two maximum V_{pk} values adjacent to the center of the vortex as outlined earlier in Section 2.1.2 and the photographic vortex tracks were used to determine the vortex location. It was found that this technique was very sensitive to errors in core radius.

The circulation time history computed from the low-speed data vortex tracks is shown in Appendix G. The computed circulation is shown from 20 seconds to the time of the last measurement. At periods earlier than 20 seconds, circulations are not shown since the vortex may not be fully rolled up. The general circulation decay trend is similar to the velocity decay trends noted earlier – relatively small decay initially followed by rapid decay in the far wake. More scatter is evident in the circulation distributions than the velocity or core radius distributions presented earlier because the circulation involves the product of the scatter of the previous two measurements. To reduce this scatter, the circulation has been recomputed using the photographic vortex tracks to define the vortex center more closely.

The circulation time history recomputed for flybys 27 and 28 from the high-speed data using the photographic tracks as a position reference is shown in Figs. 31 and 32 where the computed data points are connected by a smooth line. The circulation time history has been also recomputed for flyby 44 (Fig. 37) using the predicted vortex tracks to define the vortex location. The recomputed circulation time histories indicate a constant circulation over the time range 0 to 40 seconds and are similar to the results shown earlier in Appendix G and exhibit somewhat less scatter. However, the variation in the computed circulation is still large and makes comparisons between different flybys difficult.

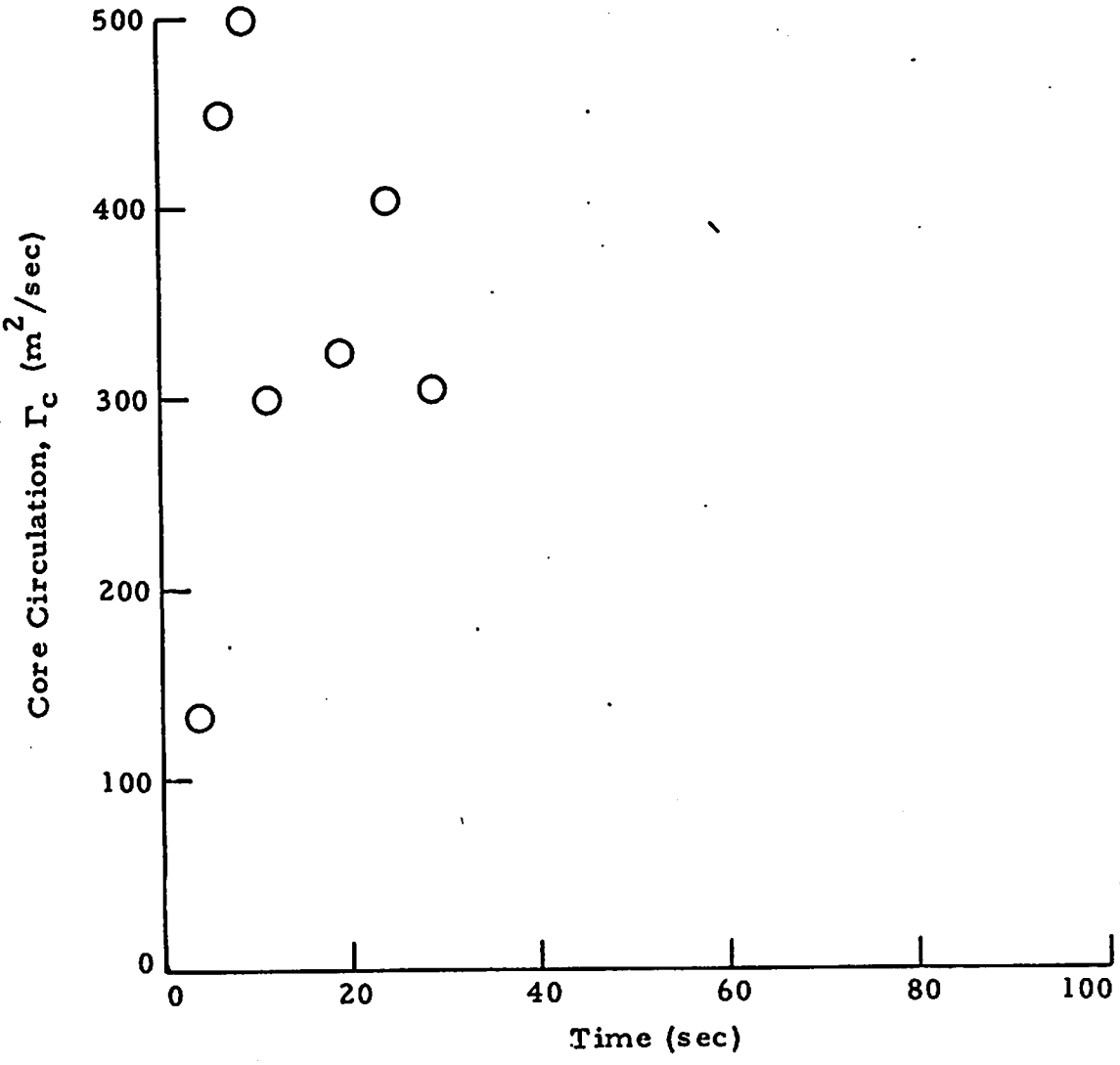

Fig. 31 - Vortex Core Circulation as a Fuction of Time for Flyby 27

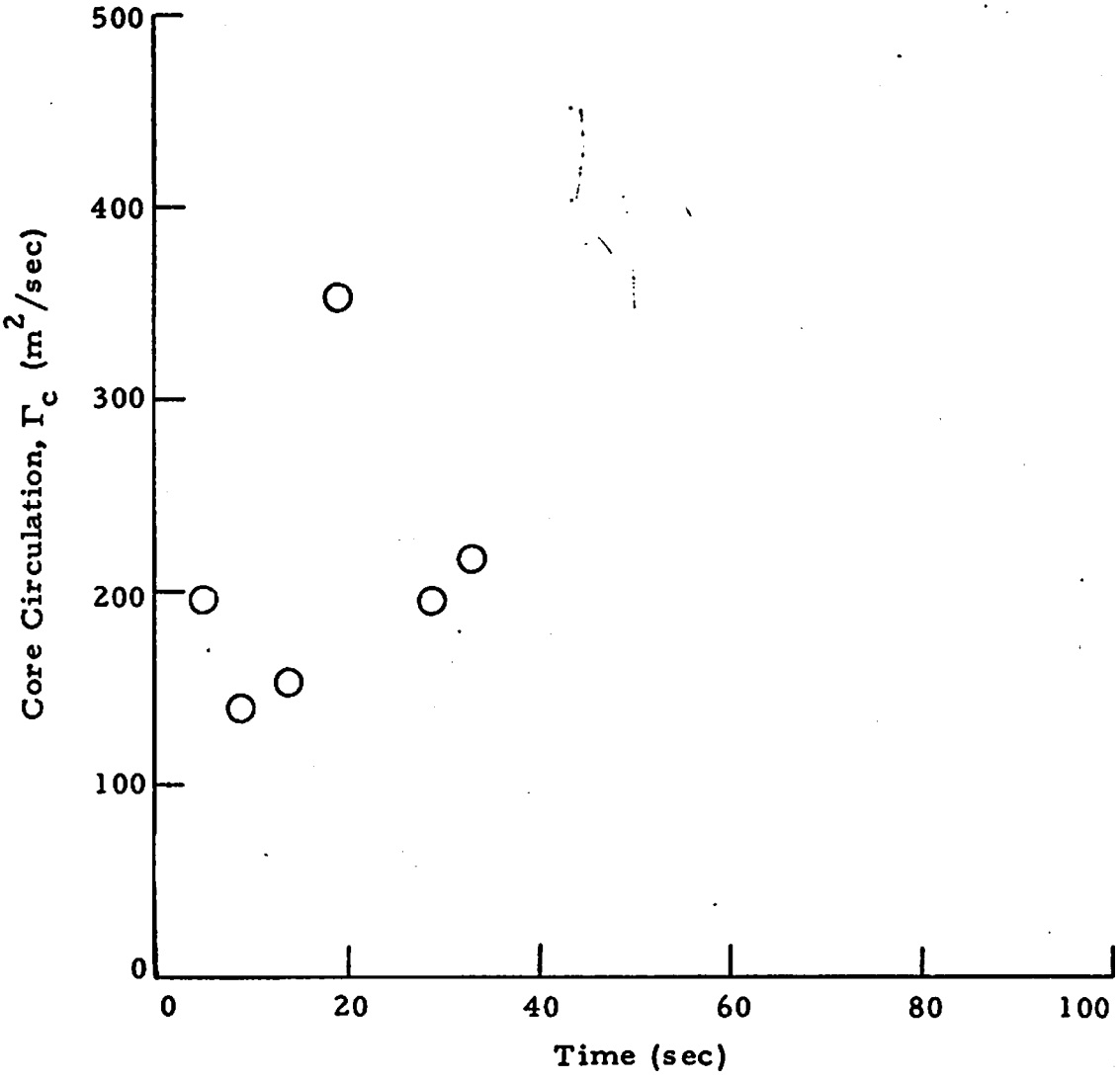

Fig. 32 - Vortex Core Circulation as a Function of Time for Flyby 28

4.3.4 Comparison of Vortex Decay Trends for Different Flight Configurations

To determine the vortex decay trends for different flight configurations, the time history of the vortex rotational velocity, circulation and core radius presented earlier can be cross correlated. The decay of the wake vortex rotational velocity for different spoiler and flap and landing gear settings and flight paths is compared in Figs. 33 through 36, respectively. These results indicate that the deployment of spoilers decreases the vortex rotational velocity in the near wake while flap and landing gear settings and aircraft flight path angle do not appear to have a significant effect. However, care must be used in interpreting the above results since for some of the runs the wake vortices drited out of the field of view (see Appendix D).

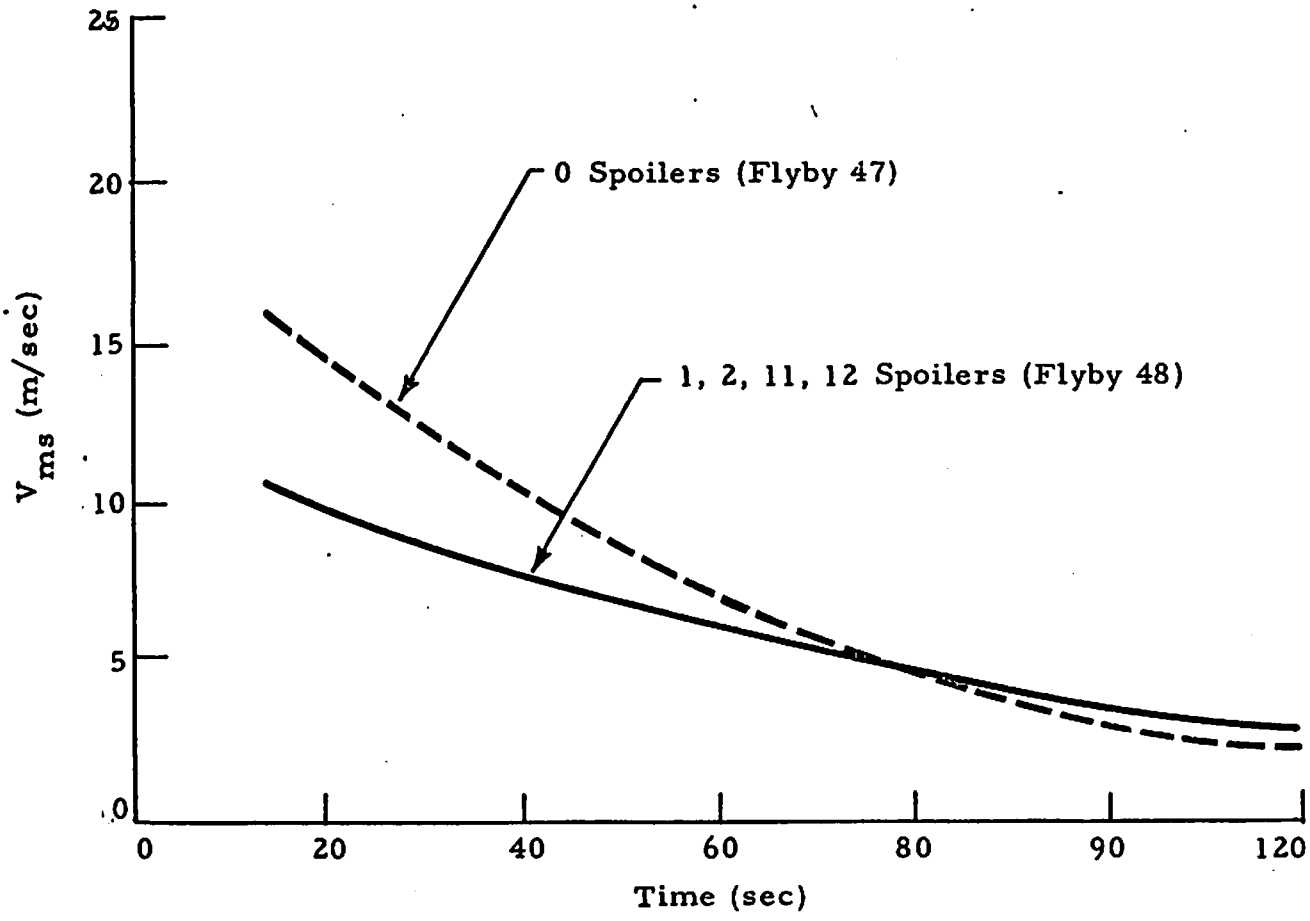

Fig. 33 - Comparison of Wake Vortex Rotational Velocity for B-747 Flybys With and Without Spoilers

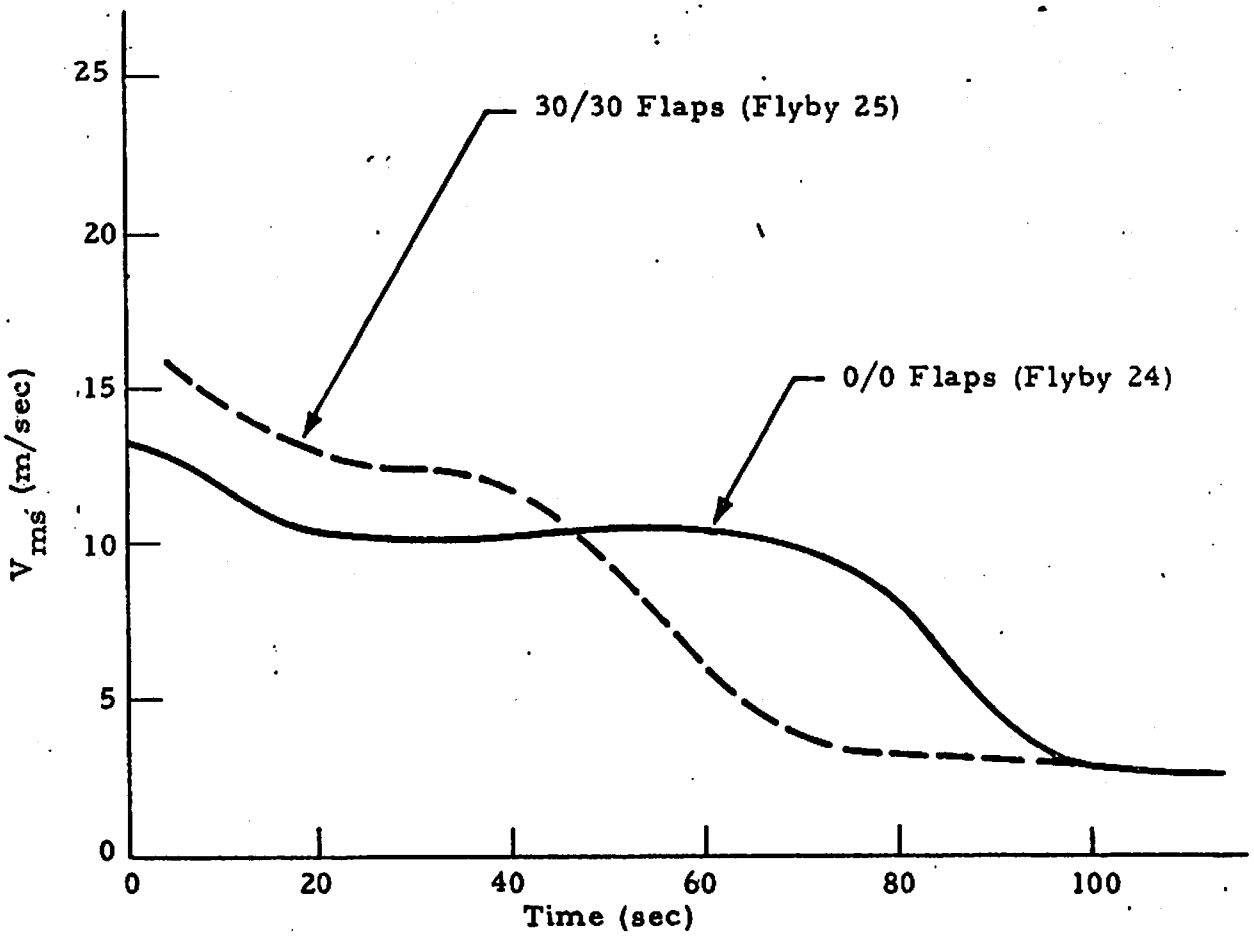

Fig. 34 - Comparison of Wake Vortex Rotational Velocity for B-747 Flyby With and Without Flaps

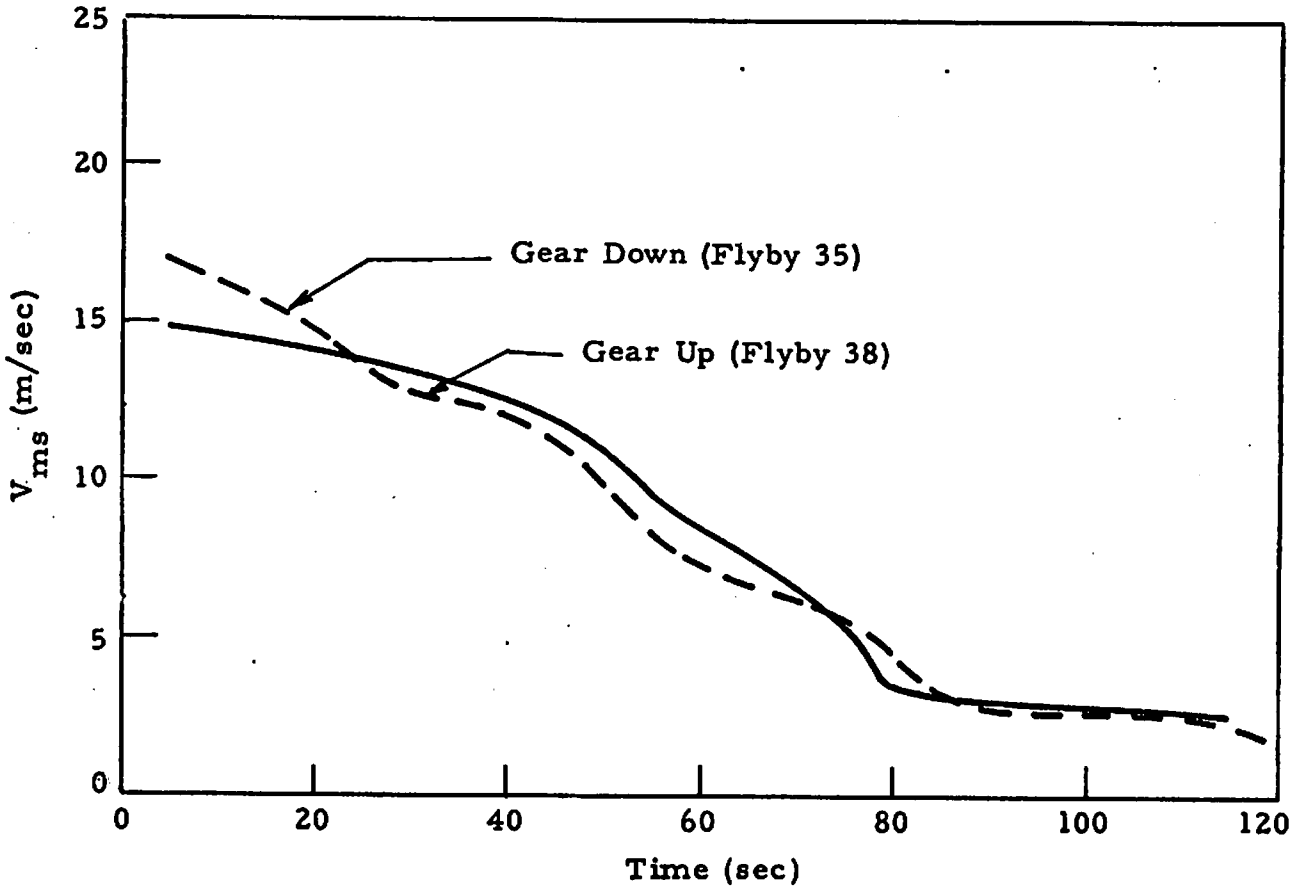

Fig. 35 - Comparison of Wake Vortex Rotational Velocity for B-747 Flybys With and Without Gear Down

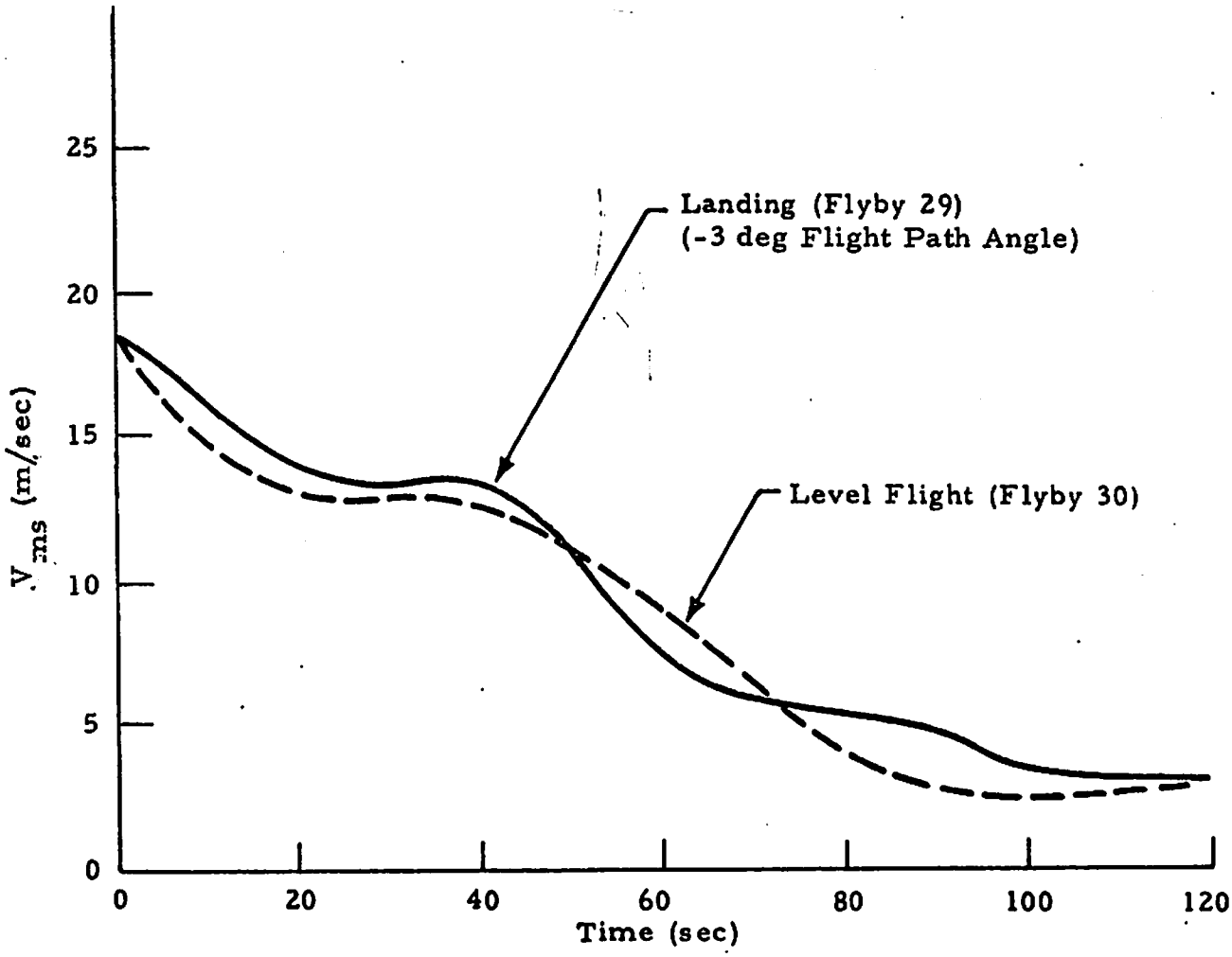

Fig. 36 - Comparison of Wake Vortex Rotational Velocity for B-747 in Level Flight and in Descending Flight

5. CONCLUSIONS

Laser Doppler velocimeter measurements of the wake vortex characteristics of a B-747 aircraft in various configurations have shown the following trends.

For vortex formation:

1. The rollup of the vortex sheet occurred rapidly within a few spans downstream of the aircraft.
2. The observed location, spacing, and strength of the multiple vortices were in general agreement with theoretical rollup calculations.
3. The peak tangential velocity and circulation of the merged vortices remained nearly constant in the near wake.
4. The B-747 spoilers affected the vortices, producing vortices with large cores.

For vortex transport:

1. The wake vortices descended vertically with little horizontal motion.

For vortex decay:

1. A decrease in the peak tangential velocity and circulation and an increase in the core radius was observed in the far wake.
2. Deployment of spoilers and flaps enhanced the vortex peak tangential velocity decay process in the near wake.

It is recommended that the existing capabilities of the LDV system be extended and additional wake vortex surveys conducted of full-scale aircraft to continue the wake vortex decay surveys initiated under this program.

REFERENCES

1. Krause, M. C. et al., "Development of Theory and Experiments to Improve Understanding of Laser Doppler Systems — Final Report;" LMSC-HREC TR D306632, Lockheed Missiles & Space Company, Hunsville, Ala., June 1973.
2. Wilson, D. J. et al., "Development and Testing of Laser Doppler System Components for Wake Vortex Monitoring — Volume I — Scanner Development, Laboratory and Field Testing and System Modeling," LMSC-HREC TR D390159-I, Lockheed Missiles & Space Company, Huntsville, Ala., August 1974.
3. Lawrence, T. R. et al., "Application of a Laser Velocimeter for Remote Wind Velocity and Turbulence Measurements," Proceedings of the International Conference on Aerospace and Aeronautical Meteorology, 22-26 May 1972, Washington, D. C. (published by the American Meteorological Society).
4. Brashears, M. R., T. R. Lawrence and A. D. Zalay, "Mobile Laser Doppler System Check Out and Calibration," LMSC-HREC TR D497036, Lockheed Missiles & Space Company, Huntsville, Ala., September 1976.
5. Garodz, L. J., David M. Lawrence and Nelson J. Miller, "Measurement of the Trailing Vortex Systems of Large Transport Aircraft, Using Tower Flyby and Flow Visualization," FAA-RD-75-127, January 1976.
6. Bilbro, J. W. et al., "Laser Doppler Velocimeter Wake Vortex Tests," FAA-RD-76-11 (also NASA TM X 64988), March 1976.
7. Hoffman, E. R., and P. M. Joubert, "Turbulent Line Vortices," J. Fluid Mech., Vol. 16, Part 3, July 1963, pp. 395-411.
8. Snedeker, R. S., and A. J. Bilanin, "Analysis of the Vortex Wakes of the Boeing 727, Lockheed L-1011, McDonnell Douglas DC-10, and Boeing 747 Aircraft," ARAP Report No. 245, July 1975.
9. Brashears, M. R. et al., "Analysis of Predicted Aircraft Wake Vortex Transport and Comparison with Experiment," FAA-RD-74-74, April 1974.

Appendix A

MVU EXTERNAL LOGS FOR ROSAMOND TESTS

Location: Rosamond Dry Lake
Date: 12/2/15 - Day 1
Sheet 1 of 2

Van X Position Ref. Pt. _____
Van Y Position Ref. Pt. Center of RW

Runway Azimuth: _____
Mirror Azimuth for Switch _____

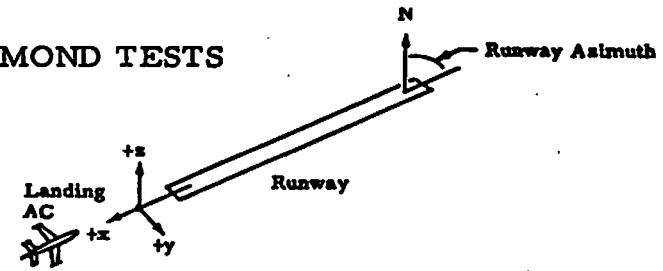

Run ID		Spectrum Analyzer						Scanner						Computer		Time		Estimated Wind Azimuth (from)	azimuth 42° is normal to runway. Comments
				Freq. Span (MHz)				Range			Elevation								
No.	AC Type or VAD	B.W. (kHz)	Log Lin	Min.	f_c	Max.	Rate (msec)	Max.	Min.	Rate	Max.	Min.	Rate	Tape No.	No. Records	Start	Stop		
1	VAD	10	LN	0	2cm.	.5	1							DRY01		6:05:00	6:49:30	est. from North	alt. @ 31,46,61,76,91,122,
																			244, 488 @ 1 Rev/alt.
2	VAD															6:50:00	6:59:00		same alt.
3	AC 1	30		1	0	2		57			63°15	3	.1kg			7:04:14	7:06:06		
4	AC 2	100		1		6							.5kg			7:09:37	7:11:25		
5	AC 3															7:15:04	7:17:17		
6	AC 4			0	1cm	5		60								7:20:49	7:22:53		
7	AC 5							118			63	20				7:25:56	7:27:40		Time mark on sight; act horiz AV going 5-10° past 90°
8	AC 6	30						118			63	03				7:31:07	7:33:25		
9	AC 7										63	30				7:35:53	7:37:42		Run stop-comp. halt; Gen. fail; Processor run number 6 till No. 6
10	AC 8							240			63	21				7:40:39	7:42:46		azimuth 180° + 42° (= 222°)
11	VAD	10		0		.5	1									7:50:00	7:58:00		Same alt. as run 1. Sync. clock 07:56:00 Our clock 07:56:05
12	AC 9	30		0	1/2cm	5		58			63	03	.5			8:12:49	8:15:17		222° azimuth
13	AC 10							120			63	15				8:18:08	8:19:56		
14	AC 11							183			63	25				8:23:37	8:25:39		
15	AC 12							240			62	35				8:29:21	8:31:31		
16	AC 13							57			62	03				8:35:07	8:36:34		
17	AC 14							57								8:40:30	8:42:50		Precisely in middle for 1st min (or longer) / Analog tape run out this run.
18	AC 15							57								8:46:06	8:48:19		
19	AC 16							68								8:51:47	8:53:41		Range, 68 m; Az. at 42°; Amplitude threshold not changed.
20	VAD	10		0	1.3cm	.5										8:58:00	9:07:02	Act. from north	same alt. as run 1.
21	AC 17	30		0	.6cm	5		35			62	03				9:32:12	9:33:32		Az. 42°. Corrected time code this run.
22	AC 18															9:37:44	9:38:50		repeat of previous run (run 17)
23	AC 18															9:42:16	9:43:09		

Appendix A (Continued)

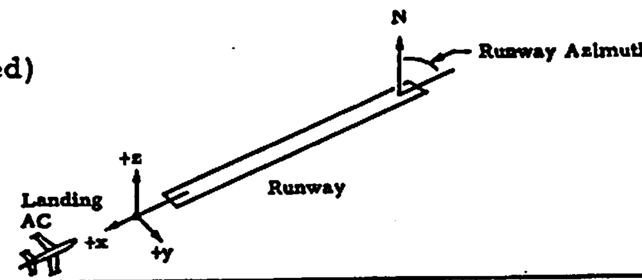

Location: Rosamond Dry Lake
Date: 12/2/75 - Day 1
Sheet 2 of 2

Van X Position: ______
Ref. Pt. ______
Van Y Position: ______
Ref. Pt. Center of RW

Runway Azimuth: ______
Mirror Azimuth for Switch ______

Run ID		Spectrum Analyzer						Scanner						Computer		Time		Estimated Wind Azimuth (from)	Comments
				Freq. Span (MHz)				Range			Elevation								
No.	AC Type or VAD	B.W. (kHz)	Log/Lin	Min.	f_c	Max.	Rate (msec)	Max.	Min.	Rate	Max.	Min.	Rate	Tape No.	No. Records	Start	Stop		
24	AC 19	30		0	.6cm	5		63			62	03				9:46:21	9:48:22		
25	AC 20							63								9:50:58	9:52:33		
26	AC 21							90								9:55:08	9:57:53		Good Run. Vortices over van – high velocities
27	AC 22																		*4 see NFO
28	VAD	10		0	1¼cm	.5										10:03	11:12	st. from north	same alt. as run 1.
																			* NOTE: 3rd SORTIE aborted due to
																			hydraulic problem on 747.

Appendix (Continued)

Location: Roosevelt Dry Lake
Date: 12/3/75 - Day 2
Sheet 1 of 2

Van X Position: Ref. Pt. _____
Van Y Position: Ref. Pt. 200' N of RW

Runway Azimuth: _____
Mirror Azimuth for Switch _____

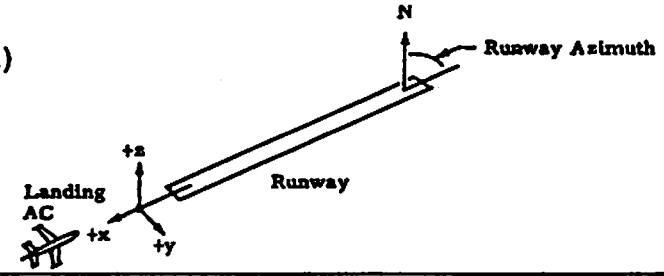

Run ID		Spectrum Analyzer						Scanner						Computer		Time		Estimated Wind Azimuth (from)	Comments
				Freq. Span (MHz)				Range			Elevation								
No.	AC Type or VAD	B.W. (kHz)	Log Lin	Min.	f_c	Max.	Rate (msec)	Max.	Min.	Rate	Max.	Min.	Rate	Tape No.	No. Records	Start	Stop		
1	VAD	10	Lin	0	2cm.	.5	1							D6902		6:29	6:35	est. from switch	alt. at 31, 46, 61, 76, 91, 122, 244, 488 at 1 rev./alt,
2	AC 23	30		0	1cm	5	1	190	35	3.5	63	10	.2			6:55:06	6:57:03		processor run no. not updated for
3	AC 24															6:59:04	7:01:12		run 3 (AC run 24)
4	AC 25															7:03:32	7:05:38		
5	AC 26															7:07:47	7:10:01		
6	AC 27										95	17				7:12:33	7:14:41		
7	AC 28										40	17				7:16:50	7:18:58		
8	AC 29															7:21:23	7:23:37		
9	AC 30										45	17				7:25:17	7:27:18		
10	VAD	10		0	2cm	.5										7:31	7:39		alt. same as run 1.
11	AC 31	30		0	.8cm	5		190	35	3.5	45	17	.2			7:56:09	1:58:30		pilot cone is at 350 ft. instead of 200.
12	AC 32															8:00:47	8:04:11		elev. scanner turned up prior to this run but turned
13	AC 33										55	30				8:06:09	8:08:16		to work ok. before run started.
14	AC 34															8:11:02	8:12:44		Run AC 33 : pilot cone in at 210 ft. Also,
15	AC 35															8:15:44	8:17:59		Mel switch run no. on processor to 34
16	AC 36															8:20:07	8:22:43		during runs.
17	AC 37															8:25:17	8:27:19		Run AC 35 : Analog tape run not this run.
18	AC 38															8:30:30	8:32:35		Run AC 36 : Lost CPU power during
																			run 36. Plug to mainframe pulled out.
																			noticed at 8:22:30. Also, our
																			time "mark" and AV "mark" not
																			synchronous for run 36.
19	VAD	10		0	1.5cm	.5										8:34	8:46		alt. same as run 1.

Appendix A (Concluded)

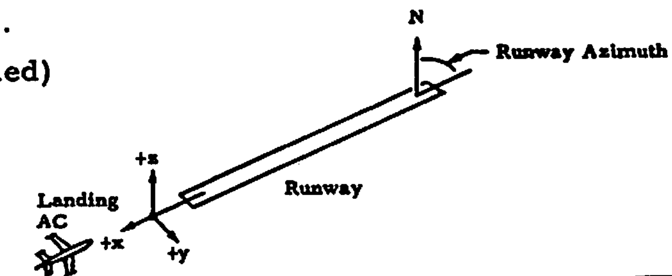

Location: Rosamond Dry Lake Date: 12/3/75 - Day 2 Sheet 2 of 2

Van X Position: Ref. Pt. ______

Van Y Position: Ref. Pt. 200' N of RW

Runway Azimuth: ______

Mirror Azimuth for Switch ______

Run ID		Spectrum Analyzer						Scanner						Computer		Time		Estimated Wind Azimuth (from)	Comments
				Freq. Span (MHz)				Range			Elevation								
No.	AC Type or VAD	B.W. (kHz)	Log / Lin	Min.	f_c	Max.	Rate (msec)	Max.	Min.	Rate	Max.	Min.	Rate	Tape No.	No. Records	Start	Stop		
20	AC 39	30	Lin	0	.6cm	5	1	140	35	3.5			.2			9:01:11	9:02:39	W. from N.W.	
21	AC 40										55	23				9:06:52	9:08:57		
22	AC 41															9:12:36	9:14:34		
23	AC 42															9:18:06	9:20:26		
24	AC 43							150	35							9:23:37	9:26:24		
25	AC 44							160	35							9:28:40	9:30:55		
26	AC 45															9:33:57	9:36:46		
27	AC 46							180	35							9:39:09	9:42:11		
28	VAD	10		0	2cm	.5										9:44	9:52		alt. same as run 1. (sheet 1)
29	AC 47	30		0	.8cm	5		140	35	3.5	63	23	.2			10:10:37	10:13:11		
30	AC 48							160	35							10:15:13	10:17:17		wind from south, both vortices drift toward van.
31	AC 49															10:20:26	10:23:10		interesting run, 180 ft. stdy. dust storms, vortices, etc. by van.
32	AC 50							140	35							10:24:49	10:27:44		Rotated scan 180° at 10:25:47
33	AC 51															10:29:31	10:32:13		Rotated scan 90° @ 10:30:46 (aft)
34	AC 52															10:33:37	10:36:26		Rotated scan forward 90° @ 10:35:00
35	AC 53															10:37:50	10:41:50		Rotated scan aft 90° @ 10:38:58; rotated 90° @ 10:39:55
36	AC 54															10:41:59	10:46:56		Rotated scan aft 90° @ 10:43:29
																			NOTE: AC Run 53: picked up vortices at 10:39:16 after 1st rotation.
37	VAD	10		0	2cm	.5										10:49:20	10:54:15		alt. same as run 1. (sheet 1)

NOTES: TIME CHECK @ END OF SORTIE 4

OUR TIME	AV TIME
10:46:13	10:48:10

Range checkout after runs O.K.

Appendix B

SAMPLE OUTPUT FROM VAD AND VORTEX TRACKER PROGRAM FOR ROSAMOND FLYBY 25

Page B-2 indicates the relative intensity (INTENSITY) and V_{ms} (SPEED (ft/sec)) of the LDV signal as a function of time and space for one sweep between the minimum and maximum elevation angle setting in the finger-scan mode. A list of the data sorted according to INTENSITY is given on page B-3 followed by the list of the values selected for determining the vortex location on page B-4. A "scatter plot" showing the location of the intensity points in units of ft and their relative magnitude (on a scale of A – O) is given on page B-5 along with the selected center of the two correlation circles (labeled Z) and the centroid of the correlation circles (the vortex locations labeled P and S for port and starboard, respectively). On page B-6 the points used in determining the vortex location are listed. The data are printed out on pages B-7 - B-12 and B-13 - B-17 for two other sample scans during flyby 25. A summary of the port and vortex starboard locations from each of the scans is given on pages B-18 through B-20. The vortex trajectories are displayed on the last two pages of Appendix B including time versus lateral displacement of the vortices (page B-21) and time versus vertical location as a function of time (page B-22).

TIME OF SWEEP START = 3.272 SEC.
TIME OF SWEEP END = 4.841 SEC.
MID TIME OF SWEEP = 4.056 SEC.

IP	TIME	RANGE	ANGLE	YP	ZP	DELTA TIME	C WIND	SPEED	IFREQ	INTENSITY
1	3.272	386.2	62.6	22.1	349.7	.784	.00	15.65	18	256
2	3.287	359.2	62.3	33.2	325.7	.769	.00	13.04	15	190
3	3.302	326.9	62.0	46.3	295.6	.754	.00	16.52	19	158
4	3.317	293.8	61.8	61.0	265.8	.740	.00	18.26	21	200
5	3.332	259.7	61.6	76.3	235.4	.725	.00	19.13	22	112
6	3.451	267.6	59.5	64.4	237.4	.605	.00	23.47	27	126
7	3.466	291.0	59.3	51.6	257.3	.590	.00	13.04	15	126
8	3.496	350.1	58.8	18.4	306.4	.560	.00	16.52	19	124
9	3.511	380.4	58.6	1.6	331.6	.545	.00	13.91	16	128
10	3.541	437.9	58.1	-31.6	378.4	.515	.00	27.82	32	124
11	3.795	319.1	53.9	12.0	264.8	.261	.00	20.87	24	126
12	3.810	341.7	53.6	-2.8	281.9	.247	.00	8.69	10	148
13	3.825	376.4	53.4	-24.6	309.1	.232	.00	16.52	19	158
14	3.855	432.6	52.9	-61.2	351.9	.202	.00	29.56	34	126
15	3.869	434.6	52.5	-64.4	351.8	.187	.00	35.65	41	124
16	3.884	418.5	52.3	-55.7	338.3	.172	.00	23.47	27	144
17	3.899	391.2	52.1	-40.1	315.8	.157	.00	26.95	31	166
18	3.914	360.5	51.8	-22.8	290.4	.142	.00	39.99	46	112
19	3.929	331.7	51.5	-6.4	266.7	.127	.00	35.65	41	126
20	3.944	310.2	51.4	6.3	249.4	.112	.00	10.43	12	126
21	3.959	274.4	51.2	27.9	220.7	.097	.00	15.65	18	120
22	3.974	240.0	51.0	46.8	193.4	.082	.00	16.52	19	128
23	4.079	262.2	49.1	28.3	205.1	-.022	.00	46.95	54	184
24	4.094	292.1	48.9	8.0	227.1	-.037	.00	46.08	53	220
25	4.109	322.0	48.6	-13.1	248.4	-.052	.00	50.43	58	256
26	4.123	348.1	48.3	-31.6	266.9	-.067	.00	42.60	49	256
27	4.138	375.3	48.1	-50.5	286.4	-.082	.00	36.52	42	192
28	4.153	402.2	47.9	-69.5	305.4	-.097	.00	30.43	35	280
29	4.168	434.0	47.7	-91.9	328.9	-.112	.00	26.08	30	318
30	4.183	438.8	47.4	-97.2	329.8	-.127	.00	13.04	15	320
31	4.198	425.8	47.2	-89.4	319.1	-.142	.00	9.56	11	190
32	4.213	401.4	47.0	-73.9	300.6	-.157	.00	9.56	11	192
33	4.228	371.4	46.7	-54.6	277.4	-.172	.00	29.56	34	222
34	4.243	348.9	46.6	-39.9	260.4	-.187	.00	7.82	9	320
35	4.258	308.0	46.1	-13.5	229.0	-.202	.00	33.04	38	164
36	4.273	277.6	45.9	7.0	206.5	-.217	.00	24.34	28	168
37	4.467	393.9	42.8	-89.2	274.4	-.411	.00	17.39	20	158
38	4.482	420.7	42.6	-109.9	291.5	-.426	.00	20.87	24	128
39	4.497	438.9	42.3	-124.5	302.6	-.441	.00	16.52	19	174
40	4.512	427.5	42.0	-117.9	292.8	-.456	.00	17.39	20	128
41	4.527	406.9	41.8	-103.5	278.0	-.471	.00	16.52	19	192
42	4.781	384.1	37.6	-104.4	241.9	-.725	.00	8.69	10	128
43	4.796	409.6	37.4	-125.5	255.7	-.740	.00	8.69	10	118
44	4.811	437.7	37.2	-148.8	271.1	-.754	.00	9.56	11	196
45	4.826	435.6	36.8	-148.9	267.8	-.769	.00	8.69	10	190
46	4.841	414.7	36.6	-133.0	254.1	-.784	.00	8.69	10	174

ORDER	VELOCITY	INTENSITY
1	25	30
2	23	34
3	24	29
4	26	28
5	18	1

6	27	25
7	15	26
8	19	33
9	35	24
10	28	4
11	14	44
12	33	27
13	10	32
14	17	41
15	29	2
16	36	31
17	6	45
18	16	23
19	11	39
20	38	46
21	5	36
22	4	17
23	37	35
24	40	3
25	3	13
26	8	37
27	13	12
28	22	16
29	39	9
30	41	22
31	1	38
32	21	40
33	9	42
34	2	6
35	7	7
36	30	11
37	20	14
38	31	19
39	32	20
40	44	8
41	12	10
42	42	15
43	43	21
44	45	43
45	46	5
46	34	18

II	II3	N1	N2	R2
30	29	2	2	30.15
30	28	3	3	1355.06
30	32	4	4	1405.40
30	41	5	5	2727.48
30	31	6	6	171.75
30	39	7	7	1492.69
30	17	8	8	3453.66
30	37	9	9	3134.18
30	16	10	10	1796.11
30	38	11	11	1633.05
30	40	12	12	1798.91
30	14	13	13	1782.36
30	15	14	14	1556.26

KV = 1 JJJ = 30 YC = -81.6 ZC = 316.6

II	III	N1	N2	R2
24	23	2	2	897.96
24	36	3	3	425.12
24	35	4	4	463.56
24	12	5	5	3123.12
24	22	6	6	2803.32
24	6	7	7	3296.32
24	7	8	8	2819.10
24	11	9	9	1438.20
24	19	10	10	1772.64
24	20	11	11	499.09
24	21	12	12	440.48

KV = 2 JJJ = 24 YC = 15.2 ZC = 229.4

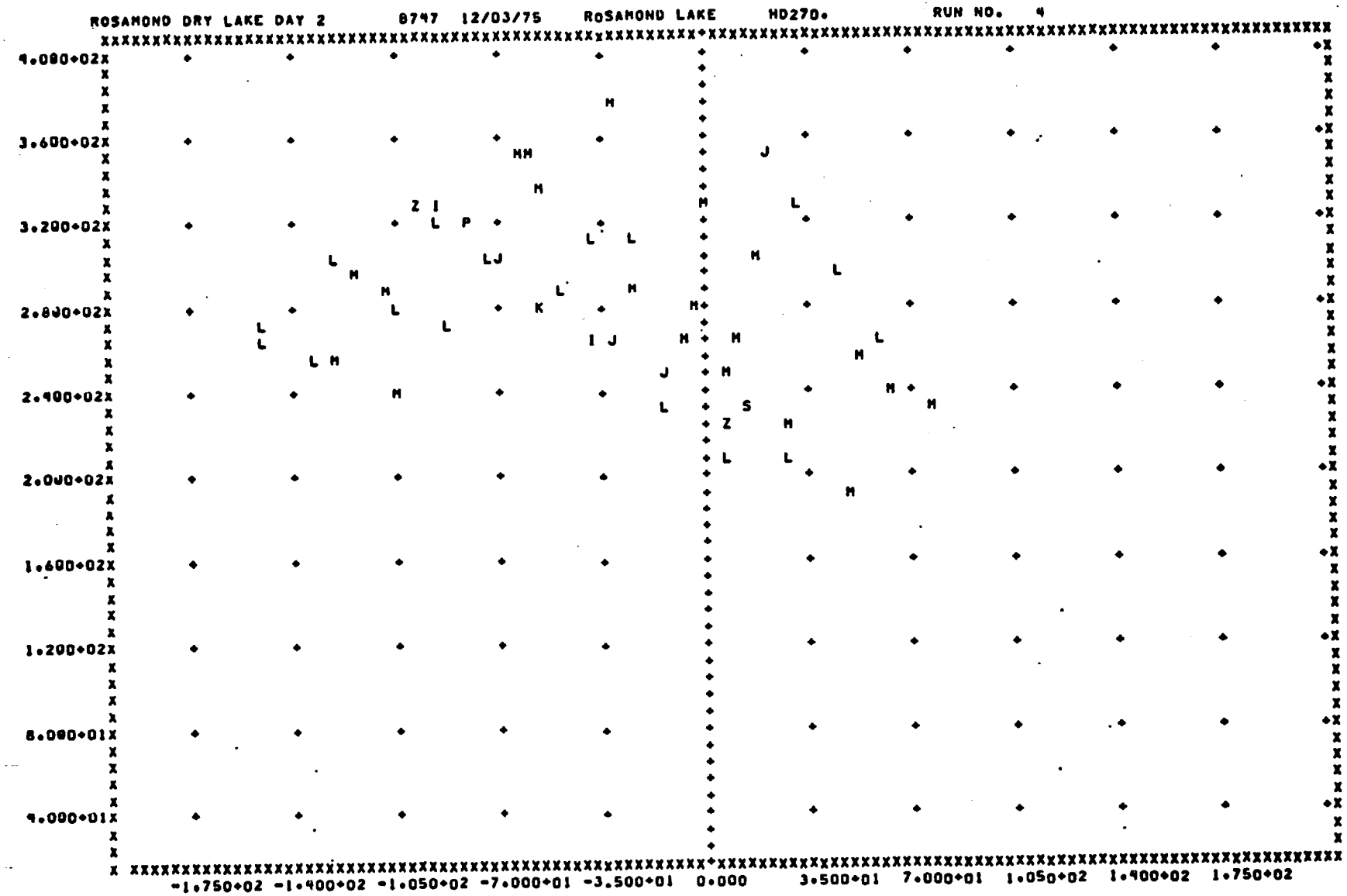
ROSAMOND DRY LAKE DAY 2 8747 12/03/75 ROSAMOND LAKE HD270. RUN NO. 4
4.000+02
3.600+02
3.200+02
2.800+02
2.400+02
2.000+02
1.600+02
1.200+02
8.000+01
4.000+01
-1.750+02 -1.400+02 -1.050+02 -7.000+01 -3.500+01 0.000 3.500+01 7.000+01 1.050+02 1.400+02 1.750+02
O=0-5 N=5-10 M=10-15 L=15-20 K=20-25 J=25-30 I=30-35 H=35-40 G=40-45 F=45-50 E=50-55 D=55-60 C=60-65 B=65-70 A=70-
NPHV= 1 KD= 239 RANGEP= 432.80 ANGLEP= 44.42 NSAMPL= 9 RANGEI= 434.71 RANGEN= 414.37
NPHV= 2 KD= 241 RANGEP= 388.45 ANGLEP= 44.84 NSAMPL= 9 RANGEI= 391.08 RANGEN= 361.88
NPHV= 3 KD= 243 RANGEP= 326.44 ANGLEP= 45.42 NSAMPL= 9 RANGEI= 329.40 RANGEN= 296.59

NPHV=	4	KD=	244	RANGEP=	293.44	ANGLEP=	45.62	NSAMPL=	10	RANGEI=	296.59	RANGEN=	265.09
NPHV=	5	KD=	256	RANGEP=	351.49	ANGLEP=	48.62	NSAMPL=	11	RANGEI=	347.77	RANGEN=	381.56
NPHV=	6	KD=	258	RANGEP=	407.88	ANGLEP=	49.05	NSAMPL=	13	RANGEI=	403.87	RANGEN=	434.71
NPHV=	7	KD=	259	RANGEP=	435.10	ANGLEP=	49.43	NSAMPL=	13	RANGEI=	434.71	RANGEN=	437.66
NPHV=	8	KD=	260	RANGEP=	435.54	ANGLEP=	49.62	NSAMPL=	12	RANGEI=	437.66	RANGEN=	419.95
NPHV=	9	KD=	261	RANGEP=	416.27	ANGLEP=	49.83	NSAMPL=	14	RANGEI=	419.95	RANGEN=	393.70
NPHV=	10	KD=	264	RANGEP=	332.55	ANGLEP=	50.62	NSAMPL=	12	RANGEI=	336.29	RANGEN=	305.12
NPHV=	11	KD=	275	RANGEP=	291.67	ANGLEP=	53.30	NSAMPL=	26	RANGEI=	283.14	RANGEN=	315.94
NPHV=	12	KD=	277	RANGEP=	345.14	ANGLEP=	53.82	NSAMPL=	10	RANGEI=	341.86	RANGEN=	374.67
NPHV=	13	KD=	278	RANGEP=	381.86	ANGLEP=	54.06	NSAMPL=	30	RANGEI=	374.67	RANGEN=	398.62
NPHV=	14	KD=	279	RANGEP=	408.18	ANGLEP=	54.33	NSAMPL=	32	RANGEI=	398.62	RANGEN=	428.48
NPHV=	15	KD=	280	RANGEP=	438.03	ANGLEP=	54.73	NSAMPL=	32	RANGEI=	428.48	RANGEN=	428.48
NPHV=	16	KD=	1	RANGEP=	435.45	ANGLEP=	54.87	NSAMPL=	35	RANGEI=	440.62	RANGEN=	425.85
NPHV=	17	KD=	2	RANGEP=	416.75	ANGLEP=	55.07	NSAMPL=	37	RANGEI=	425.85	RANGEN=	401.25
NPHV=	18	KD=	3	RANGEP=	390.35	ANGLEP=	55.28	NSAMPL=	41	RANGEI=	401.25	RANGEN=	374.67
NPHV=	19	KD=	4	RANGEP=	360.89	ANGLEP=	55.57	NSAMPL=	42	RANGEI=	374.67	RANGEN=	341.86
NPHV=	20	KD=	5	RANGEP=	329.96	ANGLEP=	55.88	NSAMPL=	39	RANGEI=	341.86	RANGEN=	311.35
NPHV=	21	KD=	6	RANGEP=	297.67	ANGLEP=	56.09	NSAMPL=	43	RANGEI=	311.35	RANGEN=	279.53
NPHV=	22	KD=	7	RANGEP=	272.57	ANGLEP=	56.24	NSAMPL=	21	RANGEI=	279.53	RANGEN=	246.39
NPHV=	23	KD=	17	RANGEP=	287.93	ANGLEP=	58.54	NSAMPL=	35	RANGEI=	276.90	RANGEN=	308.40
NPHV=	24	KD=	18	RANGEP=	320.95	ANGLEP=	58.89	NSAMPL=	45	RANGEI=	308.40	RANGEN=	336.29
NPHV=	25	KD=	19	RANGEP=	351.24	ANGLEP=	59.09	NSAMPL=	47	RANGEI=	336.29	RANGEN=	368.11
NPHV=	26	KD=	20	RANGEP=	375.79	ANGLEP=	59.26	NSAMPL=	30	RANGEI=	368.11	RANGEN=	393.70
NPHV=	27	KD=	21	RANGEP=	405.09	ANGLEP=	59.48	NSAMPL=	39	RANGEI=	393.70	RANGEN=	422.90
NPHV=	28	KD=	22	RANGEP=	430.70	ANGLEP=	59.78	NSAMPL=	44	RANGEI=	422.90	RANGEN=	440.62
NPHV=	29	KD=	23	RANGEP=	436.37	ANGLEP=	60.07	NSAMPL=	35	RANGEI=	440.62	RANGEN=	428.48
NPHV=	30	KD=	24	RANGEP=	419.37	ANGLEP=	60.27	NSAMPL=	37	RANGEI=	428.48	RANGEN=	403.87
NPHV=	31	KD=	25	RANGEP=	395.17	ANGLEP=	60.48	NSAMPL=	39	RANGEI=	403.87	RANGEN=	381.56
NPHV=	32	KD=	26	RANGEP=	370.74	ANGLEP=	60.74	NSAMPL=	34	RANGEI=	381.56	RANGEN=	349.74
NPHV=	33	KD=	27	RANGEP=	339.06	ANGLEP=	61.07	NSAMPL=	35	RANGEI=	349.74	RANGEN=	319.23
NPHV=	34	KD=	28	RANGEP=	305.17	ANGLEP=	61.28	NSAMPL=	42	RANGEI=	319.23	RANGEN=	285.76
NPHV=	35	KD=	29	RANGEP=	273.09	ANGLEP=	61.48	NSAMPL=	39	RANGEI=	285.76	RANGEN=	253.28

TIME OF SWEEP START = 23.516 SEC.
TIME OF SWEEP END = 25.114 SEC.
MID TIME OF SWEEP = 24.315 SEC.

IP	TIME	RANGE	ANGLE	YP	ZP	DELTA TIME	C WIND	SPEED	IFREQ	INTENSITY
1	23.516	378.9	36.8	-103.2	234.1	.799	.00	7.82	9	148
2	23.770	392.6	40.8	-97.1	263.7	.545	.00	13.04	15	144
3	23.799	440.0	41.2	-130.8	297.1	.515	.00	9.56	11	128
4	23.844	381.9	42.0	-83.7	262.7	.471	.00	13.04	15	112
5	23.889	288.2	42.8	-11.4	203.0	.426	.00	18.26	21	126
6	24.024	273.4	45.1	6.9	200.5	.291	.00	23.47	27	126
7	24.053	333.0	45.5	-33.3	244.4	.261	.00	26.08	30	208
8	24.068	361.0	45.9	-51.4	266.1	.247	.00	28.69	33	128
9	24.083	392.0	46.1	-72.0	289.3	.232	.00	31.30	36	188
10	24.098	416.2	46.3	-87.7	307.7	.217	.00	26.95	31	158
11	24.113	437.7	46.6	-100.8	324.9	.202	.00	39.99	46	348
12	24.128	432.2	46.9	-95.5	322.3	.187	.00	23.47	27	318
13	24.143	405.5	47.1	-76.1	304.0	.172	.00	39.12	45	256
14	24.158	381.2	47.3	-58.6	287.1	.157	.00	33.91	39	152
15	24.173	353.0	47.6	-38.2	267.4	.142	.00	35.65	41	156
16	24.188	324.6	47.9	-17.8	247.7	.127	.00	26.95	31	128
17	24.203	297.1	48.0	1.3	227.9	.112	.00	13.04	15	128
18	24.337	267.1	50.3	29.2	212.4	-.022	.00	25.21	29	126
19	24.352	299.5	50.5	9.4	236.0	-.037	.00	35.65	41	128
20	24.367	327.3	50.7	-7.2	260.4	-.052	.00	28.69	33	136
21	24.382	348.5	51.0	-19.2	277.9	-.067	.00	12.17	14	192
22	24.397	381.6	51.2	-38.9	304.6	-.082	.00	16.52	19	200
23	24.412	412.0	51.5	-56.7	329.2	-.097	.00	27.82	32	256
24	24.427	436.5	51.7	-70.4	349.7	-.112	.00	26.95	31	256
25	24.442	435.1	52.1	-67.5	350.7	-.127	.00	26.95	31	192
26	24.457	414.8	52.3	-53.9	335.0	-.142	.00	26.08	30	358
27	24.472	389.6	52.5	-37.4	315.9	-.157	.00	23.47	27	254
28	24.487	364.3	52.6	-21.0	296.4	-.172	.00	21.74	25	160
29	24.502	333.5	52.9	-1.2	273.0	-.187	.00	19.13	22	232
30	24.517	301.9	53.2	19.4	248.9	-.202	.00	20.00	23	192
31	24.531	266.4	53.5	41.4	221.0	-.217	.00	23.47	27	224
32	24.546	234.3	53.6	61.1	195.7	-.232	.00	18.26	21	126
33	24.636	225.3	55.2	71.5	192.1	-.321	.00	18.26	21	126
34	24.651	259.4	55.5	52.9	220.4	-.336	.00	22.60	26	118
35	24.666	283.5	55.6	39.9	241.0	-.351	.00	10.43	12	136
36	24.681	317.0	55.8	21.9	269.3	-.366	.00	13.91	16	172
37	24.711	375.5	56.4	-7.6	319.9	-.396	.00	17.39	20	352
38	24.726	402.2	56.6	-21.2	342.9	-.411	.00	16.52	19	128
39	24.741	430.7	56.8	-35.6	367.6	-.426	.00	15.65	18	192
40	24.771	424.1	57.4	-28.3	364.4	-.456	.00	13.91	16	200
41	24.785	397.1	57.6	-12.6	342.4	-.471	.00	14.78	17	238
42	24.800	372.9	57.8	1.4	322.4	-.486	.00	11.30	13	112
43	24.815	341.0	58.1	19.6	296.4	-.500	.00	13.91	16	126
44	24.830	310.4	58.4	37.5	271.4	-.515	.00	14.78	17	126
45	24.845	278.4	58.6	55.1	244.7	-.530	.00	12.17	14	124
46	24.950	217.7	60.3	92.0	196.0	-.635	.00	13.04	15	176
47	24.965	251.3	60.6	76.8	226.0	-.650	.00	19.13	22	160
48	24.980	279.7	60.8	63.7	251.2	-.665	.00	12.17	14	126
49	24.995	311.9	61.0	49.0	279.9	-.680	.00	20.00	23	318
50	25.010	340.8	61.3	36.3	305.9	-.695	.00	18.26	21	190
51	25.024	369.0	61.6	24.7	331.7	-.710	.00	16.52	19	152
52	25.039	396.3	61.8	13.0	356.4	-.725	.00	15.65	18	126
53	25.054	424.0	62.0	1.2	381.6	-.740	.00	14.78	17	190

54	25.069	441.8	62.3	-5.6	398.0	-.754	.00	19.78	17	158
55	25.099	401.7	62.8	16.4	364.1	-.784	.00	18.26	21	190
56	25.114	376.6	62.8	27.6	341.8	-.799	.00	20.87	24	126

ORDER	VELOCITY	INTENSITY
1	11	26
2	13	37
3	15	11
4	19	12
5	14	49
6	9	13
7	8	23
8	20	24
9	23	27
10	10	41
11	16	29
12	24	31
13	25	7
14	7	22
15	26	40
16	18	21
17	6	25
18	12	30
19	27	39
20	31	50
21	34	53
22	28	55
23	56	9
24	30	46
25	49	36
26	29	28
27	47	47
28	5	10
29	32	54
30	33	15
31	50	14
32	55	51
33	37	1
34	22	2
35	38	20
36	51	35
37	39	3
38	52	8
39	41	16
40	44	17
41	53	19
42	54	38
43	36	5
44	40	6
45	43	18
46	2	32
47	4	33
48	17	43
49	46	44
50	21	48
51	45	52
52	48	56

53	42	45
54	35	34
55	3	4
56	1	42

I1	I13	N1	N2	R2
26	37	2	2	2373.59
26	11	3	3	2301.73
26	12	4	4	1895.58
26	13	5	5	1456.54
26	23	6	6	41.24
26	24	7	7	487.28
26	27	8	8	637.40
26	41	9	9	1761.82
26	22	10	10	1155.79
26	40	11	11	1518.96
26	25	12	12	414.05
26	39	13	13	1389.64
26	9	14	14	2415.77
26	28	15	15	2556.46
26	10	16	16	1891.93
26	14	17	17	2324.26
26	38	18	18	1133.86
26	42	19	19	3215.43

KV = 1 JJJ = 26 YC = -60.9 ZC = 323.2

I1	I13	N1	N2	R2
31	30	2	2	1260.28
31	46	3	3	3191.45
31	36	4	4	2711.50
31	47	5	5	1280.65
31	35	6	6	402.96
31	17	7	7	1655.47
31	19	8	8	1310.45
31	5	9	9	3104.77
31	6	10	10	1611.90
31	18	11	11	221.90
31	32	12	12	1029.38
31	33	13	13	1742.47
31	44	14	14	2559.26
31	48	15	15	1410.64
31	45	16	16	749.01
31	34	17	17	133.03

KV = 2 JJJ = 31 YC = 37.2 ZC = 225.8

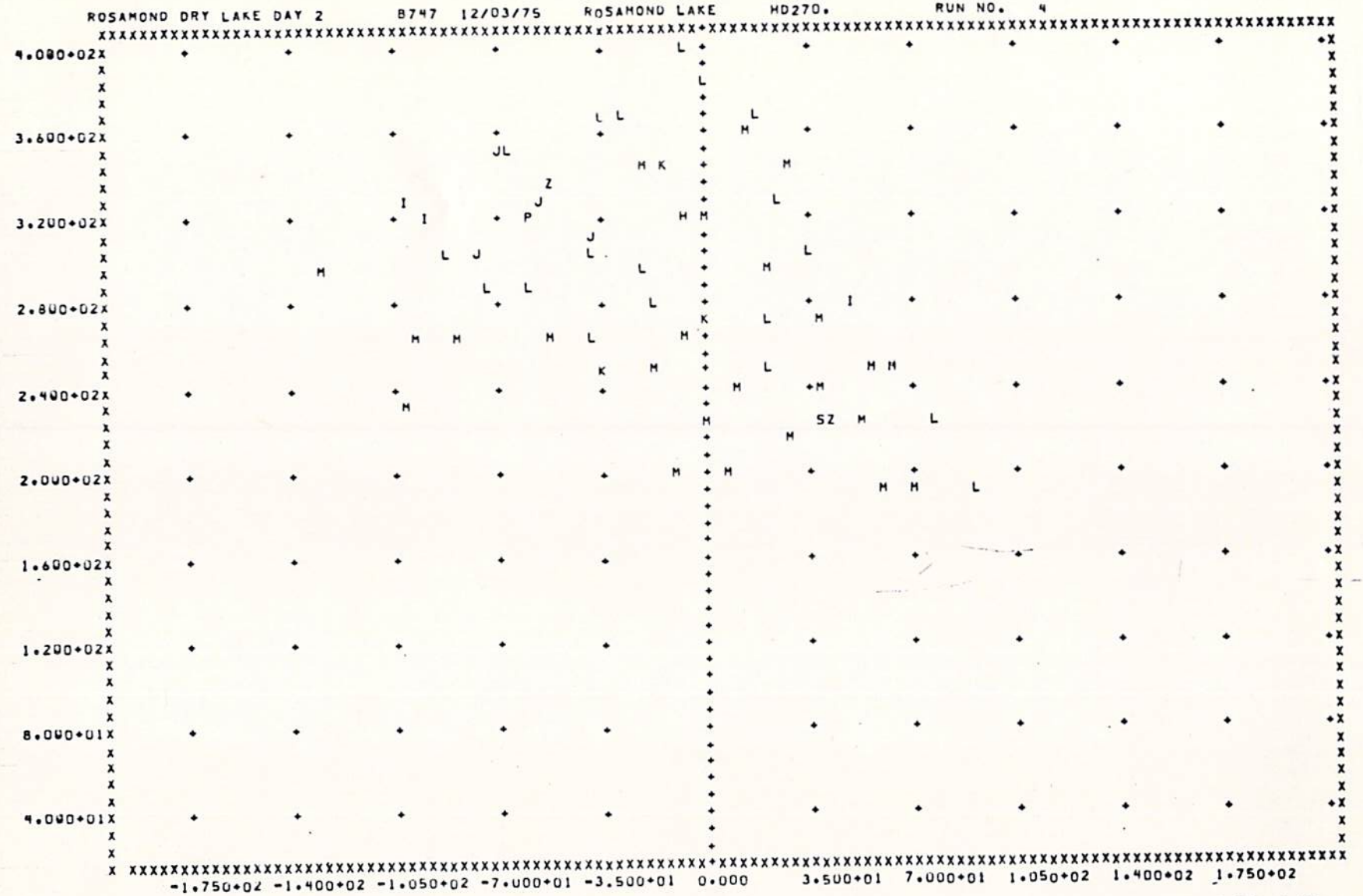
ROSAMOND DRY LAKE DAY 2 8747 12/03/75 ROSAMOND LAKE HD270. RUN NO. 4
4.000+02
3.600+02
3.200+02
2.800+02
2.400+02
2.000+02
1.600+02
1.200+02
8.000+01
4.000+01
-1.750+02 -1.400+02 -1.050+02 -7.000+01 -3.500+01 0.000 3.500+01 7.000+01 1.050+02 1.400+02 1.750+02
0=0-5 N=5-10 M=10-15 L=15-20 K=20-25 J=25-30 I=30-35 H=35-40 G=40-45 F=45-50 E=50-55 D=55-60 C=60-65 B=65-70 A=70-
NPHV= 1 KD= 276 RANGEP= 346.19 ANGLEP= 62.55 NSAMPL= 24 RANGEI= 353.67 RANGEN= 322.51
NPHV= 2 KD= 277 RANGEP= 314.30 ANGLEP= 62.30 NSAMPL= 25 RANGEI= 322.51 RANGEN= 289.70
NPHV= 3 KD= 278 RANGEP= 281.08 ANGLEP= 61.95 NSAMPL= 26 RANGEI= 289.70 RANGEN= 256.56

NPHV=	4	KD= 279	RANGEP=	249.61	ANGLEP=	61.76	NSAMPL= 20	RANGEI=	256.56	RANGEN=	221.78
NPHV=	5	KD= 280	RANGEP=	214.83	ANGLEP=	61.56	NSAMPL= 20	RANGEI=	221.78	RANGEN=	221.78
NPHV=	6	KD= 5	RANGEP=	209.80	ANGLEP=	60.37	NSAMPL= 13	RANGEI=	205.71	RANGEN=	237.20
NPHV=	7	KD= 6	RANGEP=	245.00	ANGLEP=	60.10	NSAMPL= 24	RANGEI=	237.20	RANGEN=	269.69
NPHV=	8	KD= 7	RANGEP=	278.56	ANGLEP=	59.73	NSAMPL= 33	RANGEI=	269.69	RANGEN=	296.59
NPHV=	9	KD= 8	RANGEP=	305.63	ANGLEP=	59.54	NSAMPL= 29	RANGEI=	296.59	RANGEN=	327.76
NPHV=	10	KD= 9	RANGEP=	335.79	ANGLEP=	59.34	NSAMPL= 31	RANGEI=	327.76	RANGEN=	353.67
NPHV=	11	KD= 10	RANGEP=	361.82	ANGLEP=	59.09	NSAMPL= 27	RANGEI=	353.67	RANGEN=	383.86
NPHV=	12	KD= 11	RANGEP=	391.95	ANGLEP=	58.74	NSAMPL= 29	RANGEI=	383.86	RANGEN=	411.75
NPHV=	13	KD= 12	RANGEP=	420.04	ANGLEP=	58.54	NSAMPL= 32	RANGEI=	411.75	RANGEN=	437.66
NPHV=	14	KD= 15	RANGEP=	403.30	ANGLEP=	57.73	NSAMPL= 33	RANGEI=	411.75	RANGEN=	386.15
NPHV=	15	KD= 16	RANGEP=	376.45	ANGLEP=	57.53	NSAMPL= 34	RANGEI=	386.15	RANGEN=	357.61
NPHV=	16	KD= 17	RANGEP=	347.46	ANGLEP=	57.33	NSAMPL= 34	RANGEI=	357.61	RANGEN=	327.76
NPHV=	17	KD= 18	RANGEP=	318.99	ANGLEP=	57.15	NSAMPL= 27	RANGEI=	327.76	RANGEN=	295.28
NPHV=	18	KD= 19	RANGEP=	283.56	ANGLEP=	56.86	NSAMPL= 35	RANGEI=	295.28	RANGEN=	261.81
NPHV=	19	KD= 20	RANGEP=	250.89	ANGLEP=	56.54	NSAMPL= 32	RANGEI=	261.81	RANGEN=	227.69
NPHV=	20	KD= 21	RANGEP=	217.85	ANGLEP=	56.34	NSAMPL= 30	RANGEI=	227.69	RANGEN=	194.88
NPHV=	21	KD= 26	RANGEP=	207.05	ANGLEP=	55.15	NSAMPL= 24	RANGEI=	199.80	RANGEN=	229.99
NPHV=	22	KD= 27	RANGEP=	240.91	ANGLEP=	54.87	NSAMPL= 32	RANGEI=	229.99	RANGEN=	264.11
NPHV=	23	KD= 28	RANGEP=	269.99	ANGLEP=	54.55	NSAMPL= 23	RANGEI=	264.11	RANGEN=	289.70
NPHV=	24	KD= 30	RANGEP=	300.20	ANGLEP=	54.34	NSAMPL= 32	RANGEI=	289.70	RANGEN=	322.51
NPHV=	25	KD= 31	RANGEP=	330.09	ANGLEP=	54.14	NSAMPL= 30	RANGEI=	322.51	RANGEN=	347.77
NPHV=	26	KD= 32	RANGEP=	358.24	ANGLEP=	53.88	NSAMPL= 31	RANGEI=	347.77	RANGEN=	381.56
NPHV=	27	KD= 33	RANGEP=	388.25	ANGLEP=	53.54	NSAMPL= 30	RANGEI=	381.56	RANGEN=	403.87
NPHV=	28	KD= 34	RANGEP=	411.56	ANGLEP=	53.35	NSAMPL= 25	RANGEI=	403.87	RANGEN=	434.71
NPHV=	29	KD= 35	RANGEP=	434.71	ANGLEP=	53.14	NSAMPL= 31	RANGEI=	434.71	RANGEN=	434.71
NPHV=	30	KD= 37	RANGEP=	409.97	ANGLEP=	52.69	NSAMPL= 28	RANGEI=	417.32	RANGEN=	391.08
NPHV=	31	KD= 38	RANGEP=	384.00	ANGLEP=	52.34	NSAMPL= 28	RANGEI=	391.08	RANGEN=	365.81
NPHV=	32	KD= 39	RANGEP=	357.71	ANGLEP=	52.15	NSAMPL= 26	RANGEI=	365.81	RANGEN=	334.65
NPHV=	33	KD= 40	RANGEP=	326.20	ANGLEP=	51.95	NSAMPL= 26	RANGEI=	334.65	RANGEN=	302.17
NPHV=	34	KD= 41	RANGEP=	293.72	ANGLEP=	51.70	NSAMPL= 26	RANGEI=	302.17	RANGEN=	269.69
NPHV=	35	KD= 42	RANGEP=	260.98	ANGLEP=	51.35	NSAMPL= 26	RANGEI=	269.69	RANGEN=	236.22
NPHV=	36	KD= 43	RANGEP=	228.27	ANGLEP=	51.15	NSAMPL= 24	RANGEI=	236.22	RANGEN=	203.08
NPHV=	37	KD= 49	RANGEP=	229.23	ANGLEP=	49.73	NSAMPL= 17	RANGEI=	223.43	RANGEN=	257.55
NPHV=	38	KD= 50	RANGEP=	263.43	ANGLEP=	49.35	NSAMPL= 23	RANGEI=	257.55	RANGEN=	283.14
NPHV=	39	KD= 51	RANGEP=	290.68	ANGLEP=	49.15	NSAMPL= 23	RANGEI=	263.14	RANGEN=	315.94
NPHV=	40	KD= 52	RANGEP=	321.53	ANGLEP=	48.95	NSAMPL= 23	RANGEI=	315.94	RANGEN=	340.22
NPHV=	41	KD= 53	RANGEP=	346.42	ANGLEP=	48.76	NSAMPL= 18	RANGEI=	340.22	RANGEN=	374.67
NPHV=	42	KD= 54	RANGEP=	379.46	ANGLEP=	48.52	NSAMPL= 20	RANGEI=	374.67	RANGEN=	398.62
NPHV=	43	KD= 55	RANGEP=	406.17	ANGLEP=	48.15	NSAMPL= 23	RANGEI=	398.62	RANGEN=	431.43
NPHV=	44	KD= 59	RANGEP=	392.37	ANGLEP=	47.17	NSAMPL= 17	RANGEI=	396.00	RANGEN=	374.67
NPHV=	45	KD= 60	RANGEP=	369.50	ANGLEP=	46.97	NSAMPL= 15	RANGEI=	374.67	RANGEN=	340.22
NPHV=	46	KD= 61	RANGEP=	334.73	ANGLEP=	46.76	NSAMPL= 18	RANGEI=	340.22	RANGEN=	309.71
NPHV=	47	KD= 62	RANGEP=	304.25	ANGLEP=	46.54	NSAMPL= 16	RANGEI=	309.71	RANGEN=	275.59
NPHV=	48	KD= 63	RANGEP=	270.77	ANGLEP=	46.17	NSAMPL= 15	RANGEI=	275.59	RANGEN=	243.44
NPHV=	49	KD= 64	RANGEP=	238.08	ANGLEP=	45.97	NSAMPL= 16	RANGEI=	243.44	RANGEN=	209.97
NPHV=	50	KD= 65	RANGEP=	204.57	ANGLEP=	45.77	NSAMPL= 16	RANGEI=	209.97	RANGEN=	176.18
NPHV=	51	KD= 69	RANGEP=	191.67	ANGLEP=	44.76	NSAMPL= 20	RANGEI=	185.04	RANGEN=	218.18
NPHV=	52	KD= 70	RANGEP=	223.48	ANGLEP=	44.57	NSAMPL= 16	RANGEI=	218.18	RANGEN=	251.31
NPHV=	53	KD= 71	RANGEP=	256.67	ANGLEP=	44.32	NSAMPL= 19	RANGEI=	251.31	RANGEN=	279.53
NPHV=	54	KD= 72	RANGEP=	284.06	ANGLEP=	43.97	NSAMPL= 15	RANGEI=	279.53	RANGEN=	309.71
NPHV=	55	KD= 73	RANGEP=	315.03	ANGLEP=	43.76	NSAMPL= 20	RANGEI=	309.71	RANGEN=	336.29
NPHV=	56	KD= 74	RANGEP=	341.40	ANGLEP=	43.57	NSAMPL= 15	RANGEI=	336.29	RANGEN=	370.41
NPHV=	57	KD= 75	RANGEP=	375.07	ANGLEP=	43.32	NSAMPL= 20	RANGEI=	370.41	RANGEN=	393.70
NPHV=	58	KD= 76	RANGEP=	399.81	ANGLEP=	42.96	NSAMPL= 19	RANGEI=	393.70	RANGEN=	425.85
NPHV=	59	KD= 77	RANGEP=	428.81	ANGLEP=	42.76	NSAMPL= 20	RANGEI=	425.85	RANGEN=	440.62
NPHV=	60	KD= 78	RANGEP=	437.37	ANGLEP=	42.56	NSAMPL= 22	RANGEI=	440.62	RANGEN=	425.85

NPHV= 81	KD= 79	RANGEP=	420.44	ANGLEP=	42.36	NSAMPL= 22	RANGEI=	425.85	RANGEN=	401.25
NPHV= 82	KD= 80	RANGEP=	395.97	ANGLEP=	42.10	NSAMPL= 24	RANGEI=	401.25	RANGEN=	379.27
NPHV= 83	KD= 81	RANGEP=	372.97	ANGLEP=	41.76	NSAMPL= 20	RANGEI=	379.27	RANGEN=	347.77
NPHV= 84	KD= 82	RANGEP=	342.03	ANGLEP=	41.56	NSAMPL= 19	RANGEI=	347.77	RANGEN=	317.59
NPHV= 85	KD= 83	RANGEP=	311.38	ANGLEP=	41.36	NSAMPL= 18	RANGEI=	317.59	RANGEN=	283.14
NPHV= 86	KD= 84	RANGEP=	276.57	ANGLEP=	41.12	NSAMPL= 20	RANGEI=	283.14	RANGEN=	250.33
NPHV= 87	KD= 85	RANGEP=	243.91	ANGLEP=	40.76	NSAMPL= 19	RANGEI=	250.33	RANGEN=	216.54
NPHV= 88	KD= 86	RANGEP=	212.85	ANGLEP=	40.58	NSAMPL= 11	RANGEI=	216.54	RANGEN=	183.07
NPHV= 89	KD= 92	RANGEP=	252.79	ANGLEP=	39.08	NSAMPL= 30	RANGEI=	243.44	RANGEN=	274.61
NPHV= 90	KD= 93	RANGEP=	282.60	ANGLEP=	38.74	NSAMPL= 29	RANGEI=	274.61	RANGEN=	302.17
NPHV= 91	KD= 94	RANGEP=	311.42	ANGLEP=	38.54	NSAMPL= 30	RANGEI=	302.17	RANGEN=	333.01
NPHV= 92	KD= 95	RANGEP=	342.53	ANGLEP=	38.33	NSAMPL= 33	RANGEI=	333.01	RANGEN=	361.88
NPHV= 93	KD= 96	RANGEP=	372.10	ANGLEP=	38.13	NSAMPL= 35	RANGEI=	361.88	RANGEN=	391.08
NPHV= 94	KD= 97	RANGEP=	401.05	ANGLEP=	37.85	NSAMPL= 38	RANGEI=	391.08	RANGEN=	417.32
NPHV= 95	KD= 98	RANGEP=	423.38	ANGLEP=	37.55	NSAMPL= 26	RANGEI=	417.32	RANGEN=	440.62
NPHV= 96	KD= 99	RANGEP=	436.25	ANGLEP=	37.33	NSAMPL= 36	RANGEI=	440.62	RANGEN=	428.48
NPHV= 97	KD= 100	RANGEP=	419.57	ANGLEP=	37.11	NSAMPL= 46	RANGEI=	428.48	RANGEN=	409.12
NPHV= 98	KD= 101	RANGEP=	399.77	ANGLEP=	36.85	NSAMPL= 37	RANGEI=	409.12	RANGEN=	383.86
NPHV= 99	KD= 102	RANGEP=	371.18	ANGLEP=	36.52	NSAMPL= 42	RANGEI=	383.86	RANGEN=	353.67
NPHV= 100	KD= 103	RANGEP=	349.54	ANGLEP=	36.37	NSAMPL= 14	RANGEI=	353.67	RANGEN=	324.15
NPHV= 101	KD= 105	RANGEP=	279.09	ANGLEP=	35.87	NSAMPL= 33	RANGEI=	289.70	RANGEN=	257.55
NPHV= 102	KD= 112	RANGEP=	219.44	ANGLEP=	34.11	NSAMPL= 45	RANGEI=	205.71	RANGEN=	236.22
NPHV= 83	KD= 113	RANGEP=	239.47	ANGLEP=	33.98	NSAMPL= 10	RANGEI=	236.22	RANGEN=	268.70
NPHV= 84	KD= 114	RANGEP=	280.13	ANGLEP=	33.63	NSAMPL= 43	RANGEI=	268.70	RANGEN=	295.28
NPHV= 85	KD= 115	RANGEP=	308.70	ANGLEP=	33.31	NSAMPL= 44	RANGEI=	295.26	RANGEN=	325.79
NPHV= 86	KD= 116	RANGEP=	336.66	ANGLEP=	33.12	NSAMPL= 39	RANGEI=	325.79	RANGEN=	353.67
NPHV= 87	KD= 117	RANGEP=	365.04	ANGLEP=	32.93	NSAMPL= 35	RANGEI=	353.67	RANGEN=	386.15
NPHV= 88	KD= 118	RANGEP=	391.53	ANGLEP=	32.72	NSAMPL= 21	RANGEI=	386.15	RANGEN=	411.75
NPHV= 89	KD= 119	RANGEP=	420.04	ANGLEP=	32.34	NSAMPL= 32	RANGEI=	411.75	RANGEN=	437.66
NPHV= 90	KD= 120	RANGEP=	436.69	ANGLEP=	32.13	NSAMPL= 33	RANGEI=	437.66	RANGEN=	434.71
NPHV= 91	KD= 121	RANGEP=	426.20	ANGLEP=	31.94	NSAMPL= 32	RANGEI=	434.71	RANGEN=	414.37
NPHV= 92	KD= 122	RANGEP=	409.48	ANGLEP=	31.72	NSAMPL= 21	RANGEI=	414.37	RANGEN=	391.08
NPHV= 93	KD= 124	RANGEP=	356.35	ANGLEP=	31.17	NSAMPL= 17	RANGEI=	361.88	RANGEN=	329.40
NPHV= 94	KD= 126	RANGEP=	292.69	ANGLEP=	30.78	NSAMPL= 12	RANGEI=	296.59	RANGEN=	264.11
NPHV= 95	KD= 136	RANGEP=	292.82	ANGLEP=	28.17	NSAMPL= 13	RANGEI=	288.39	RANGEN=	322.51
NPHV= 96	KD= 140	RANGEP=	408.19	ANGLEP=	27.17	NSAMPL= 14	RANGEI=	403.87	RANGEN=	434.71
NPHV= 97	KD= 141	RANGEP=	435.18	ANGLEP=	26.97	NSAMPL= 16	RANGEI=	434.71	RANGEN=	437.66
NPHV= 98	KD= 142	RANGEP=	435.01	ANGLEP=	26.77	NSAMPL= 15	RANGEI=	437.66	RANGEN=	419.95
NPHV= 99	KD= 143	RANGEP=	416.01	ANGLEP=	26.57	NSAMPL= 15	RANGEI=	419.95	RANGEN=	393.70
NPHV= 100	KD= 144	RANGEP=	390.89	ANGLEP=	26.36	NSAMPL= 11	RANGEI=	393.70	RANGEN=	368.11
NPHV= 101	KD= 145	RANGEP=	364.93	ANGLEP=	25.98	NSAMPL= 10	RANGEI=	368.11	RANGEN=	336.29
NPHV= 102	KD= 146	RANGEP=	332.39	ANGLEP=	25.78	NSAMPL= 12	RANGEI=	336.29	RANGEN=	303.81

TIME OF SWEEP START = 57.474 SEC.
TIME OF SWEEP END = 59.655 SEC.
MID TIME OF SWEEP = 58.565 SEC.

IP	TIME	RANGE	ANGLE	YP	ZP	DELTA TIME	C WIND	SPEED	IFREQ	INTENSITY
1	57.474	265.8	62.6	68.4	260.7	1.091	.00	10.43	12	254
2	57.489	253.5	62.4	82.5	231.A	1.076	.00	10.43	12	240
3	57.504	218.9	62.1	97.7	200.A	1.061	.00	11.30	13	174
4	57.519	184.9	61.8	112.6	169.9	1.046	.00	10.43	12	128
5	57.579	210.4	60.8	97.3	190.A	.986	.00	11.30	13	318
6	57.594	238.9	60.6	82.6	215.1	.971	.00	9.56	11	320
7	57.609	271.9	60.4	65.6	243.4	.956	.00	10.43	12	318
8	57.624	299.8	60.2	50.9	267.1	.941	.00	12.17	14	192
9	57.639	331.1	59.9	34.2	293.A	.926	.00	11.30	13	320
10	57.668	386.6	59.4	3.1	339.7	.896	.00	9.56	11	158
11	57.683	412.3	59.2	-11.2	361.0	.881	.00	9.56	11	124
12	57.758	354.0	58.0	12.1	307.1	.807	.00	10.43	12	112
13	57.773	323.5	57.6	26.5	280.1	.792	.00	11.30	13	224
14	57.788	290.9	57.4	43.1	252.0	.777	.00	12.17	14	222
15	57.803	260.0	57.2	59.1	225.5	.762	.00	10.43	12	240
16	57.818	225.9	57.0	76.8	196.4	.747	.00	10.43	12	160
17	57.833	192.1	56.6	94.2	167.3	.732	.00	10.43	12	190
18	57.892	202.4	55.8	86.1	174.3	.672	.00	9.56	11	124
19	57.907	232.8	55.4	67.7	198.A	.657	.00	11.30	13	256
20	57.922	266.1	55.2	48.0	225.5	.642	.00	11.30	13	288
21	57.937	292.1	55.0	32.3	246.9	.627	.00	9.56	11	238
22	57.952	325.3	54.8	12.3	272.7	.613	.00	9.56	11	200
23	57.982	383.7	54.2	-24.6	318.1	.583	.00	9.56	11	128
24	58.072	362.4	52.8	-19.2	295.A	.493	.00	9.56	11	144
25	58.087	331.1	52.6	-1.3	269.9	.478	.00	9.56	11	188
26	58.102	298.7	52.2	16.8	243.0	.463	.00	9.56	11	256
27	58.117	267.4	52.0	35.3	217.A	.448	.00	9.56	11	190
28	58.132	234.1	51.8	55.2	190.9	.433	.00	9.56	11	374
29	58.146	200.0	51.6	75.7	163.A	.418	.00	9.56	11	172
30	58.206	195.6	50.6	75.7	158.1	.359	.00	8.69	10	126
31	58.221	226.5	50.2	55.0	180.9	.344	.00	9.56	11	256
32	58.236	259.8	50.0	32.9	206.0	.329	.00	11.30	13	278
33	58.251	285.9	49.8	15.4	225.3	.314	.00	10.43	12	176
34	58.266	318.4	49.6	-6.5	249.3	.299	.00	8.69	10	142
35	58.281	344.7	49.2	-25.4	267.8	.284	.00	11.30	13	180
36	58.296	378.0	49.0	-48.1	292.7	.269	.00	12.17	14	144
37	58.311	401.6	48.8	-64.6	309.1	.254	.00	8.69	10	112
38	58.341	435.6	48.3	-89.5	332.5	.224	.00	12.17	14	128
39	58.371	394.1	47.8	-64.9	298.8	.194	.00	16.52	19	164
40	58.386	369.5	47.6	-49.3	279.7	.179	.00	13.04	15	152
41	58.400	335.6	47.3	-27.4	253.8	.164	.00	13.04	15	148
42	58.415	305.1	47.0	-8.2	230.0	.149	.00	12.17	14	152
43	58.430	273.8	46.8	12.5	206.5	.134	.00	8.69	10	254
44	58.445	242.0	46.6	33.7	182.8	.120	.00	8.69	10	432
45	58.535	220.4	45.2	44.6	163.3	.030	.00	8.69	10	128
46	58.550	252.1	44.8	21.1	184.A	.015	.00	8.69	10	128
47	58.565	280.4	44.6	.3	203.8	.000	.00	9.56	11	192
48	58.580	311.5	44.4	-22.6	224.8	-.015	.00	9.56	11	172
49	58.595	340.7	44.1	-44.5	244.3	-.030	.00	12.17	14	126
50	58.610	371.2	43.8	-68.0	263.8	-.045	.00	10.43	12	128
51	58.639	425.0	43.4	-108.9	298.9	-.075	.00	10.43	12	124
52	58.669	425.3	42.8	-112.2	295.8	-.105	.00	11.30	13	128
53	58.684	401.4	42.6	-95.6	278.A	-.120	.00	9.56	11	152

54	58.699	376.2	42.4	-77.9	260.6	-.134	.00	13.91	16	190
55	58.729	314.3	41.8	-34.4	216.4	-.164	.00	8.69	10	128
56	58.744	280.6	41.6	-9.9	193.7	-.179	.00	10.43	12	128
57	58.908	335.7	39.0	-61.0	218.1	-.344	.00	8.69	10	144
58	58.938	391.9	38.4	-107.2	250.3	-.373	.00	10.43	12	126
59	58.953	418.0	38.2	-128.6	265.4	-.388	.00	12.17	14	136
60	58.968	439.6	38.0	-146.6	277.4	-.403	.00	9.56	11	126
61	59.013	380.2	37.2	-102.9	236.7	-.448	.00	11.30	13	238
62	59.028	346.1	37.0	-78.2	216.9	-.463	.00	20.87	24	128
63	59.207	299.8	34.0	-48.6	174.6	-.642	.00	12.17	14	126
64	59.267	412.5	33.0	-146.1	231.6	-.702	.00	10.43	12	160
65	59.566	381.5	28.0	-136.9	186.0	-1.001	.00	8.69	10	128
66	59.581	404.6	27.8	-158.0	195.4	-1.016	.00	8.69	10	112
67	59.655	364.9	26.6	-126.4	170.3	-1.091	.00	8.69	10	192

ORDER	VELOCITY	INTENSITY
1	62	44
2	39	28
3	54	6
4	40	9
5	41	5
6	8	7
7	14	20
8	36	32
9	38	19
10	42	26
11	49	31
12	59	1
13	63	43
14	3	2
15	5	15
16	9	21
17	13	61
18	19	13
19	20	14
20	32	22
21	35	8
22	52	47
23	61	67
24	1	17
25	2	27
26	4	54
27	7	25
28	12	35
29	15	33
30	16	3
31	17	29
32	33	48
33	50	39
34	51	16
35	56	64
36	58	10
37	64	40
38	0	42
39	10	53
40	11	41
41	18	24

42	21	36
43	22	57
44	23	34
45	24	59
46	25	4
47	26	23
48	27	38
49	28	45
50	29	46
51	31	50
52	47	52
53	48	55
54	53	56
55	60	62
56	30	65
57	34	30
58	37	49
59	43	58
60	44	60
61	45	63
62	46	11
63	55	18
64	57	51
65	65	12
66	66	37
67	67	66

II	II3	N1	N2	R2
44	28	2	2	528.17
44	6	3	3	3443.30
44	20	4	4	2028.29
44	32	5	5	539.24
44	19	6	6	1408.77
44	31	7	7	456.58
44	43	8	8	1009.41
44	15	9	9	2470.52
44	47	10	10	1555.29
44	27	11	11	1216.85
44	33	12	12	2144.54
44	29	13	13	2129.46
44	16	14	14	2044.82
44	45	15	15	498.80
44	46	16	16	162.32
44	56	17	17	2007.23
44	30	18	18	2380.44
44	18	19	19	2824.32

KV = 1 JJJ = 44 YC = 46.4 ZC = 198.7

II	II3	N1	N2	R2
61	54	2	2	1190.72
61	64	3	3	1888.51
61	53	4	4	1807.21
61	57	5	5	2106.69
61	59	6	6	1481.17
61	50	7	7	1952.76

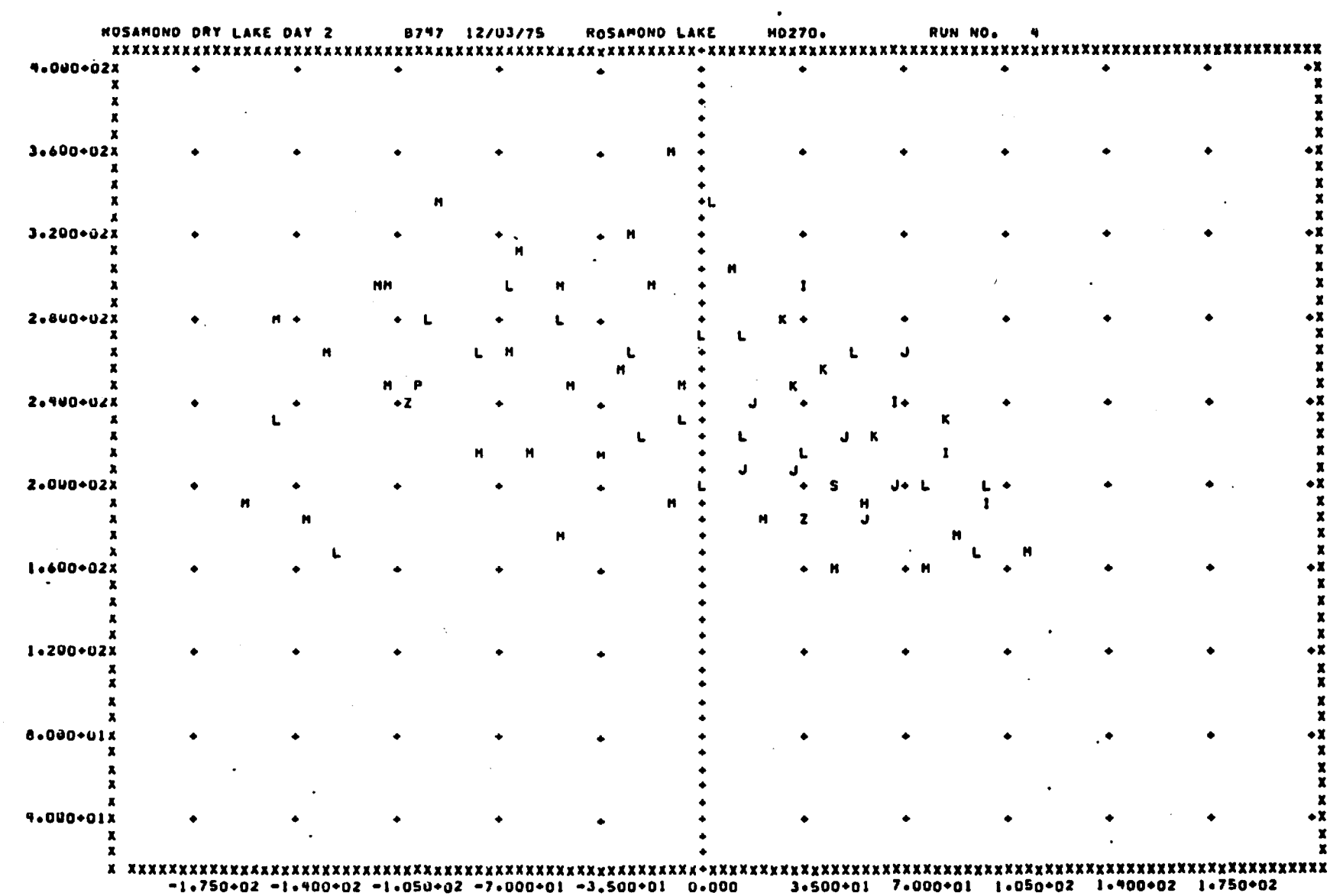
ROSAMOND DRY LAKE DAY 2 B747 12/03/75 ROSAMOND LAKE HD270. RUN NO. 4
4.000+02
3.600+02
3.200+02
2.800+02
2.400+02
2.000+02
1.600+02
1.200+02
8.000+01
4.000+01
-1.750+02 -1.400+02 -1.050+02 -7.000+01 -3.500+01 0.000 3.500+01 7.000+01 1.050+02 1.400+02 1.750+02
0=0-5 N=5-10 M=10-15 L=15-20 K=20-25 J=25-30 I=30-35 H=35-40 G=40-45 F=45-50 E=50-55 D=55-60 C=60-65 B=65-70 A=70-
NPHV= 1 KD= 174 RANGEP= 343.44 ANGLEP= 37.22 NSAMPL= 10 RANGEI= 340.22 RANGEN= 372.38
NPHV= 2 KD= 175 RANGEP= 375.21 ANGLEP= 37.42 NSAMPL= 12 RANGEI= 372.38 RANGEN= 396.00
NPHV= 3 KD= 181 RANGEP= 372.92 ANGLEP= 39.03 NSAMPL= 13 RANGEI= 376.97 RANGEN= 345.80

NPHV=	4	KD= 219	RANGEP=	538.75	ANGLEP=	48.56	NSAMPL= 12	RANGEI=	411.75	RANGEN=	1970.14
NPHV=	5	KD= 226	RANGEP=	337.17	ANGLEP=	60.22	NSAMPL= 10	RANGEI=	340.22	RANGEN=	309.71
NPHV=	6	KD= 227	RANGEP=	305.62	ANGLEP=	60.42	NSAMPL= 12	RANGEI=	309.71	RANGEN=	275.59
NPHV=	7	KD= 228	RANGEP=	271.84	ANGLEP=	60.62	NSAMPL= 11	RANGEI=	275.59	RANGEN=	241.47
NPHV=	8	KD= 229	RANGEP=	237.20	ANGLEP=	60.85	NSAMPL= 13	RANGEI=	241.47	RANGEN=	208.66
NPHV=	9	KD= 230	RANGEP=	204.94	ANGLEP=	61.22	NSAMPL= 11	RANGEI=	208.66	RANGEN=	174.87
NPHV=	10	KD= 235	RANGEP=	222.18	ANGLEP=	62.42	NSAMPL= 10	RANGEI=	218.83	RANGEN=	252.30
NPHV=	11	KD= 236	RANGEP=	255.02	ANGLEP=	62.62	NSAMPL= 10	RANGEI=	252.30	RANGEN=	279.53
NPHV=	12	KD= 237	RANGEP=	283.21	ANGLEP=	62.80	NSAMPL= 11	RANGEI=	279.53	RANGEN=	312.99
NPHV=	13	KD= 238	RANGEP=	315.52	ANGLEP=	62.78	NSAMPL= 10	RANGEI=	312.99	RANGEN=	338.25

ROSAMOND DRY LAKE DAY 2 8747 12/03/75

TIME IS 7: 3:50.

ROSAMOND LAKE HD270. RUN NO. 4

STARBOARD VORTEX

TIME	Z	Y
4.05621	260.652	44.1498
8.27676	260.229	38.5139
13.8568	212.365	47.6868
15.5002	278.173	6.46237
18.7123	271.046	36.3668
20.6620	257.905	26.2682
24.3148	224.413	55.0379
26.2645	177.873	46.3209
29.8949	259.492	26.9209
31.6056	171.146	59.0845
34.7579	230.324	46.7477
37.0064	220.007	5.36603
40.5472	241.469	61.3459
42.5118	244.896	40.6397
45.4176	230.303	52.5408
47.4121	192.493	60.0888
51.1471	205.975	83.2493
53.0743	192.320	58.7777
63.6145	233.186	37.4797
69.2095	220.445	35.1234

PORT VORTEX

TIME	Z	Y
4.05621	316.589	-81.6382
8.27676	357.333	-29.5650
13.8568	349.730	-34.7920
15.5002	258.296	-114.384
18.7123	323.249	-69.0965
20.6620	269.113	-123.139
24.3148	323.246	-60.4487
26.2645	273.360	14.0868
29.8949	323.499	-74.6053
31.6056	232.370	-37.9057
34.7579	334.106	-23.4391
37.0064	243.742	-125.949
40.5472	289.022	-84.2635
42.5118	258.368	-105.767
45.4176	318.621	-45.9242
47.4121	269.746	-97.0168
51.1471	354.548	-20.3668
53.0743	237.969	-126.092
63.6145	297.511	-90.3922
69.2095	308.295	-82.9007

UNKNOWN TYPE OF VORTEX

TIME	Z	Y
2.89089	286.775	31.5946
9.94257	297.216	-87.3446
56.5852	253.098	45.4470
58.5648	198.678	46.4100
61.9412	252.638	67.2202
67.1926	342.761	-.433675
73.0118	342.916	-59.9073
77.9868	296.564	-91.7344
80.8926	230.220	-141.526
89.0200	261.570	-43.6382
91.4552	235.385	-136.489
94.5179	262.498	-29.0438
96.8784	248.933	-124.571

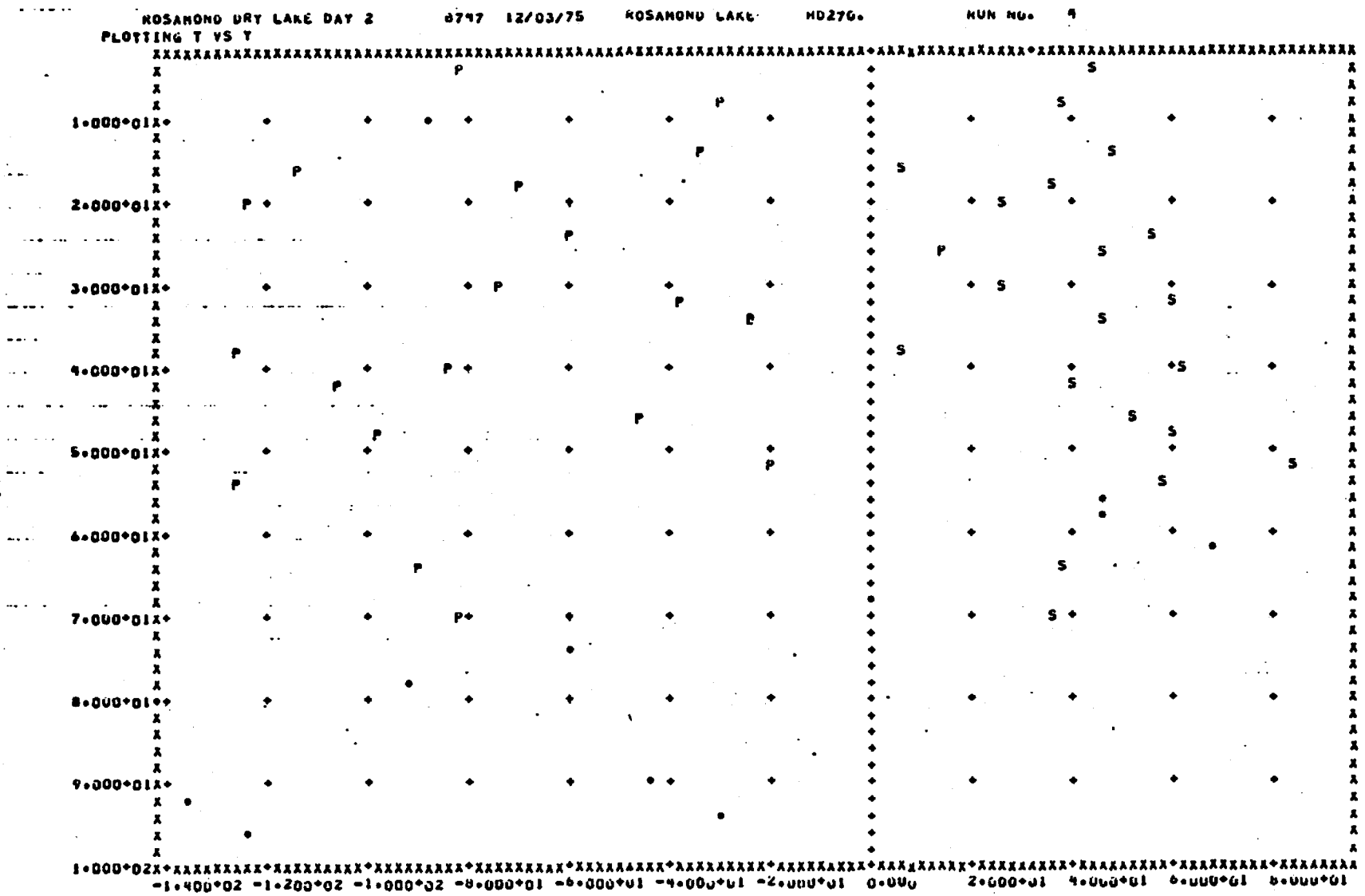

THE INTERPRETATION OF MEANINGLESS INPUT WAS ATTEMPTED.
THE FOLLOWING RECORD IS ERRONEOUS OR DOES NOT CORRESPOND TO FORMAT SPECIFICATIONS:

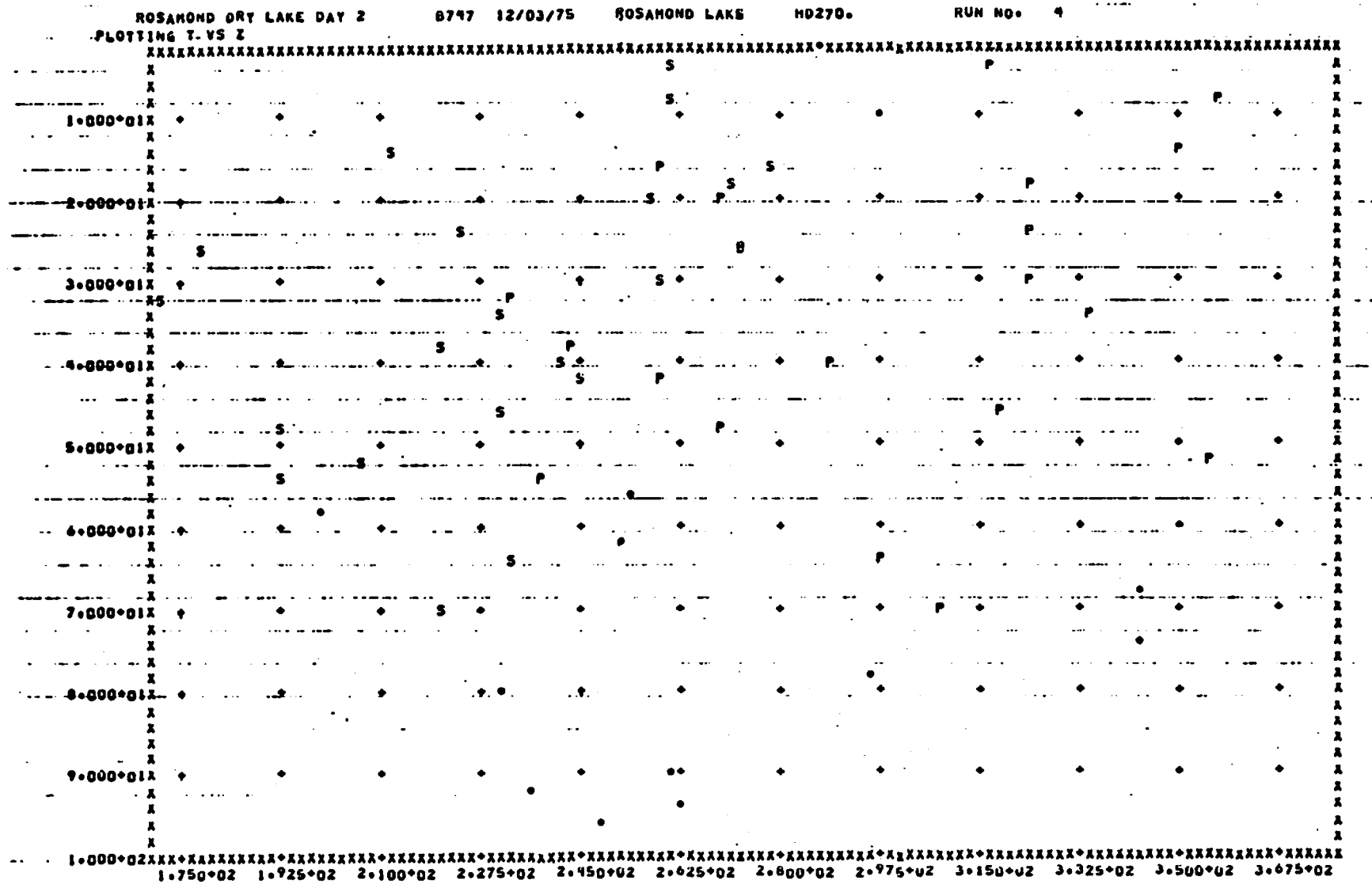
ROSAMOND DRY LAKE DAY 2 8747 12/03/75 ROSAMOND LAKE MD270. RUN NO. 4
PLOTTING T VS Z
1.000+01
2.000+01
3.000+01
4.000+01
5.000+01
6.000+01
7.000+01
8.000+01
9.000+01
1.000+02
1.750+02 1.925+02 2.100+02 2.275+02 2.450+02 2.625+02 2.800+02 2.975+02 3.150+02 3.325+02 3.500+02 3.675+02

Appendix C

SAMPLE OUTPUT FROM NASA-MSFC LDV DATA PROCESSING ROUTINES FOR ROSAMOND FLYBY 47

Results from the Rosamond high-speed data are given on page C-2 including a printout of the relative intensity of the LDV signal (IPEAK) and the frequency (or velocity) of the flow field including V_{ms} and V_{pk} in units of meters per second (VMAX and VPEAK, respectively). The sweep count from the start of the flyby is shown by the column labeled SCAN while the lateral and vertical location and range and elevation angle of the focal volume are given by X (m), Y (m), R (m) and T (deg), respectively. The time at which the LDV signal was sampled is contained in the frame count (1 FRAME = 1/500 sec).

From the array of LDV sample points illustrated on page C-2, plots of VPEAK versus the scan elevation angle in degrees, THETA, are generated as illustrated on pages C-3 - C-6. Note that the characteristic double peak signature of the wake vortex is evident in the sample plots.

Applying the "I_{pk}" algorithm (p. 4-7 of Ref. 7) to the threshold LDV spectrum illustrated above, the vortex location is determined. The vortex trajectory for flyby 47 as computed from the high speed data is shown on pages C-7 - C-9. On page C-7 the vertical and lateral motion of the vortices is given as a function of time, while page C-8 shows the altitude versus lateral position of the wake vortex. Page C-9 gives a listing of the vortex locations. For additional information regarding the vortex location, criteria and coefficients used in the "I_{pk}" algorithm and shown in the plots refer to Ref. 7.

Note that the coordinate system used in the NASA-MSFC data processing routines is not the same as the coordinate system used in the text earlier. The runway centerline is located at y = -200 ft in the NASA plots.

SCAN	FRAME	X	Y	R	T	IPEAK	VMAX	VPEAK	VAVG	VWIDTH
4	4150	219.4	245.0	328.9	48.2	127	9.8	10.9	9.0	8
4	4151	216.9	242.5	325.3	48.2	131	8.2	10.4	8.7	8
4	4152	218.8	240.0	324.7	47.7	134	8.2	10.9	8.8	8
4	4153	216.9	237.5	321.6	47.6	134	9.3	10.4	9.0	8
4	4154	208.7	235.0	314.3	48.4	123	10.4	10.9	9.1	8
4	4155	206.2	232.5	310.8	48.4	121	9.3	10.4	8.5	8
4	4156	208.1	229.4	309.7	47.8	121	10.4	10.4	8.8	8
4	4157	205.0	226.2	305.3	47.8	124	8.2	10.4	8.5	8
4	4158	196.9	223.7	298.0	48.7	118	8.2	10.4	8.2	8
4	4159	199.4	221.2	297.8	48.0	131	8.2	10.9	8.5	9
4	4160	196.9	217.5	293.4	47.8	136	7.1	10.4	8.0	9
4	4161	189.4	215.6	287.0	48.7	128	9.3	10.4	8.7	7
4	4162	186.2	212.5	282.6	48.8	125	9.3	10.9	9.4	8
4	4163	187.5	209.4	281.1	48.2	116	10.9	10.9	9.1	8
4	4164	185.6	206.9	277.9	48.1	123	8.7	10.9	8.8	5
4	4165	178.1	204.4	271.1	48.9	117	8.7	10.9	9.4	6
4	4166	179.4	201.2	269.6	48.3	111	7.1	10.4	7.8	4
4	4167	177.5	198.7	266.5	48.2	116	9.3	10.4	9.0	6
4	4168	169.4	195.6	258.8	49.1	118	9.3	9.8	8.8	5
4	4169	166.2	192.5	254.4	49.2	131	8.7	9.3	8.5	4
4	4170	169.4	190.6	255.9	48.4	119	8.7	10.9	8.8	4
4	4171	166.2	187.5	250.6	48.4	130	8.7	10.4	8.9	5
4	4172	158.7	185.0	243.8	49.4	126	8.7	8.7	8.3	3
4	4173	155.6	181.9	239.4	49.4	131	8.2	8.7	8.2	3
4	4174	158.1	179.4	239.1	48.6	136	8.2	10.4	8.5	5
4	4175	155.0	176.2	234.7	48.7	128	8.7	10.4	7.5	6
4	4176	147.5	173.1	227.4	49.6	129	8.7	9.8	8.1	5
4	4177	145.0	170.6	223.9	49.6	136	8.7	9.3	8.1	6
4	4178	146.9	168.1	223.2	48.9	120	8.2	8.7	7.5	5
4	4179	139.4	165.0	216.0	49.8	132	7.6	8.7	7.7	4
4	4180	136.2	161.9	211.6	49.9	134	8.2	9.3	8.0	5
4	4181	138.7	159.4	211.3	49.0	128	8.2	8.7	7.5	6
4	4182	136.2	156.3	207.3	48.9	130	8.2	8.7	8.4	2
4	4183	128.1	153.7	200.1	50.2	130	8.2	9.3	8.1	5
4	4184	126.2	151.2	197.0	50.1	117	9.3	9.3	8.5	5
4	4185	128.1	148.1	195.8	49.1	121	7.6	8.7	7.8	4
4	4186	125.6	145.0	191.9	49.1	116	6.0	9.3	7.3	5
4	4187	118.1	141.9	184.6	50.2	106	8.2	8.2	8.2	1
4	4188	115.0	139.4	180.7	50.5	115	8.2	8.7	8.2	2
4	4189	117.5	136.9	180.4	49.4					
4	4190	115.0	134.4	176.9	49.4					
4	4191	107.5	131.2	169.7	50.7					
4	4192	109.4	127.5	168.0	49.4					
4	4193	106.9	125.0	164.5	49.5					
4	4194	99.4	121.9	157.3	50.8					
4	4195	96.2	120.0	153.8	51.3					
4	4196	99.4	117.5	153.9	49.8					
4	4197	96.2	114.4	149.5	49.9					
4	4198	88.7	111.2	142.3	51.4					
4	4199	85.6	108.7	138.4	51.8					

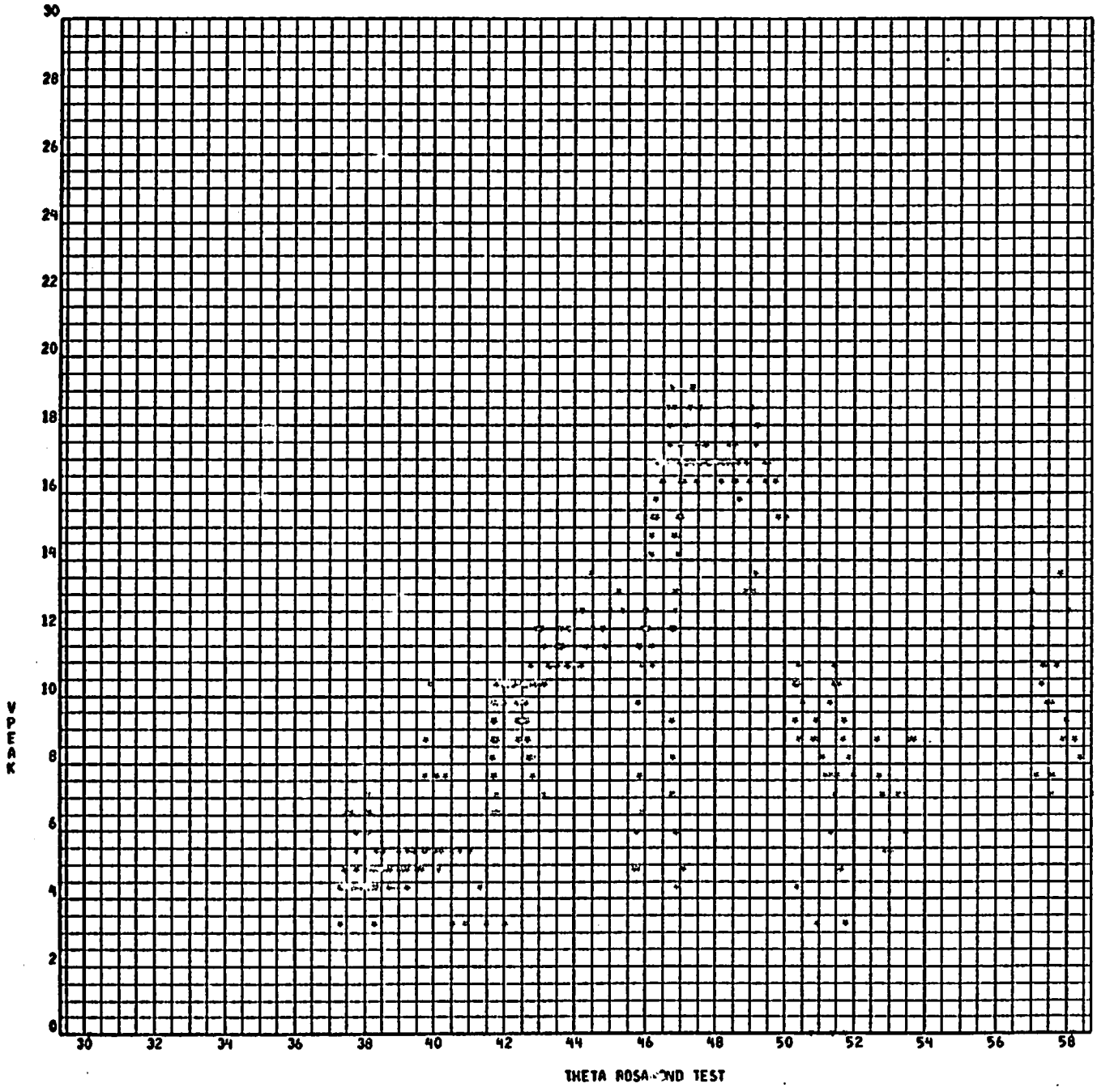
30
28
26
24
22
20
18
16
14
12
10
8
6
4
2
0
VPEAK
30
32
34
36
38
40
42
44
46
48
50
52
54
56
58
THETA ROSA··ND TEST

SCAN = 3

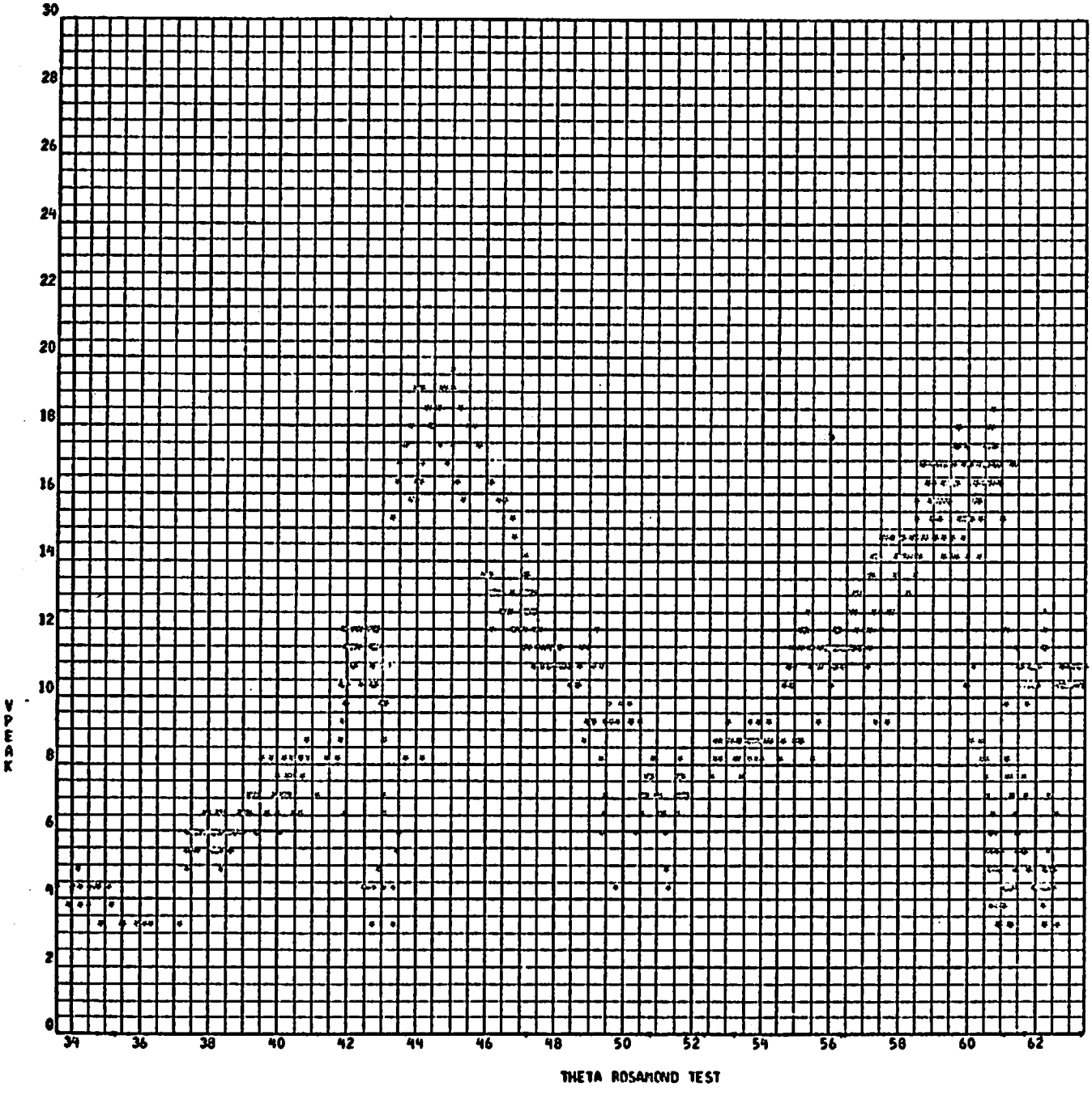
30
28
26
24
22
20
18
16
14
12
10
8
6
4
2
0
VPEAK
34
36
38
40
42
44
46
48
50
52
54
56
58
60
62
THETA ROSAMOND TEST

SCAN = 4

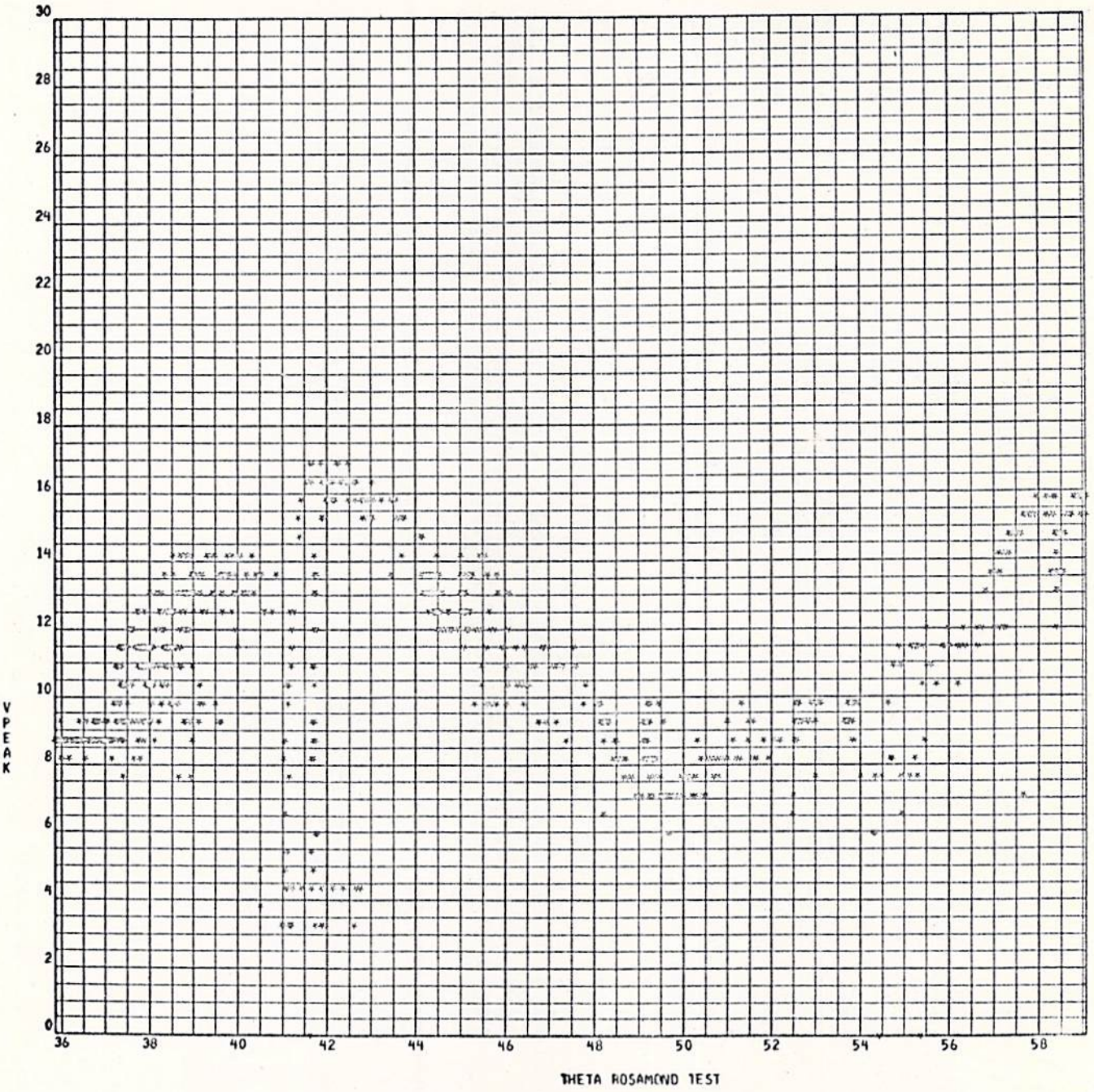
30
28
26
24
22
20
18
16
14
12
10
8
6
4
2
0
VPEAK
36
38
40
42
44
46
48
50
52
54
56
58
THETA ROSAMOND TEST

SCAN = 5

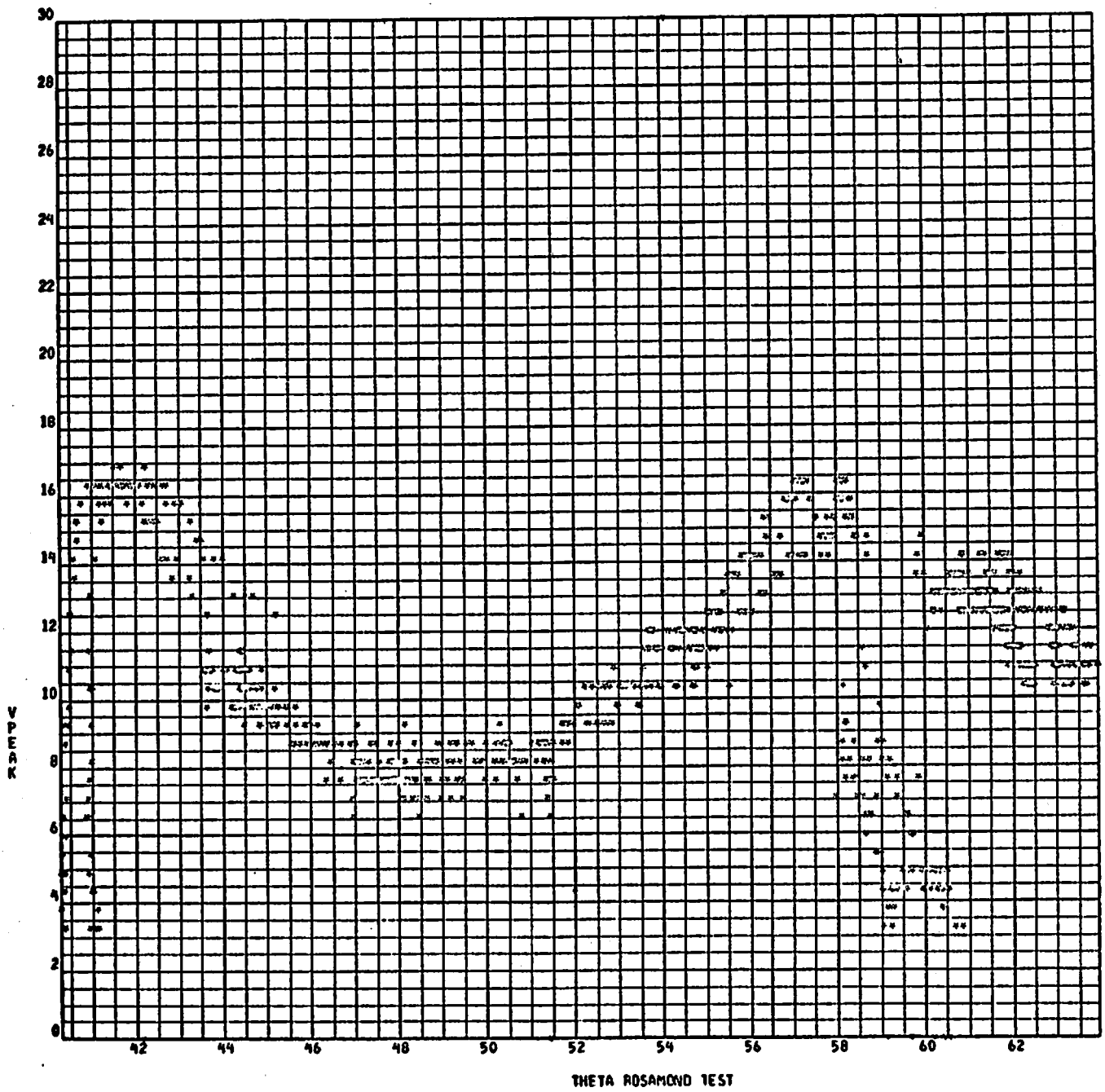
30
28
26
24
22
20
18
16
14
12
10
8
6
4
2
0
VPEAK
42
44
46
48
50
52
54
56
58
60
62
THETA ROSAMOND TEST

SCAN = 6

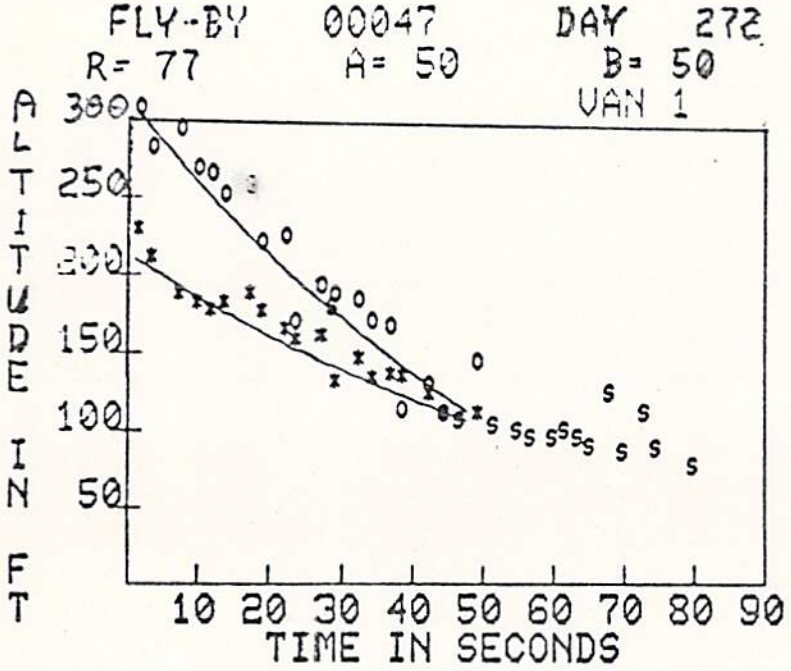
FLY-BY 00047 DAY 272
R= 77 A= 50 B= 50
VAN 1
ALTITUDE IN FT
300
250
200
150
100
50
10 20 30 40 50 60 70 80 90
TIME IN SECONDS

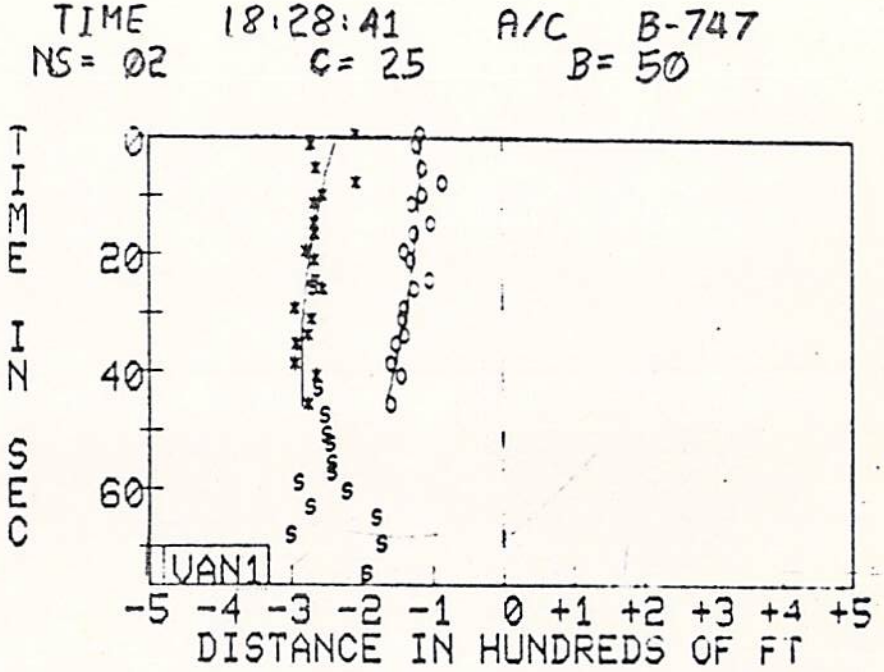
TIME 18:28:41 A/C B-747
NS= 02 C= 25 B= 50
TIME IN SEC
0
20
40
60
VAN1
-5 -4 -3 -2 -1 0 +1 +2 +3 +4 +5
DISTANCE IN HUNDREDS OF FT

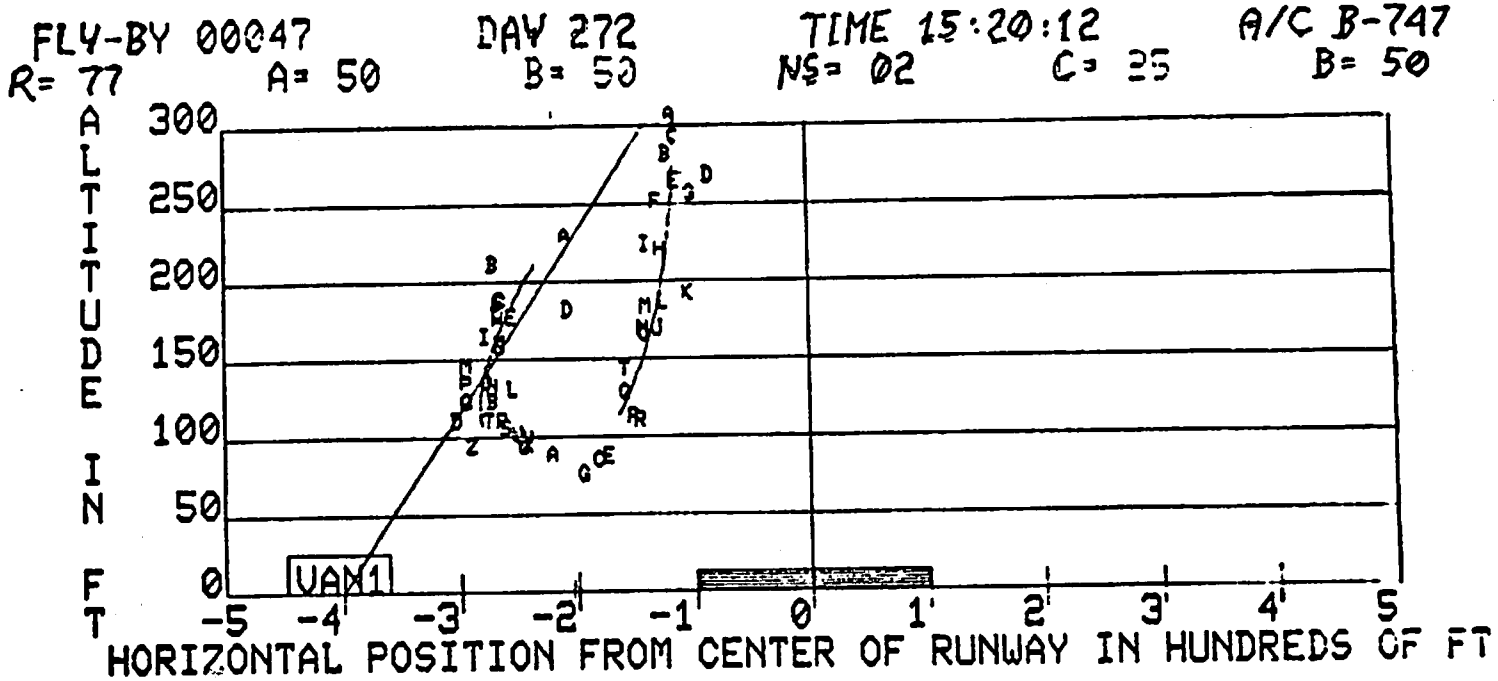
FLY-BY 00047
DAY 272
TIME 15:20:12
A/C B-747
R= 77
A= 50
B= 50
NS= 02
C= 25
B= 50
ALTITUDE IN FT
300
250
200
150
100
50
0
UAM1
-5
-4
-3
-2
-1
0
1
2
3
4
5
HORIZONTAL POSITION FROM CENTER OF RUNWAY IN HUNDREDS OF FT

FLY-BY 00047 DAY 272 TIME 15:28:32 A/C B-747

R = 77 A = 50 B = 50 NS = 02 C = 25 D = 50

FR	DATA PTS	COR P	COR S	PT P	PT S	NOISE P	NOISE S	ANGLE MN	ANGLE MX	PK P	PAR S	TIME	PORT X	PORT Y	STARB X	STARB Y
01	2270	151	055	00	00	44	61	230	200	000.8			-211	225	-120	303
02	2491	128	128	00	00	37	62	230	221	002.8			-274	207	-124	277
03	2529	150	099	00	00	33	60	241	210	006.8			-268	183	-117	288
04	2753	250	146	00	00	37	61	222	208	009.4			-210	178	-089	263
05	2931	250	238	00	00	37	61	257	225	011.4			-259	173	-117	260
06	2917	238	250	00	00	36	61	258	209	013.2			-270	177	-133	247
07	2685	252	112	00	00	37	63	248	214	016.7			-271	183	-104	252
08	2715	233	222	00	00	38	61	260	223	018.3			-270	171	-130	216
09	2569	186	135	00	00	38	60	249	185	021.6			-281	160	-144	219
10	2682	229	224	00	00	29	59	248	196	023.2			-269	153	-133	165
11	2577	250	125	00	00	28	62	262	189	026.5			-268	156	-107	187
12	2486	098	080	00	00	00	00	250	000	028.0			-298	128	-129	181
13	2454	151	179	00	00	31	62	265	189	031.8			-298	141	-143	179
14	2421	158	098	00	00	29	60	272	172	033.6			-276	128	-146	165
15	2286	111	068	00	00	30	61	265	170	036.3			-280	131	-144	162
16	2311	056	114	00	00	18	61	276	176	038.0			-297	130	-154	108
17	2187	036	077	00	00	20	63	273	176	041.7			-298	118	-162	124
18	2178	057	025	00	00	18	62	237	145	043.8			-268	105	-148	105
19	2167	062	020	00	02	18	62	238	000	046.0			-264	101		
20	2142	043	019	00	00	19	62	212	144	048.7			-278	106	-162	139
21	2132	062	000	00	00	19	61	218	000	050.9			-254	098		
22	2116	054	000	00	00	19	54	220	000	054.0			-252	094		
23	2097	051	000	00	00	18	51	202	000	055.9			-248	090		
24	2092	023	000	00	00	07	50	103	000	059.2			-246	090		
25	2052	040	000	00	00	20	45	188	000	060.8			-246	094		
26	2032	022	000	00	00	37	42	174	000	062.8			-293	089		
27	2050	048	000	00	00	30	36	198	000	064.3			-224	084		
28	2026	006	000	00	00	39	45	166	000	067.1			-276	118		
29	2072	000	078	00	00	23	32	000	186	069.1					-184	080
30	2002	002	000	00	00	47	49	174	000	072.3			-306	106		
31	2058	000	068	00	00	24	25	000	176	073.8					-176	083
32	2020	000		00		00	00	000								
33	2033	000	024	00	00	19	21	000	196	079.1					-198	072
34	2020	000		00		00	00	000								
35	2020	000		00		00	00	000								
36	0000	000		00		00	00	000								

Appendix D

WAKE VORTEX TRACKS COMPUTED FROM LOW SPEED MEASUREMENTS

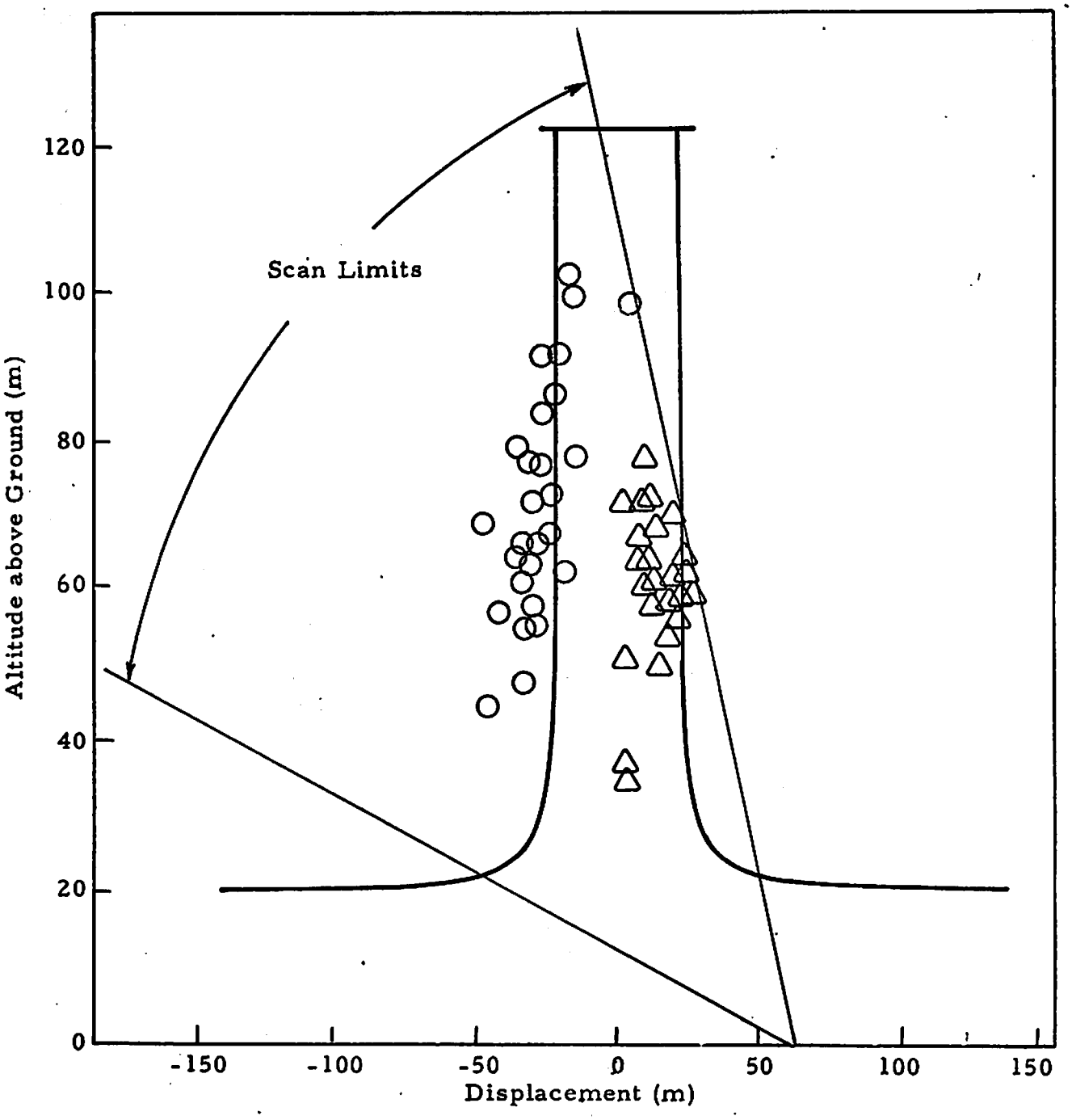

Wake Vortex Trajectory for Rosamond Fly-By 23

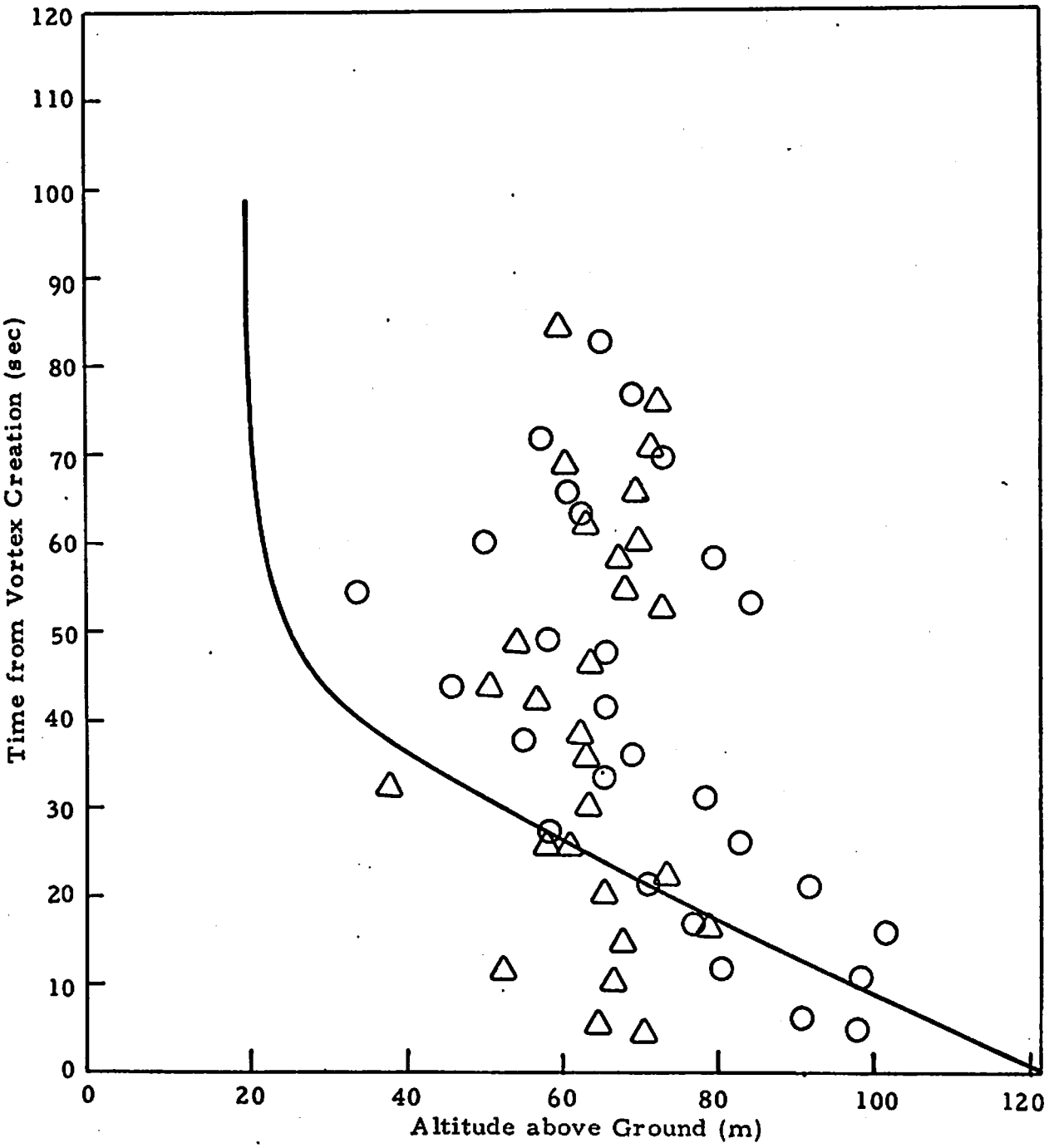
Time from Vortex Creation (sec)
120
110
100
90
80
70
60
50
40
30
20
10
0
0
20
40
60
80
100
120
Altitude above Ground (m)

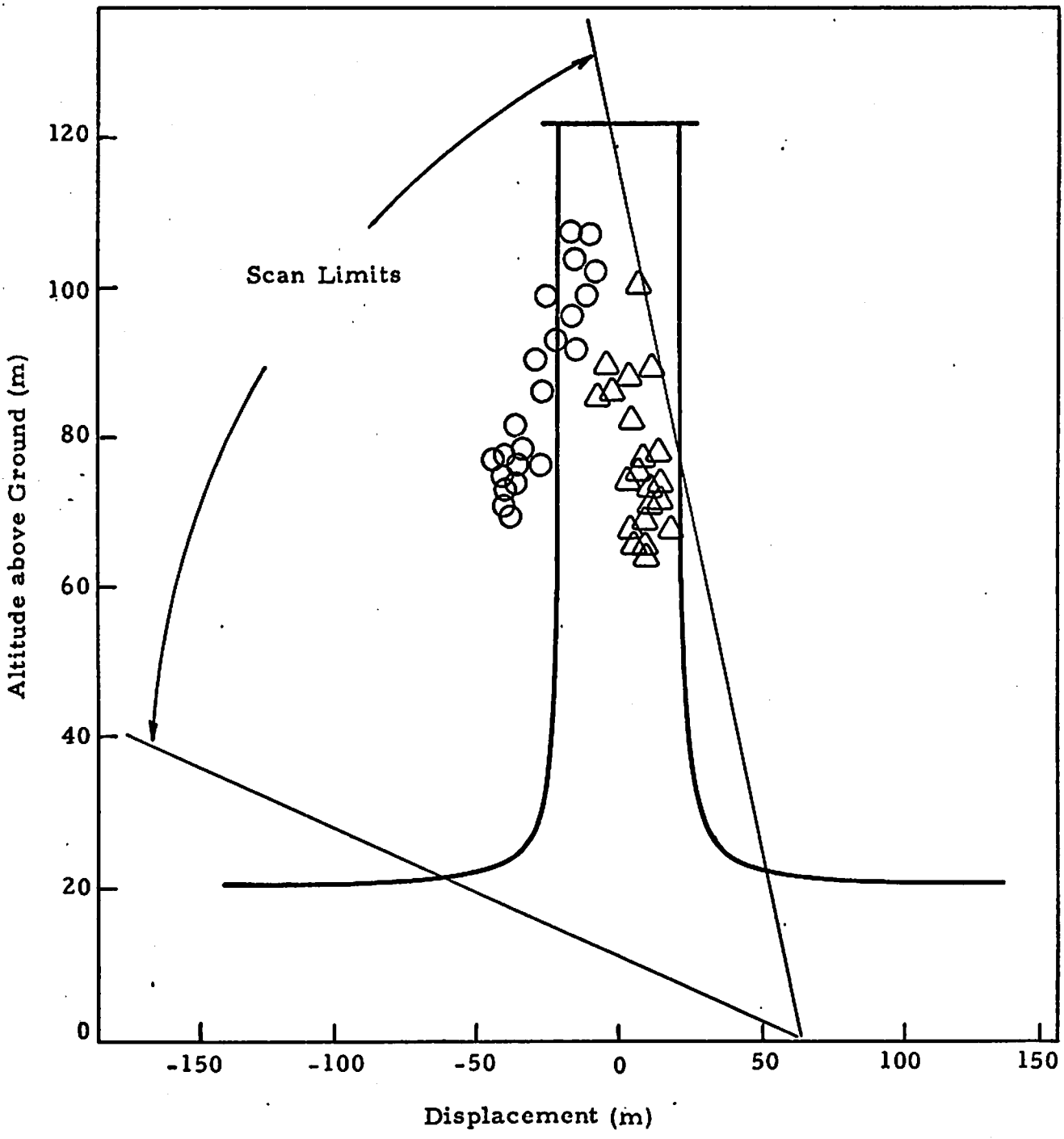

Wake Vortex Trajectory for Rosamond Fly-By 24

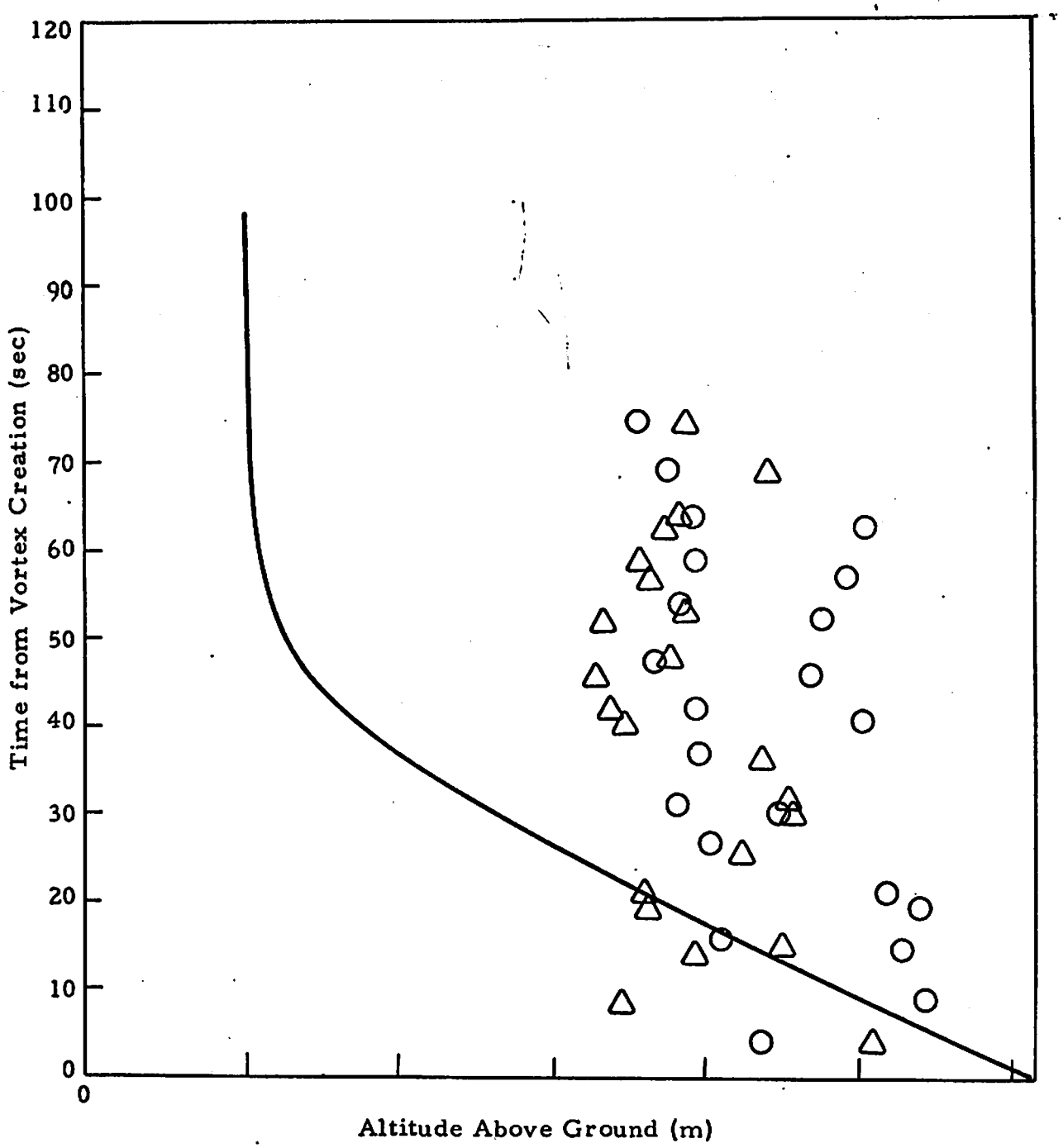
120
110
100
90
80
70
60
50
40
30
20
10
0
0
Time from Vortex Creation (sec)
Altitude Above Ground (m)

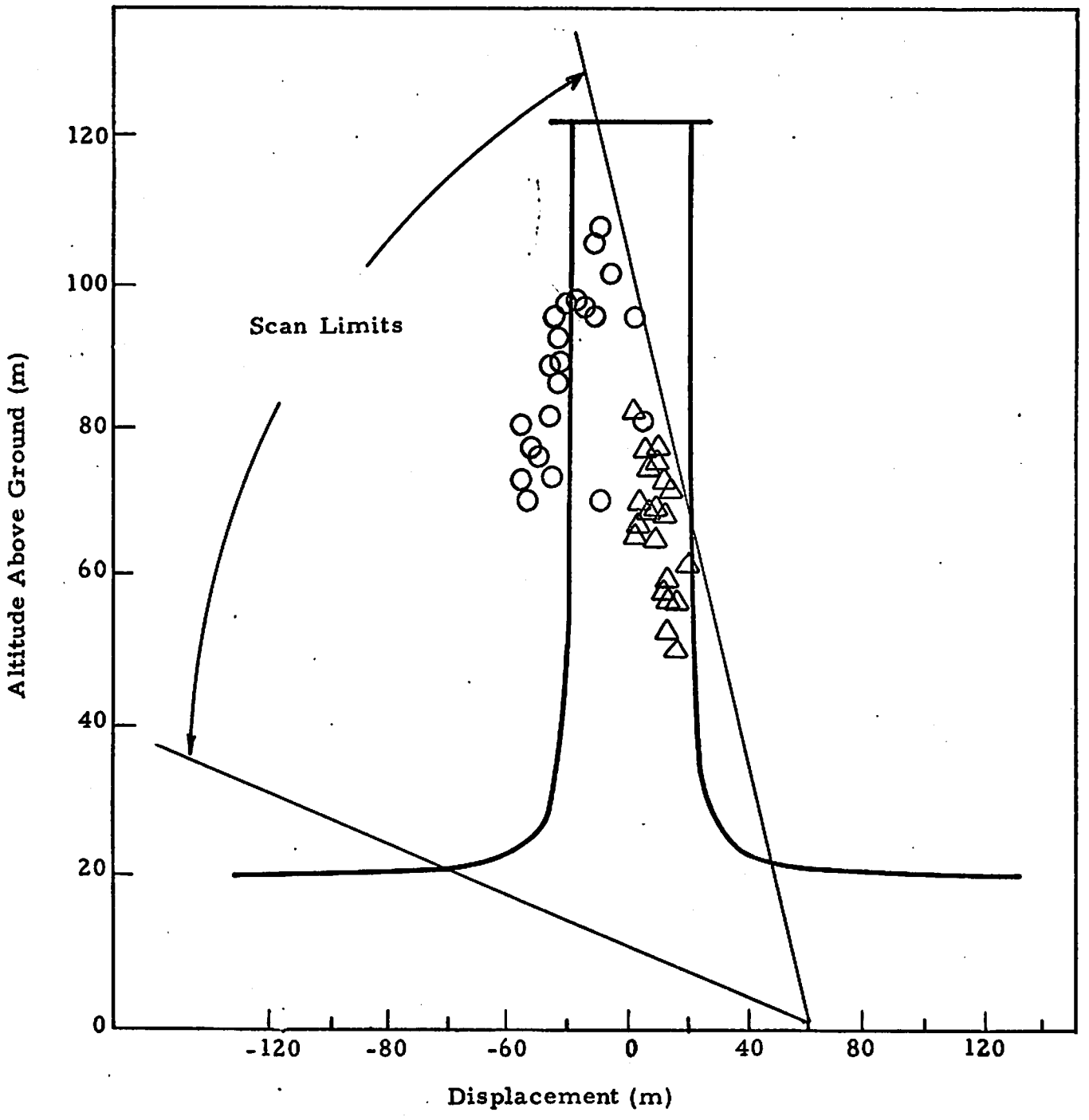

Wake Vortex Trajectory for Rosamond Fly-By 25

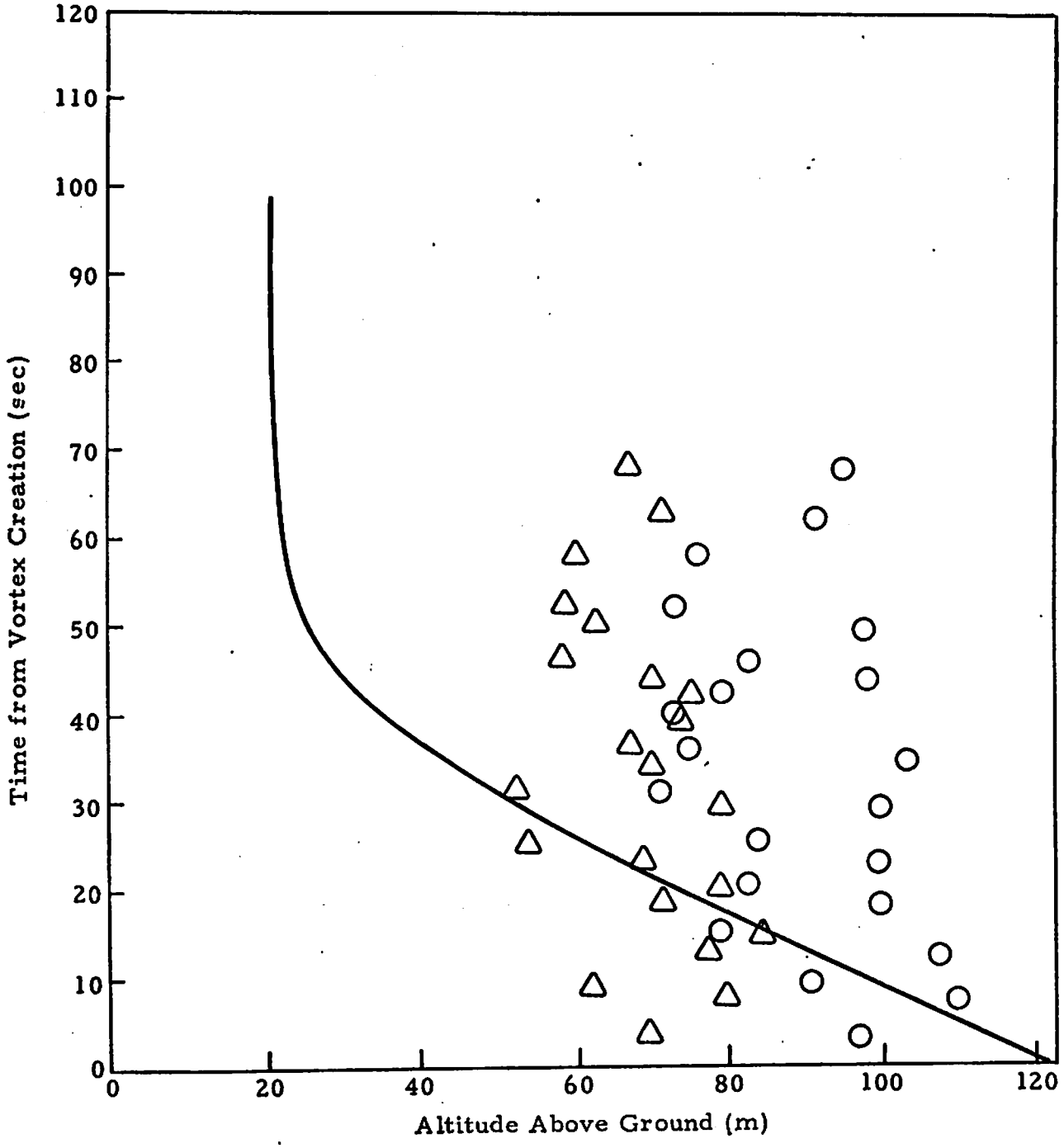
Time from Vortex Creation (sec)
120
110
100
90
80
70
60
50
40
30
20
10
0
0
20
40
60
80
100
120
Altitude Above Ground (m)

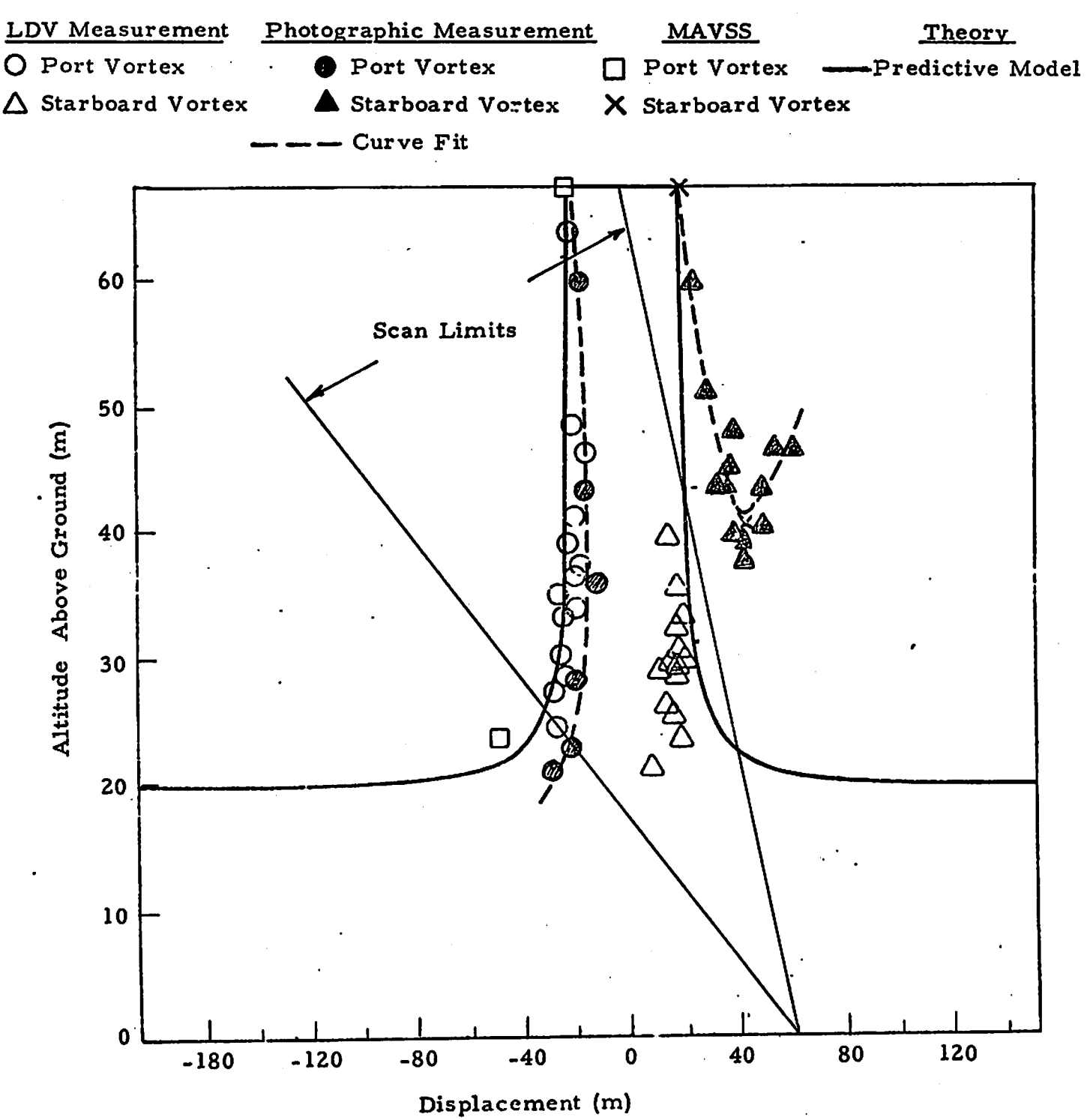

Wake Vortex Trajectory for Rosamond Flyby 27

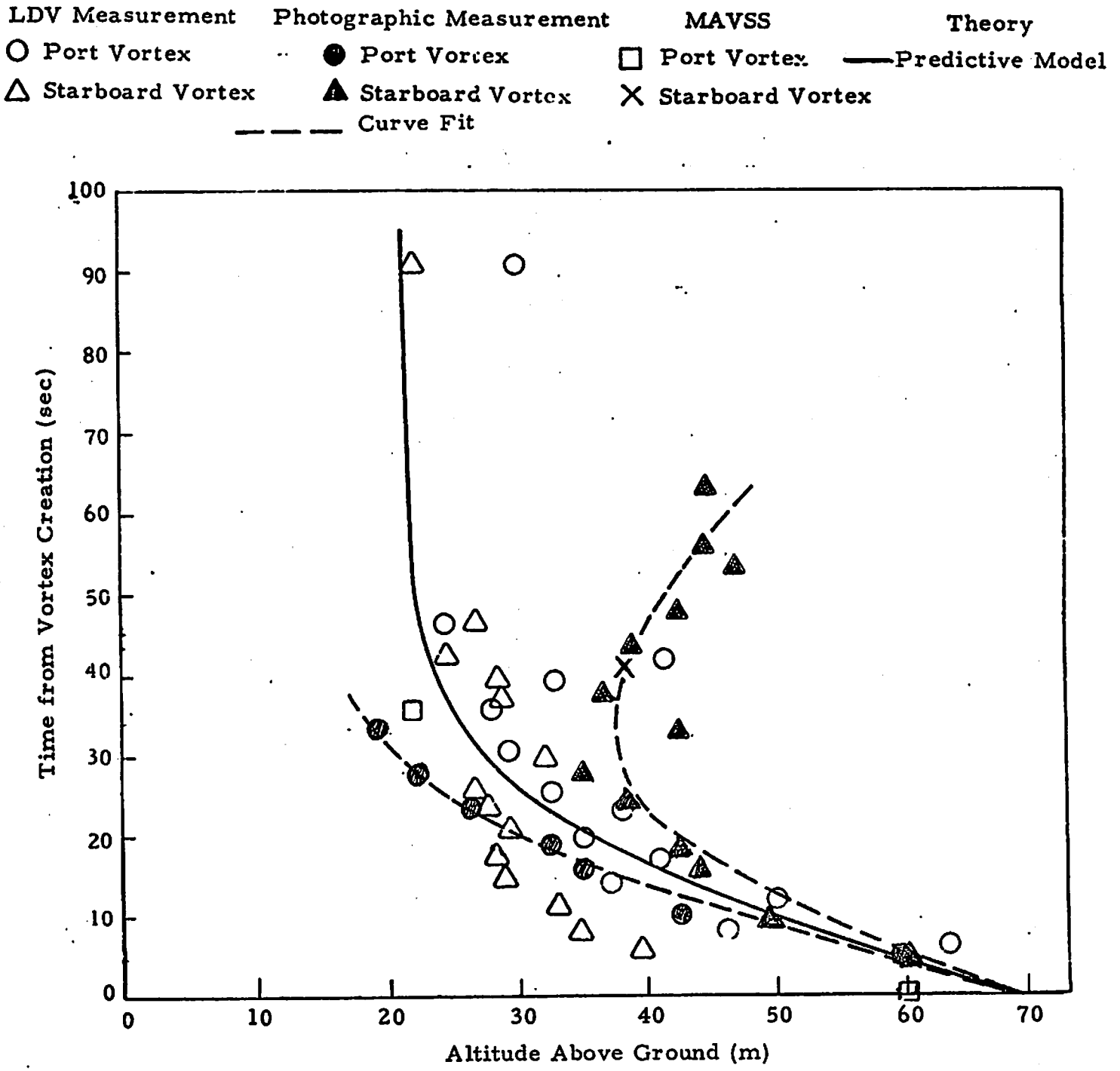
LDV Measurement
Port Vortex
Starboard Vortex
Photographic Measurement
Port Vortex
Starboard Vortex
Curve Fit
MAVSS
Port Vortex
Starboard Vortex
Theory
Predictive Model
Time from Vortex Creation (sec)
Altitude Above Ground (m)
0
10
20
30
40
50
60
70
80
90
100

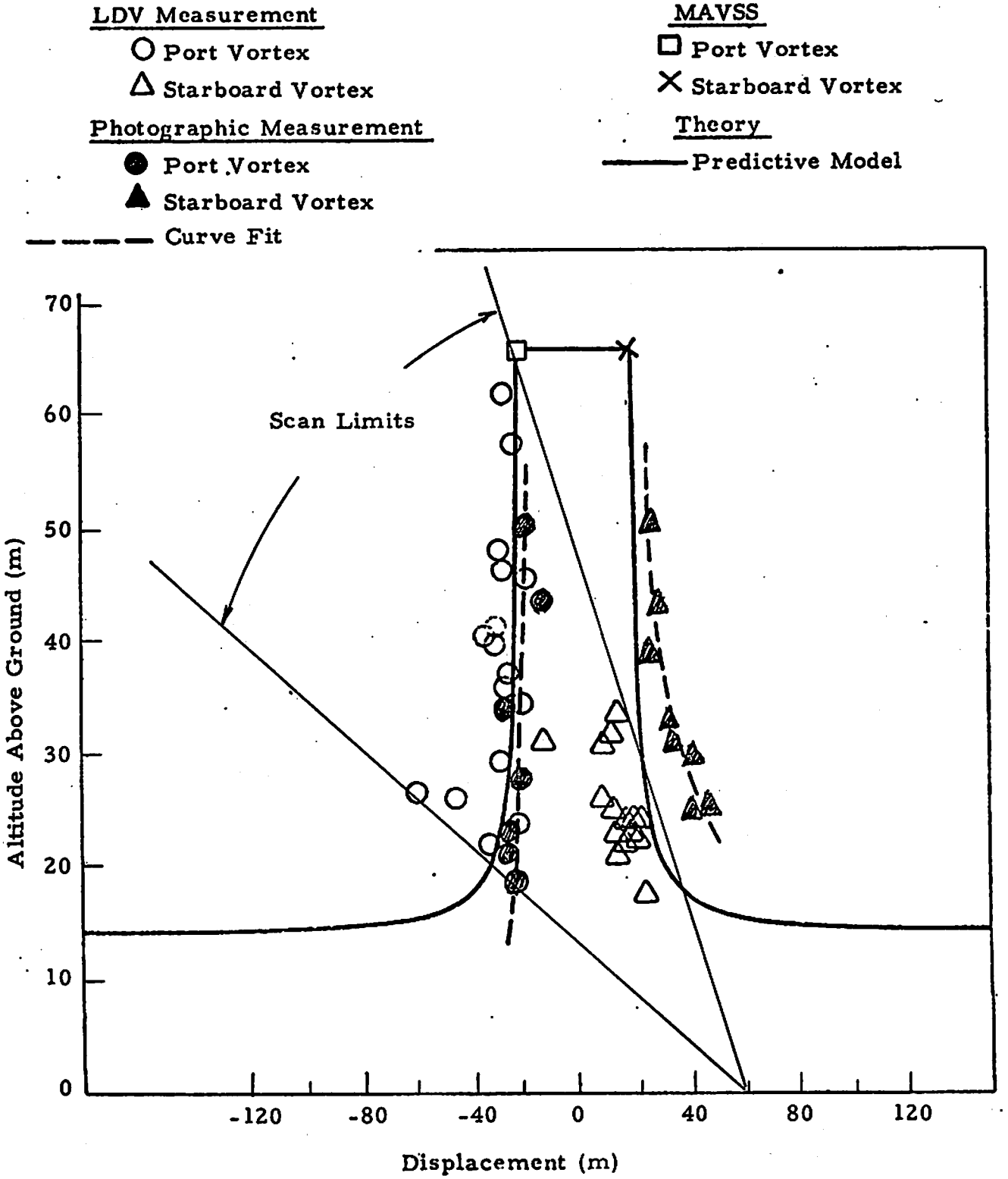

Wake Vortex Trajectory for Rosamond Flyby 28

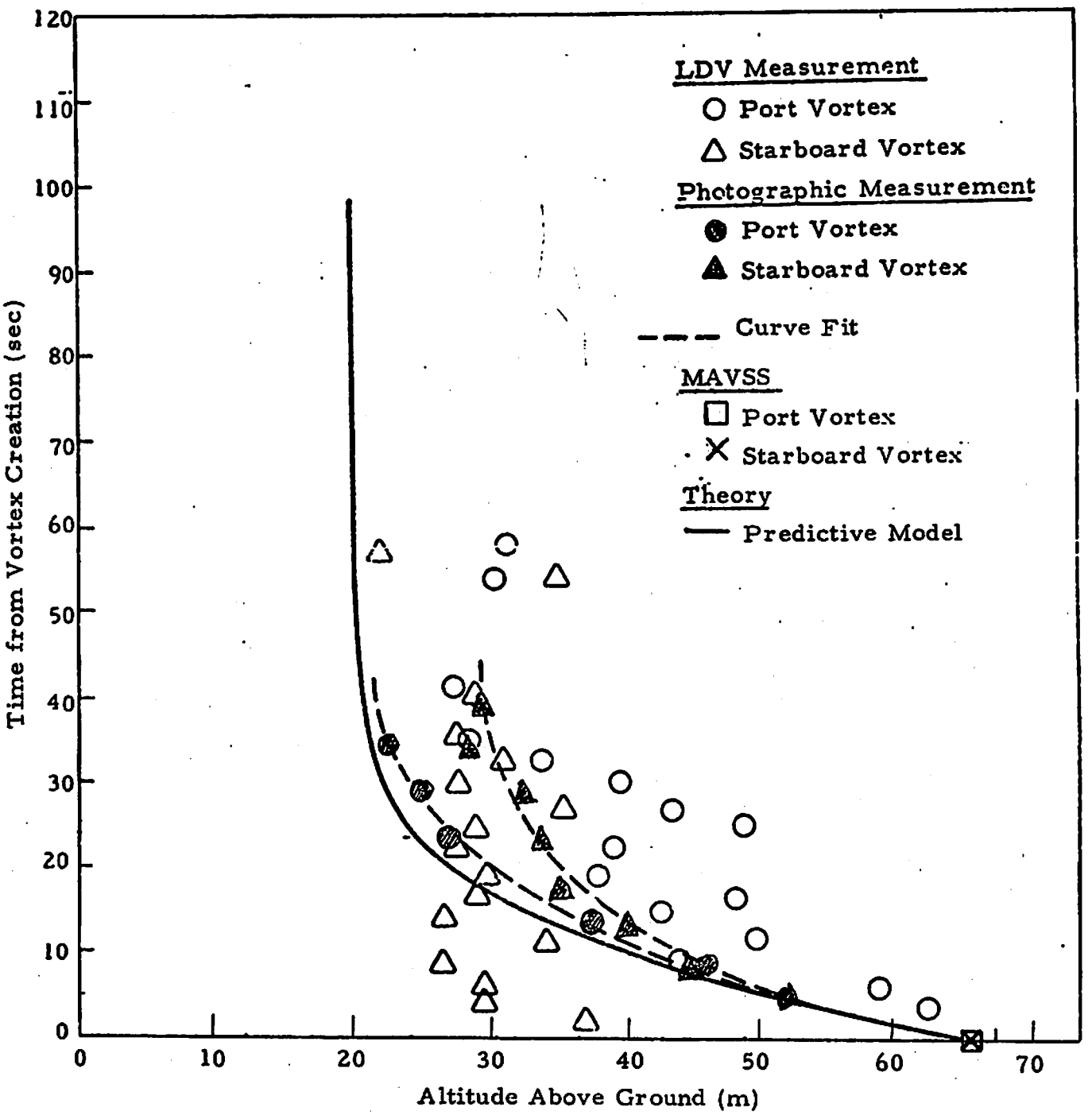
LDV Measurement
Port Vortex
Starboard Vortex
Photographic Measurement
Port Vortex
Starboard Vortex
Curve Fit
MAVSS
Port Vortex
Starboard Vortex
Theory
Predictive Model
Time from Vortex Creation (sec)
Altitude Above Ground (m)
0
10
20
30
40
50
60
70
80
90
100
110
120

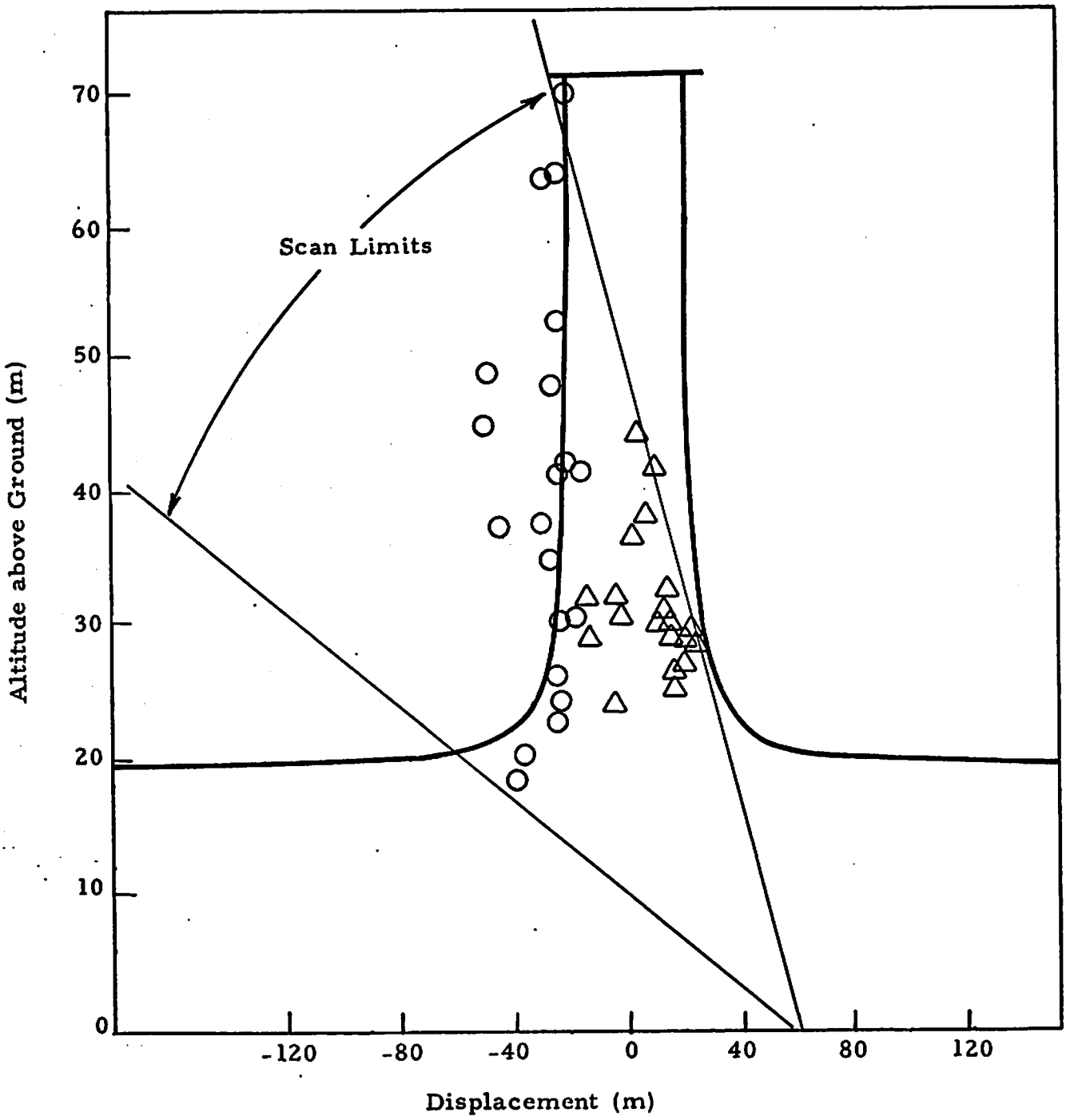

Wake Vortex Trajectory for Rosamond Fly-By 29

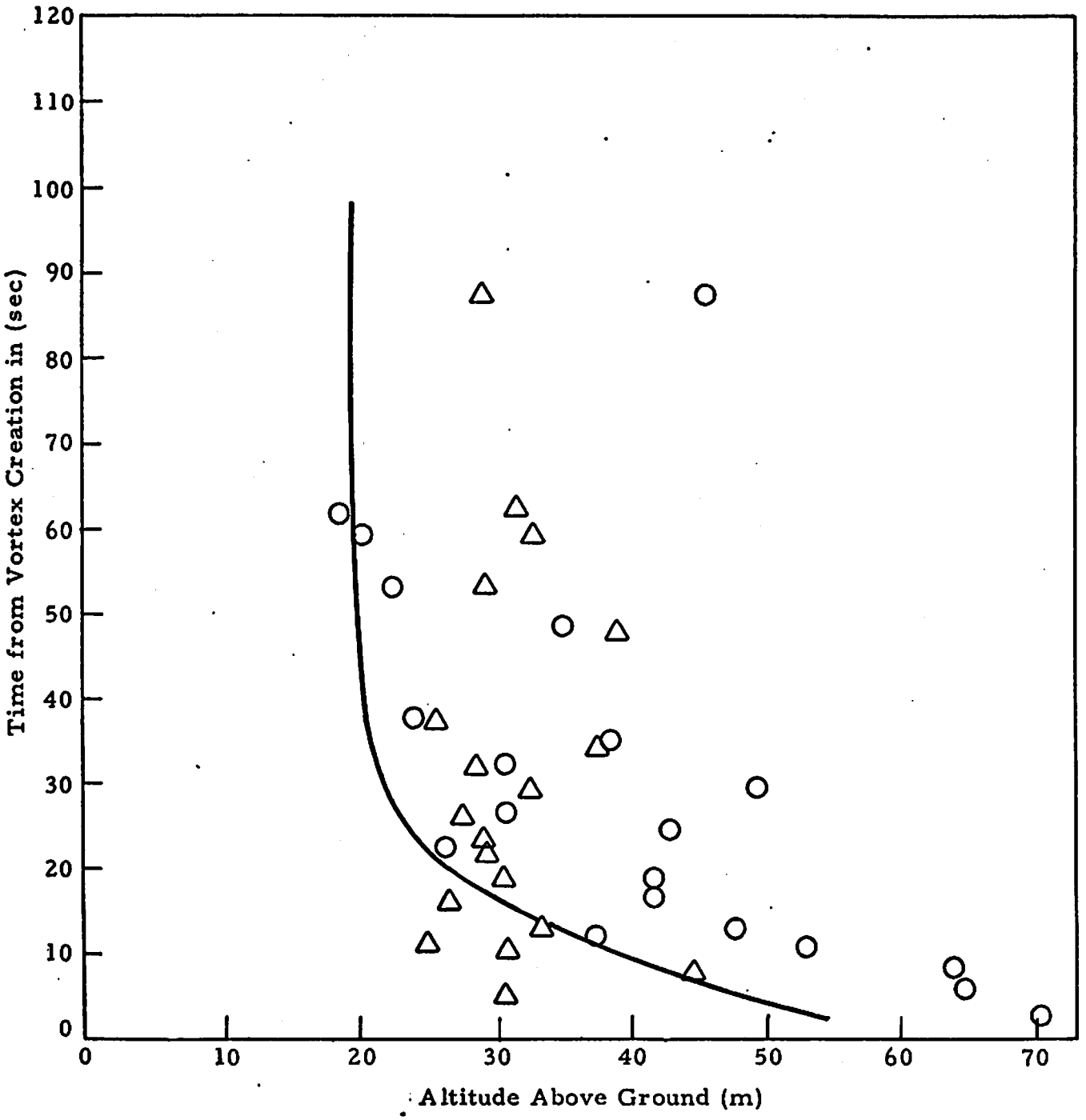
Time from Vortex Creation in (sec)
120
110
100
90
80
70
60
50
40
30
20
10
0
0
10
20
30
40
50
60
70
Altitude Above Ground (m)

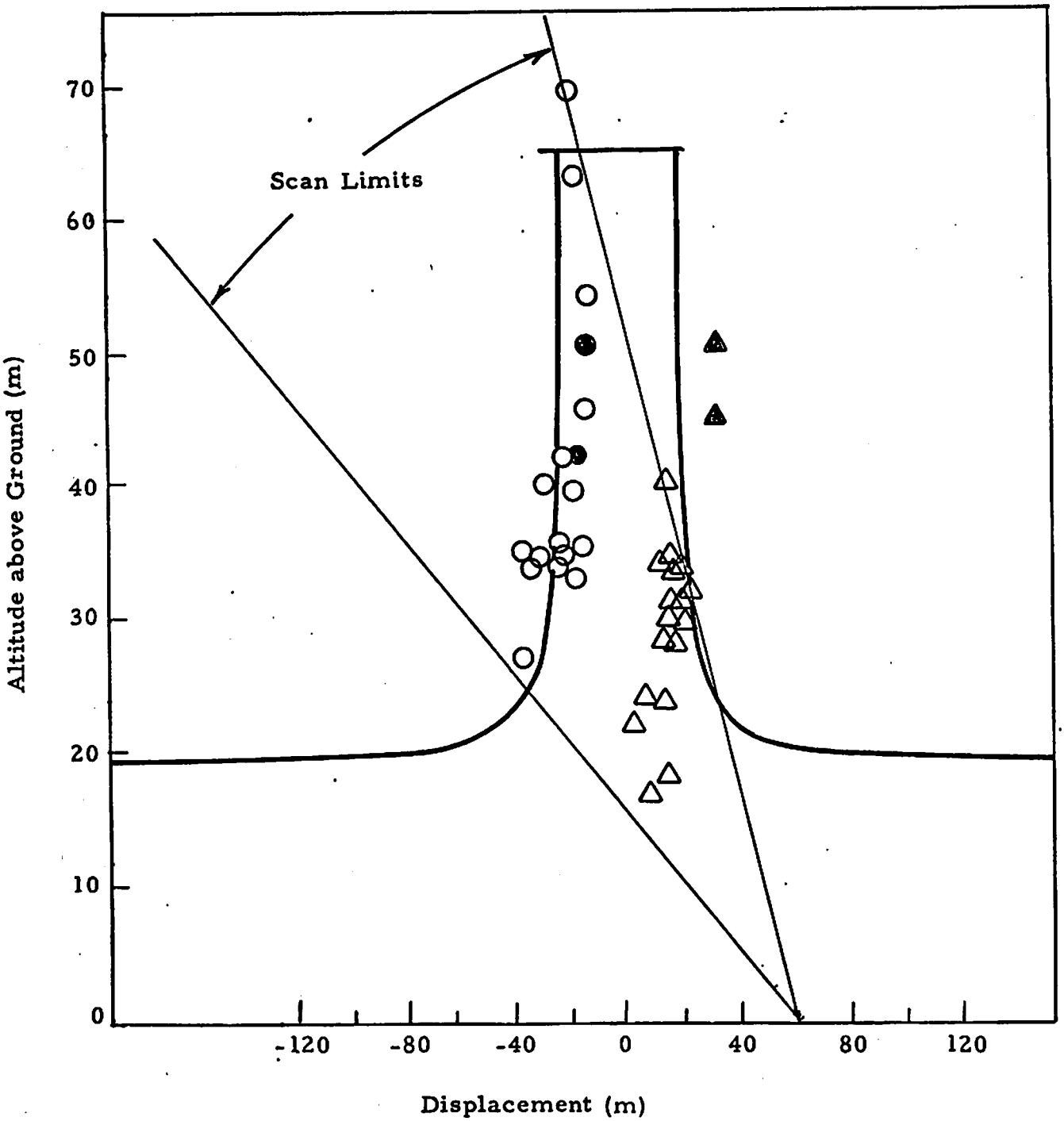

Wake Vortex Trajectory for Rosamond Fly-By 30

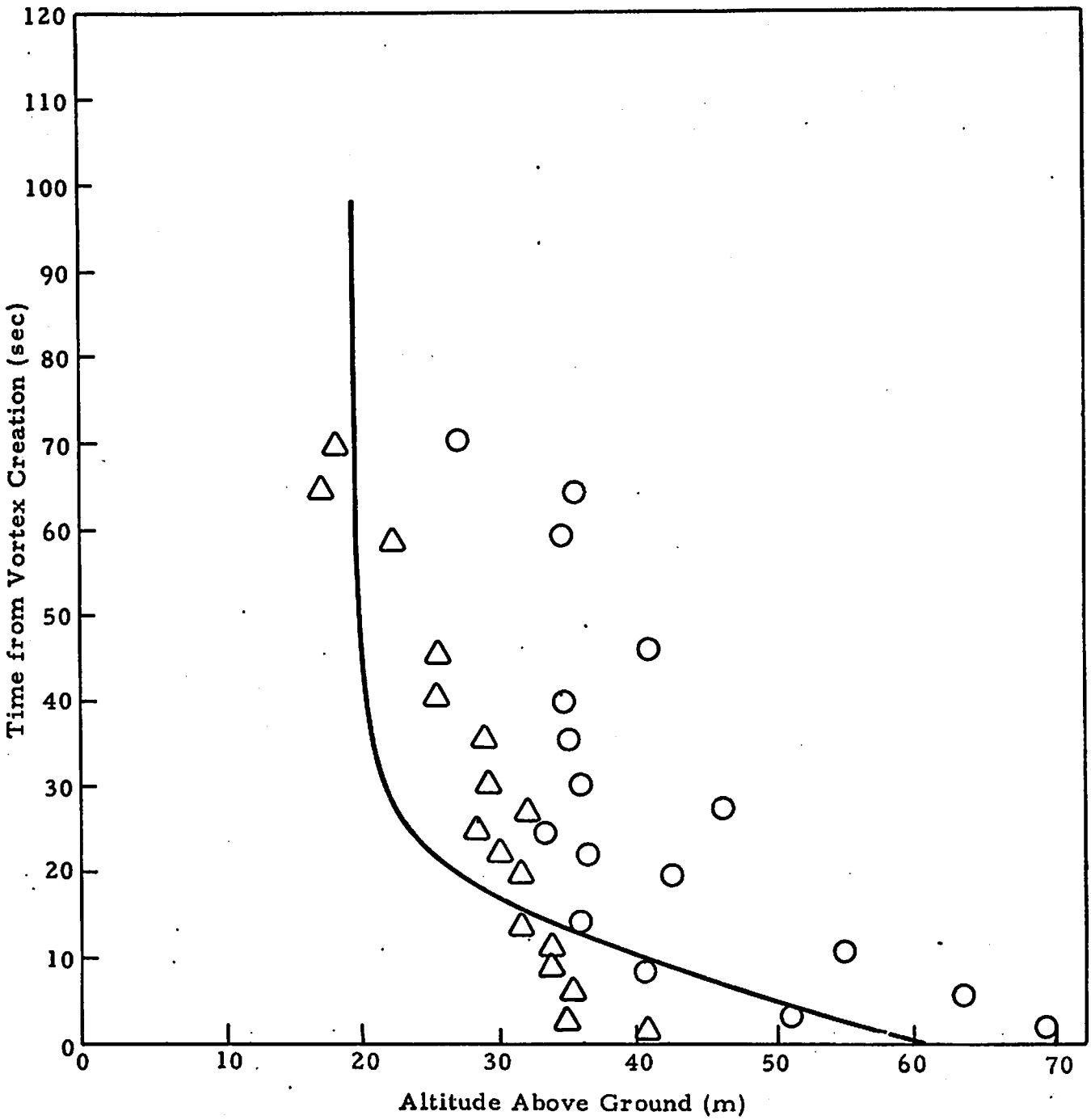
Time from Vortex Creation (sec)
120
110
100
90
80
70
60
50
40
30
20
10
0
0
10
20
30
40
50
60
70
Altitude Above Ground (m)

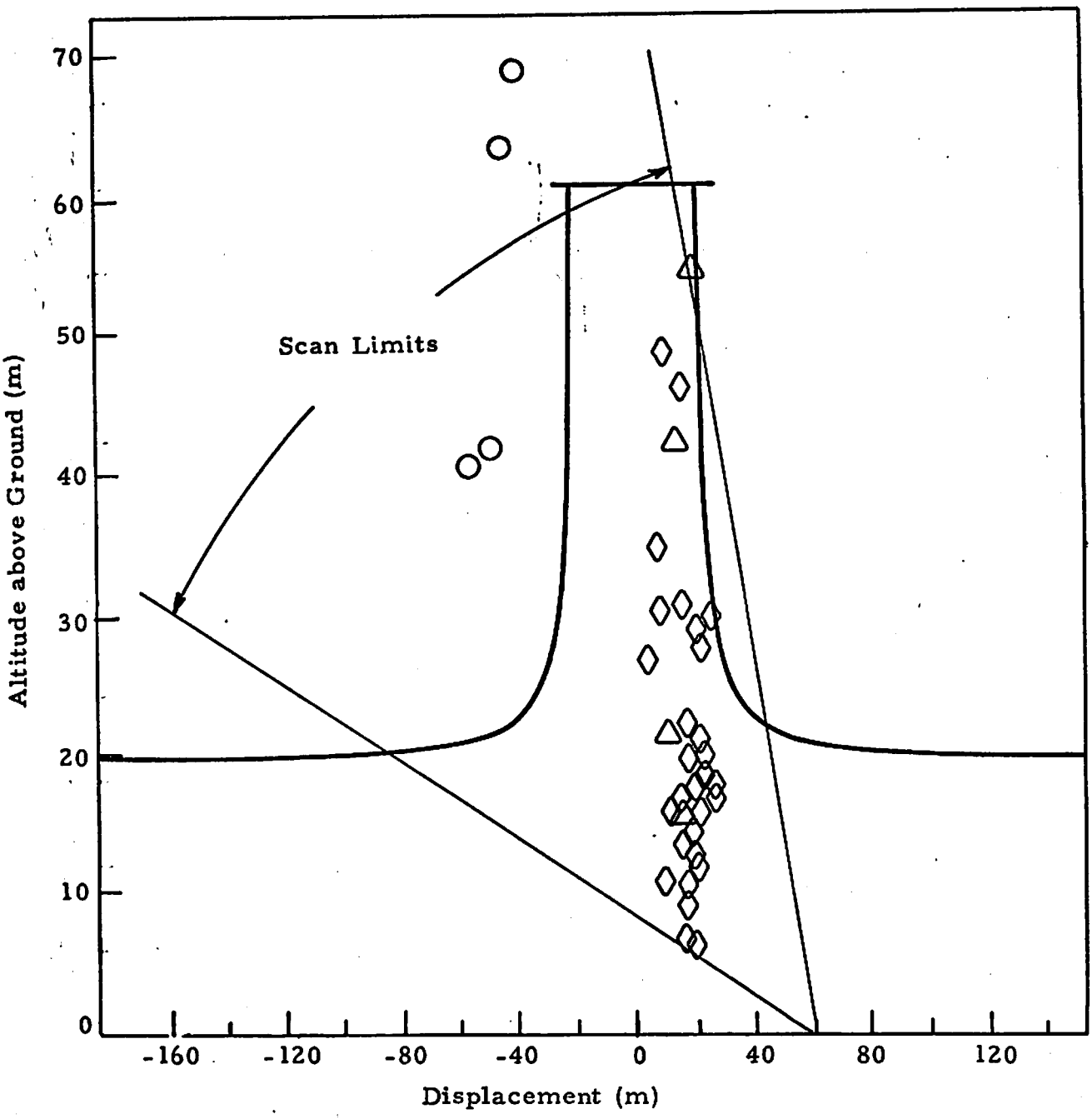

Wake Vortex Trajectory for Rosamond Fly-By 40

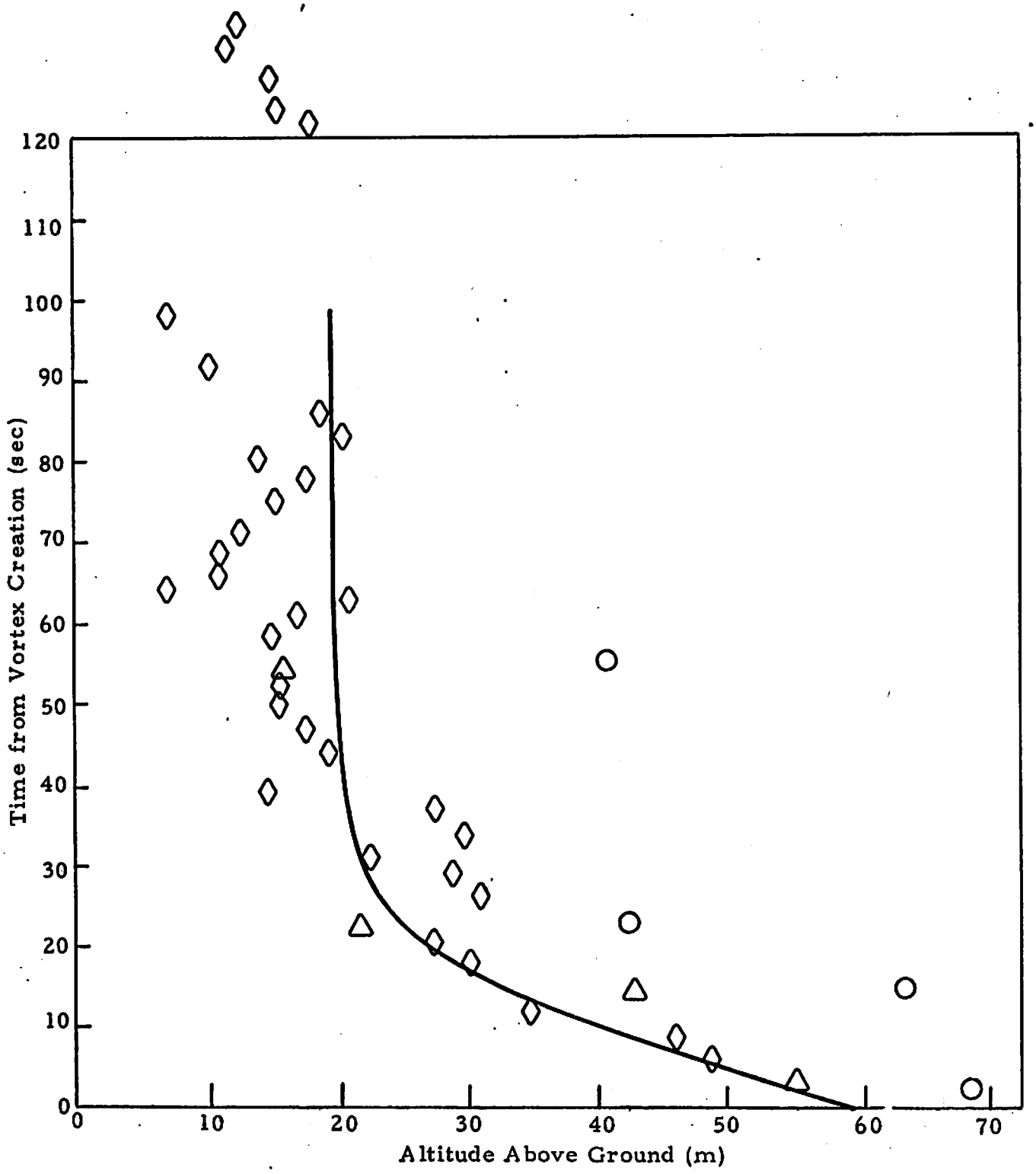
Time from Vortex Creation (sec)
120
110
100
90
80
70
60
50
40
30
20
10
0
0
10
20
30
40
50
60
70
Altitude Above Ground (m)

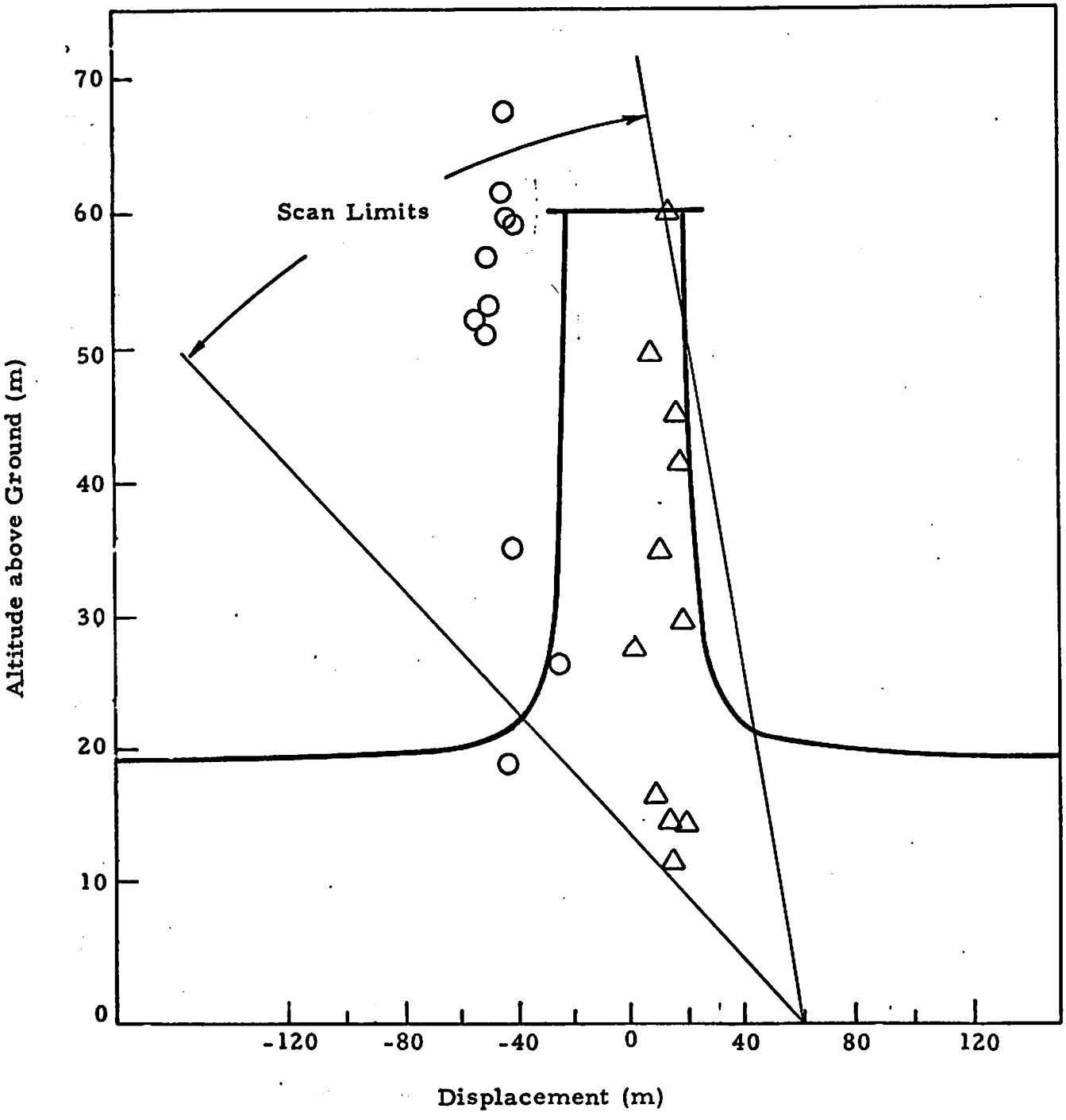

Wake Vortex Trajectory for Rosamond Fly-By 42

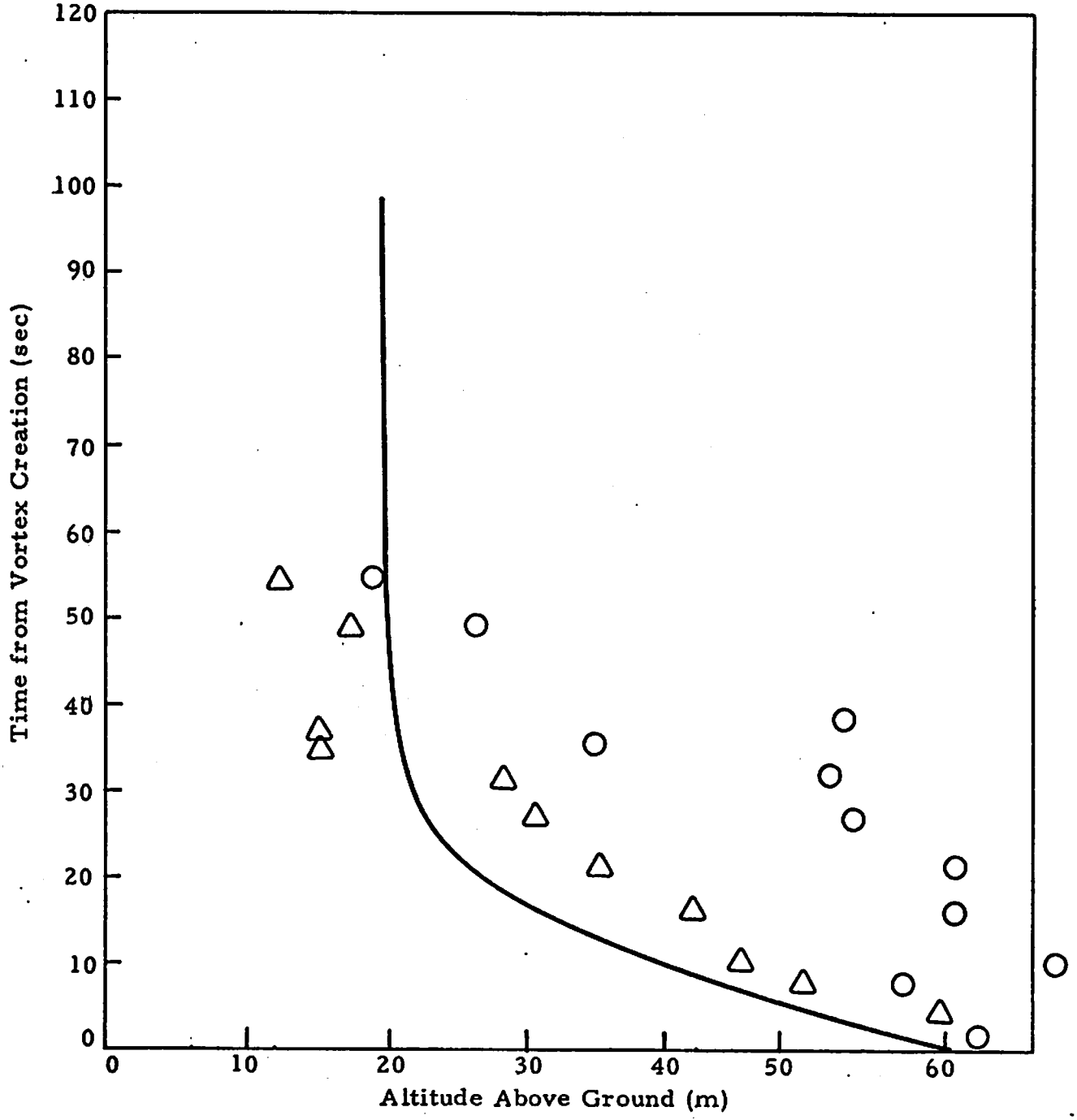
Time from Vortex Creation (sec)
120
110
100
90
80
70
60
50
40
30
20
10
0
0
10
20
30
40
50
60
Altitude Above Ground (m)

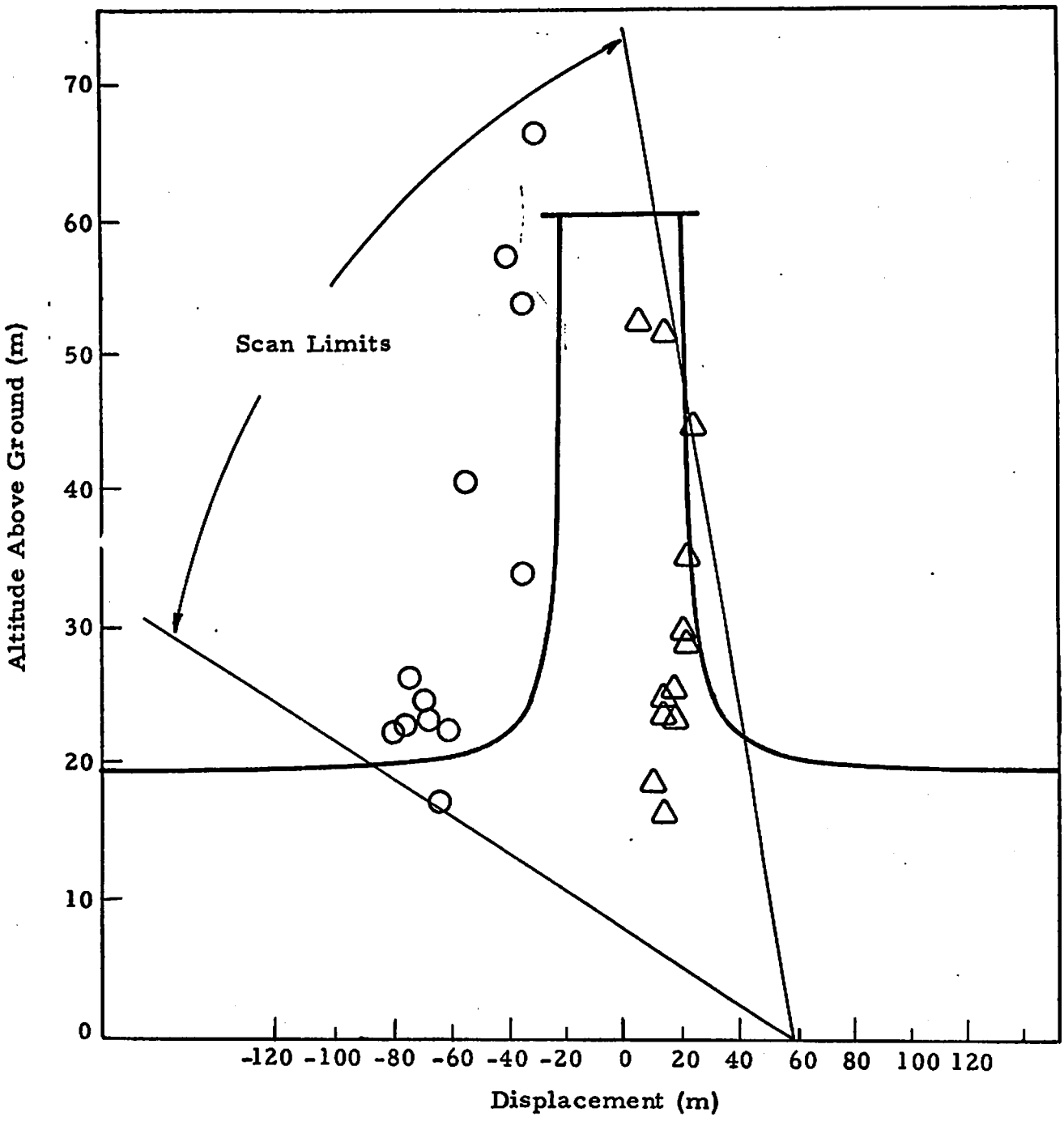

Wake Vortex Trajectory for Rosamond Flyby 44

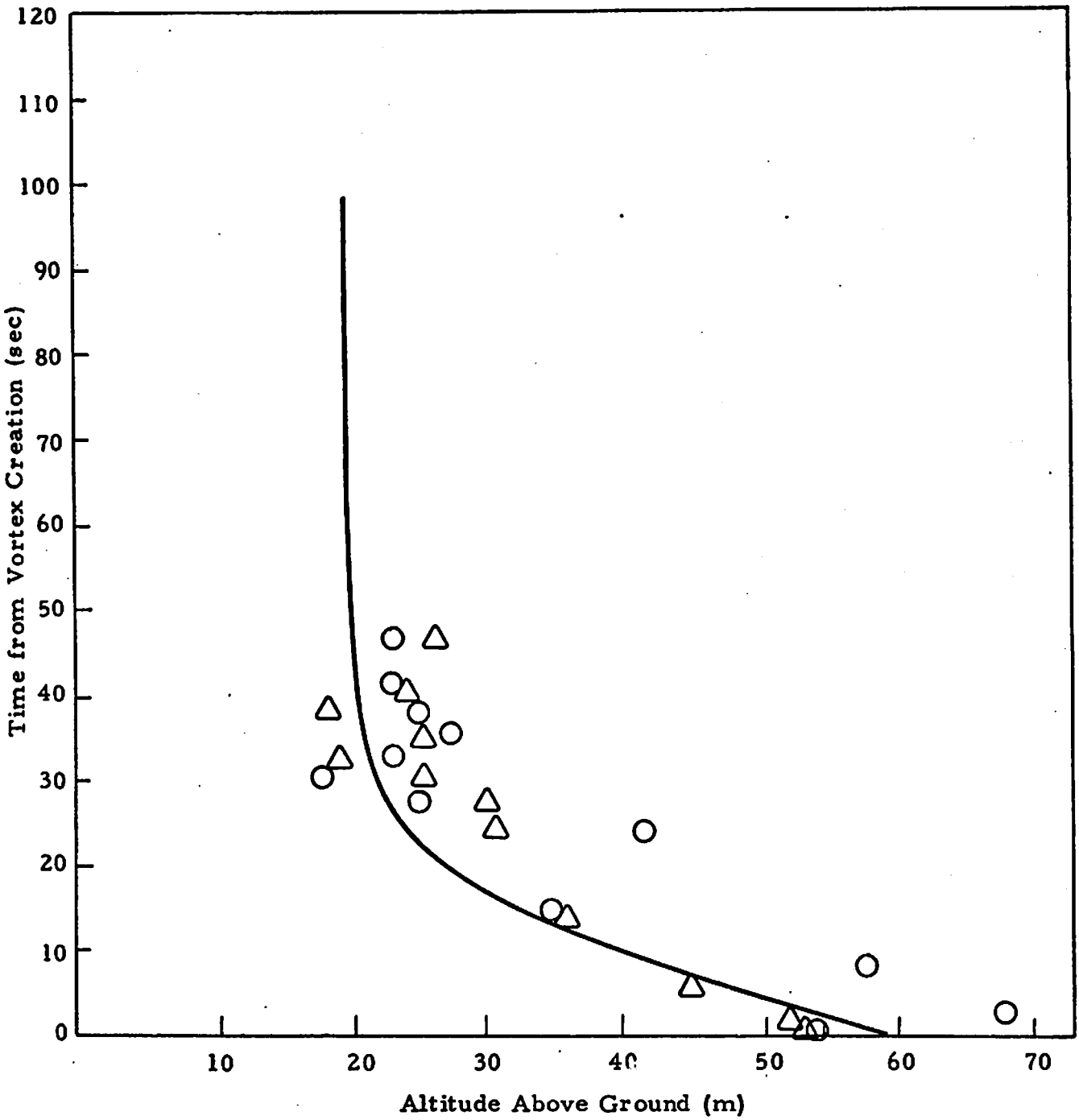
Time from Vortex Creation (sec)
120
110
100
90
80
70
60
50
40
30
20
10
0
10
20
30
40
50
60
70
Altitude Above Ground (m)

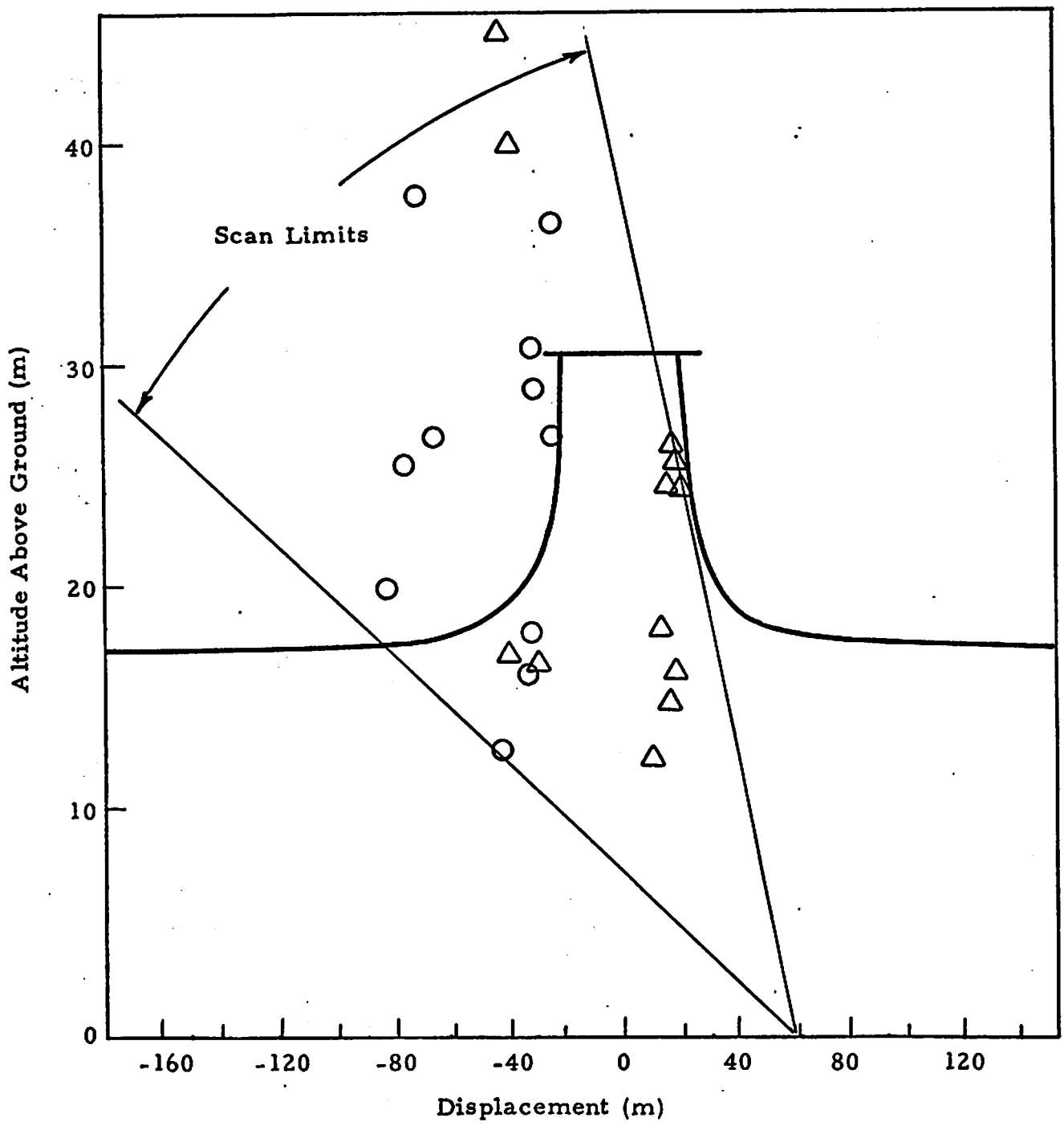

Wake Vortex Trajectory for Rosamond Fly-By 46

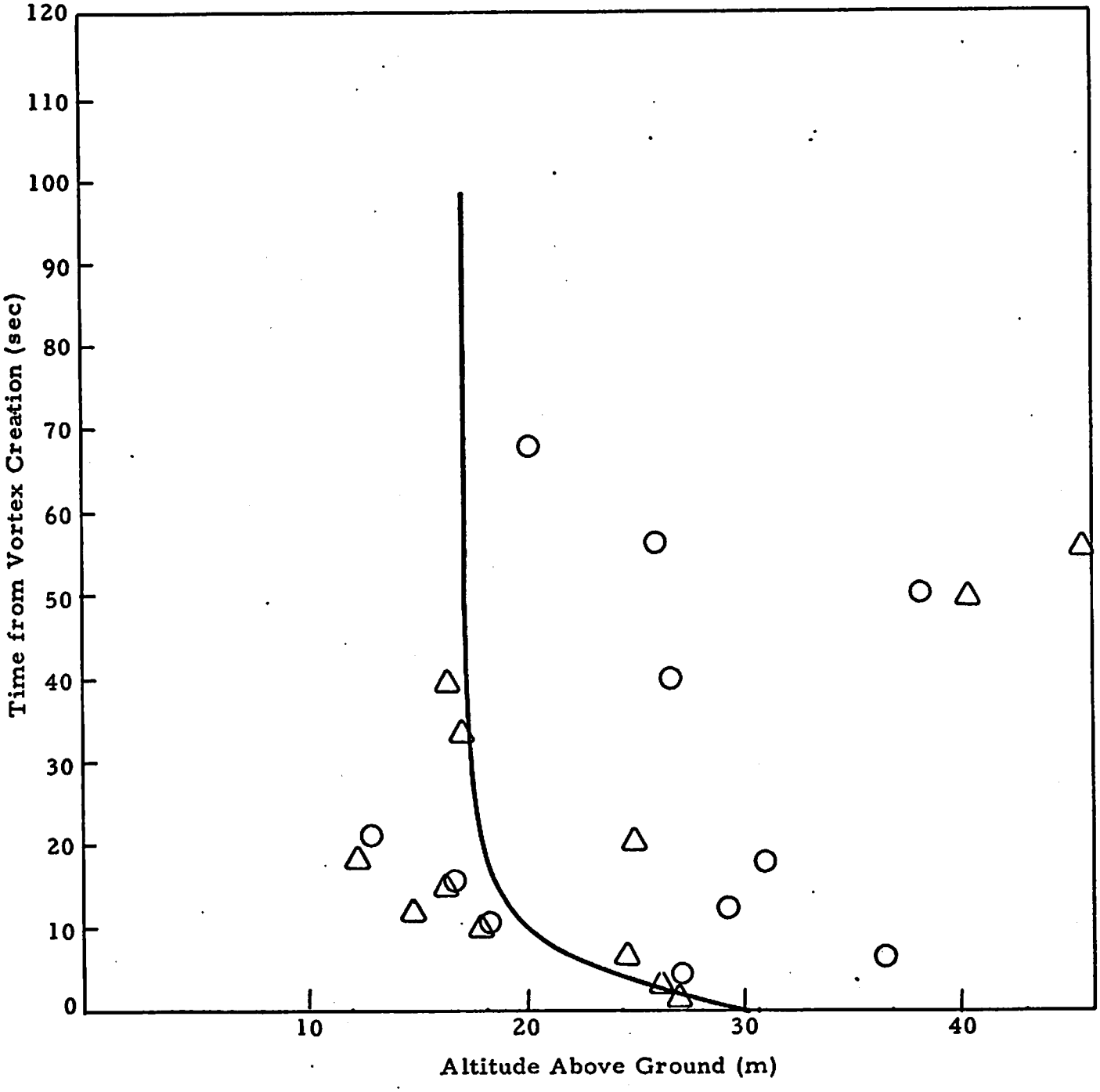
120
110
100
90
80
70
60
50
40
30
20
10
0
Time from Vortex Creation (sec)
10
20
30
40
Altitude Above Ground (m)

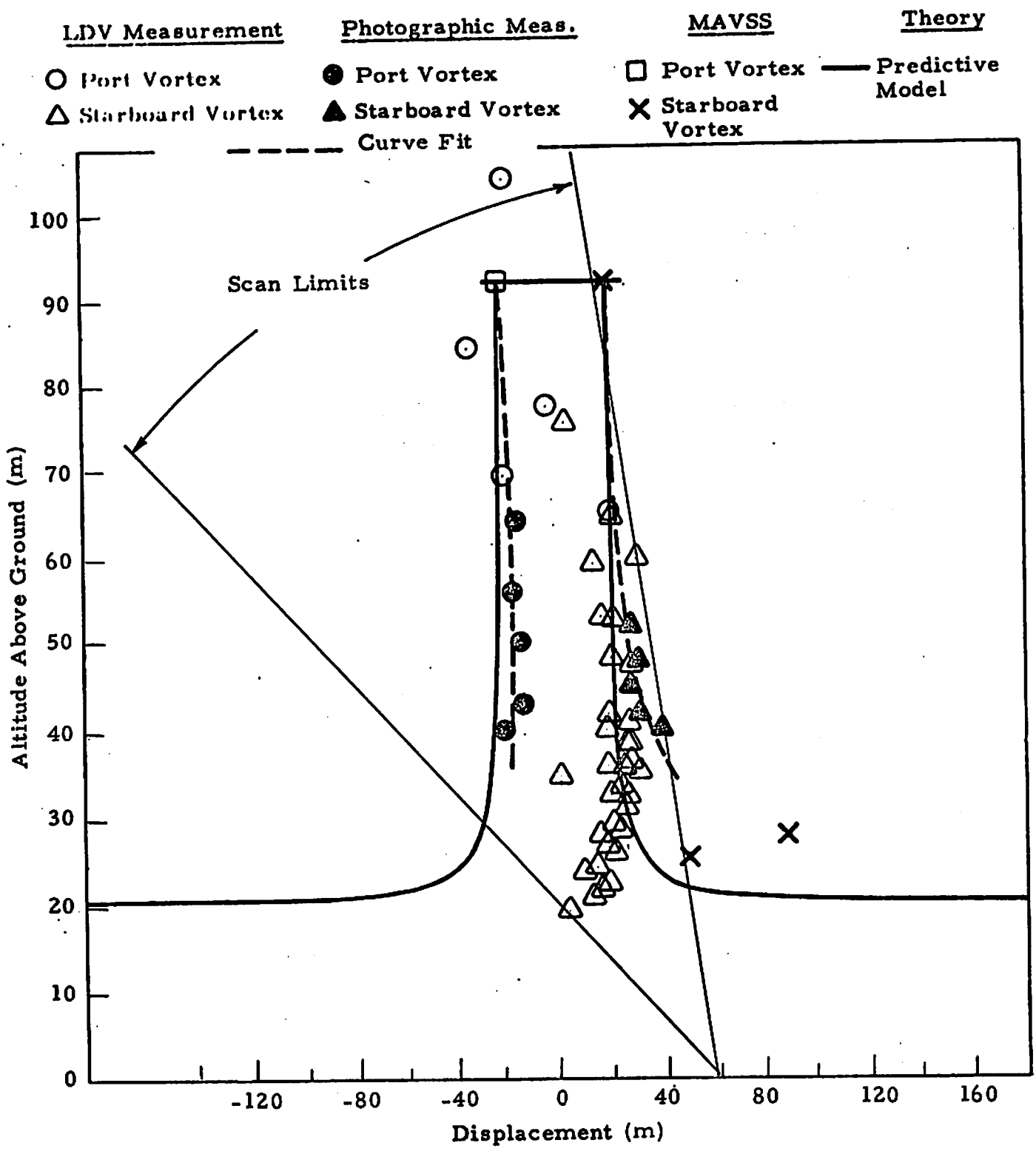

Wake Vortex Trajectory for Rosamond Flyby 47

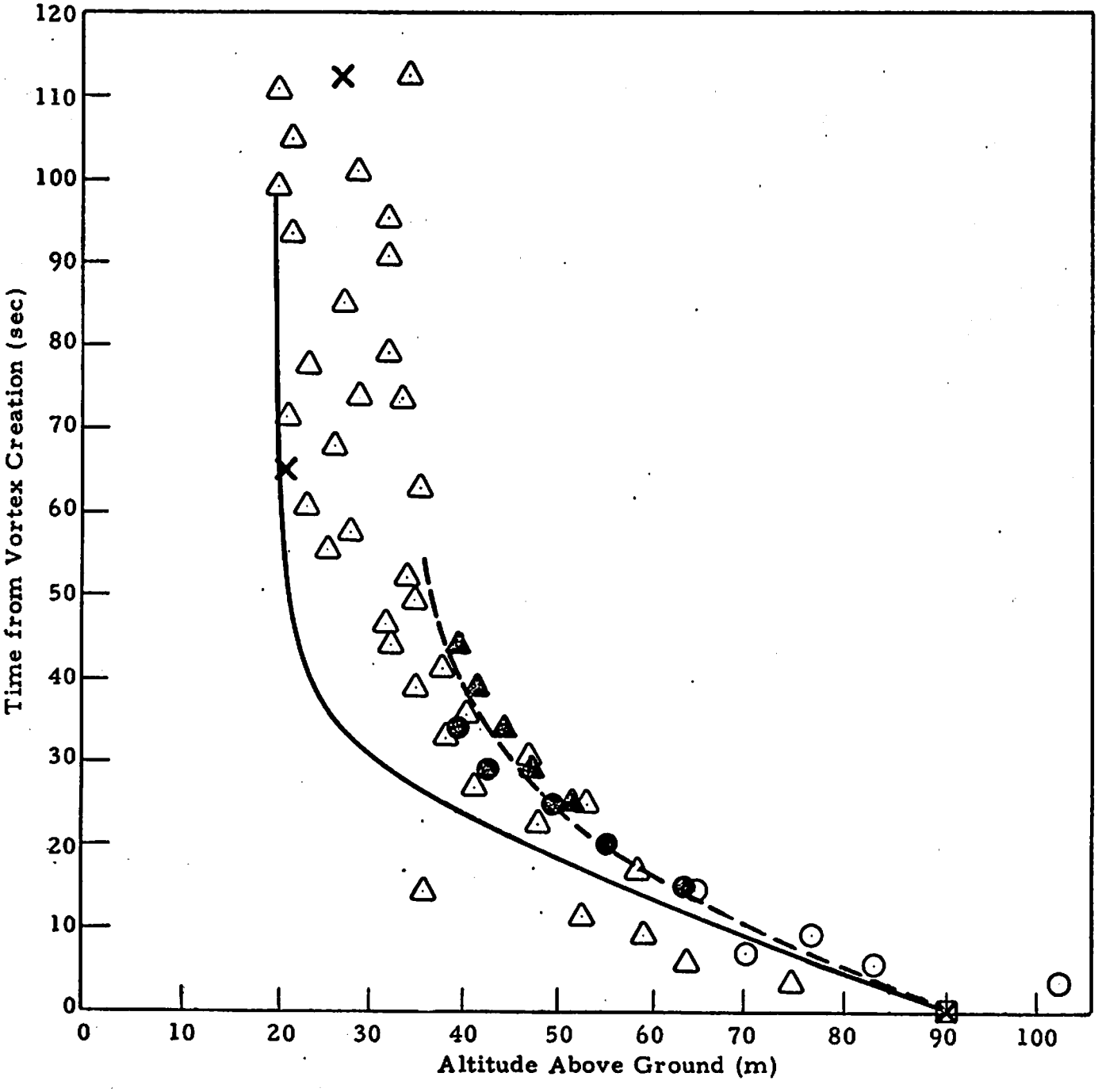
Time from Vortex Creation (sec)
120
110
100
90
80
70
60
50
40
30
20
10
0
0
10
20
30
40
50
60
70
80
90
100
Altitude Above Ground (m)

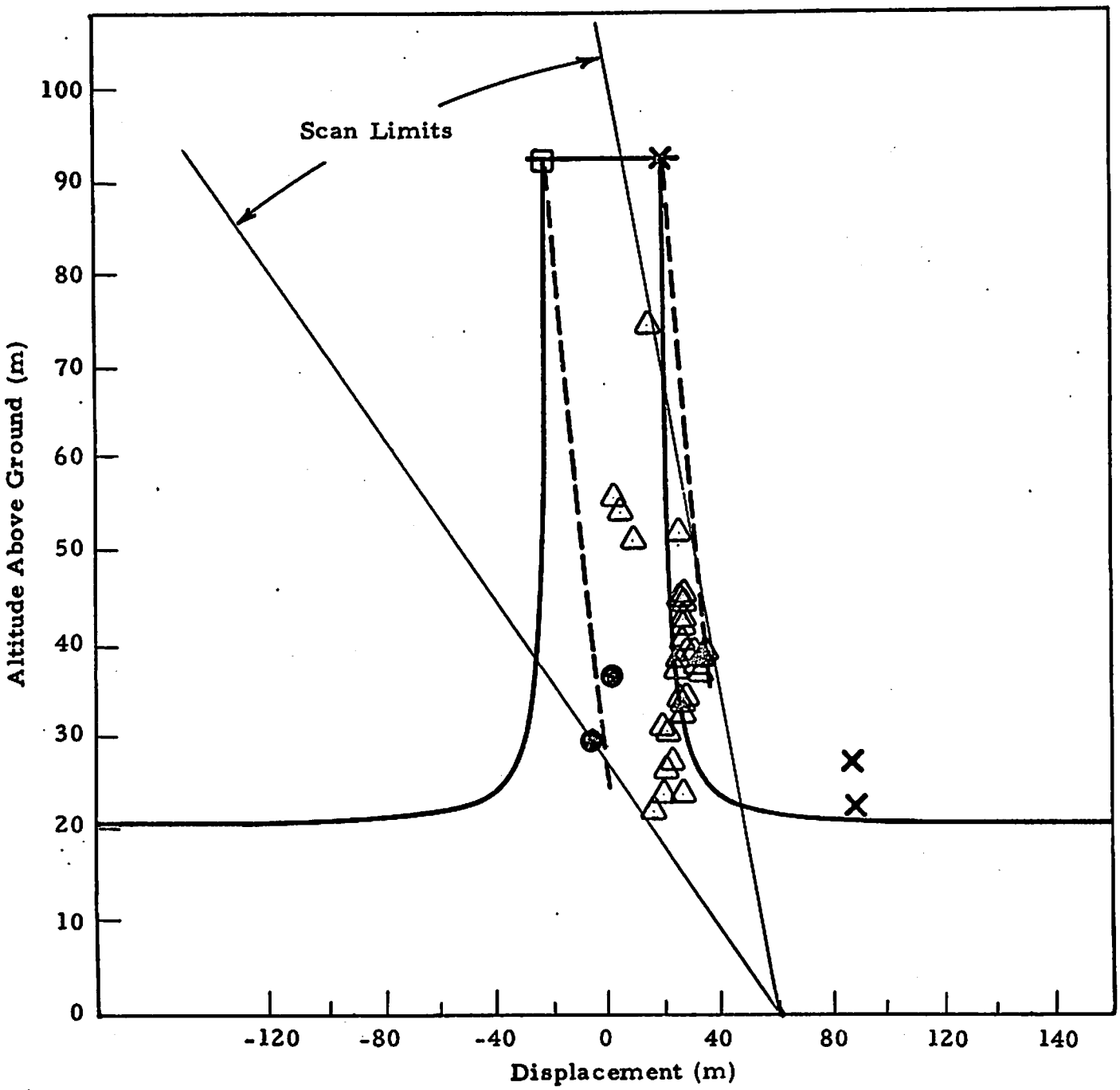

Wake Vortex Trajectory for Rosamond Flyby 48

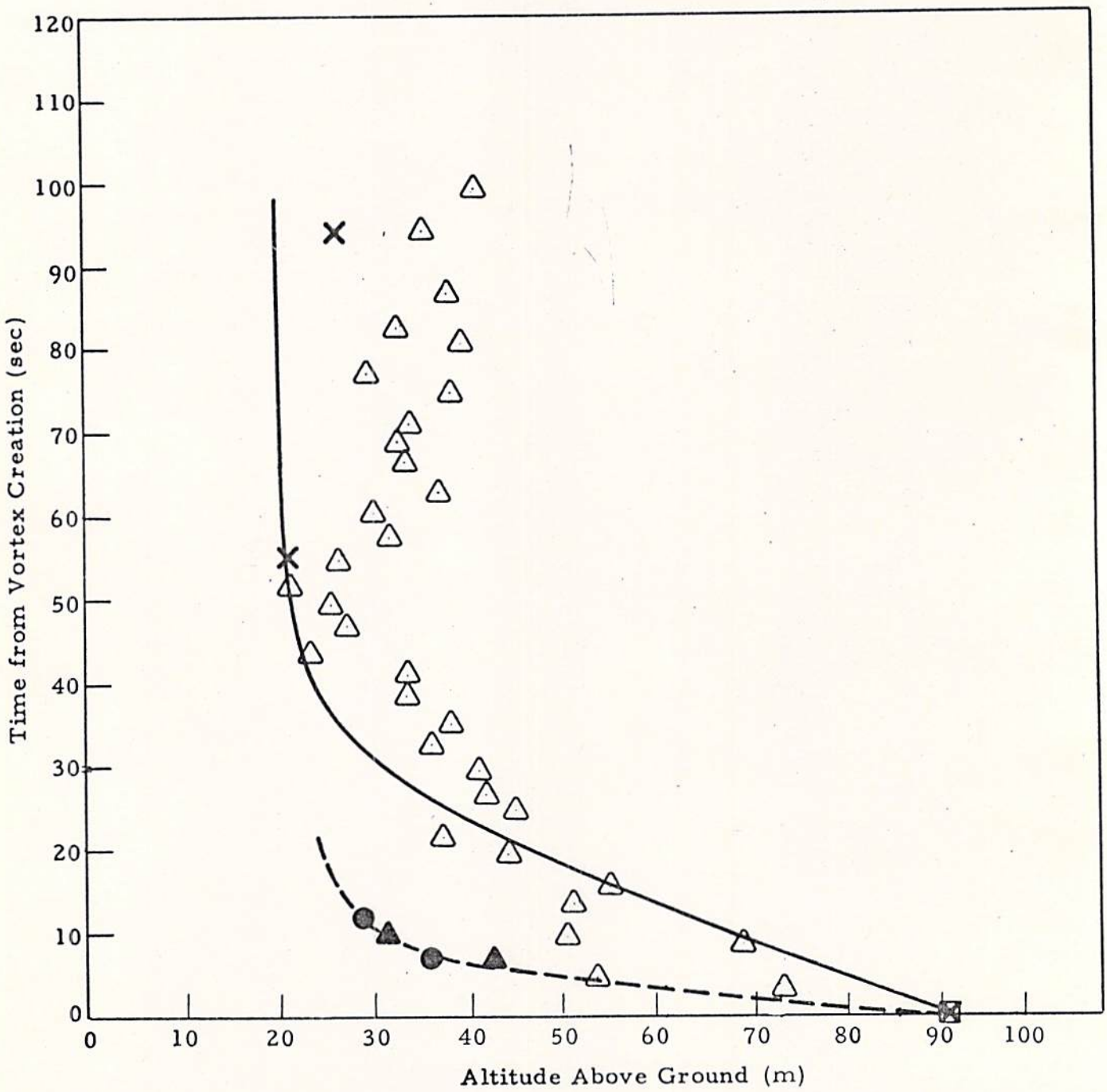
Time from Vortex Creation (sec)
120
110
100
90
80
70
60
50
40
30
20
10
0
0
10
20
30
40
50
60
70
80
90
100
Altitude Above Ground (m)

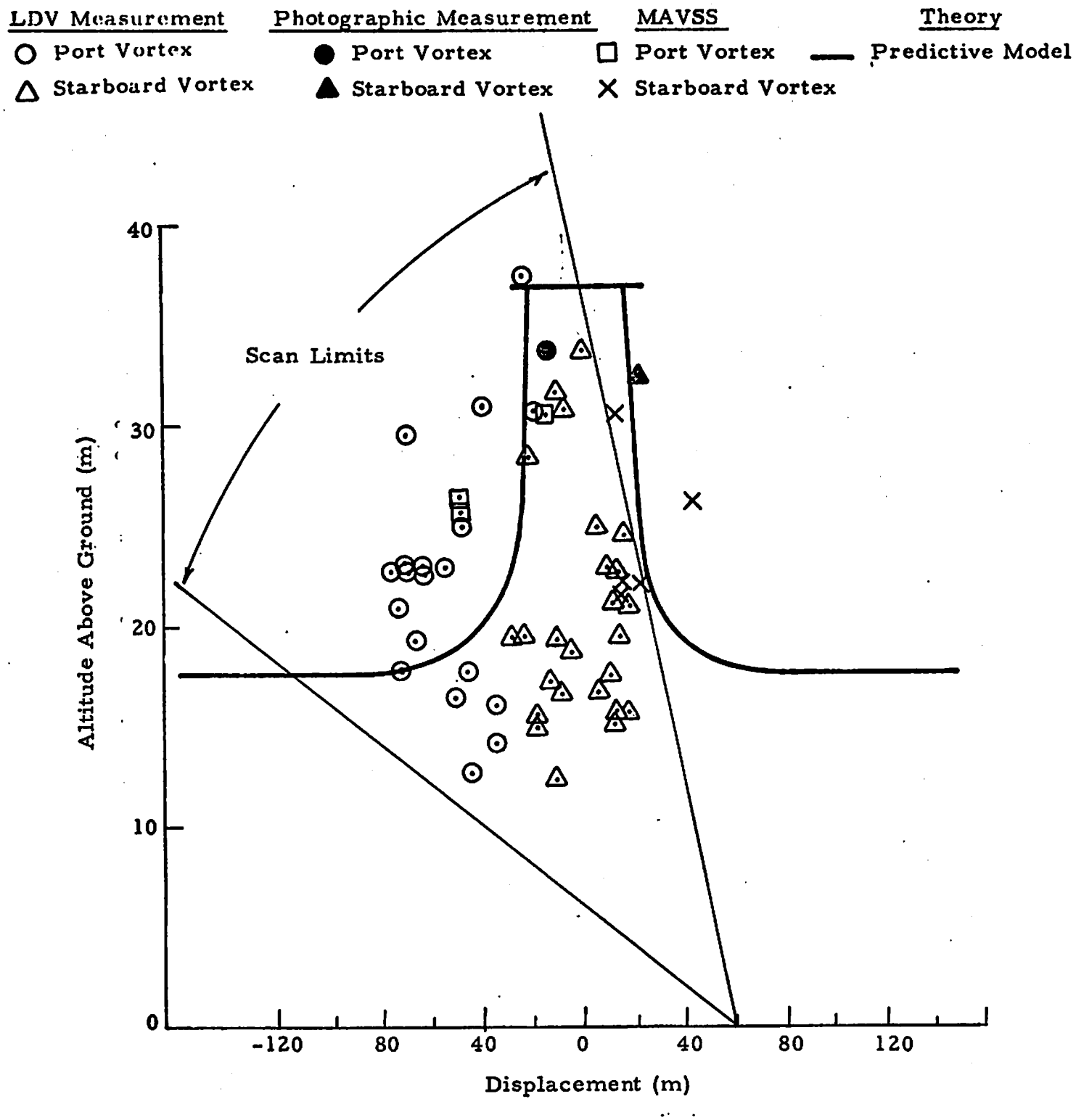

Wake Vortex Trajectory for Rosamond Flyby 49

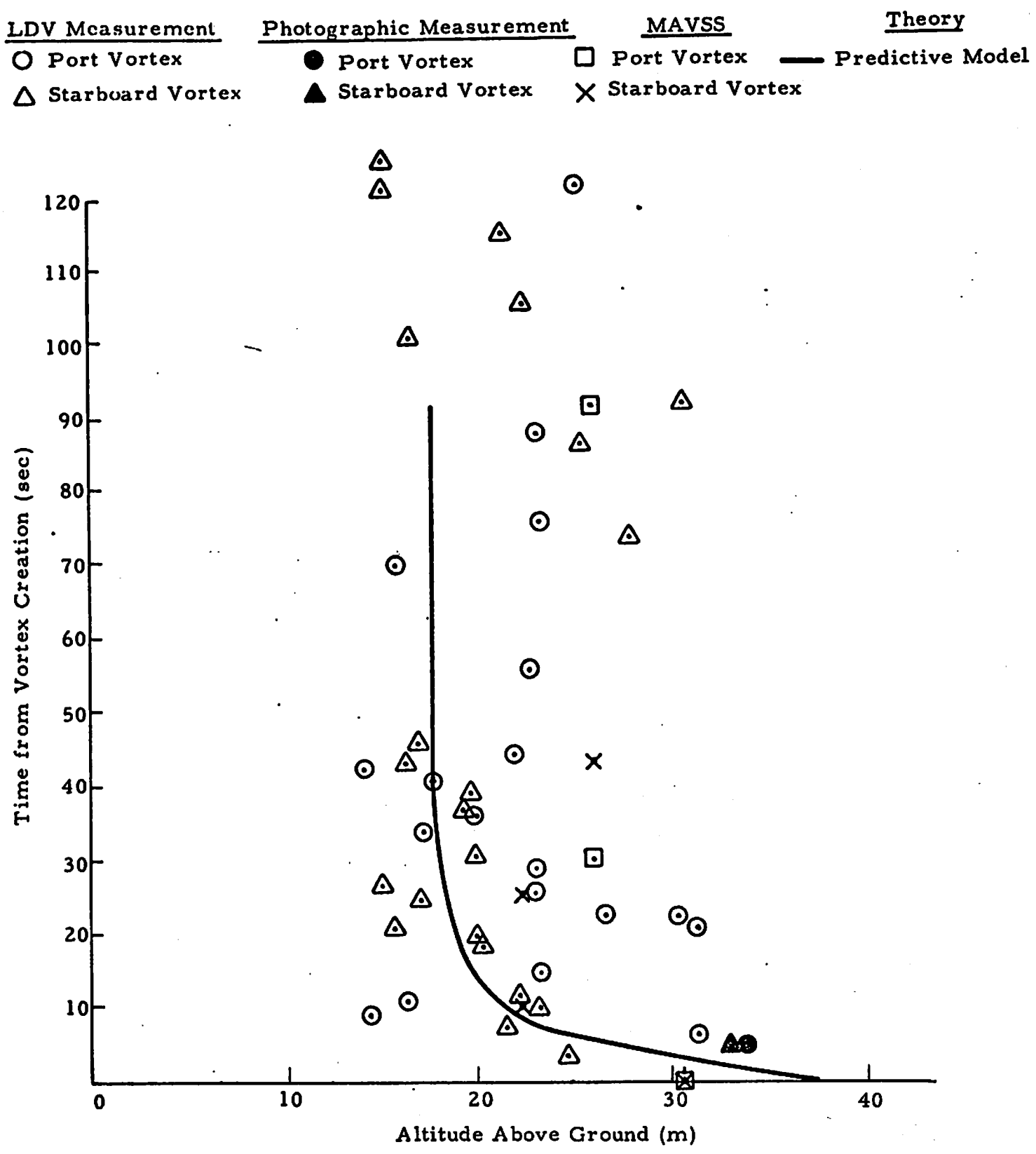
LDV Measurement
Port Vortex
Starboard Vortex
Photographic Measurement
Port Vortex
Starboard Vortex
MAVSS
Port Vortex
Starboard Vortex
Theory
Predictive Model
Time from Vortex Creation (sec)
120
110
100
90
80
70
60
50
40
30
20
10
0
10
20
30
40
Altitude Above Ground (m)

Appendix E

WAKE VORTEX TRACKS COMPUTED FROM HIGH SPEED MEASUREMENTS

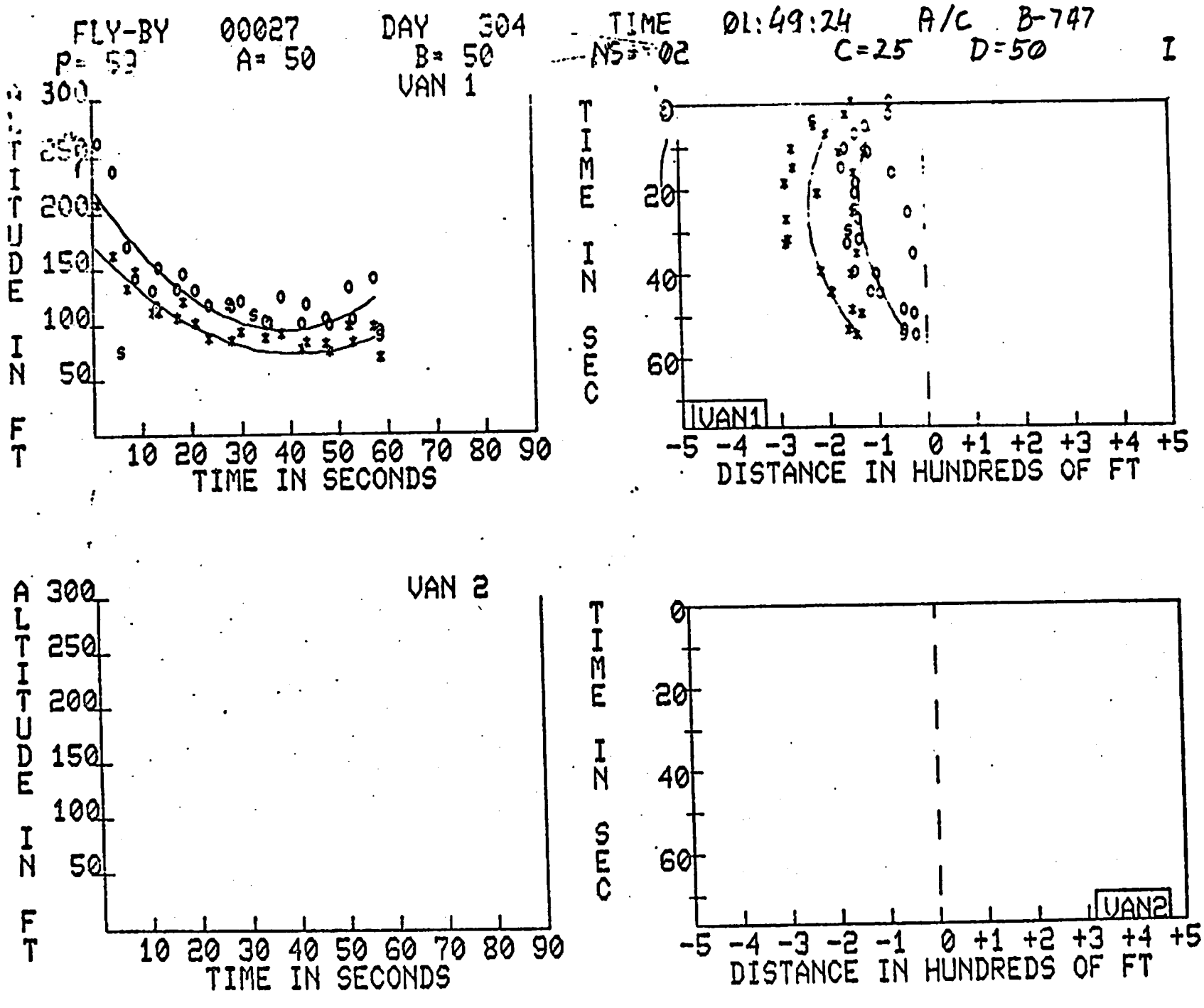
FLY-BY 00027 DAY 304 TIME 01:49:24 A/C B-747
P= 53 A= 50 B= 50 NS= 02 C=25 D=50 I
VAN 1
ALTITUDE IN FT
300
250
200
150
100
50
10 20 30 40 50 60 70 80 90
TIME IN SECONDS
TIME IN SEC
0
20
40
60
VAN1
-5 -4 -3 -2 -1 0 +1 +2 +3 +4 +5
DISTANCE IN HUNDREDS OF FT
VAN 2
ALTITUDE IN FT
300
250
200
150
100
50
10 20 30 40 50 60 70 80 90
TIME IN SECONDS
TIME IN SEC
0
20
40
60
VAN2
-5 -4 -3 -2 -1 0 +1 +2 +3 +4 +5
DISTANCE IN HUNDREDS OF FT

FLY-BY 00027 DAY 304 TIME 01 49 29 A/C B-747
E= 50 A= 50 B= 50 NS= 02 C= 25 D= 50

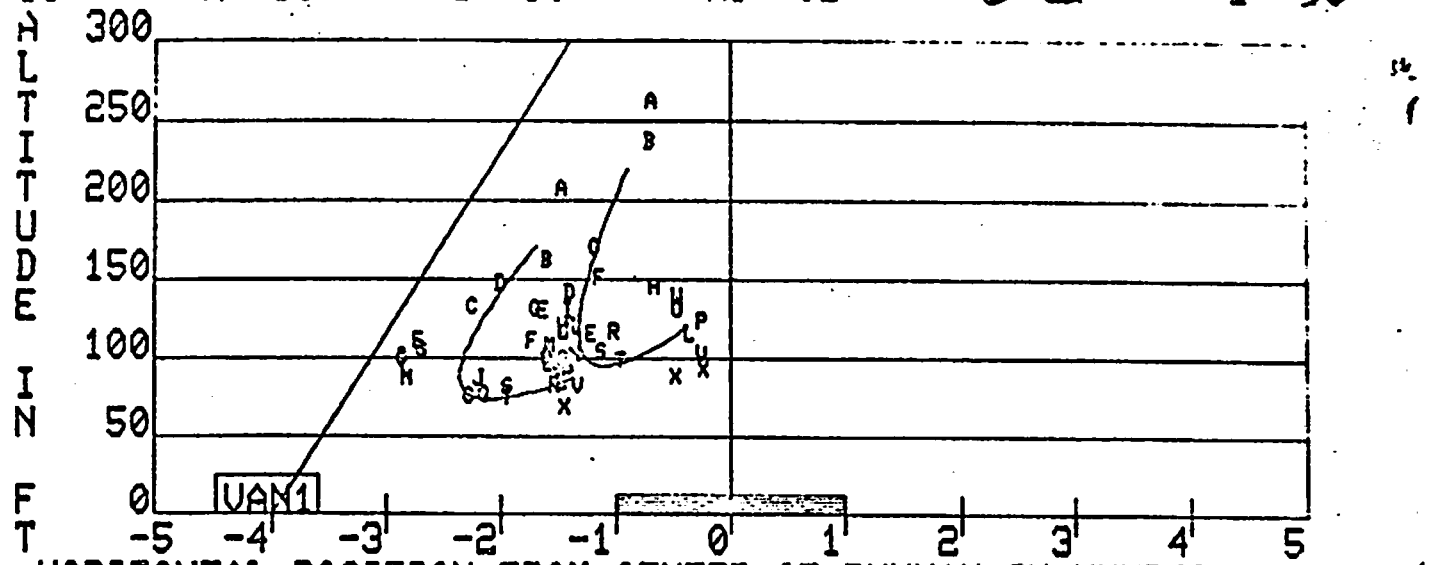

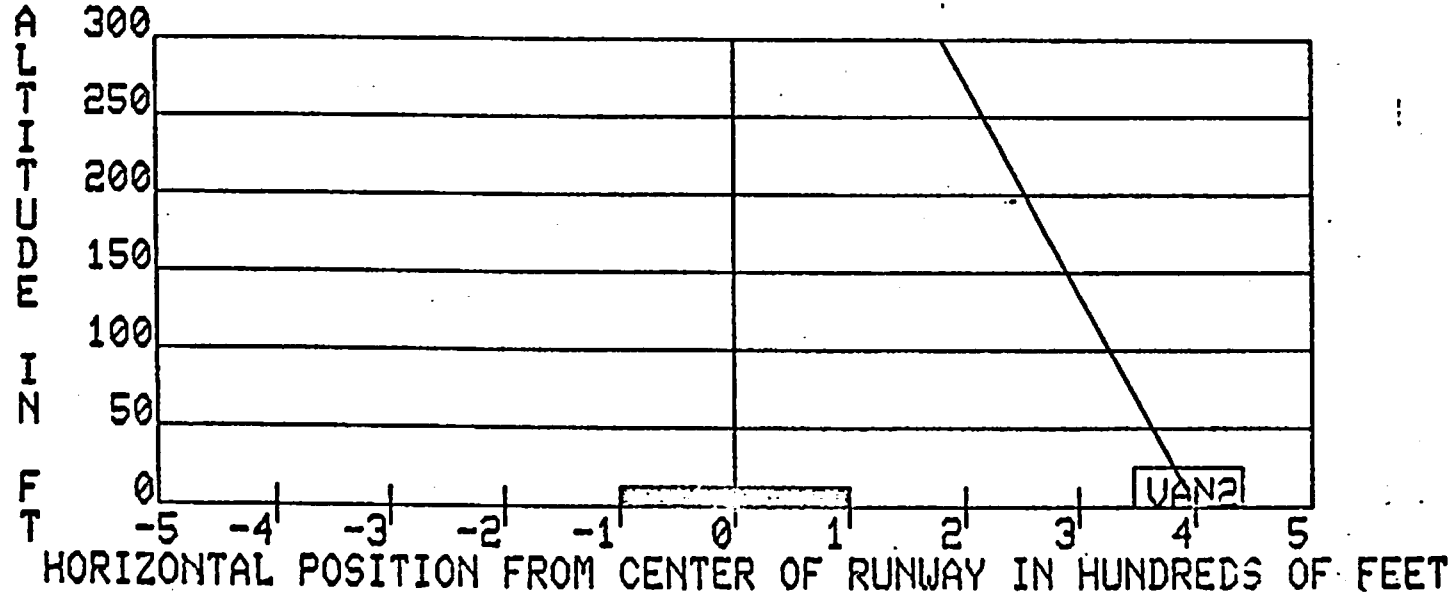

FLY-BY 00027 DAY 304 TIME 01 49 24 A/C B-747

R= 59 A= 50 B= 50 NS= 02 C= 25 D= 50 I

FR	DATA PTS	COR PT P	S	NOISE P	S	ANGLE MN	MX	PK P	PAR S	TIME	PORT POS X	Y	STARB POS X	Y
01	0747	250	099	00	00	24	44	258	216	000.6	-150	203	-073	258
02	0713	250	141	00	00	23	43	273	218	003.7	-163	158	-074	233
03	0003	000	000	00	00	00	00	000	000	005.5	-220	029	-121	166
04	0533	169	250	01	00	22	43	289	235	003.2	-203	143	-143	138
05	0003	000	000	00	00	00	00	000	000	012.4	-274	107	-183	188
06	0506	250	183	00	01	21	43	277	250	012.9	-176	107	-117	147
07	0749	075	247	00	00	22	45	245	205	016.7	-272	101	-173	128
08	0750	250	031	00	01	21	42	261	233	017.8	-148	116	-071	141
09	0555	033	195	00	00	20	45	201	228	020.3	-209	097	-144	126
10	0540	104	250	01	00	20	43	222	208	022.9	-222	083	-147	113
11	0455	033	180	05	00	18	43	210	253	026.9			-149	114
12	0103	000	000	00	00	10	00	000	000	030.8	-200	089	-000	110
13	0444	025	158	05	00	17	45	225	244	032.0			-160	104
14	0508	011	225	00	00	17	41	256	240	034.4	-224	083	-139	098
15	0004	016	165	00	00	19	42	241	229	035.1	-200	095	-164	097
16	0004	174	137	00	00	17	33	224	177	037.7	-144	087	-089	120
17	0005	040	144	01	00	15	46	103	230	040.0	-210	073	-148	095
18	0407	196	117	00	01	15	36	221	193	042.8	-186	078	-105	112
19	0005	000	180	01	00	16	35	170	224	047.1	-197	078	-117	101
20	0003	000	161	01	00	16	00	100	218	047.7	-197	071	-099	094
21	0015	181	004	00	00	17	03	004	100	051.6	-155	003	-000	127
22	0411	204	002	00	00	17	00	242	158	052.5	-135	078	-000	000
23	0018	100	003	00	00	17	32	000	194	055.8	-100	003	-000	135
24	0003	000	000	00	00	13	18	000	100	057.8	-148	005	-000	000

FR	DATA PTS	COR PT P	S	NOISE P	S	ANGLE MN	MX	PK P	PAR S	TIME	PORT POS X	Y	STARB POS X	Y

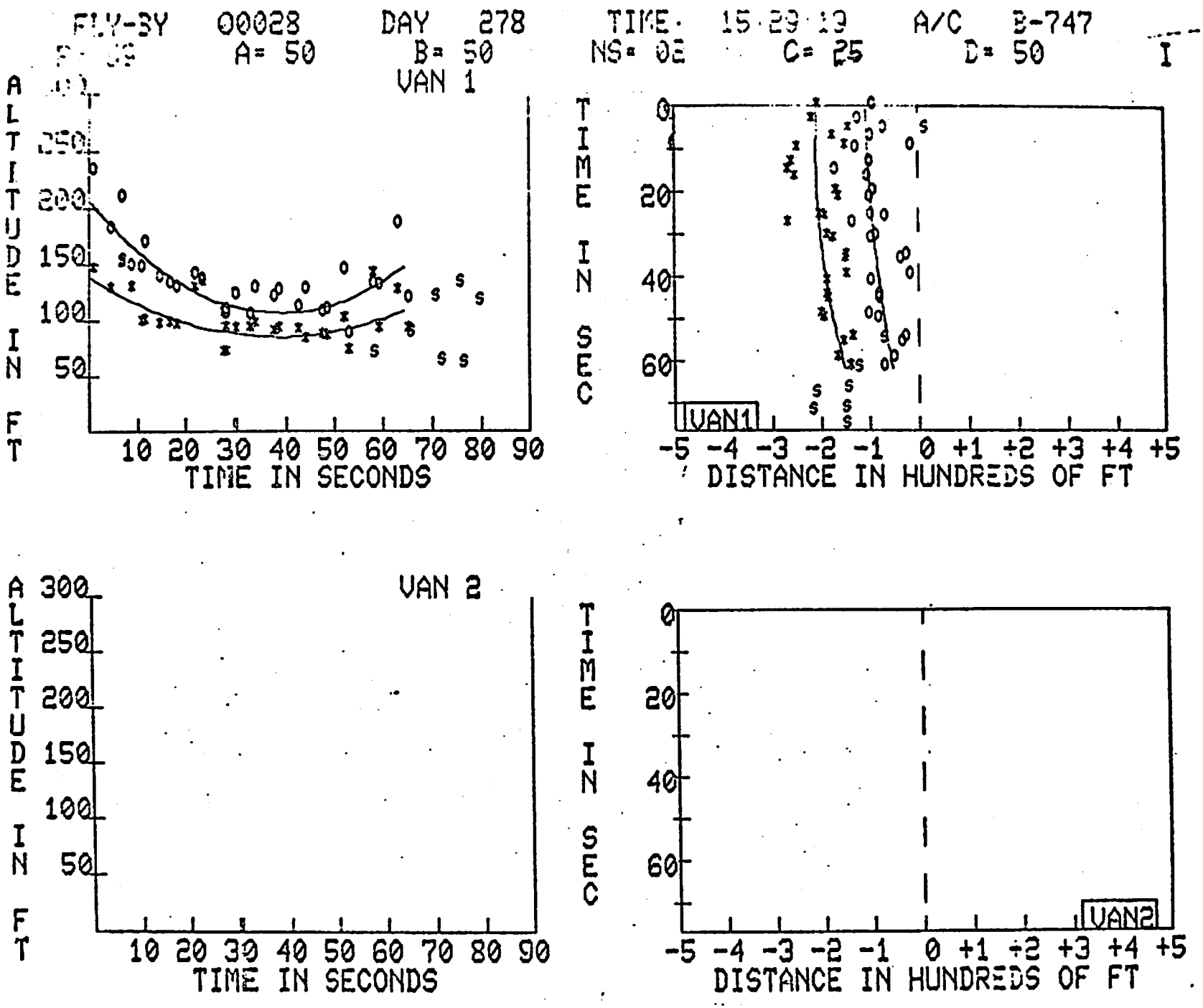
FLY-BY 00028 DAY 278 TIME 15:29:19 A/C B-747
A= 50 B= 50 C= 25 D= 50
VAN 1
ALTITUDE IN FT
300
250
200
150
100
50
10 20 30 40 50 60 70 80 90
TIME IN SECONDS
TIME IN SEC
0
20
40
60
VAN1
-5 -4 -3 -2 -1 0 +1 +2 +3 +4 +5
DISTANCE IN HUNDREDS OF FT
VAN 2
ALTITUDE IN FT
300
250
200
150
100
50
10 20 30 40 50 60 70 80 90
TIME IN SECONDS
TIME IN SEC
0
20
40
60
VAN2
-5 -4 -3 -2 -1 0 +1 +2 +3 +4 +5
DISTANCE IN HUNDREDS OF FT

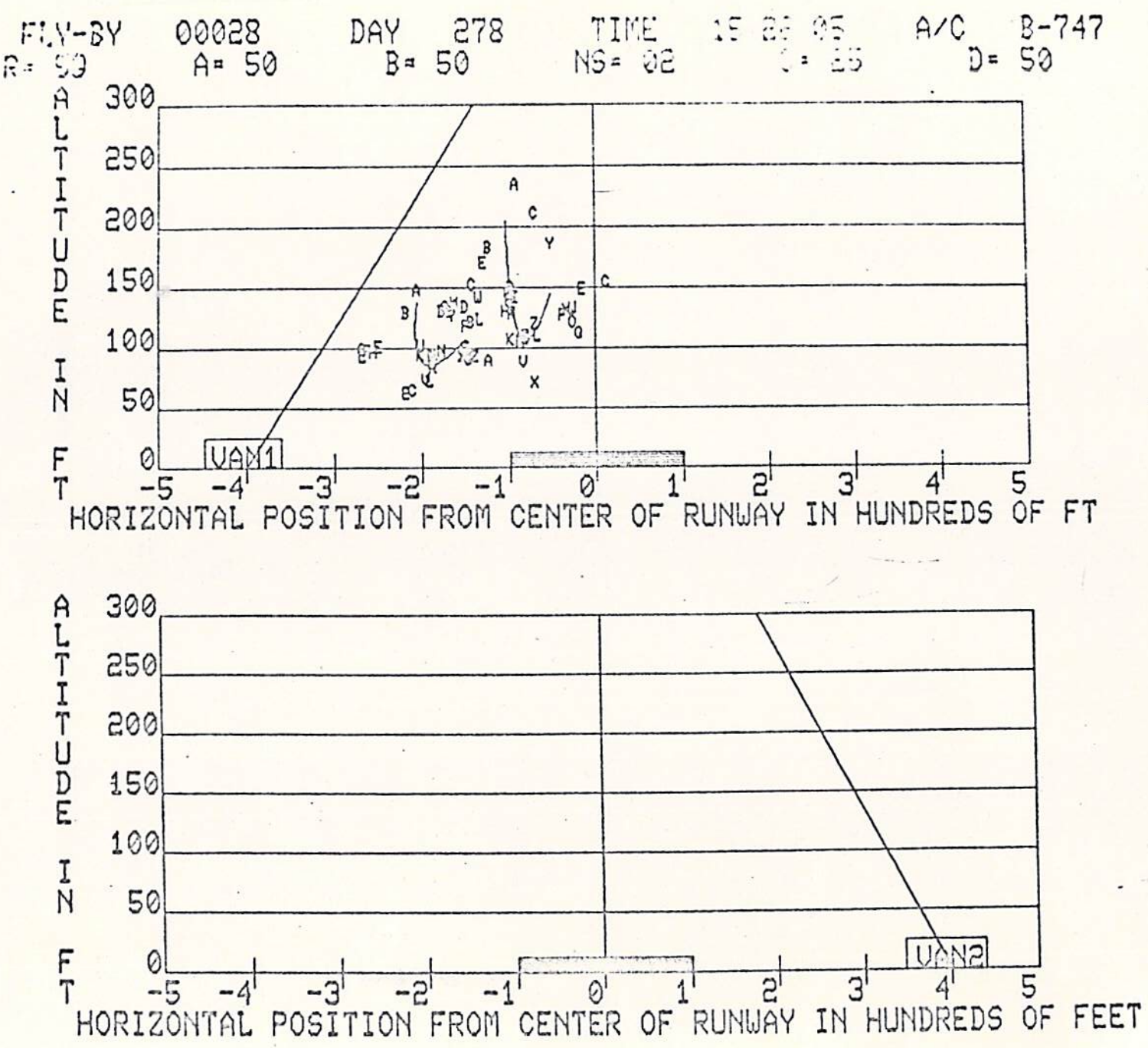
FLY-BY 00028 DAY 278 TIME 15 06 05 A/C B-747
R= 50 A= 50 B= 50 NS= 02 D= 50
ALTITUDE IN FT
300
250
200
150
100
50
0
-5 -4 -3 -2 -1 0 1 2 3 4 5
VAN1
HORIZONTAL POSITION FROM CENTER OF RUNWAY IN HUNDREDS OF FT
ALTITUDE IN FT
300
250
200
150
100
50
0
-5 -4 -3 -2 -1 0 1 2 3 4 5
VAN2
HORIZONTAL POSITION FROM CENTER OF RUNWAY IN HUNDREDS OF FEET

FLT-SY 00028 DAY 278 TIME 15 38 27 A/C B-747

P= 50 A= 50 B= 50 NS= 02 C= 00 D= 50 I

FR	DATA PTS	COR PT P	S	NOISE P	S	ANGLE MN	MX	PK P	PAR S	TIME	PORT X	POS Y	STARB X	POS Y
01	0537	250	199	00	00	21	40	261	273	000.3	-209	144	-096	230
02	0500	178	250	00	00	21	40	226	262	004.0	-221	185	-127	178
03	0003	000	003	00	00	00	00	003	005	006.2	-146	148	0000	000
04	0000	003	250	00	00	00	00	003	266	008.2	-150	126	-102	145
05	0000	003	000	00	00	00	00	006	278	010.9	-253	093	-093	103
06	0503	259	213	00	00	21	40	004	258	014.2	-206	093	-103	136
07	0574	089	250	00	00	20	40	260	266	016.2	-271	094	-175	130
08	0003	073	223	00	00	21	41	242	261	017.7	-258	092	-107	126
09	0000	250	161	00	01	19	42	257	233	021.4	-172	126	-096	138
10	0753	150	213	01	00	19	39	217	237	023.0	-167	130	-102	133
11	0503	250	193	00	00	18	39	233	253	027.4	-205	090	-101	103
12	0013	003	000	00	00	18	00	000	004	029.9	-003	089	-003	100
13	0510	203	180	01	00	16	39	226	257	032.2	-192	090	-091	101
14	0510	172	233	01	00	16	39	238	254	033.1	-160	093	-100	126
15	0712	173	160	00	00	14	41	248	192	037.0	-190	087	-090	117
16	0537	164	000	00	00	14	41	249	194	037.9	-154	000	-041	123
17	0506	206	105	00	00	15	34	246	204	041.9	-190	088	-088	103
18	0507	073	244	01	00	16	33	198	240	043.4	-191	079	-100	124
19	0134	182	197	00	00	13	34	200	245	046.9	-188	093	-094	104
20	0000	115	148	00	00	13	37	213	242	048.0	-183	081	-084	105
21	0506	078	237	02	00	18	39	173	231	051.6	-204	080	-105	141
22	0752	118	000	00	00	18	25	173	233	053.5	-190	070	-097	094
23	0001	210	187	00	00	14	25	202	172	057.5	-183	100	-091	109
24	0013	000	000	00	00	14	00	000	150	059.8	-157	000	-000	097
25	0527	210	197	00	00	15	25	231	193	062.5	-190	100	-095	101
26	0161	083	003	01	00	18	21	140	183	064.6	-142	000	-075	115
27	0000	074	000	00	04	17	21	173	000	065.0	-187	005		
28	0013	005	000	00	00	00	20	184	000	070.0	-140	117		
29	0000	002	000	00	00	17	18	146	000	071.3	-215	000		
30	0163	100	000	00	00	21	21	100	000	075.0	-194	120		
31	0003	003	000	00	00	17	18	170	000	075.8	-202	058		
32	0013	003	000	00	00	19	27	140	000	079.1	-159	113		
33	0000	000		00		00	00	000						
34	0003	007	000	00	00	00	00	153	000	085.0	-165	133		
35	0013	000		00		00	00	000						
36	0003	000		00		00	00	000						

FR	DATA PTS	COR PT P	S	NOISE P	S	ANGLE MN	MX	PK P	PAR S	TIME	PORT X	POS Y	STARB X	POS Y

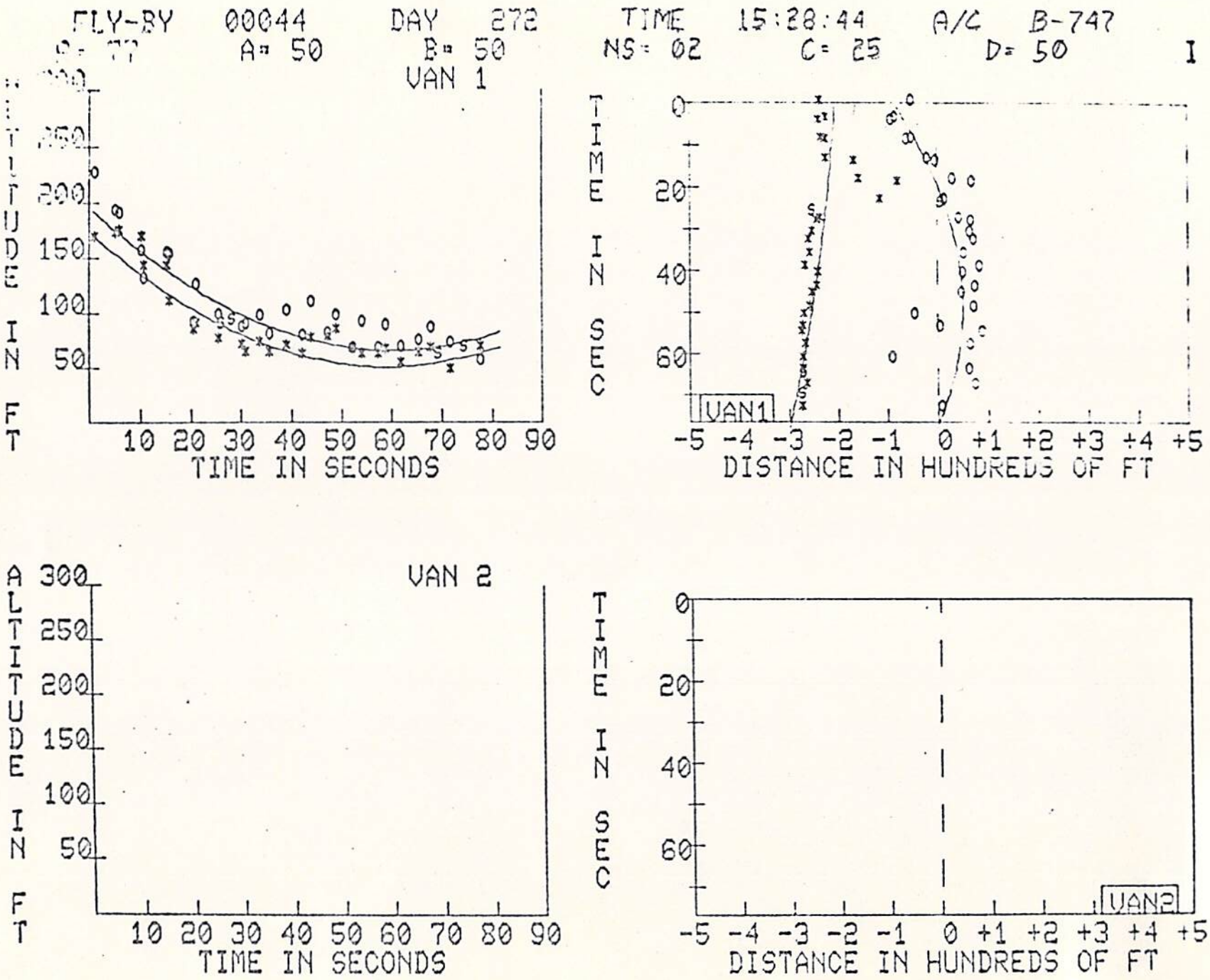
FLY-BY 00044 DAY 272
C= 77 A= 50 B= 50
VAN 1
ALTITUDE IN FT
TIME IN SECONDS
TIME 15:28:44 A/C B-747
NS= 02 C= 25 D= 50
TIME IN SEC
VAN1
DISTANCE IN HUNDREDS OF FT
VAN 2
ALTITUDE IN FT
TIME IN SECONDS
TIME IN SEC
VAN2
DISTANCE IN HUNDREDS OF FT

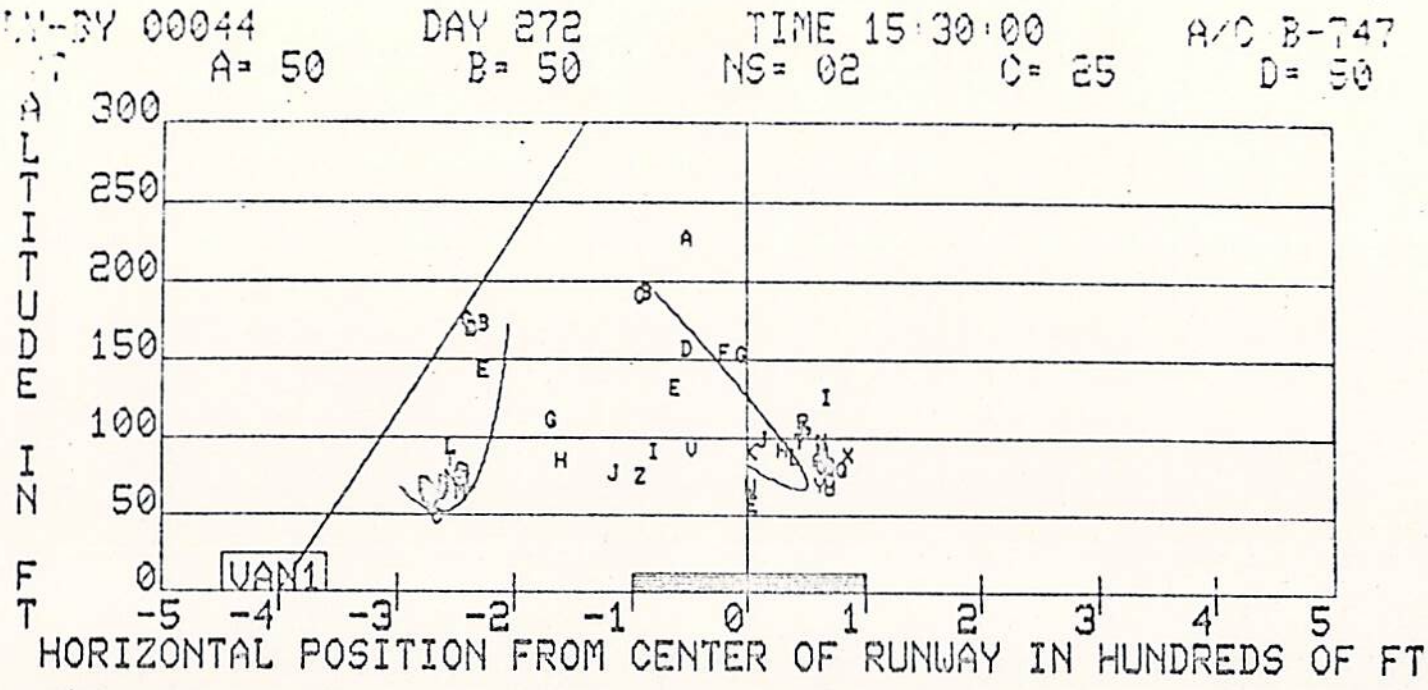
TUNBY 00044
DAY 272
TIME 15:30:00
A/C B-747
A= 50
B= 50
NS= 02
C= 25
D= 50
ALTITUDE IN FT
300
250
200
150
100
50
0
VAN1
-5 -4 -3 -2 -1 0 1 2 3 4 5
HORIZONTAL POSITION FROM CENTER OF RUNWAY IN HUNDREDS OF FT

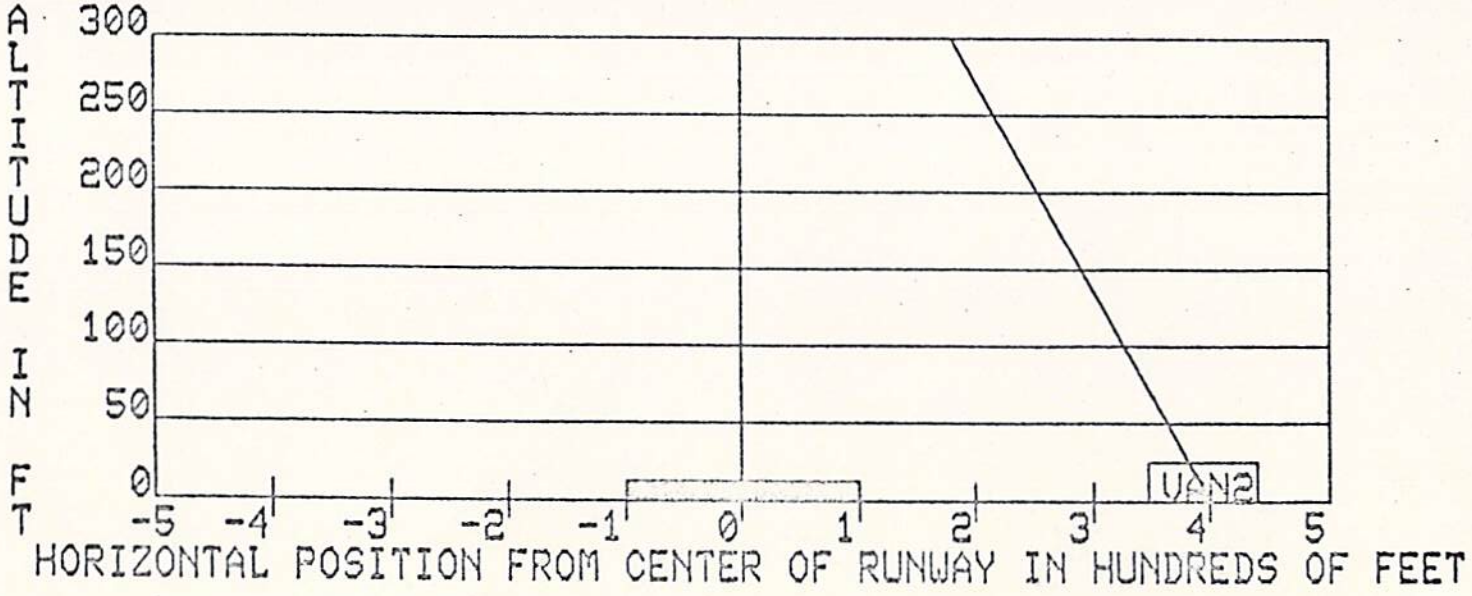
ALTITUDE IN FT
300
250
200
150
100
50
0
VAN2
-5 -4 -3 -2 -1 0 1 2 3 4 5
HORIZONTAL POSITION FROM CENTER OF RUNWAY IN HUNDREDS OF FEET

TLV-BY 00044 DAY 272 TIME 15:28:32 A/C B-747

A= 50 B= 50 NS= 02 C= 25 D= 50

FR	DATA PTS	COR P	PT S	NOISE P	NOISE S	ANGLE MN	ANGLE MX	PK P	PAR S	TIME	PORT POS X	PORT POS Y	STARB POS X	STARB POS Y
01	0876	194	200	00	00	27	54	262	282	000 5	-240	165	-056	223
02	0865	241	224	00	00	27	53	262	270	004 5	-228	168	-090	189
03	0867	174	187	00	00	27	54	243	274	005 3	-243	170	-097	186
04	0862	156	221	00	00	19	53	234	266	009 6	-238	164	-055	153
05	0782	178	154	00	00	19	53	248	281	010 1	-228	139	-065	127
06	0666	166	134	00	00	17	54	253	258	014 7	-230	139	-024	150
07	0528	131	141	00	00	17	52	197	237	015.2	-172	107	-009	149
08	0553	123	146	00	00	09	54	224	252	019 8	-163	081	0025	087
09	0561	132	050	00	00	09	55	256	234	020.3	-085	086	0063	121
10	0519	119	122	01	00	10	51	224	256	024 8	-119	073	0009	094
11	0312	035	218	05	00	08	33	220	249	025.3			0000	087
12	0093	258	000	00	00	02	30	220	000	029.6	-287	000	0036	083
13	0620	241	131	00	00	07	32	250	260	030.3	-249	060	0061	085
14	0441	028	100	00	00	09	33	245	224	033.1	-257	070	0059	094
15	0406	021	034	00	00	08	36	222	240	035.0	-265	060	0036	076
16	0292	021	123	00	00	10	35	229	200	038.4	-263	066	0046	098
17	0420	021	081	00	00	08	34	214	214	041.5	-271	058	0076	076
18	0178	026	079	00	00	08	33	214	178	043.2	-246	072	0044	106
19	0343	024	106	00	00	08	36	217	194	046.6	-249	074	0066	077
20	0008	024	040	00	00	09	37	203	169	048.2	-257	081	0040	093
21	0190	014	039	00	00	11	34	225	176	051.5	-263	064	0065	064
22	0048	010	023	00	00	11	34	212	153	053.4	-275	058	-051	037
23	0192	009	101	00	00	09	33	193	165	056.6	-276	058	-001	034
24	0000	000	004	00	00	90	90	000	134	058 1	-278	063	0032	004
25	0005	003	006	00	00	09	35	173	103	061.1	-272	050	0058	064
26	0008	002	006	00	00	11	29	153	103	064.7	-273	050	-006	071
27	0019	004	014	00	00	08	28	158	148	067.3	-276	063	0057	002
28	0003	003	000	00	00	14	33	184	000	068.5	-276	058		
29	0018	010	006	00	00	09	30	180	133	071.1	-289	044	0067	068
30	0004	004	000	00	00	23	33	150	000	073.7	-279	065		
31	0003	005	002	00	00	07	33	196	134	077.0	-280	085	0000	053
32	0000	000		00		90	90	000						
33	0003	004	003	00	01	10	27	172	140	081.6	-273	050	0059	077
34	0000	000		00		90	90	000						
35	0000	000		00		90	90	000						
36	0000	000		00		90	90	000						

FR	DATA PTS	COR P	PT S	NOISE P	NOISE S	ANGLE MN	ANGLE MX	PK P	PAR S	TIME	PORT POS X	PORT POS Y	STARB POS X	STARB POS Y

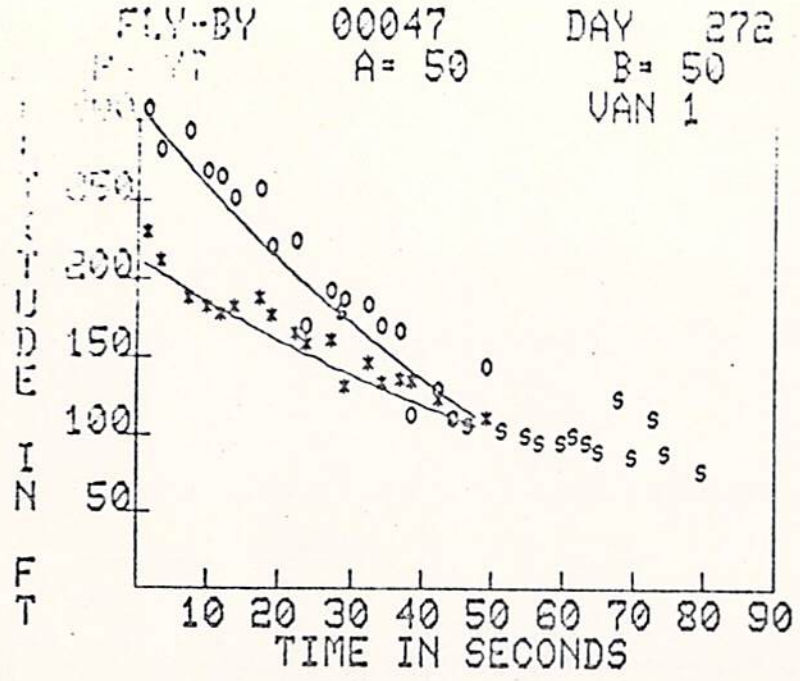
FLY-BY 00047 DAY 272
A= 50 B= 50
VAN 1
ALTITUDE IN FT
300
250
200
150
100
50
10 20 30 40 50 60 70 80 90
TIME IN SECONDS

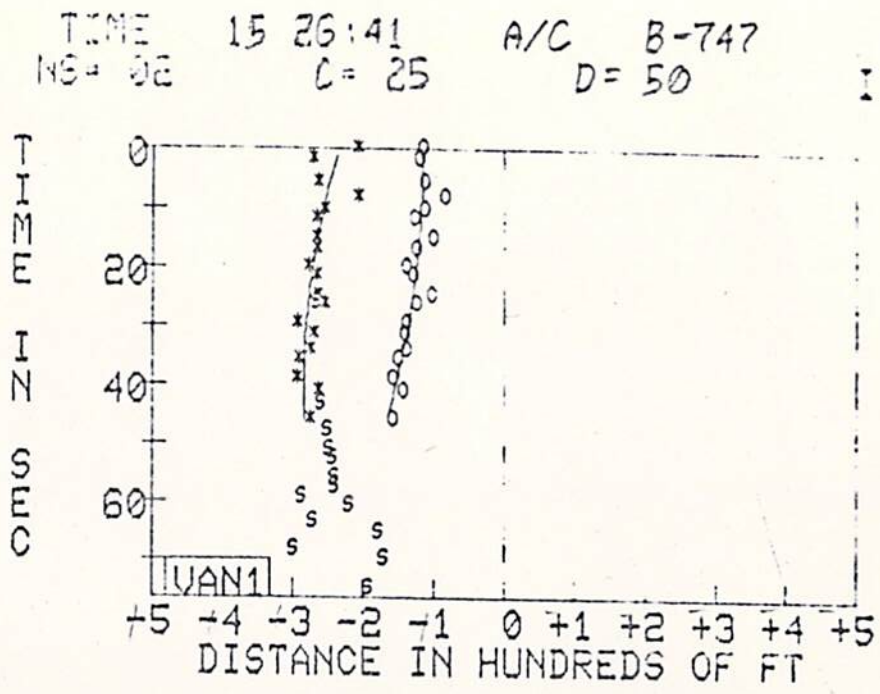
TIME 15 26:41 A/C B-747
C= 25 D= 50
TIME IN SEC
0
20
40
60
VAN1
+5 -4 -3 -2 -1 0 +1 +2 +3 +4 +5
DISTANCE IN HUNDREDS OF FT

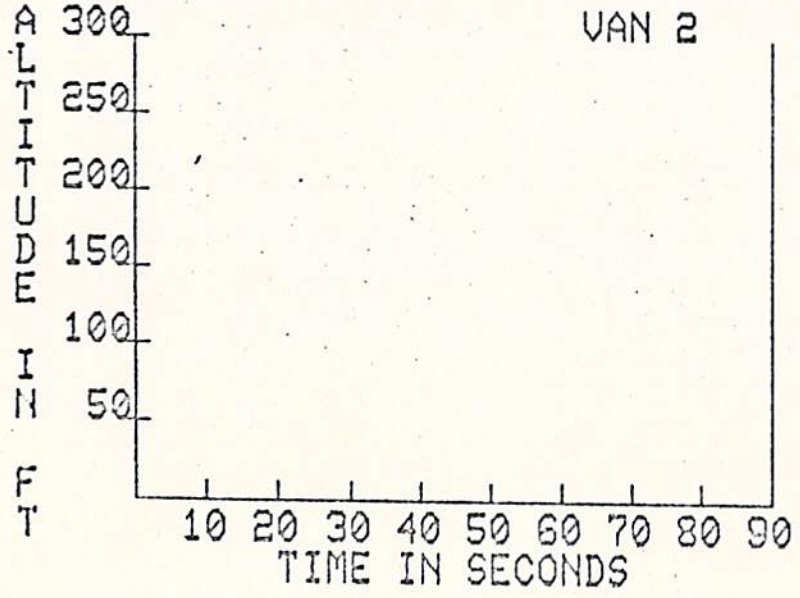
VAN 2
ALTITUDE IN FT
300
250
200
150
100
50
10 20 30 40 50 60 70 80 90
TIME IN SECONDS

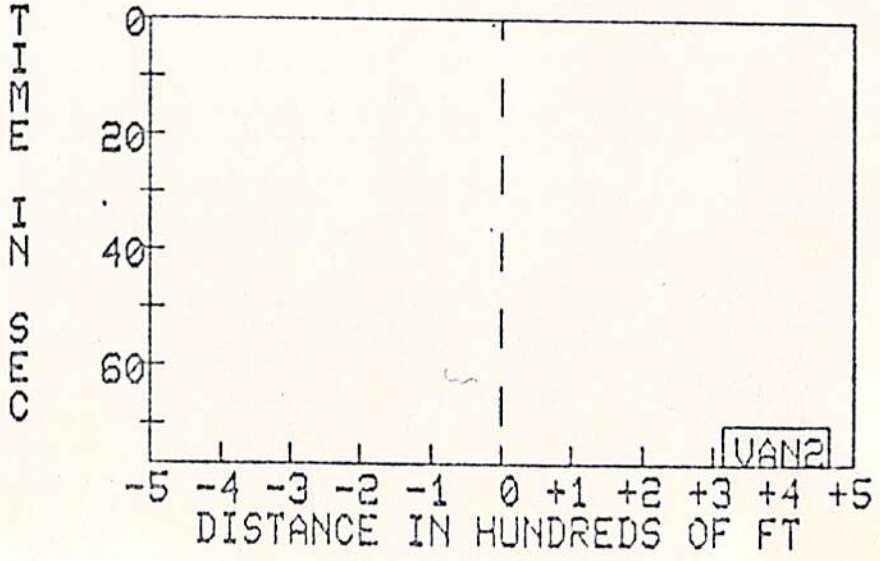
TIME IN SEC
0
20
40
60
VAN2
-5 -4 -3 -2 -1 0 +1 +2 +3 +4 +5
DISTANCE IN HUNDREDS OF FT

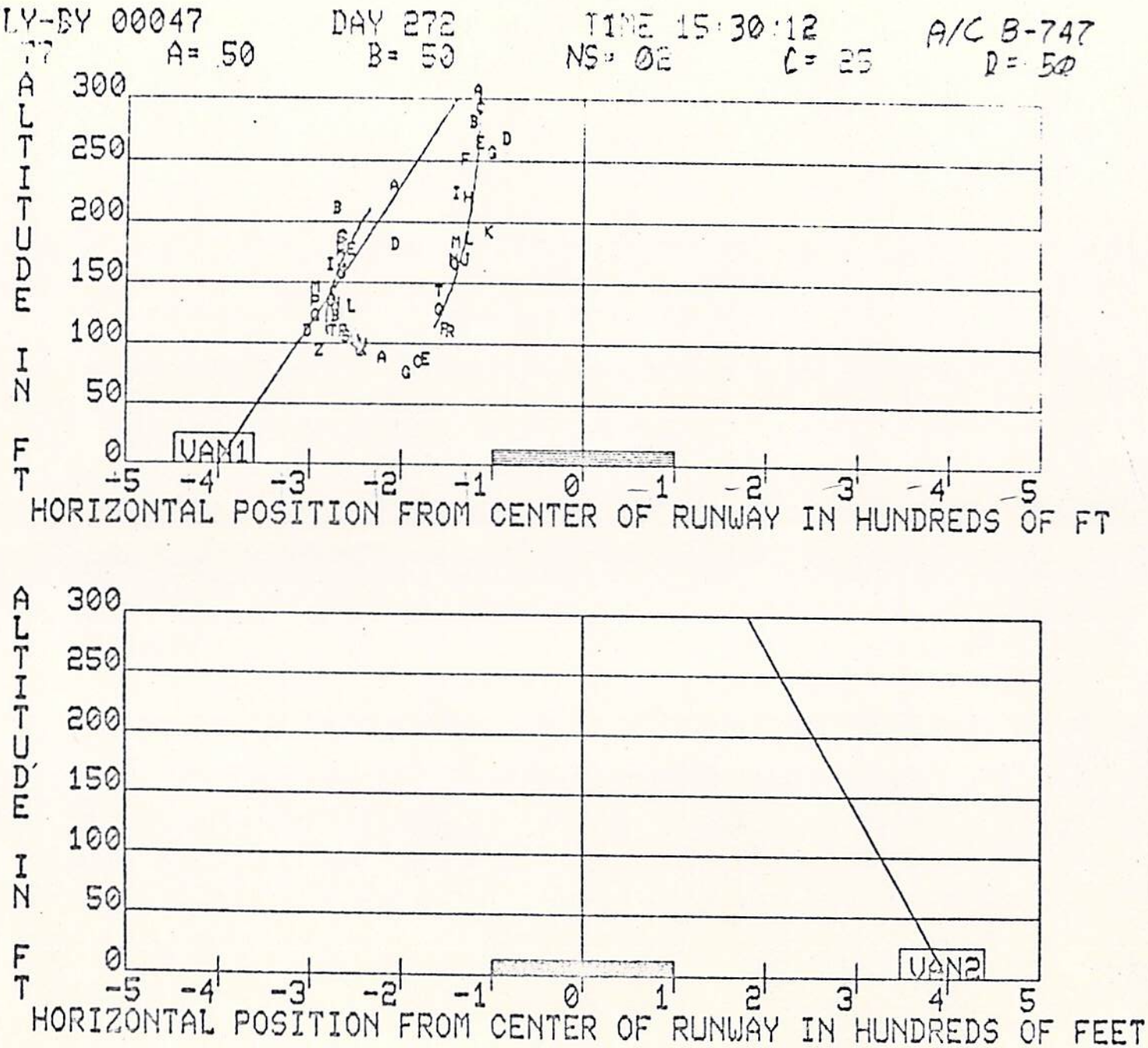
FLY-BY 00047
DAY 272
TIME 15:30:12
A/C B-747
A= 50
B= 50
NS= 0E
C= 25
D= 50
ALTITUDE IN FT
300
250
200
150
100
50
0
VAN1
-5 -4 -3 -2 -1 0 1 2 3 4 5
HORIZONTAL POSITION FROM CENTER OF RUNWAY IN HUNDREDS OF FT
ALTITUDE IN FT
300
250
200
150
100
50
0
VAN2
-5 -4 -3 -2 -1 0 1 2 3 4 5
HORIZONTAL POSITION FROM CENTER OF RUNWAY IN HUNDREDS OF FEET

FLY-BY 00047 DAY 272 TIME 15 28:32 A/C B-747

T A= 50 B= 50 NS= 02 C= 25 D= 50

FR	DATA PTS	COR PT P	S	NOISE P	S	ANGLE MN	MX	PK P	PAR S	TIME	PORT POS X	Y	STARB POS X	Y
01	0270	151	055	00	00	44	61	230	200	000.8	-211	225	-120	303
02	0491	128	128	00	00	37	62	230	221	002.8	-274	207	-124	277
03	0509	150	089	00	00	33	60	241	210	006.8	-268	183	-117	288
04	0753	250	146	00	00	37	61	232	208	009.4	-210	178	-089	263
05	0931	250	238	00	00	37	61	257	225	011.4	-259	173	-117	260
06	0917	238	250	00	00	36	61	258	209	013.2	-270	177	-139	247
07	0885	250	112	00	00	37	63	248	214	016.7	-271	183	-104	252
08	0719	233	222	00	00	38	61	230	220	018.3	-270	171	-130	216
09	0589	186	135	00	00	38	60	249	185	021.6	-281	160	-144	219
10	0680	209	224	00	00	29	59	248	196	023.2	-269	153	-133	165
11	0577	250	185	00	00	33	62	262	189	026.5	-268	156	-107	187
12	0416	003	000	00	00	43	09	250	000	028.8	-283	123	-129	181
13	0494	151	179	00	00	31	62	265	189	031.8	-293	141	-143	179
14	0491	158	093	00	00	29	60	272	172	033.6	-276	128	-146	165
15	0285	111	088	00	00	30	61	265	170	036.3	-280	131	-144	162
16	0311	086	114	00	00	18	61	276	176	038.0	-287	130	-154	108
17	0187	085	077	00	00	20	63	273	176	041.7	-293	118	-162	124
18	0178	057	085	00	00	18	62	237	145	043.8	-269	105	-148	105
19	0167	002	000	00	02	18	62	238	000	046.0	-284	101		
20	0142	043	019	00	00	19	62	212	144	048.7	-278	106	-162	139
21	0133	002	000	00	00	19	61	218	000	050.9	-284	098		
22	0116	054	000	00	00	19	54	220	000	054.0	-282	094		
23	0097	051	000	00	00	18	51	202	000	055.9	-248	090		
24	0081	000	000	00	00	52	59	101	000	059.2	-245	090		
25	0082	000	000	00	00	20	45	188	000	060.8	-246	094		
26	0082	002	000	00	00	37	48	174	000	062.8	-293	089		
27	0086	048	000	00	00	30	36	198	000	064.3	-284	084		
28	0086	086	000	00	00	39	45	186	000	067.1	-276	118		
29	0080	000	078	00	00	23	32	000	186	069.1			-184	080
30	0082	002	000	00	00	47	49	174	000	072.3	-306	106		
31	0088	002	088	00	00	24	25	000	176	073.8			-176	083
32	0090	000		00		50	90	000						
33	0093	000	024	00	00	19	21	000	196	079.1			-198	072
34	0100	000		00		90	90	000						
35	0099	000		00		90	90	000						
36	0100	000		00		90	90	000						

FR	DATA PTS	COR PT P	S	NOISE P	S	ANGLE MN	MX	PK P	PAR S	TIME	PORT POS X	Y	STARB POS X	Y

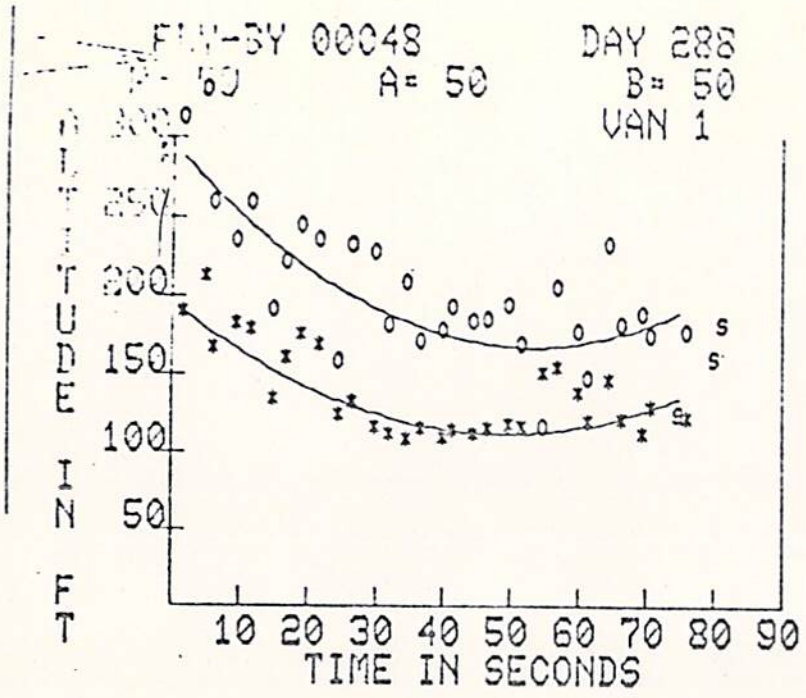
FLY-BY 00048
DAY 288
A= 50
B= 50
VAN 1
ALTITUDE IN FT
300
250
200
150
100
50
10 20 30 40 50 60 70 80 90
TIME IN SECONDS

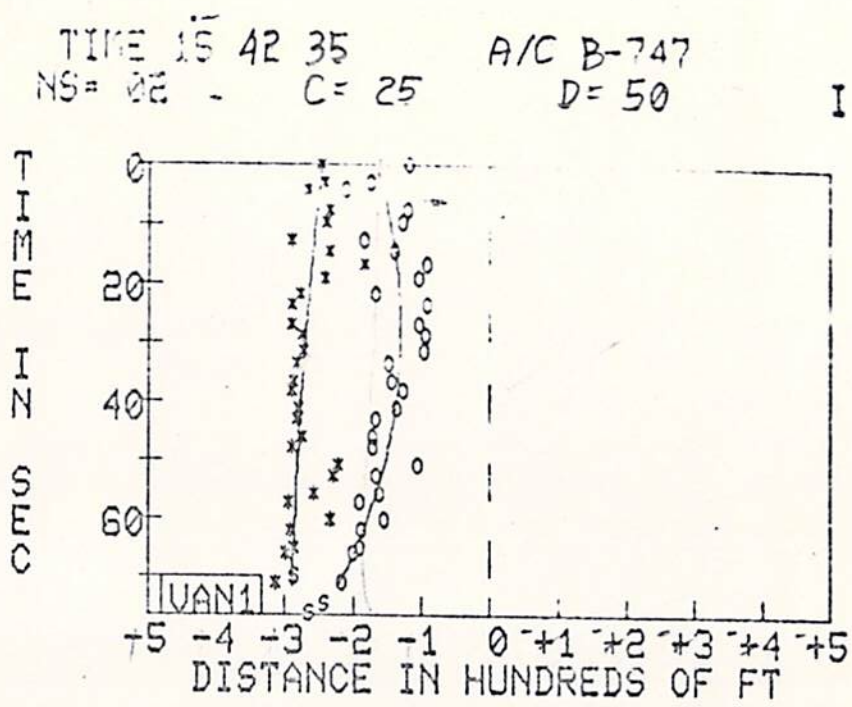
TIME 15 42 35
A/C B-747
NS= 02
C= 25
D= 50
I
TIME IN SEC
0
20
40
60
VAN1
-5 -4 -3 -2 -1 0 +1 +2 +3 +4 +5
DISTANCE IN HUNDREDS OF FT

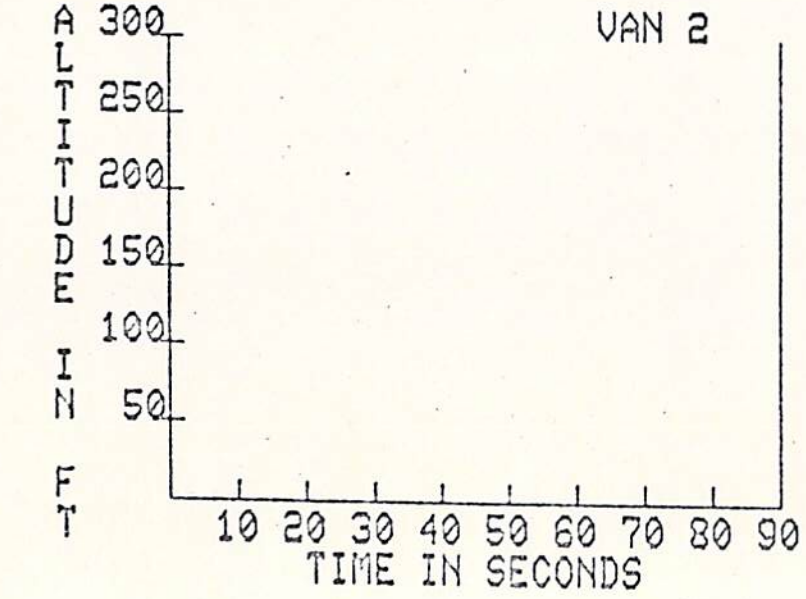
VAN 2
ALTITUDE IN FT
300
250
200
150
100
50
10 20 30 40 50 60 70 80 90
TIME IN SECONDS

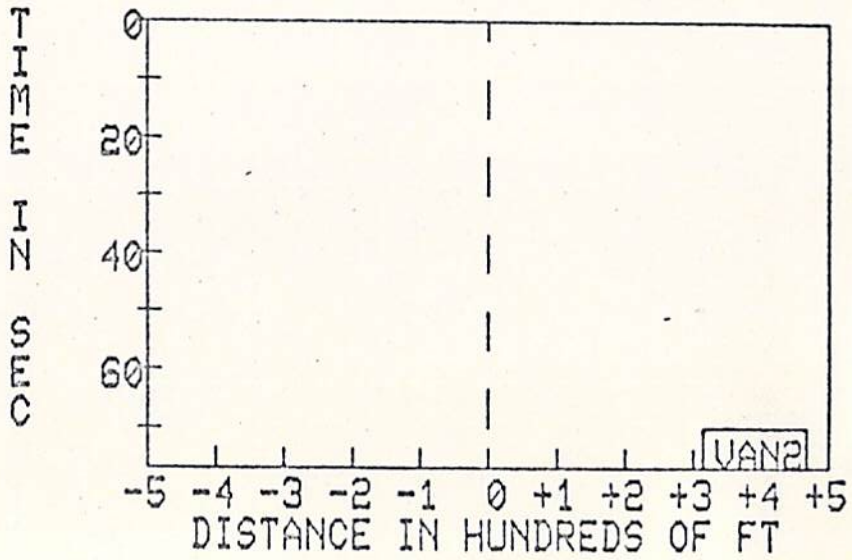
TIME IN SEC
0
20
40
60
VAN2
-5 -4 -3 -2 -1 0 +1 +2 +3 +4 +5
DISTANCE IN HUNDREDS OF FT

FLY-BY 00048 DAY-288 TIME 15 41 28 A/C B-747

R= 50 A= 50 B= 50 MS= 02 C=25 D= 50

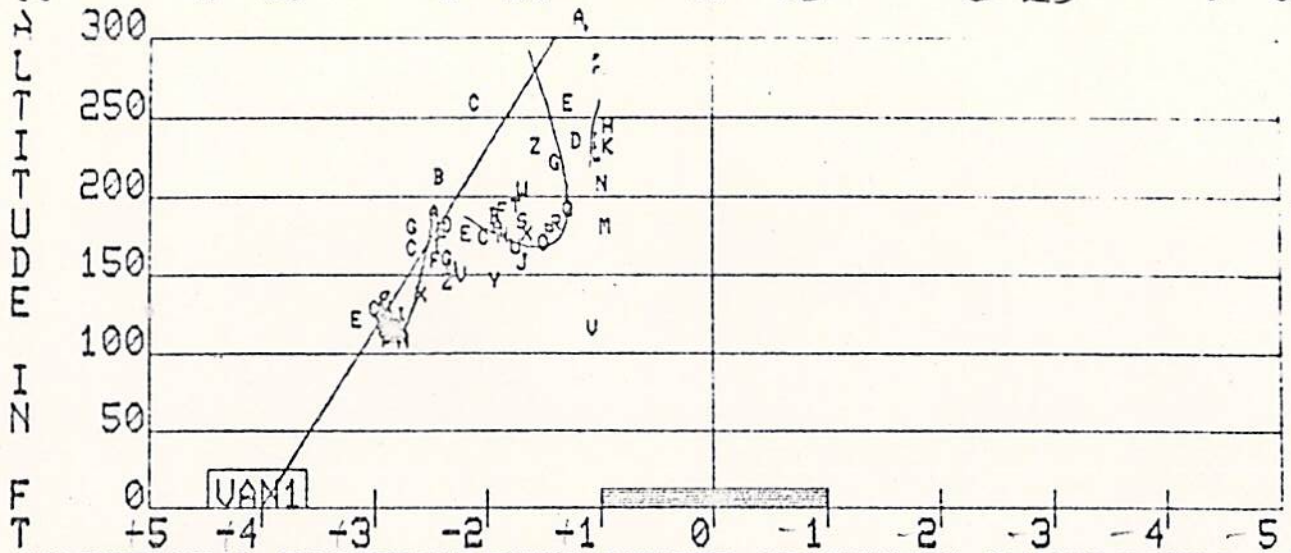

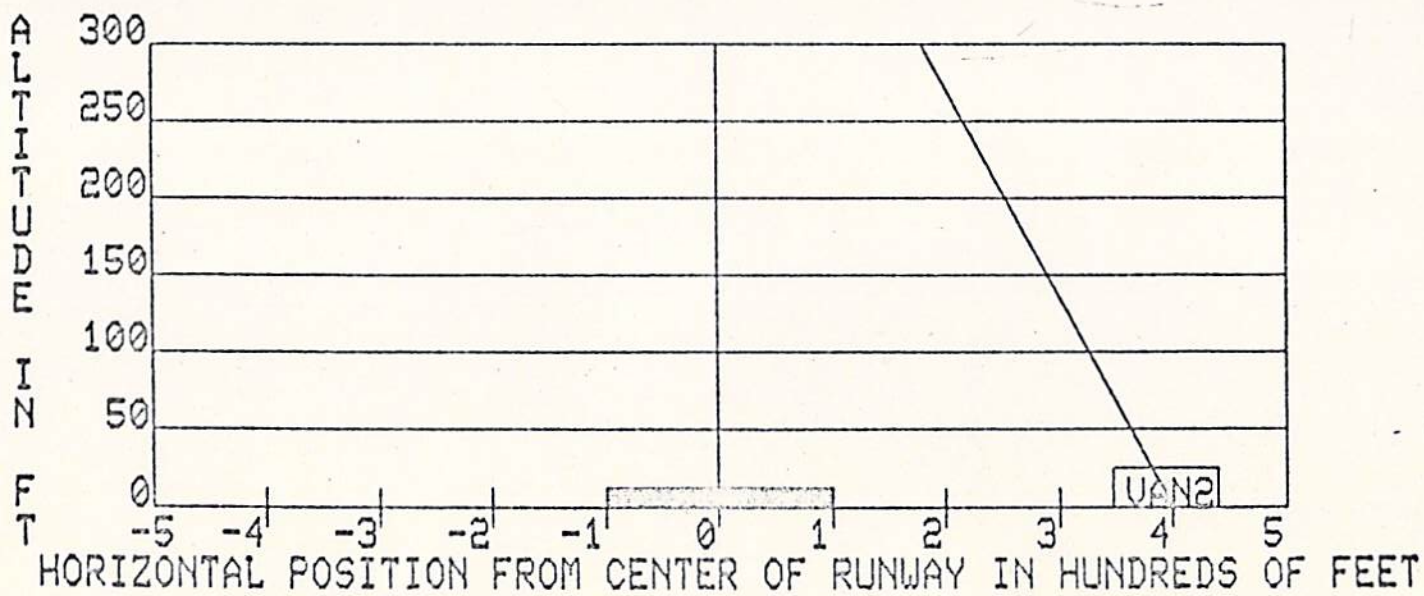

FLY-BY 00048 DAY 288 TIME 15:44:12 A/C B=747

P 50 A= 50 B= 50 NS= 0E C= 25 D = 50 I

FR	DATA PTS	COR P	PT S	NOISE P	NOISE S	ANGLE MN	ANGLE MX	PK P	PAR S	TIME	PORT POS X	PORT POS Y	STARB POS X	STARB POS Y
01	0409	068	079	00	00	35	61	234	218	020.9	-250	186	-121	328
02	0508	154	073	00	00	33	61	248	192	004.2	-246	208	-180	326
03	0673	059	129	00	00	30	62	205	235	005.6	-270	162	-214	254
04	0602	159	108	00	00	26	63	241	222	008.9	-239	177	-124	231
05	0644	148	110	00	00	27	63	230	203	011.0	-243	174	-132	255
06	0594	043	144	00	00	23	61	269	212	014.3	-292	130	-169	187
07	0525	137	116	00	00	27	61	233	209	016.3	-230	156	-143	217
08	0495	133	054	00	00	25	60	217	214	018.4	-169	170	-093	239
09	0530	149	053	00	00	23	61	233	205	020.9	-247	164	-103	231
10	0537	026	104	00	00	21	62	222	214	024.0	-281	120	-171	153
11	[illegible]	020	107	00	00	20	60	[illegible]	212	025.8	-204	127	-097	228
12	0450	022	055	00	00	22	60	253	201	029.1	-204	111	-107	223
13	0407	032	031	00	00	21	61	276	197	031.2	-279	107	-259	176
14	0472	043	035	00	00	19	58	250	202	033.8	-278	104	-102	233
15	0424	041	127	00	00	21	63	222	205	036.1	-236	110	-153	165
16	0337	017	103	00	00	19	54	250	213	039.3	-292	165	-148	173
17	0357	032	117	00	00	21	59	259	210	040.9	-234	110	-131	180
18	0433	040	103	00	00	21	57	[illegible]	224	044.0	-234	107	-142	178
19	[illegible]	032	165	00	00	25	56	245	184	046.0	-257	110	-171	179
20	0550	033	053	00	00	25	53	243	163	049.1	[illegible]	112	-178	189
21	0247	021	119	00	00	24	63	241	213	051.1	-233	112	-178	193
22	0237	[illegible]	032	00	00	21	52	231	177	054.1	-237	145	-111	112
23	[illegible]	000	019	00	03	[illegible]	[illegible]	[illegible]	140	[illegible]	-234	140	-172	200
24	0153	040	041	00	00	19	53	213	104	060.3	[illegible]	133	-167	171
25	0165	065	035	00	00	27	53	217	104	[illegible]	-207	114	-195	142
26	0151	075	018	00	00	23	51	205	143	064.0	[illegible]	141	-100	237
27	0116	024	047	00	00	[illegible]	55	244	173	065.7	-207	116	-193	176
28	[illegible]	010	045	00	00	[illegible]	55	217	103	068.9	[illegible]	103	-193	183
29	0057	031	031	00	00	[illegible]	53	[illegible]	176	070.1	-303	124	[illegible]	109
30	0055	024	000	00	00	30	53	153	000	074.2	-202	120		
31	[illegible]	003	037	00	00	33	57	202	142	075.3	-318	117	-221	172
32	[illegible]	000	003	00	00	40	47	000	156	078.3			-248	154
33	[illegible]	002	000	00	00	53	54	104	000	000.6	-270	176		
34	0000	000		00		50	50	000						
35	0000	000		00		50	00	000						

FR	DATA PTS	COR P	PT S	NOISE P	NOISE S	ANGLE MN	ANGLE MX	PK P	PAR S	TIME	PORT POS X	PORT POS Y	STARB POS X	STARB POS Y

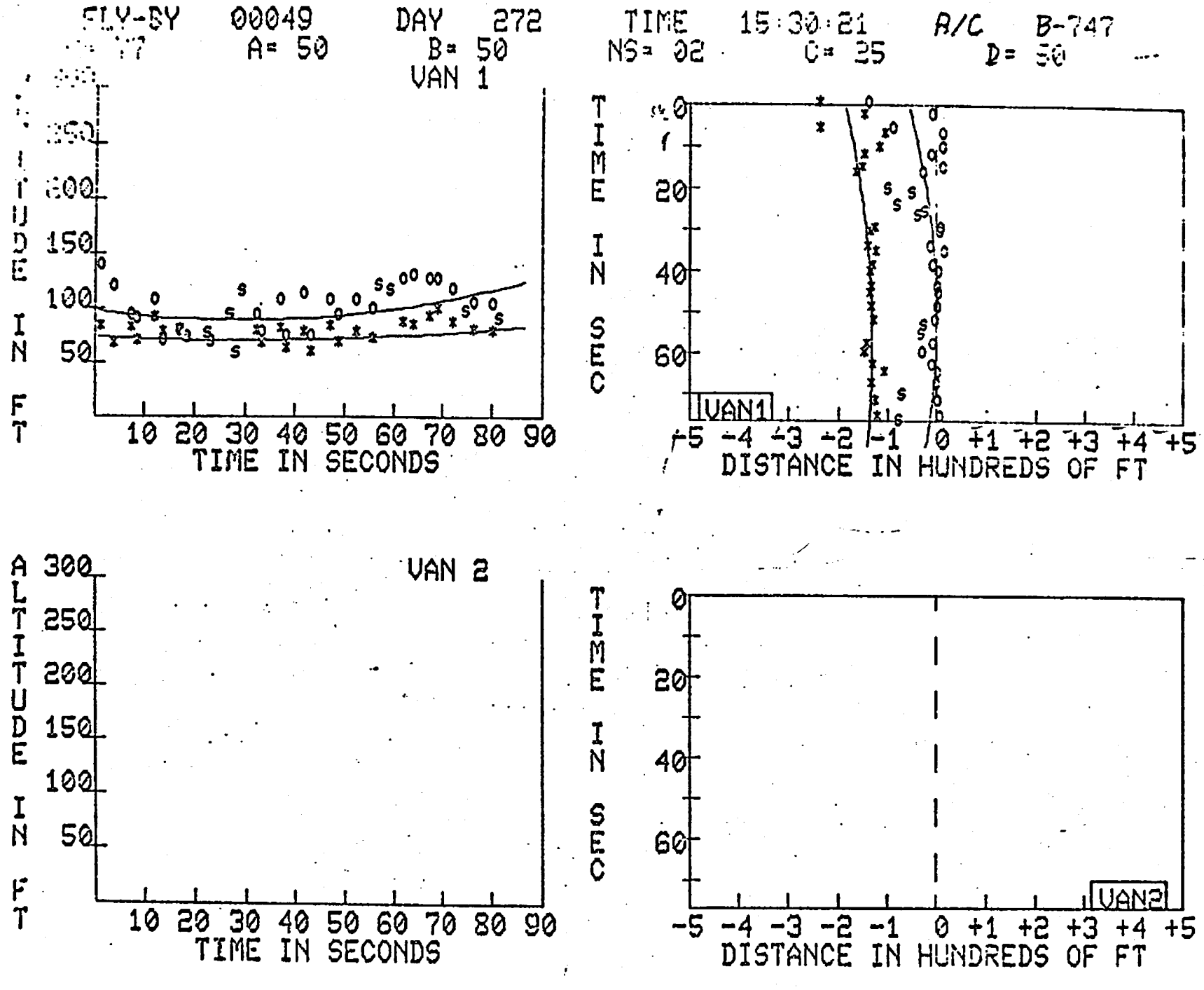
FLY-BY 00049 DAY 272 TIME 15:30:21 A/C B-747
A= 50 B= 50
NS= 02 C= 25 D= 50
VAN 1
ALTITUDE IN FT
TIME IN SECONDS
TIME IN SEC
DISTANCE IN HUNDREDS OF FT
VAN1
VAN 2
VAN2

FLY-BY 00049 DAY 272 TIME 15:56 52 A/C B-747

A= 50 B= 50 NS= 02 C= 24 D= 50

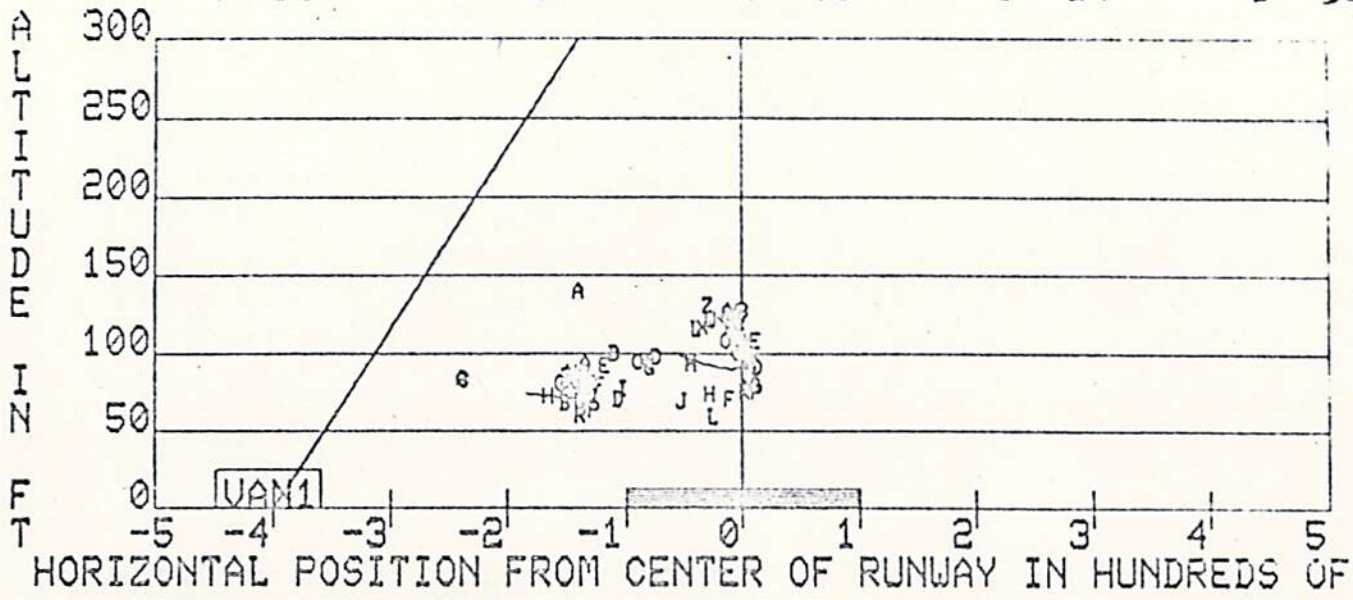

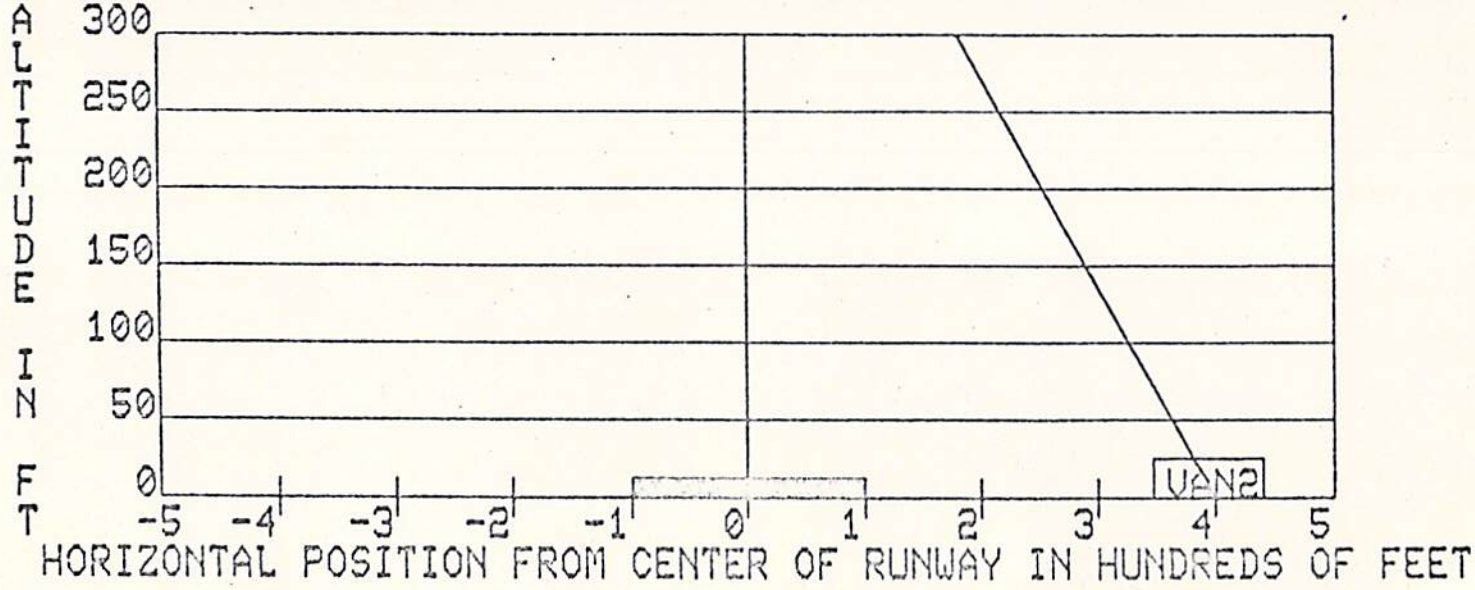

FLY-BY 00049 DAY 272 TIME 15:51:55 A/C -- B-747

77 A= 50 B= 50 NS= 02 C= 24 D= 50 I

FR	DATA PTS	COR PT P	S	NOISE P	S	ANGLE MN	MX	PK P	PAR S	TIME	PORT POS X	Y	STARB POS X	Y
01	0393	062	250	00	00	07	35	220	262	000.6	-241	080	-144	135
02	0969	250	229	00	00	07	34	273	213	003 1	-154	064	-013	116
03	0937	068	250	00	00	08	33	262	268	006.7	-240	079	-093	090
04	0933	250	099	00	00	08	33	265	240	007.9	-110	066	0009	086
05	0711	250	106	00	00	08	32	261	214	011.5	-122	087	0007	103
06	0950	250	156	00	00	08	33	261	244	013.3	-153	074	-014	086
07	0979	250	096	00	00	07	33	278	269	016.5	-158	076	0007	075
08	0997	227	214	00	00	07	28	252	276	017.9	-169	088	-031	089
09	0587	248	000	00	02	09	28	269	000	021.9	-106	073		
10	0583	016	250	05	00	08	22	170	208	022 8			-056	065
11	0376	000	221	00	00	08	23	000	249	026.2			-085	000
12	0283	000	089	05	00	00	50	000	000	028 6			-000	088
13	0987	131	120	00	00	08	21	214	244	031.6	-132	075	0004	089
14	0985	150	139	00	00	08	25	241	250	038.8	-142	064	0002	074
15	0971	106	171	00	00	10	23	214	242	036.6	-145	077	-017	104
16	0470	169	122	00	00	09	20	216	242	037.6	-130	059	0003	071
17	0957	169	112	00	00	09	22	209	000	041.2	-137	074	-012	110
18	0907	159	198	00	00	09	22	217	236	042.7	-142	056	0000	071
19	0915	078	146	00	00	10	23	196	240	043.6	-139	000	-003	103
20	0485	131	191	00	00	09	22	200	000	048.1	-141	065	0000	000
21	0240	087	000	00	00	12	21	184	000	051.8	-139	074	-004	103
22	0582	134	250	00	00	09	10	209	000	055.0	-134	000	-007	095
23	0215	000	000	04	00	00	24	000	224	056.4			-000	117
24	0000	000	103	00	00	00	00	000	217	058.7			-037	113
25	0000	000	110	00	00	10	25	209	000	061.1	-148	000	-011	123
26	0000	000	103	00	00	10	25	178	000	063.5	-153	000	-033	135
27	0372	024	133	00	00	07	23	195	000	066.2	-137	000	-015	133
28	0554	136	041	00	00	11	22	218	176	068.3	-113	000	-008	122
29	0219	057	103	00	00	12	21	000	000	071.4	-138	000	-005	114
30	0221	186	000	00	00	10	20	000	000	074.2	-077	094		
31	0164	000	075	00	00	00	00	174	201	076.7	-139	077	-003	101
32	0174	000	076	00	00	11	20	180	000	078.7	-135	075	0001	100
33	0183	086	000	00	00	00	00	184	000	000.9	-033	097		
34	0201	000	146	04	00	00	31	000	000	004.5			-048	099
35	0185	051	033	00	00	00	18	196	177	006.8	-138	074	-006	106
36	0000	000		00		00	00	000						

FR	DATA PTS	COR PT P	S	NOISE P	S	ANGLE MN	MX	PK P	PAR S	TIME	PORT POS X	Y	STARB POS X	Y

Appendix F
TIME HISTORY OF VORTEX ROTATIONAL VELOCITY

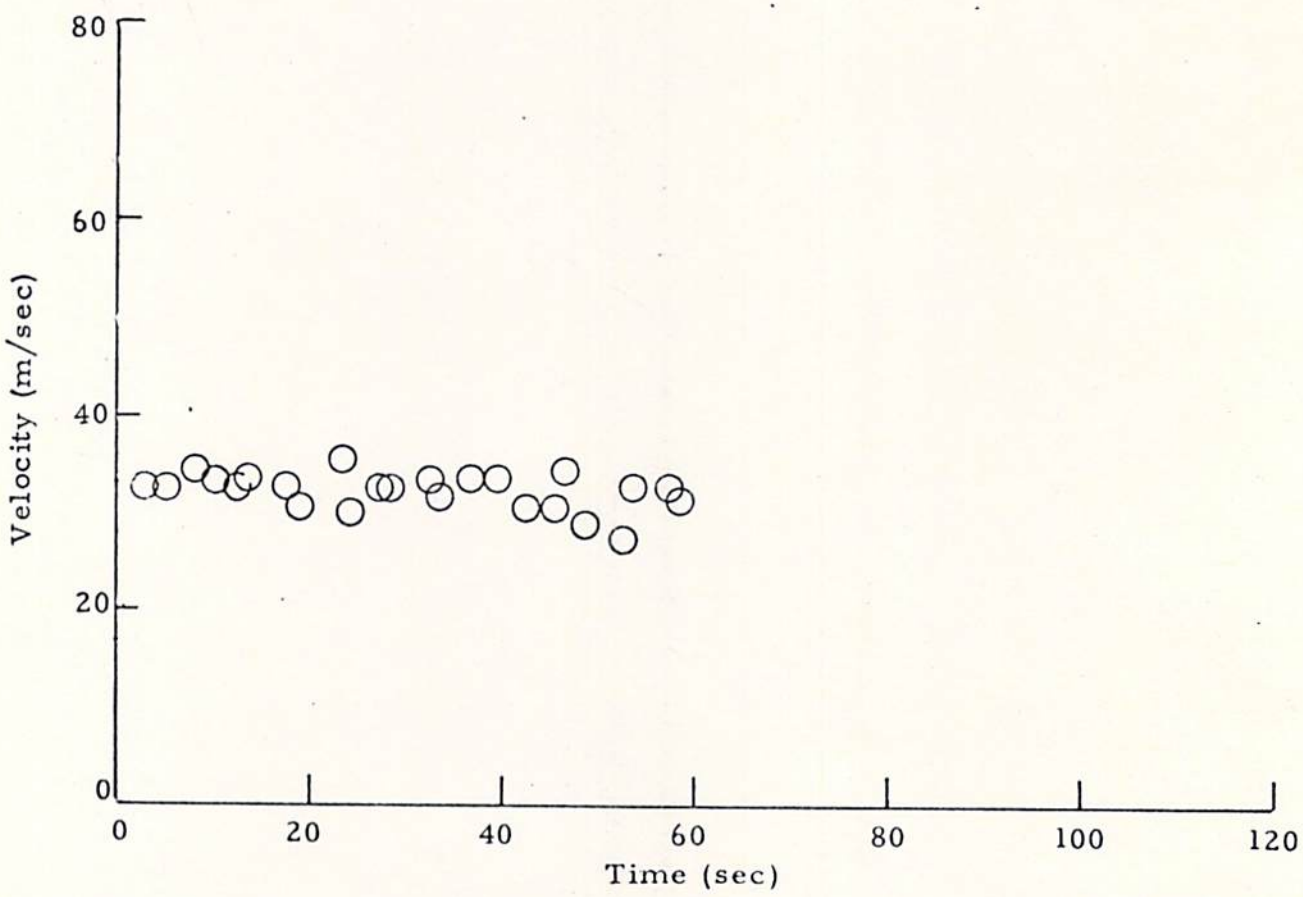

V_{pk} as a Function of Time for Rosamond B-747 Flyby 24
(from High-Speed Data)

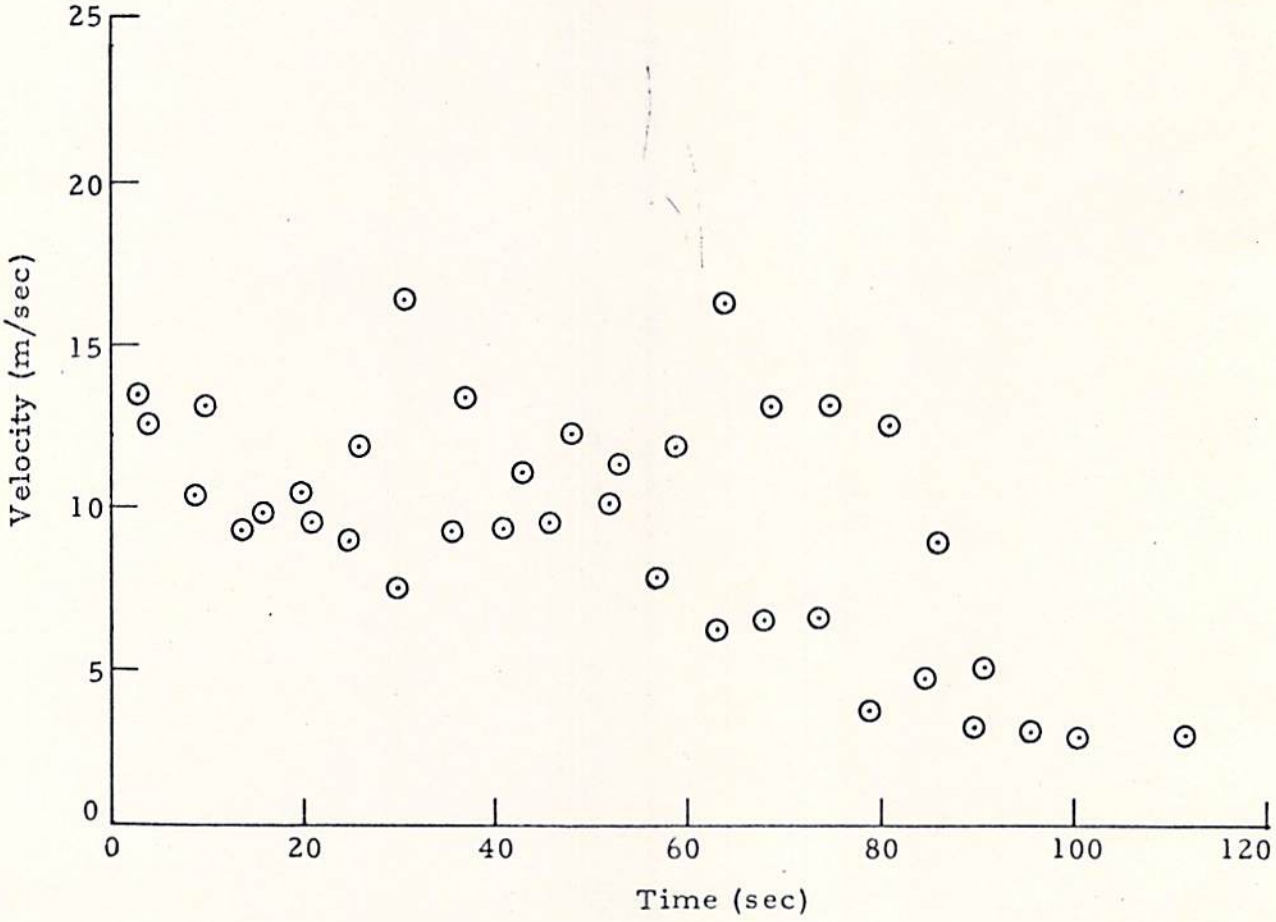

V_{ms} as a Function of Time for Rosamond B-747 Flyby 24
(from Low-Speed Data)

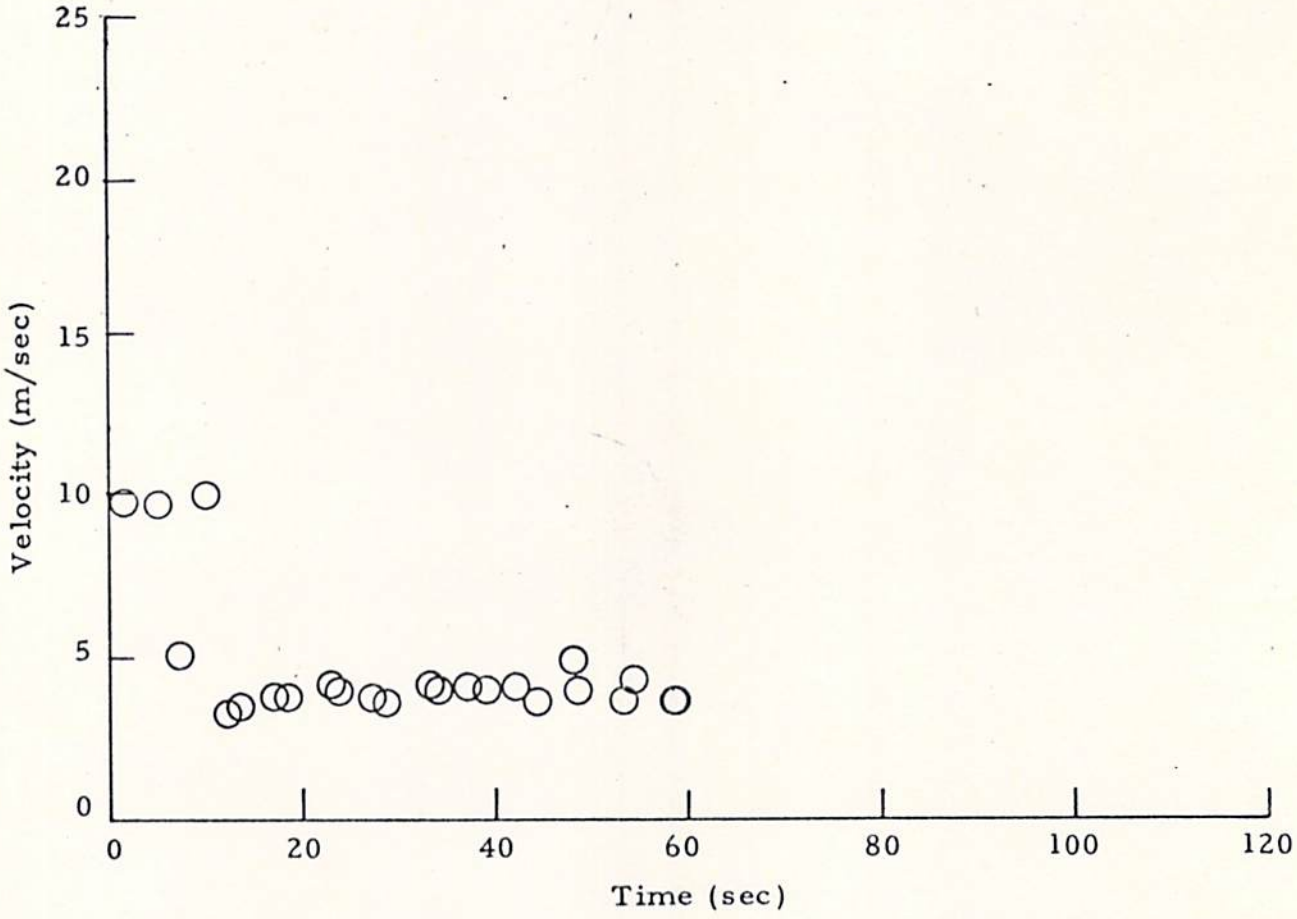

V_{ms} as a Function of Time for Rosamond B-747 Flyby 24
(from High-Speed Data)

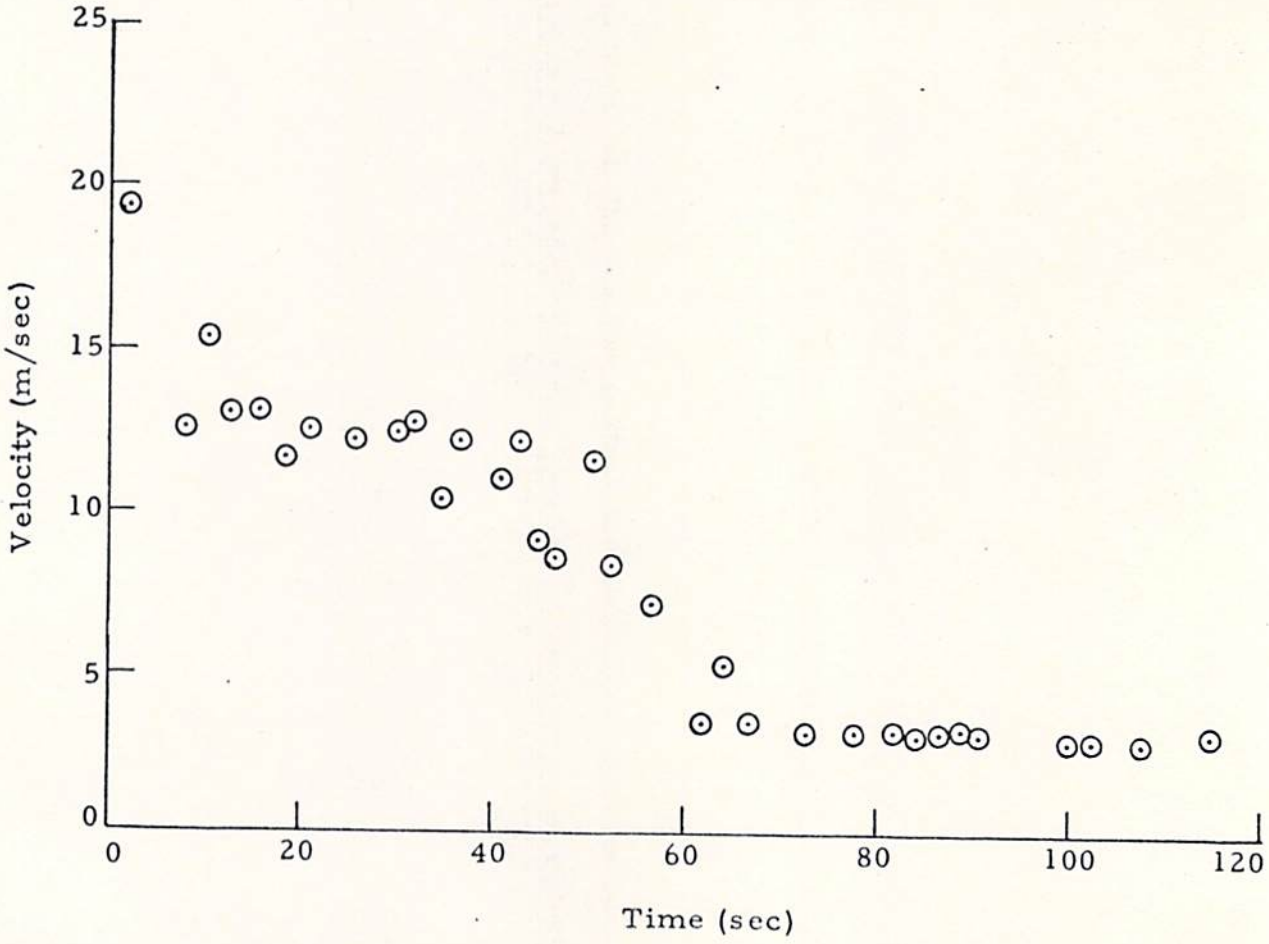

V_{ms} as a Function of Time for Rosamond B-747 Flyby 25
(from Low-Speed Data)

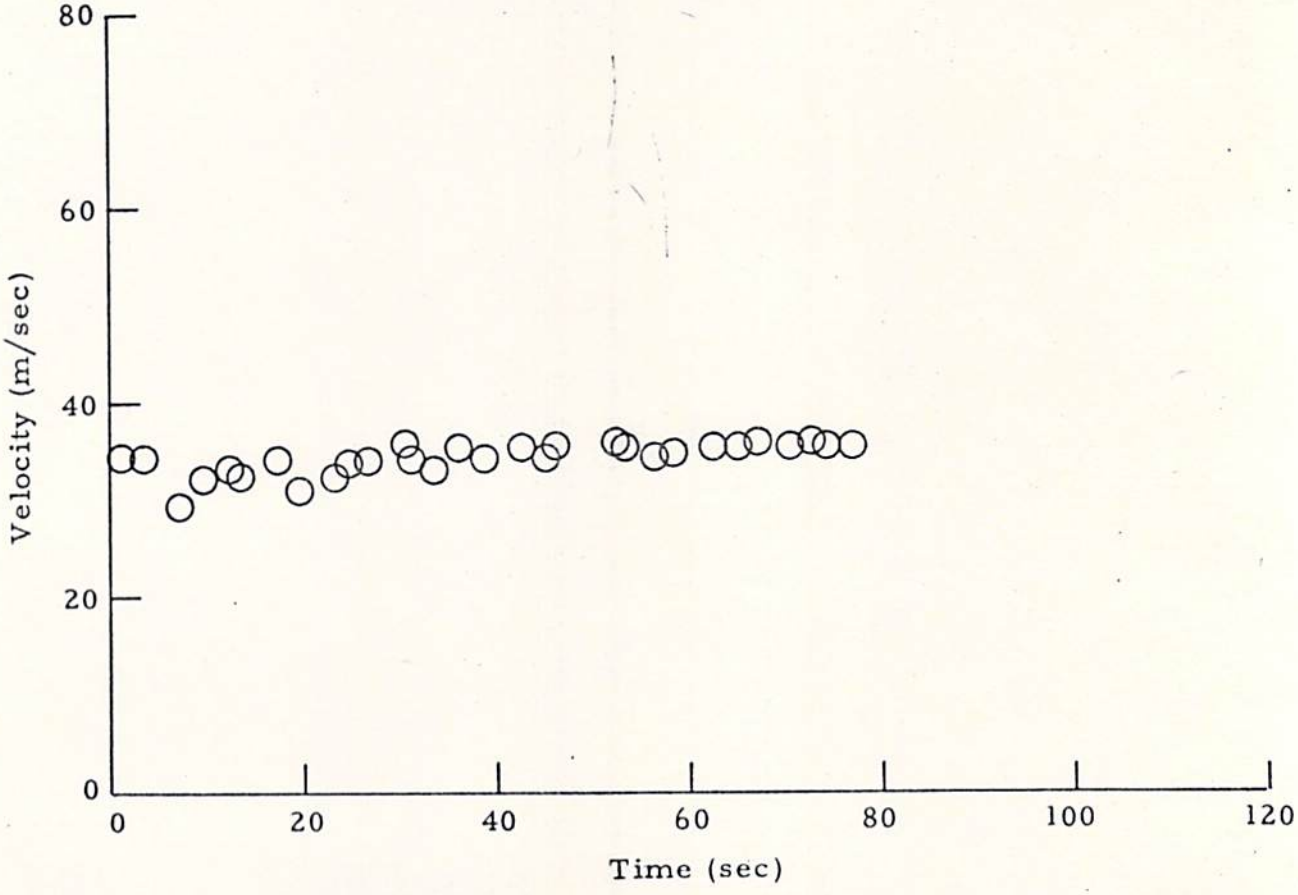

V_{pk} as a Function of Time for Rosamond B-747 Flyby 27
(from high speed data)

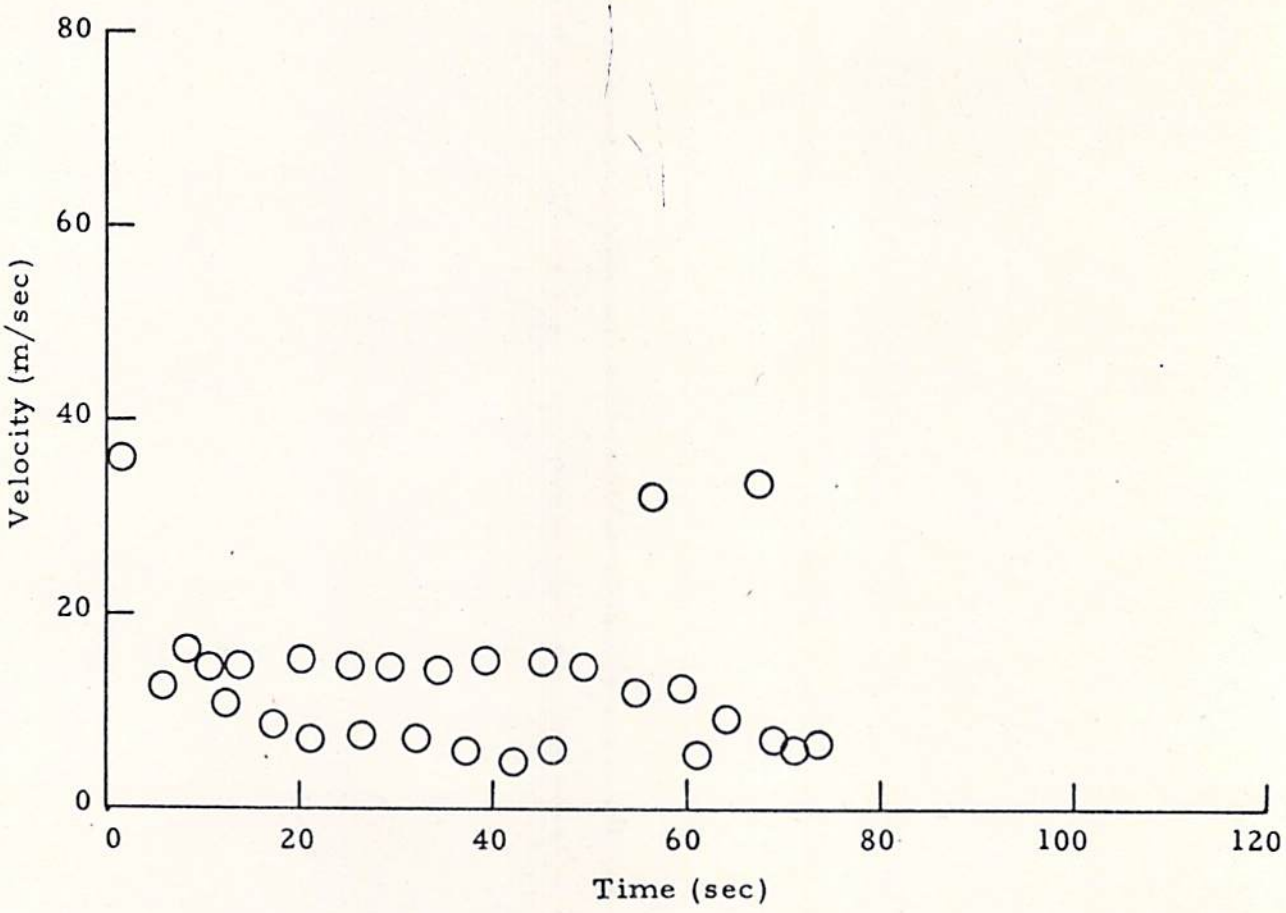

V_{ms} as a Function of Time for Rosamond B-747 Flyby 27 (from High-Speed Data)

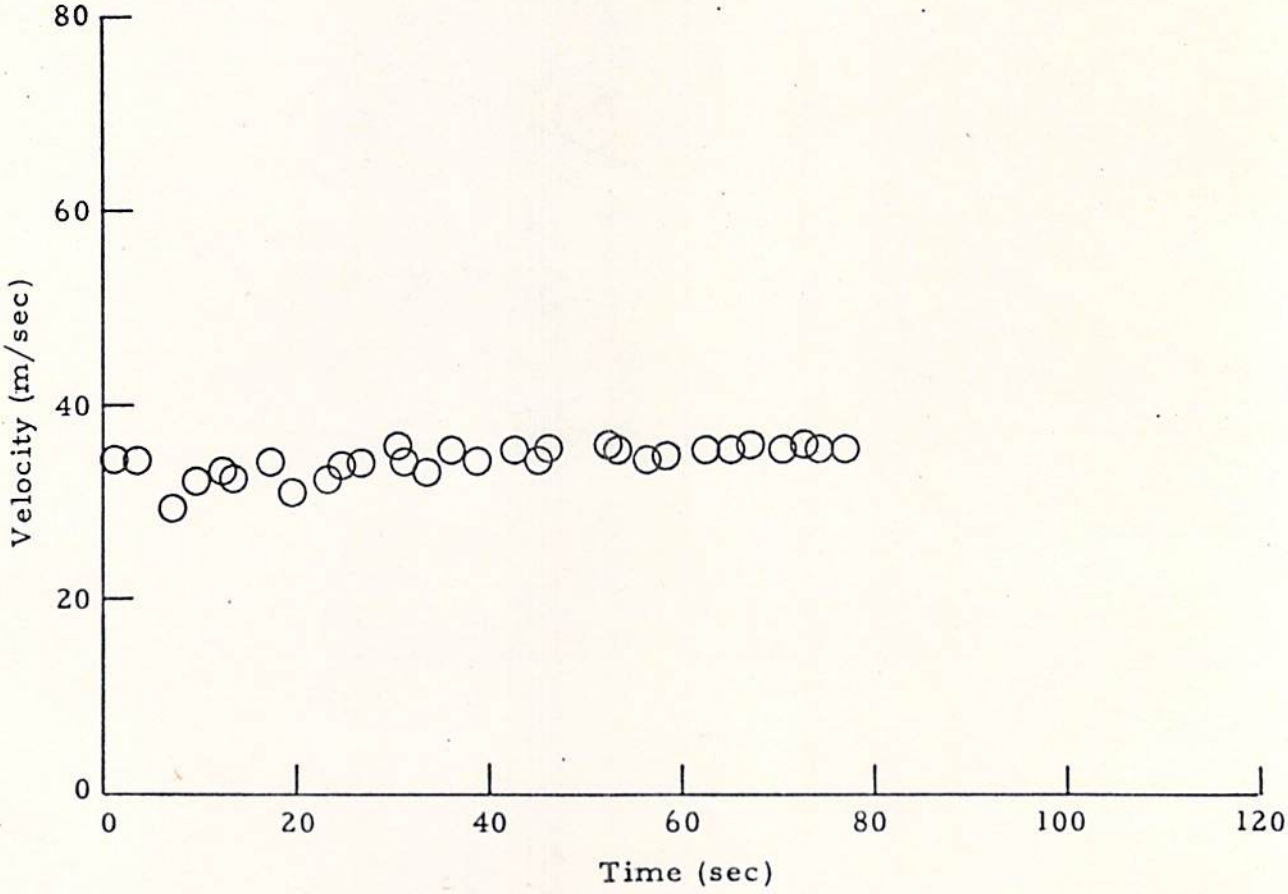

V_{pk} as a Function of Time for Rosamond B-747 Flyby 28
(from High-Speed Data)

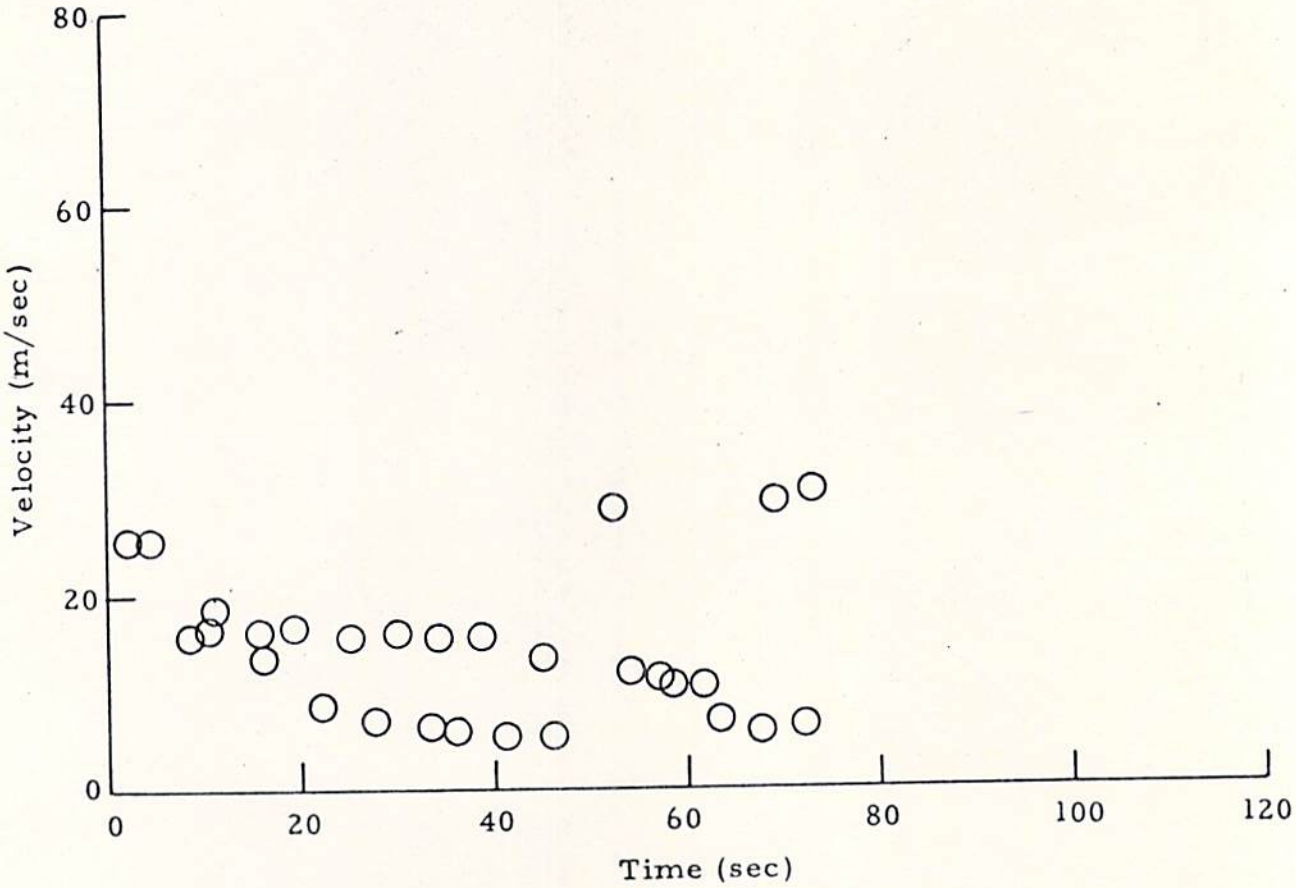

V_{ms} as a Function of Time for Rosamond B-747 Flyby 29
(from High-Speed Data)

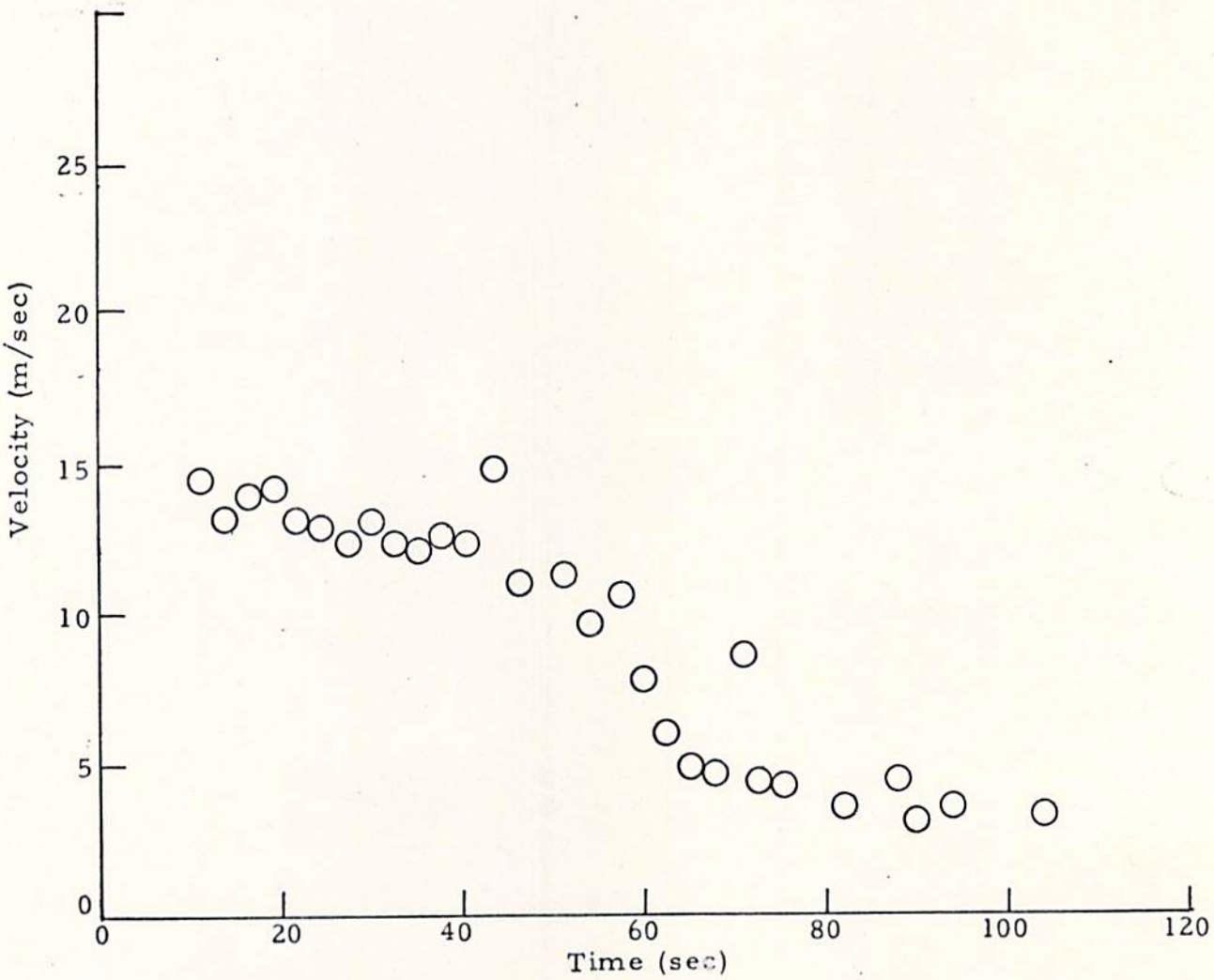

V_{ms} as a Function of Time for Rosamond Flyby 29
(from Low-Speed Data)

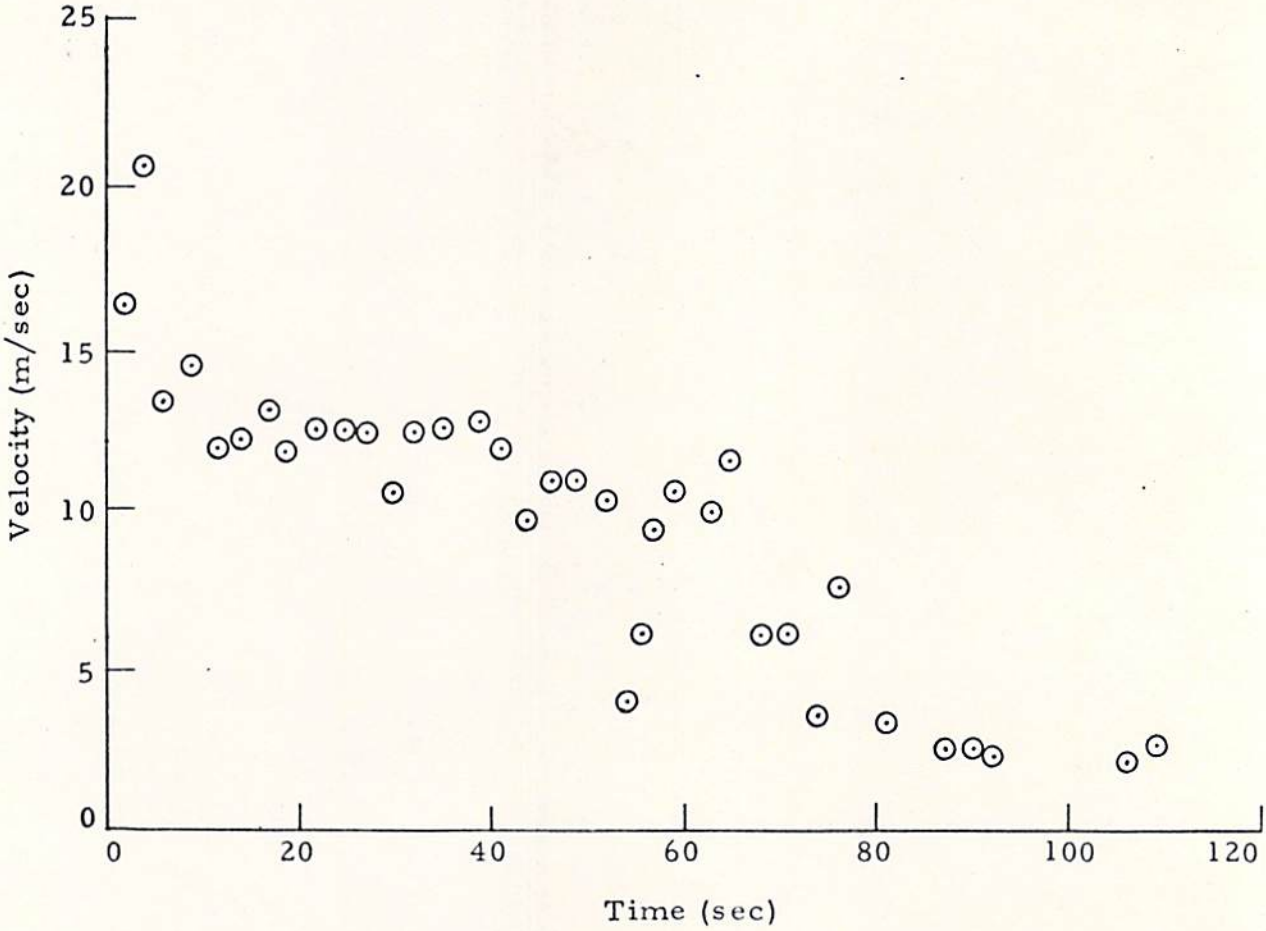

V_{ms} as a Function of Time for Rosamond B-747 Flyby 30 (from Low-Speed Data)

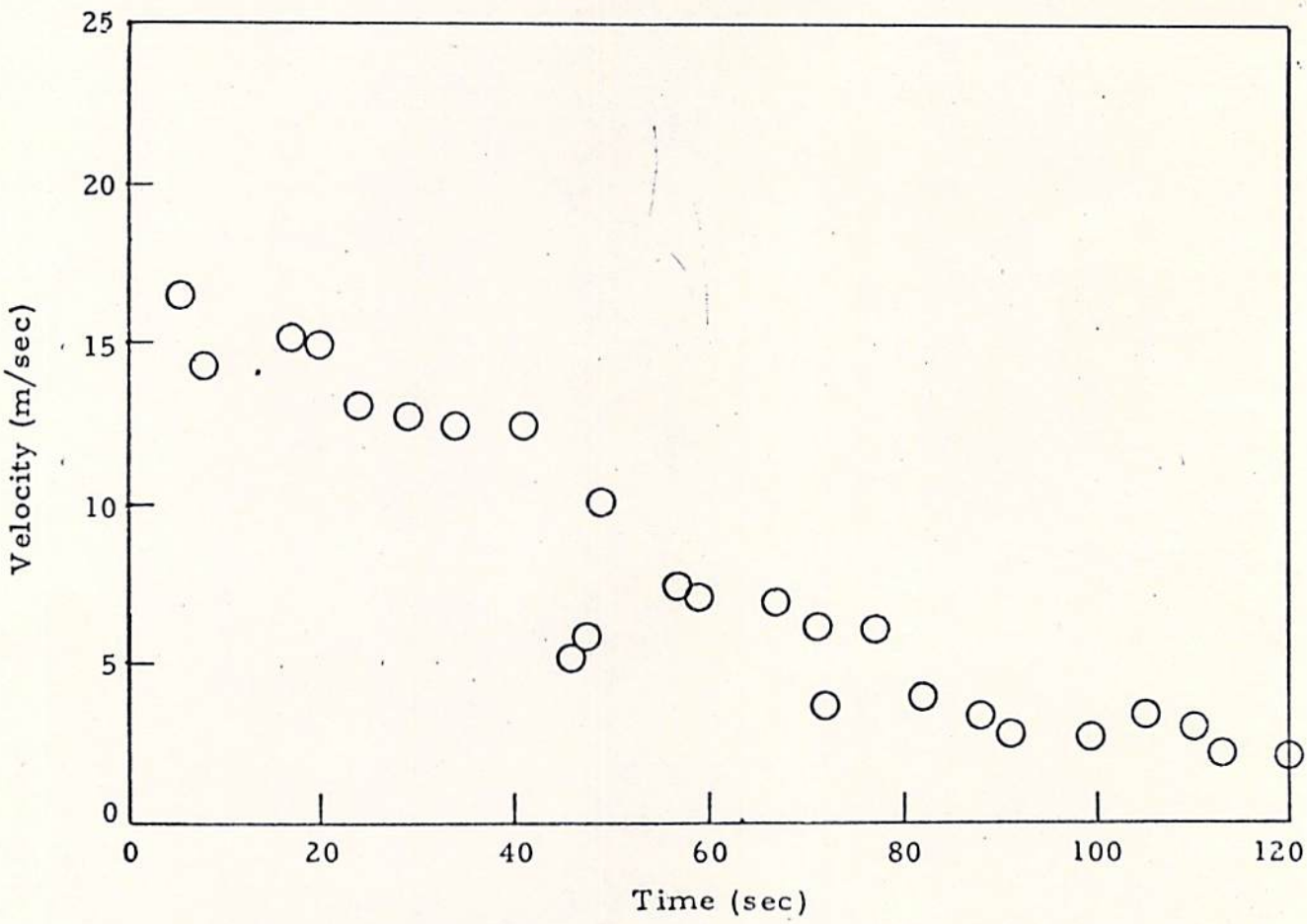

V_{ms} as a Function of Time for Rosamond B-747 Flyby 35
(from Low-Speed Data)

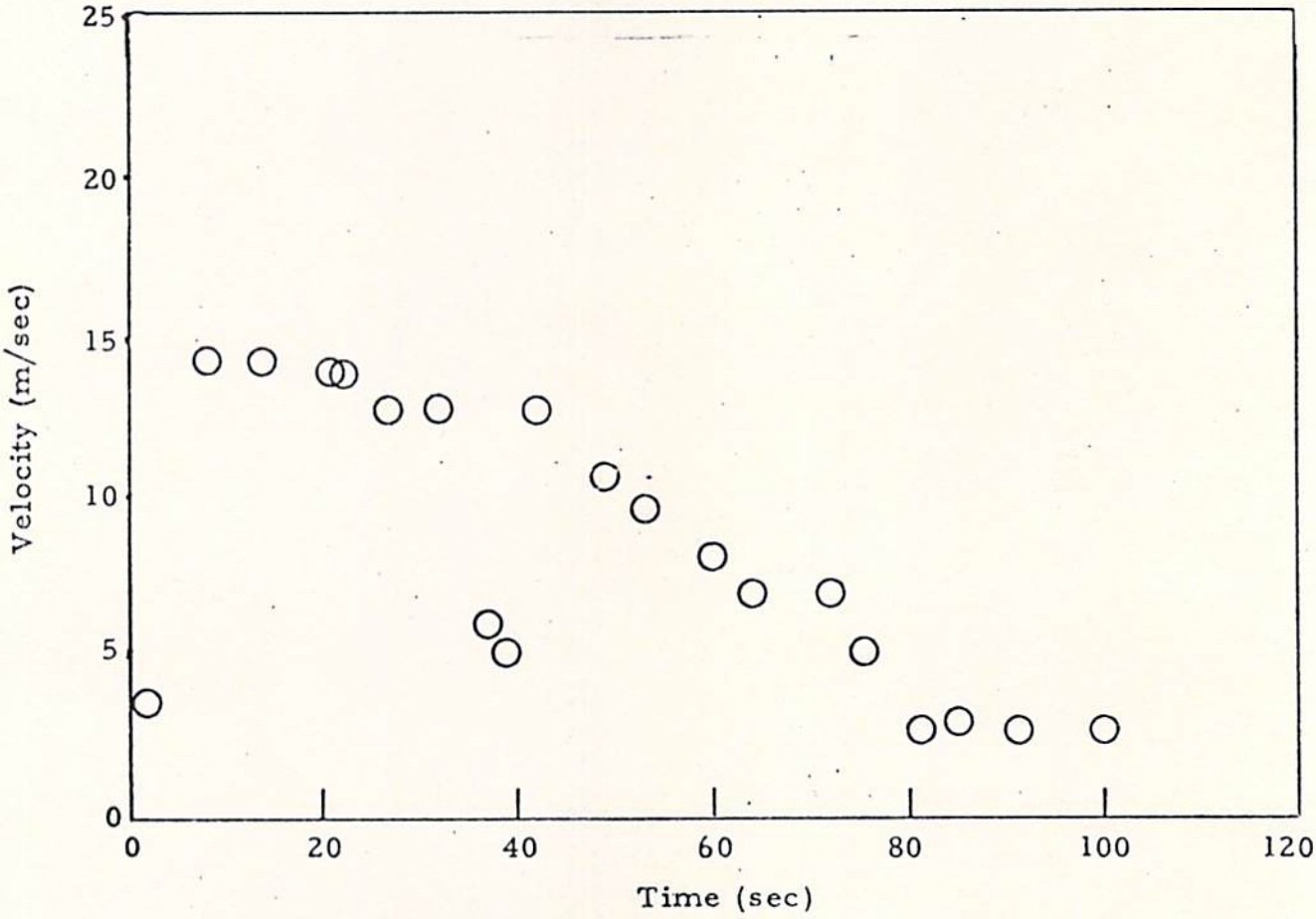

V_{ms} as a Function of Time for Rosamond B-747 Flyby 38
(from Low-Speed Data)

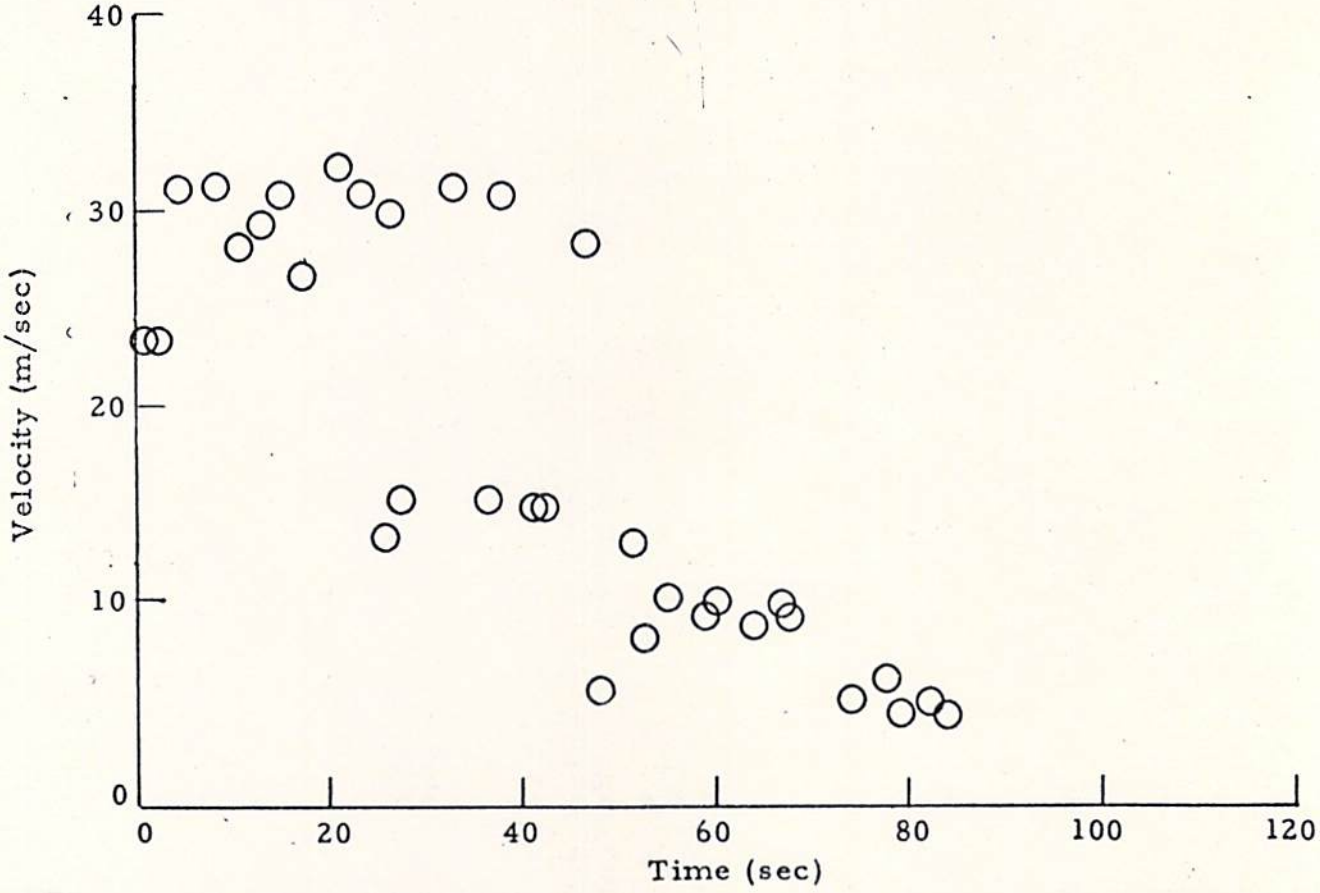

V_{pk} as a Function of Time for Rosamond B-747 Flyby 44
(from High Speed Data)

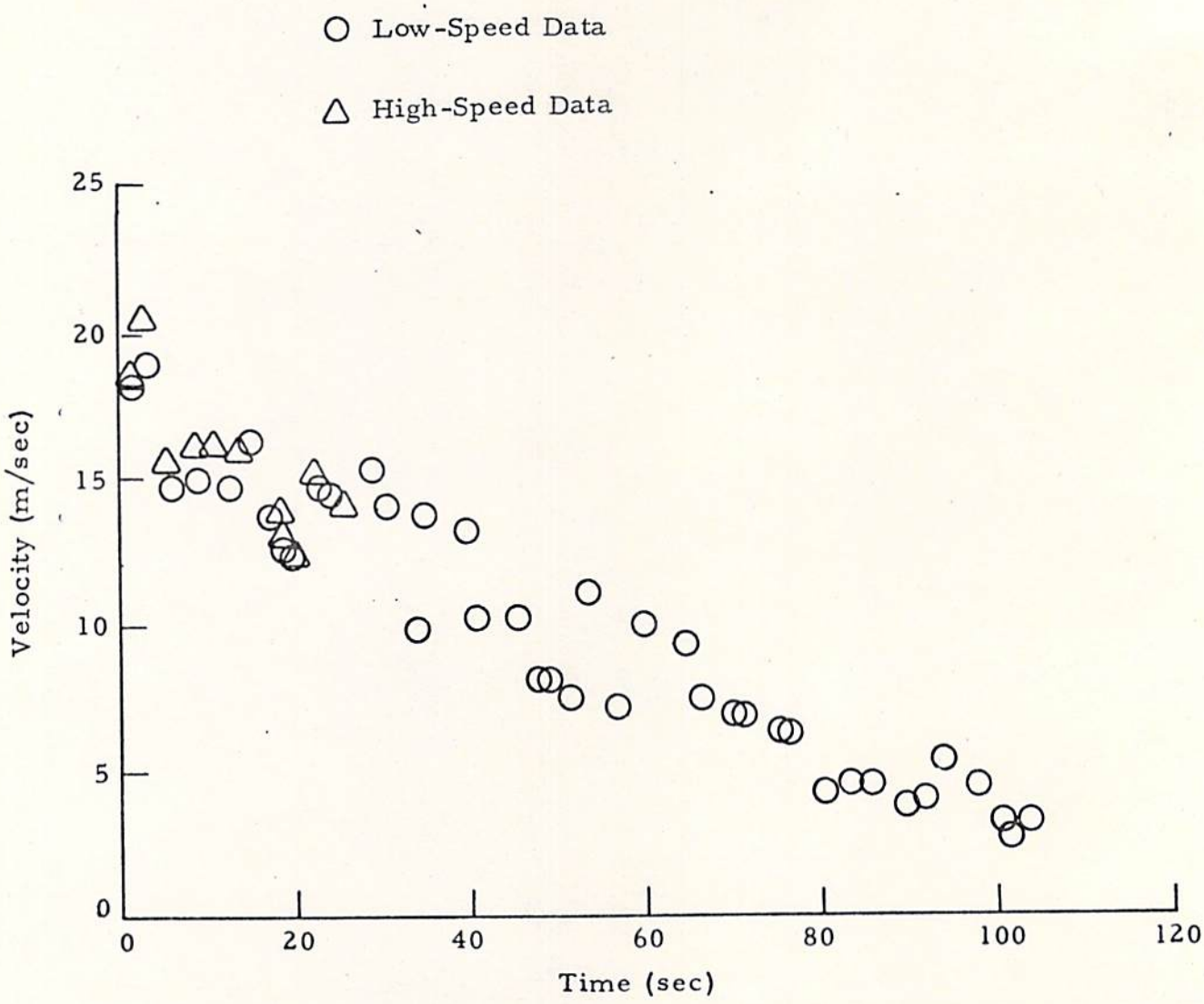

V_{ms} as a Function of Time for Rosamond B-747 Flyby 44

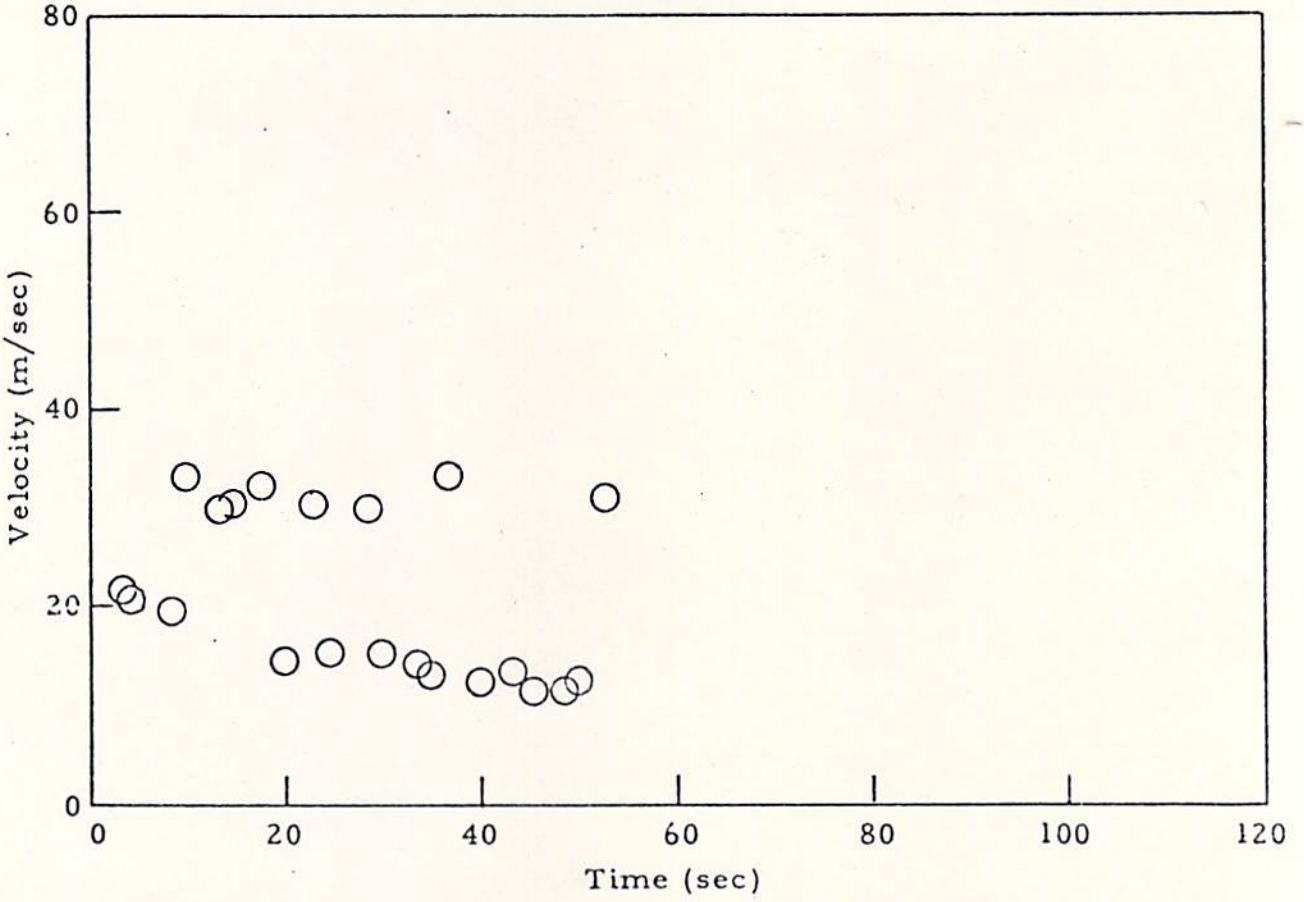

V_{pk} as a Function of Time for Rosamond B-747 Flyby 47
(from High-Speed Data)

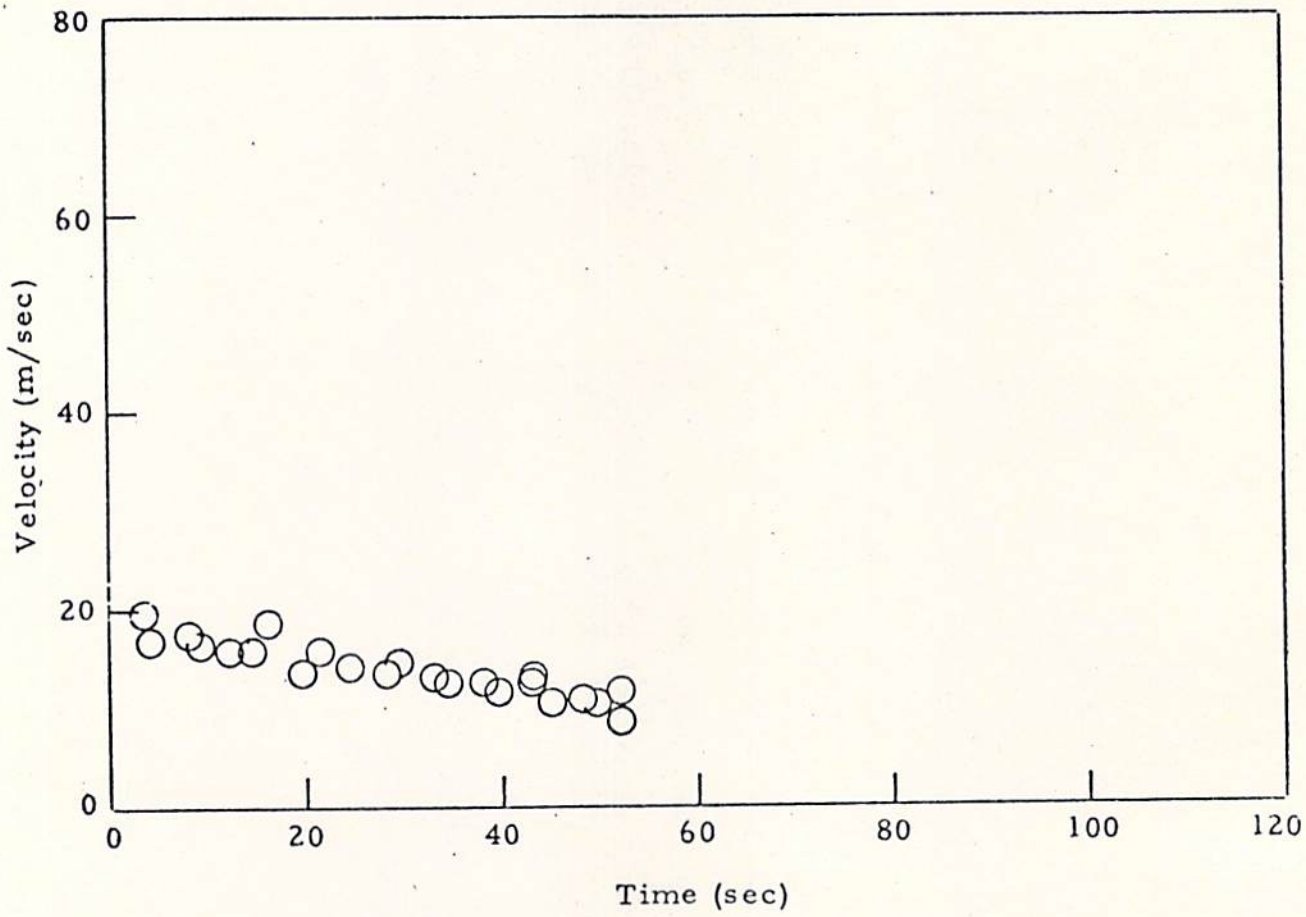

V_{ms} as a Function of Time for Rosamond B-747 Flyby 47
(from High-Speed Data)

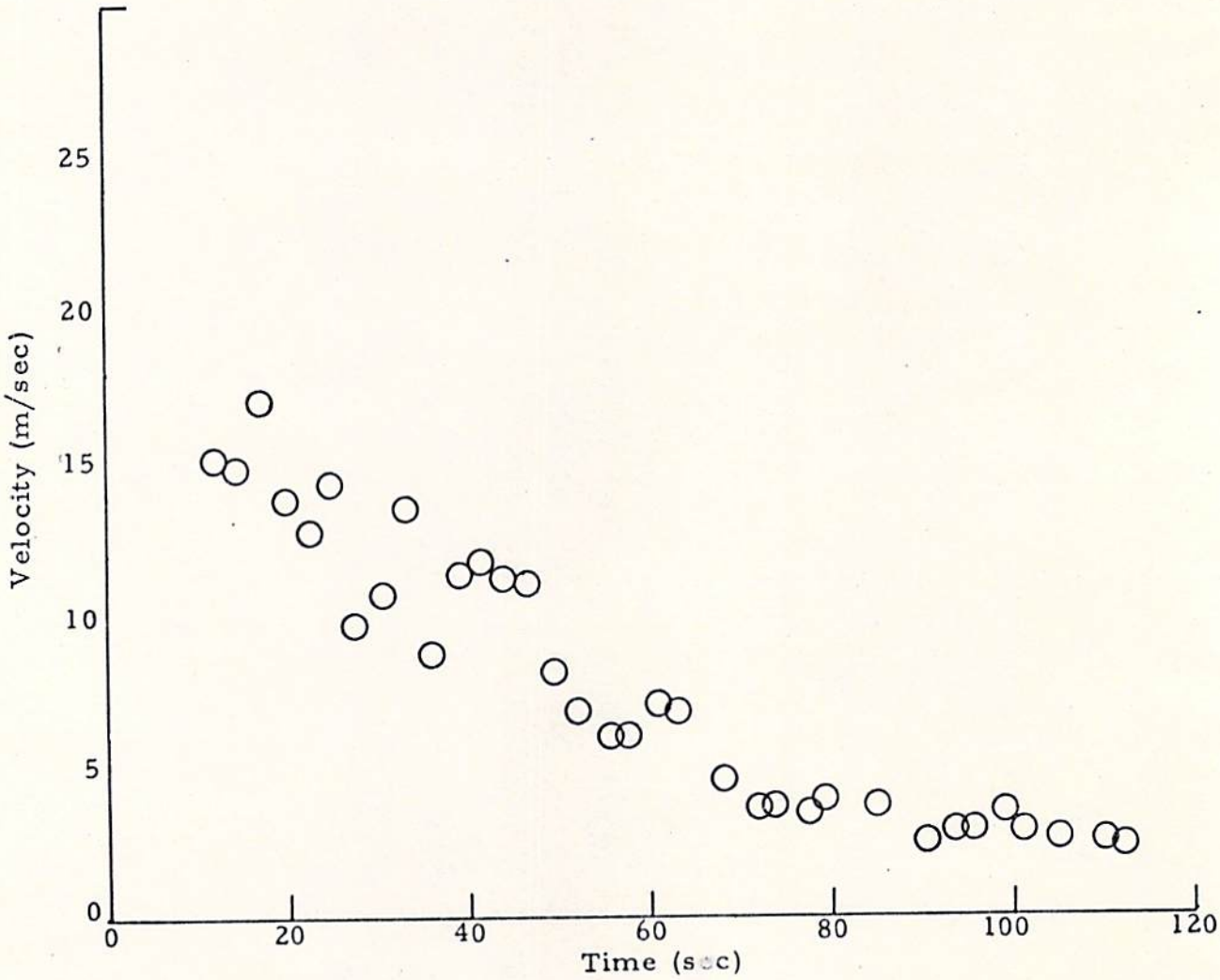

V_{ms} as a Function of Time for Rosamond B-747 Flyby 47
(from Low-Speed Data)

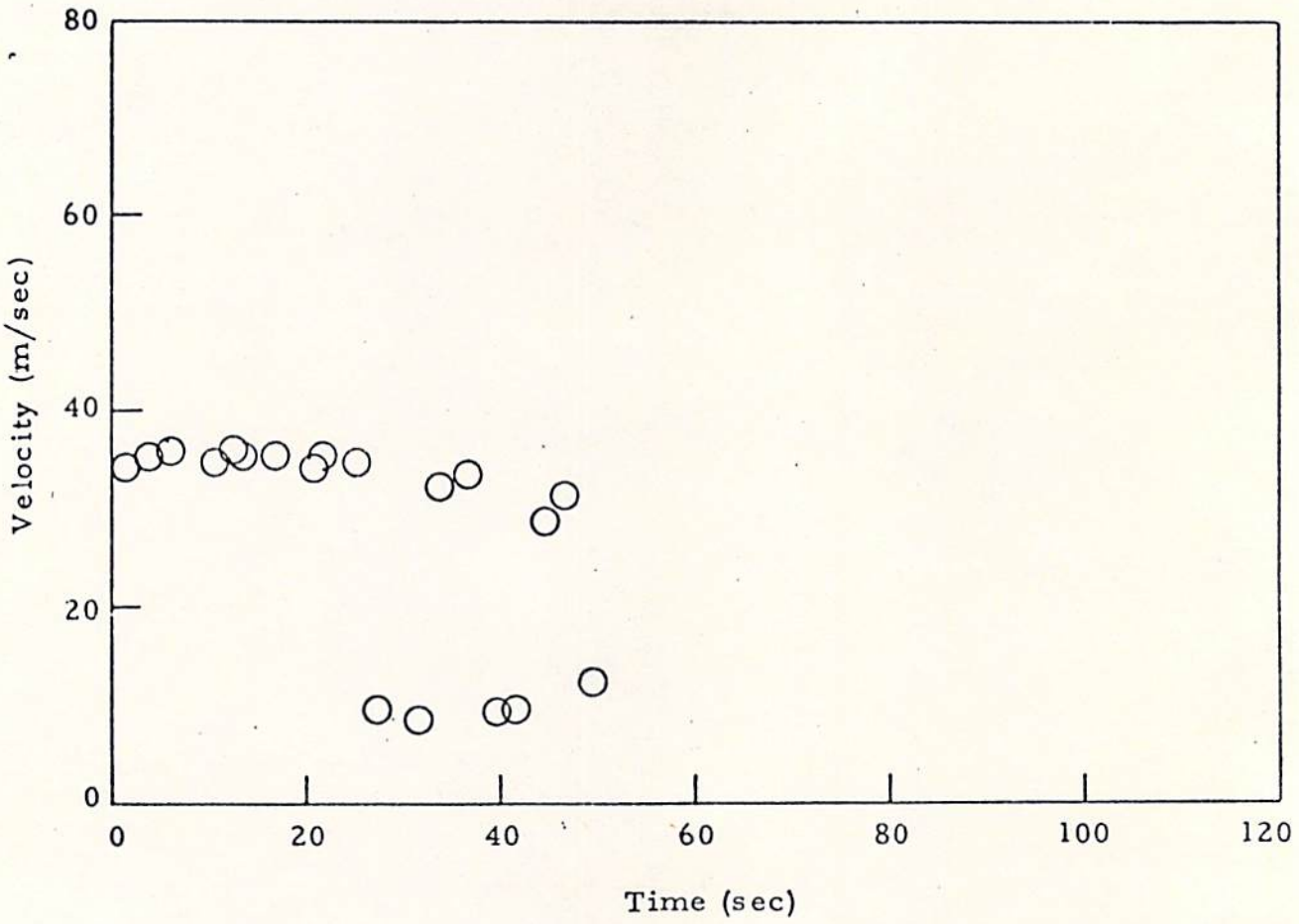

V_{pk} as a Function of Time for Rosamond B-747 Flyby 48
(from High-Speed Data)

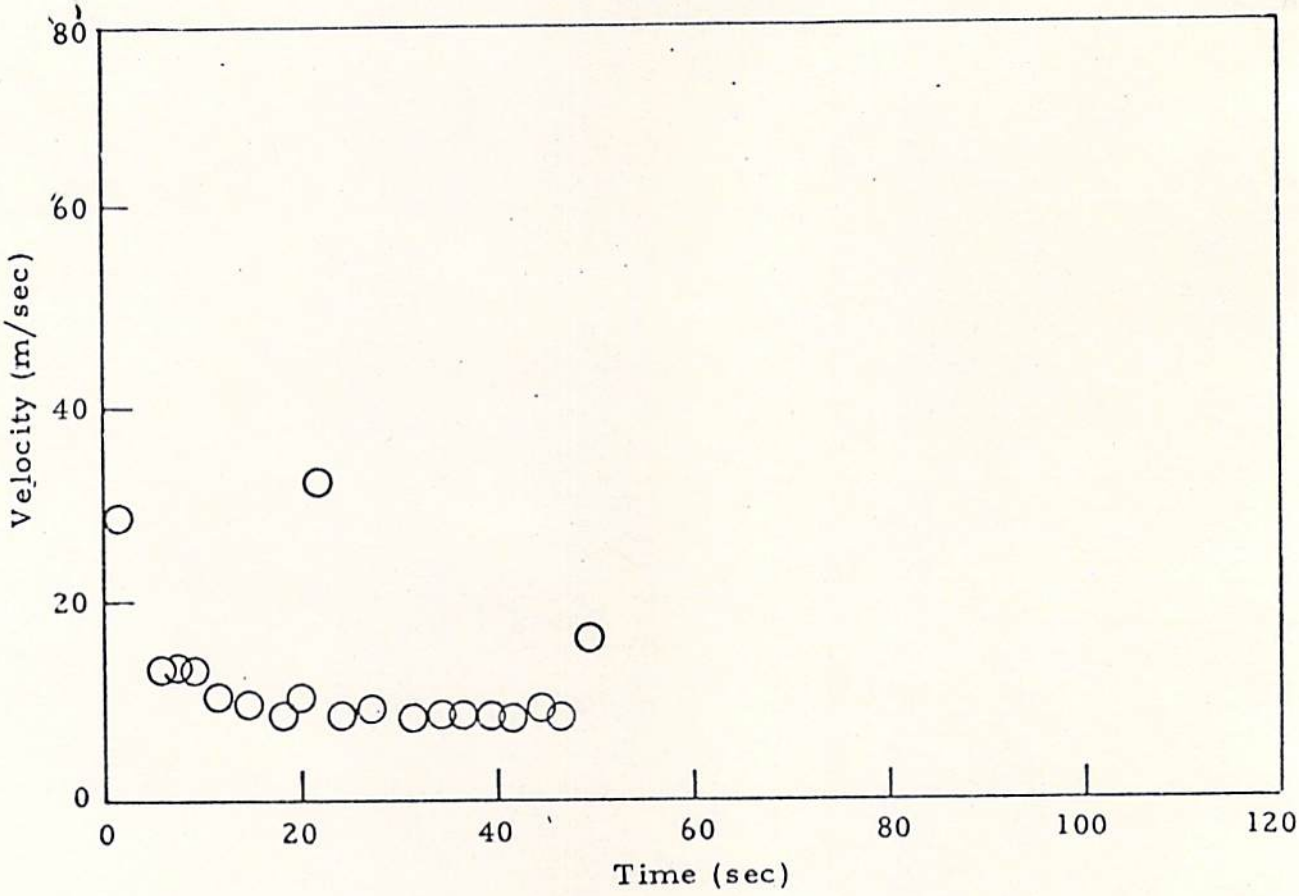

V_{ms} as a Function of Time for Rosamond B-747 Flyby 48
(from High-Speed Data)

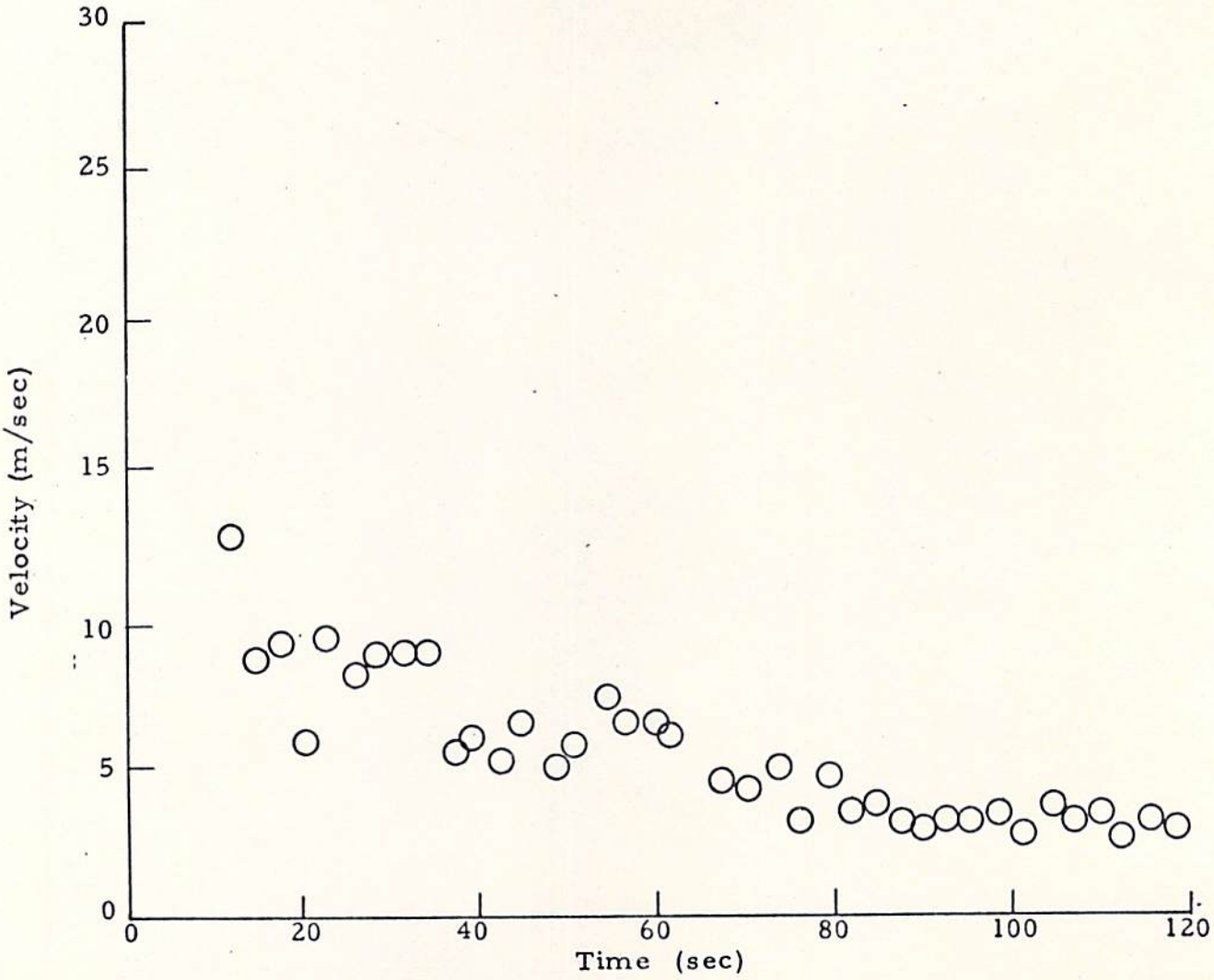

V_{ms} as a Function of Time for Rosamond B-747 Flyby 48
(from Low-Speed Data)

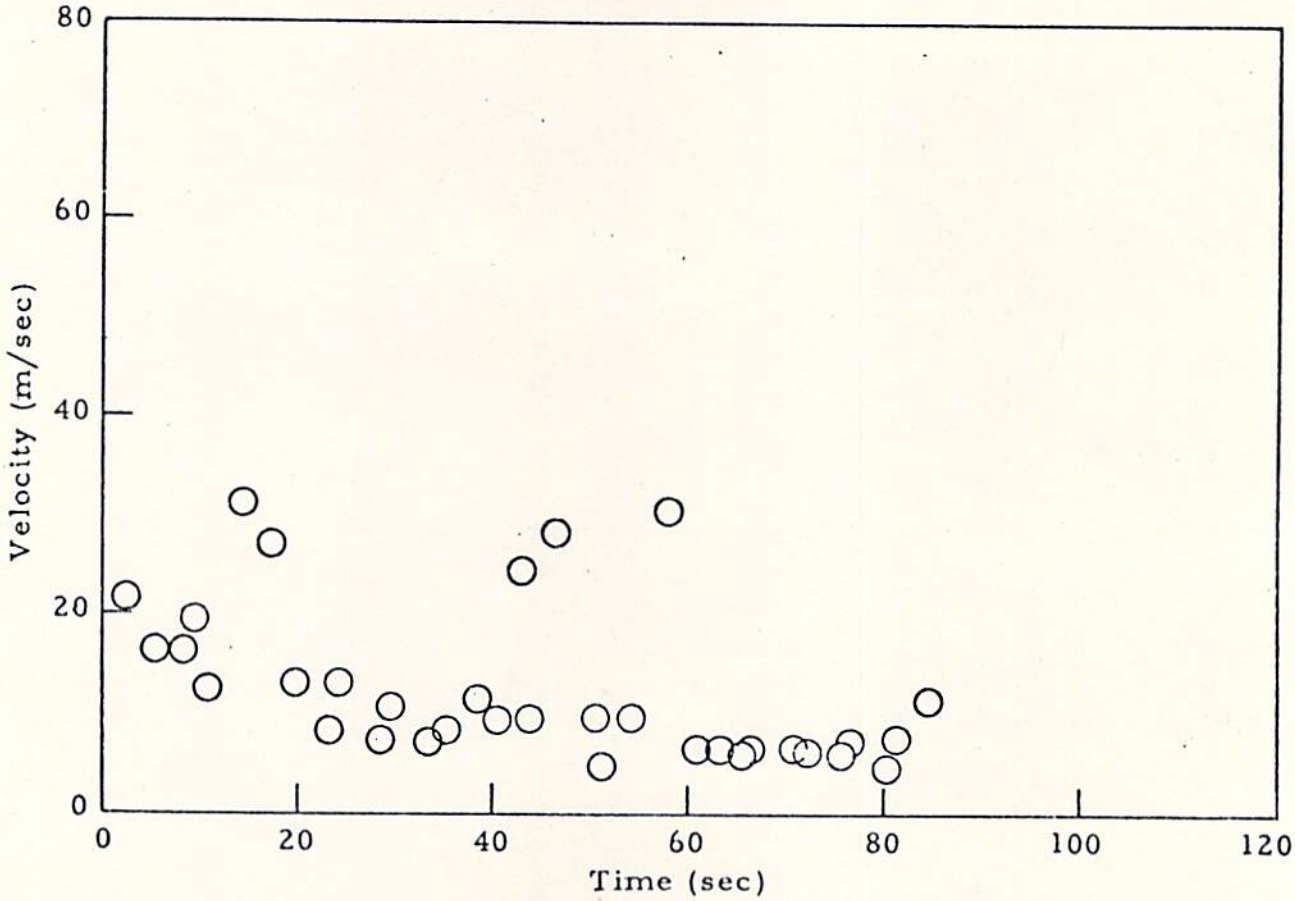

V_{pk} as a Function of Time for Rosamond B-747 Flyby 49
(from High-Speed Data)

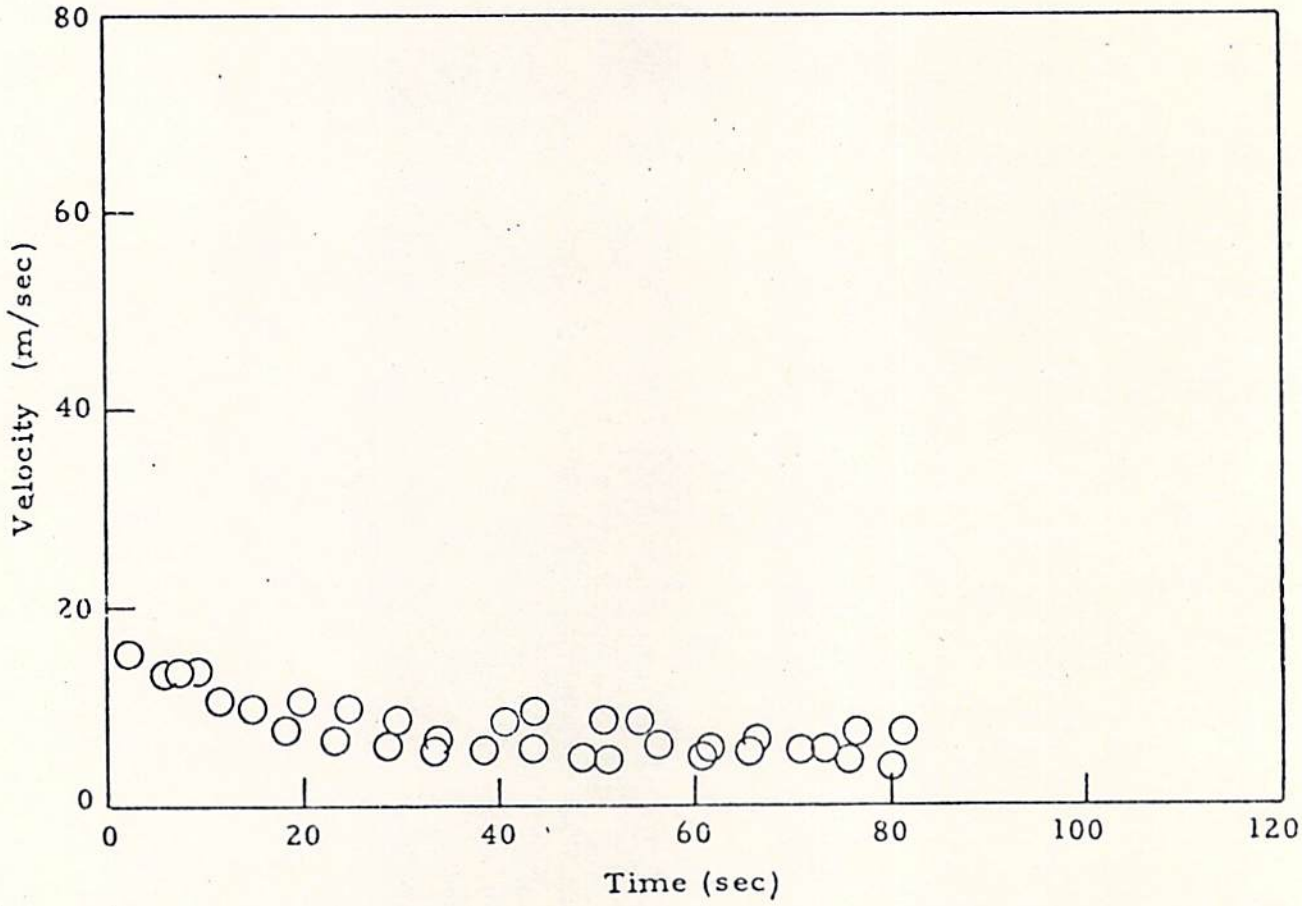

V_{ms} as a Function of Time for Rosamond B-747 Flyby 49
(from High-Speed Data)

Appendix G

TIME HISTORY OF VORTEX CIRCULATION

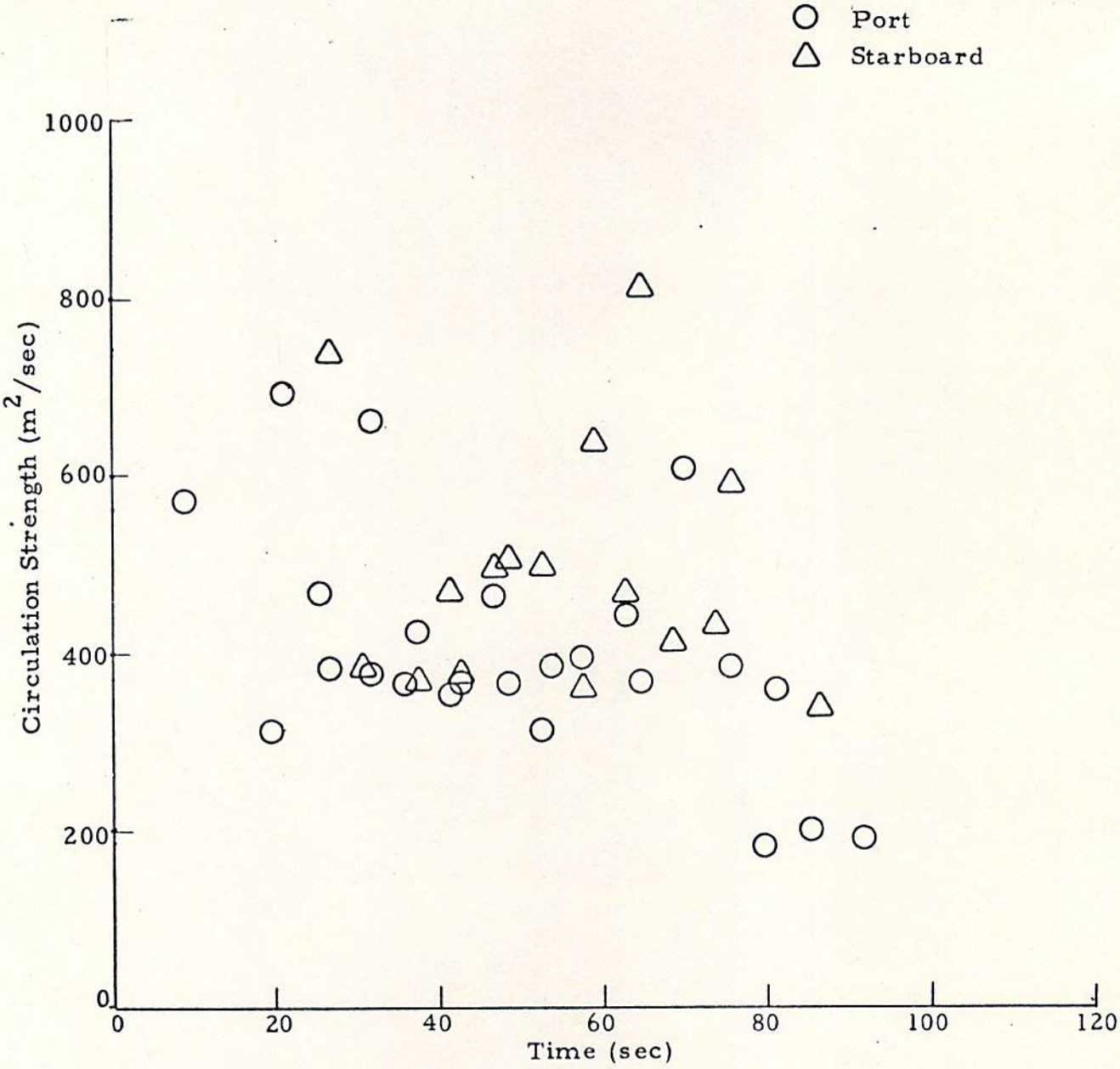

Observed Circulation Time History for Rosamond B-747 Flyby 24

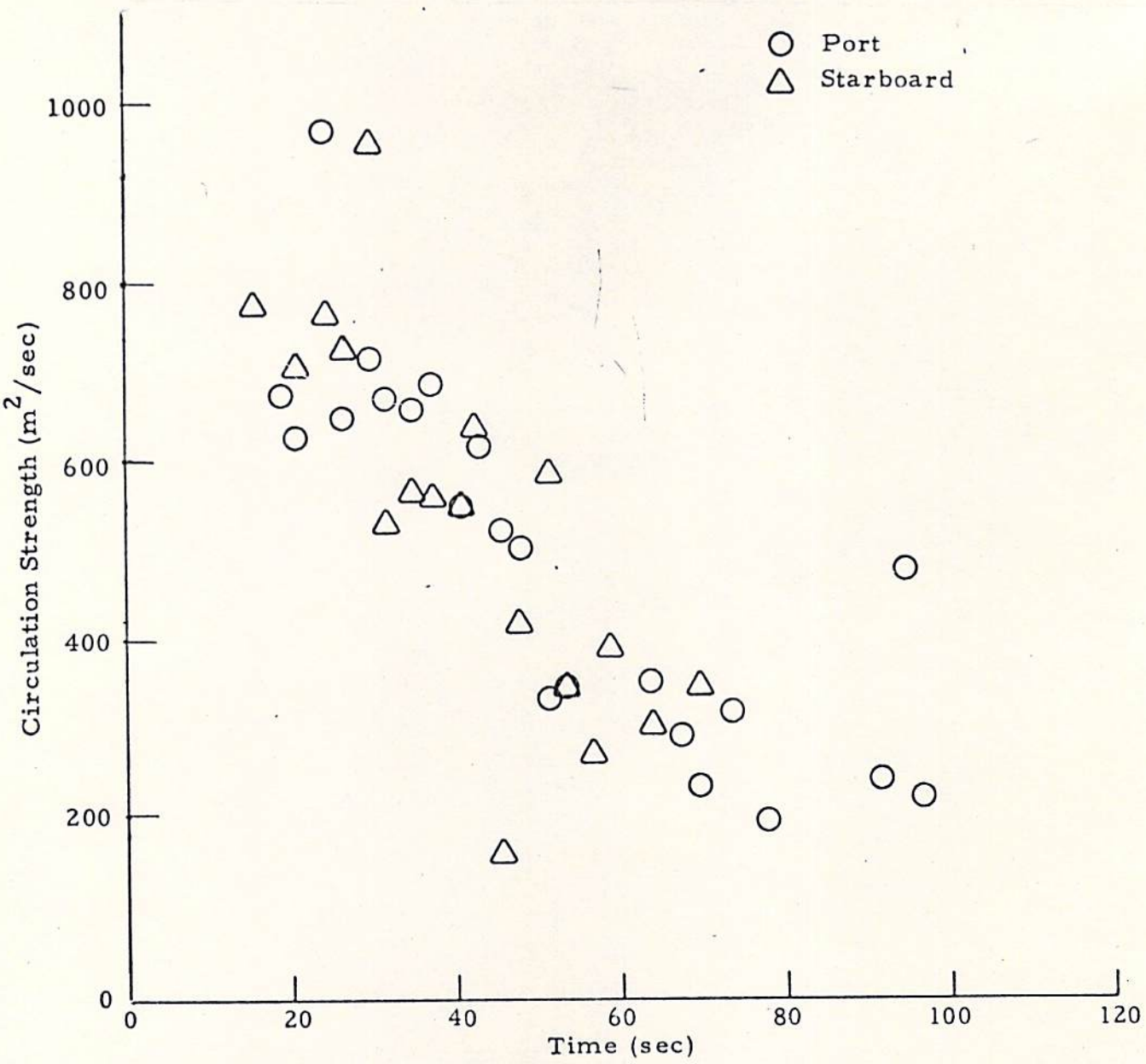

Observed Circulation Time History for Rosamond B-747 Flyby 25

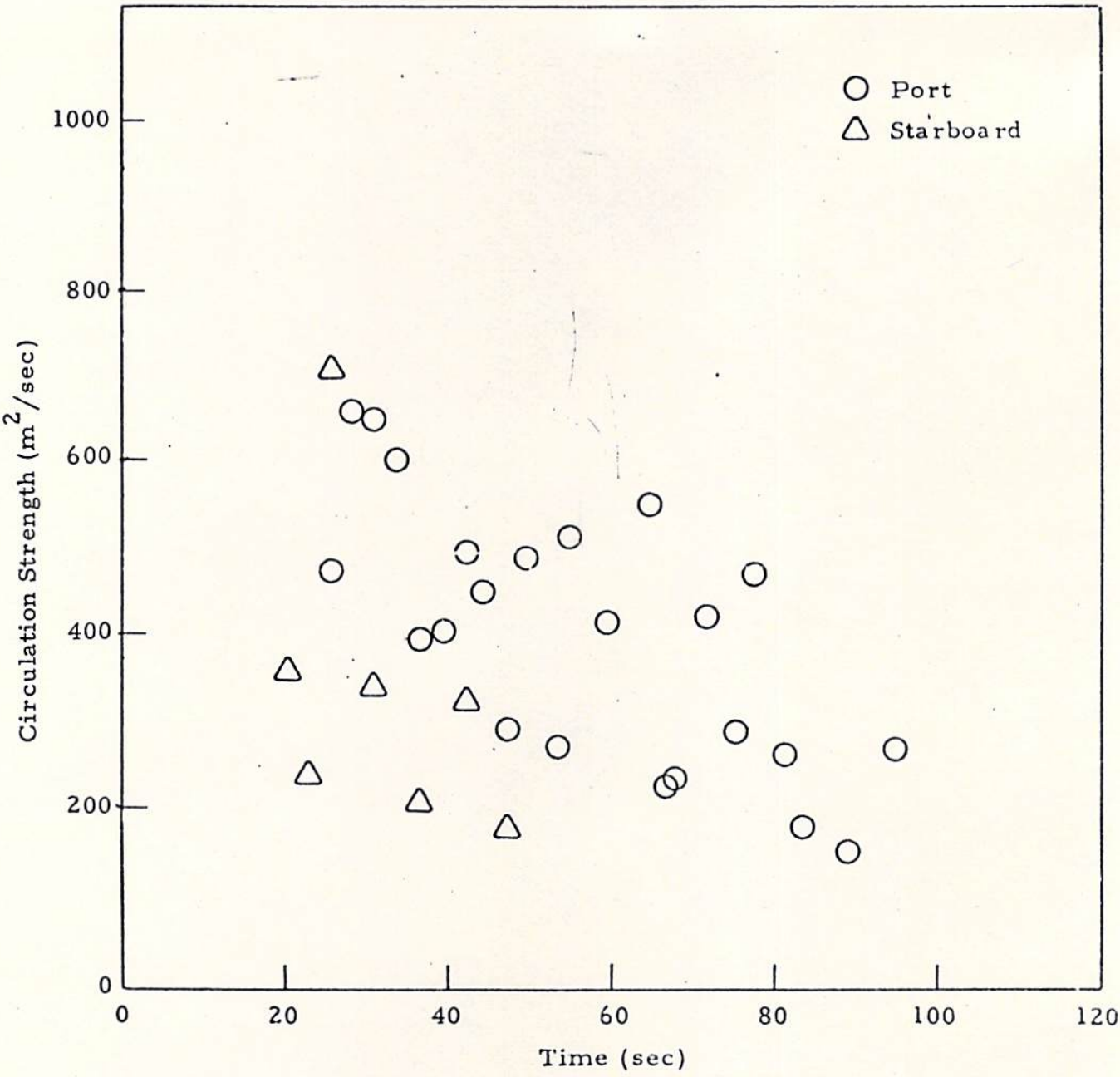

Observed Circulation Time History for Rosamond B-747 Flyby 27

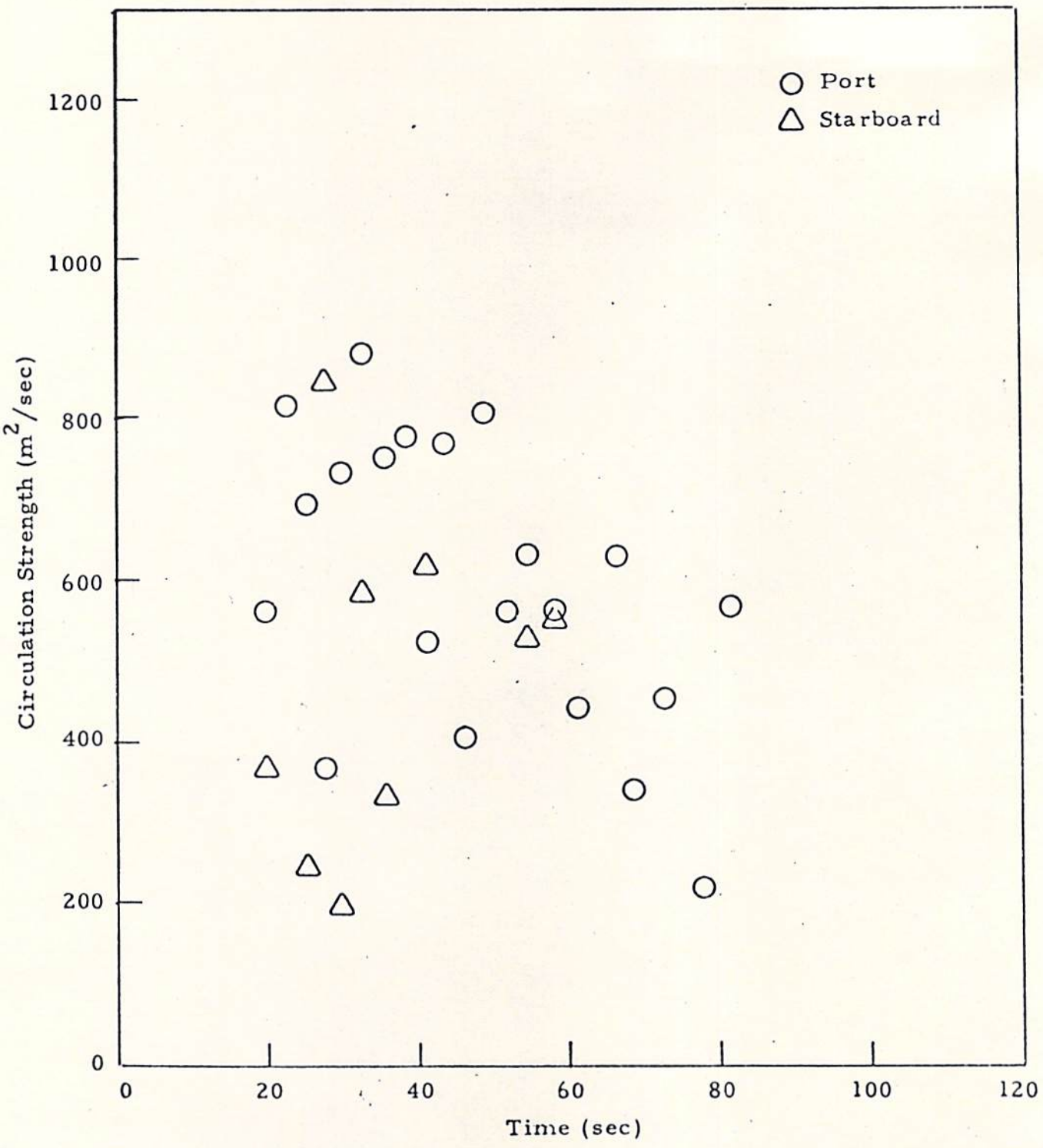

Observed Circulation Time History for Rosamond B-747 Flyby 28

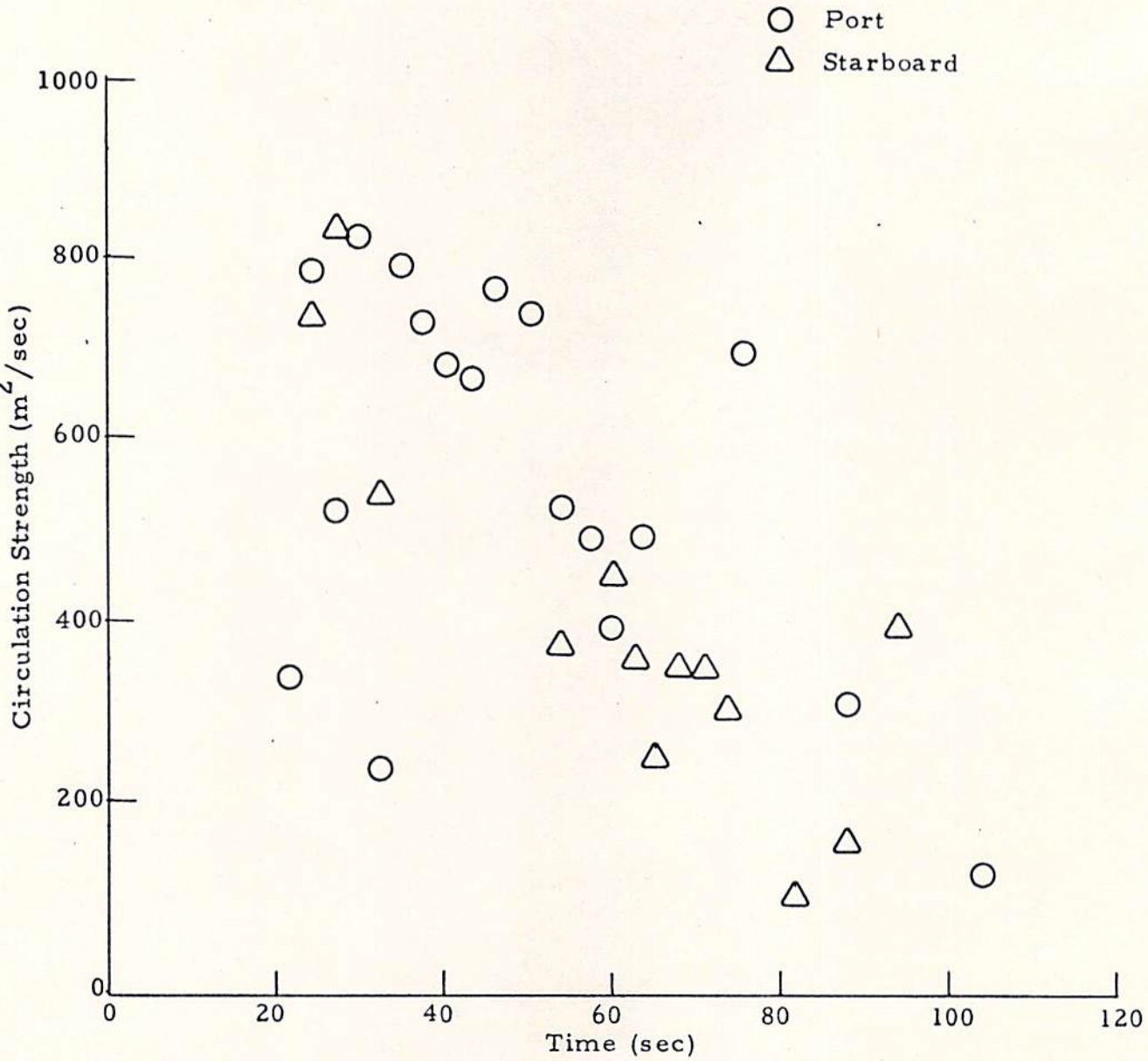

Observed Circulation Time History for Rosamond B-747 Flyby 29

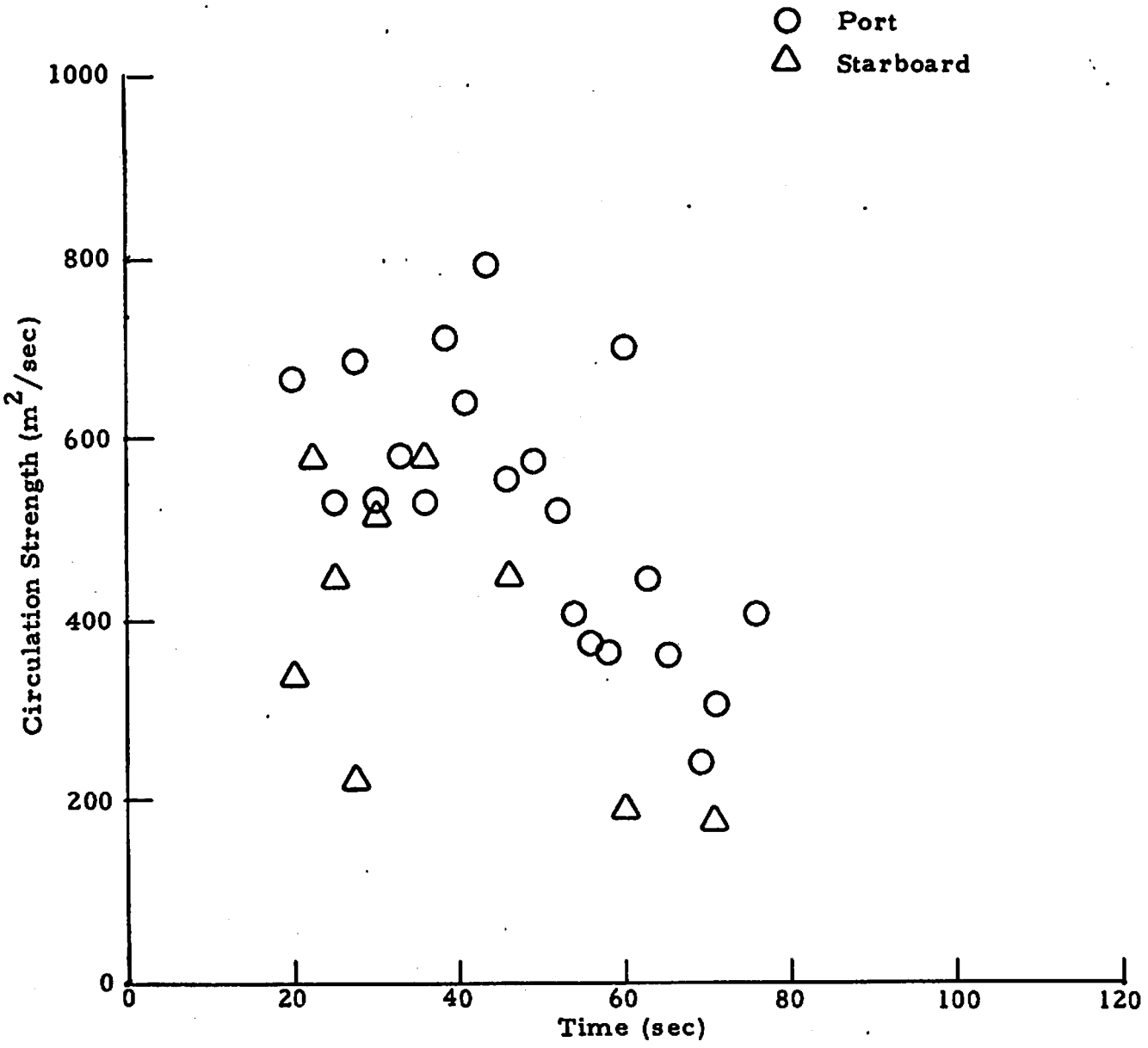

Observed Circulation Time History for Rosamond B-747 Flyby 30

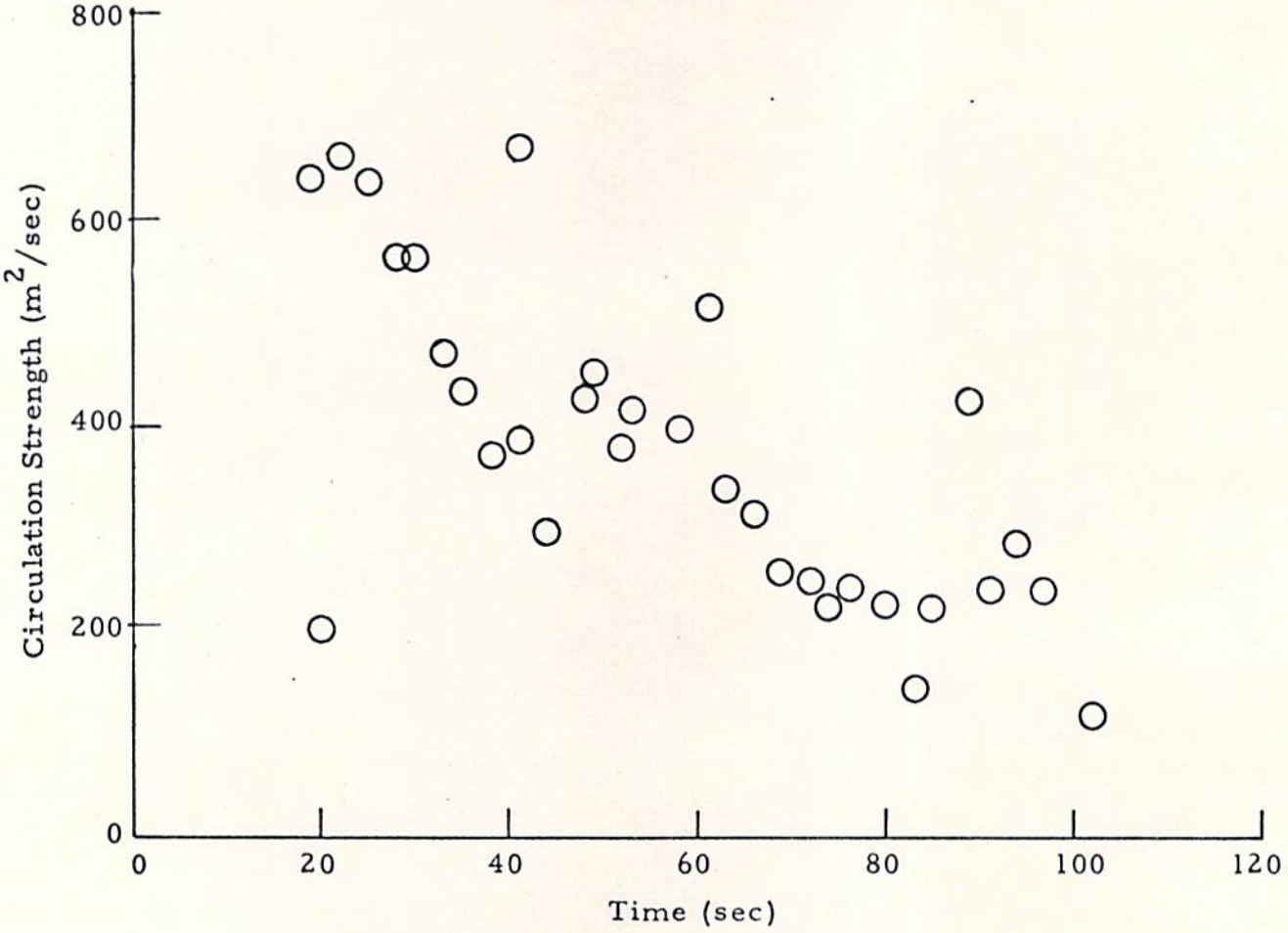

Observed Circulation Time History for Rosamond B-747
Flyby 44, Starboard Vortex

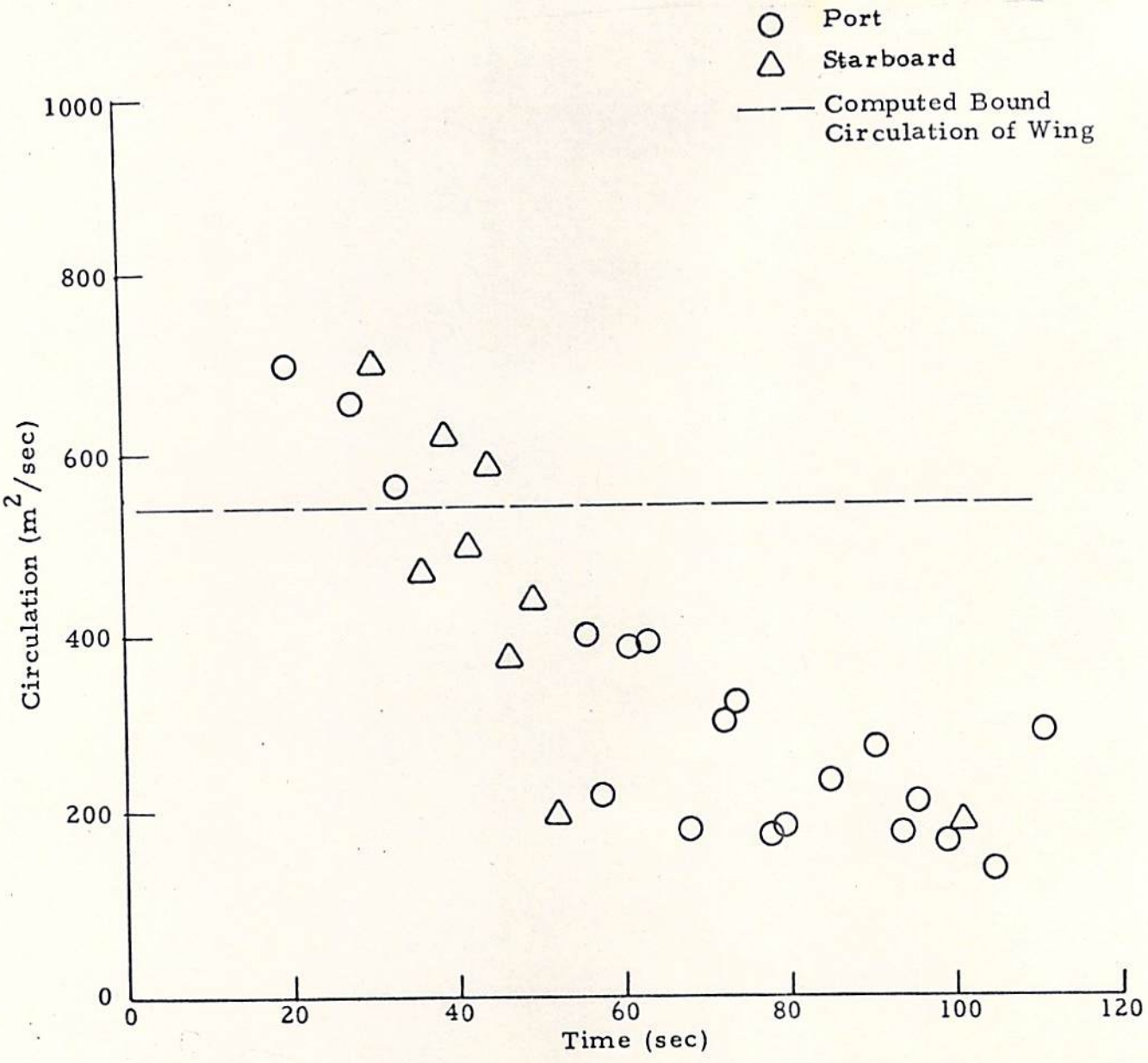

Observed Circulation Time History for Rosamond B-747 Flyby 47

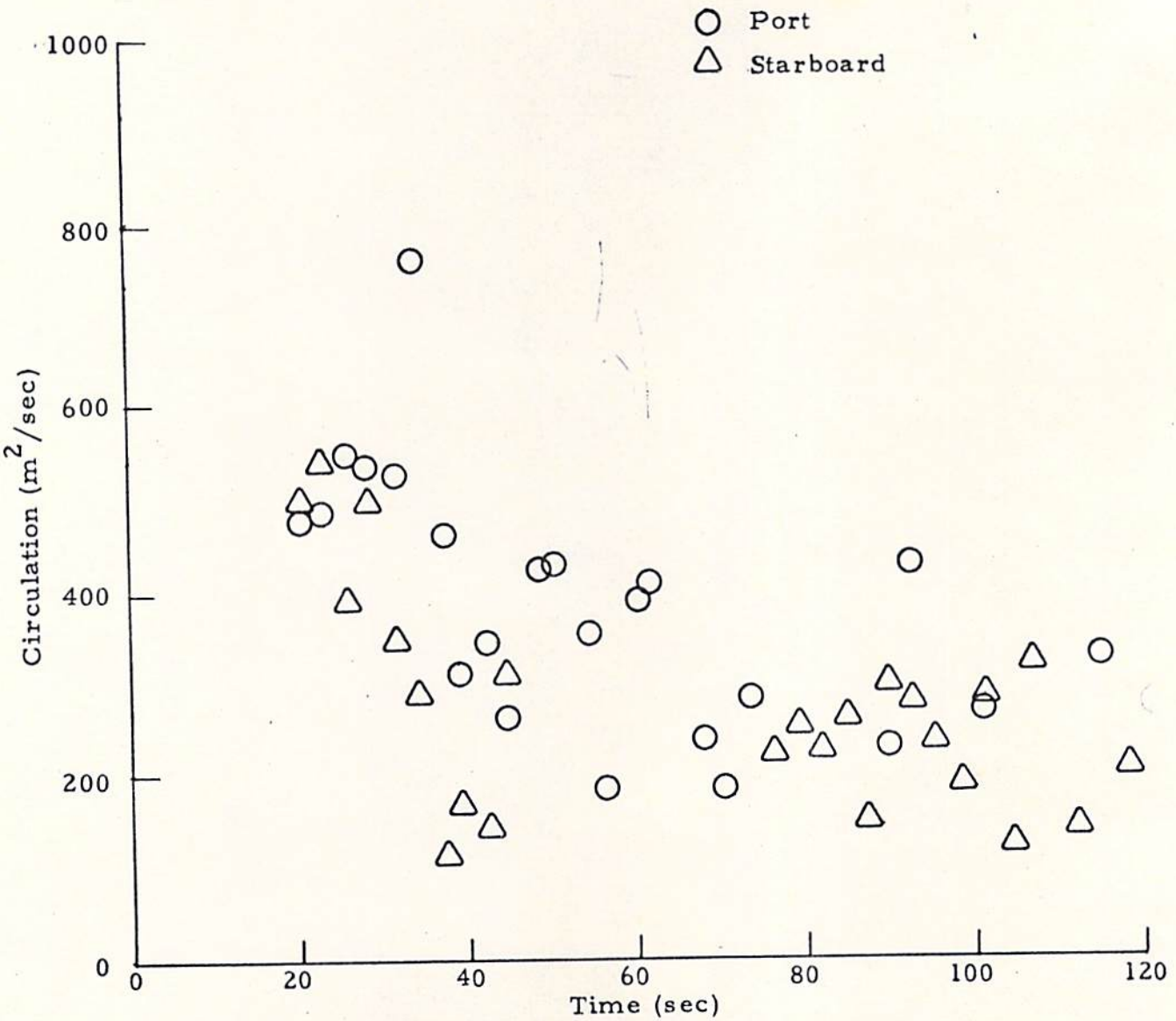

Observed Circulation Time History for Rosamond B-747 Flyby 48

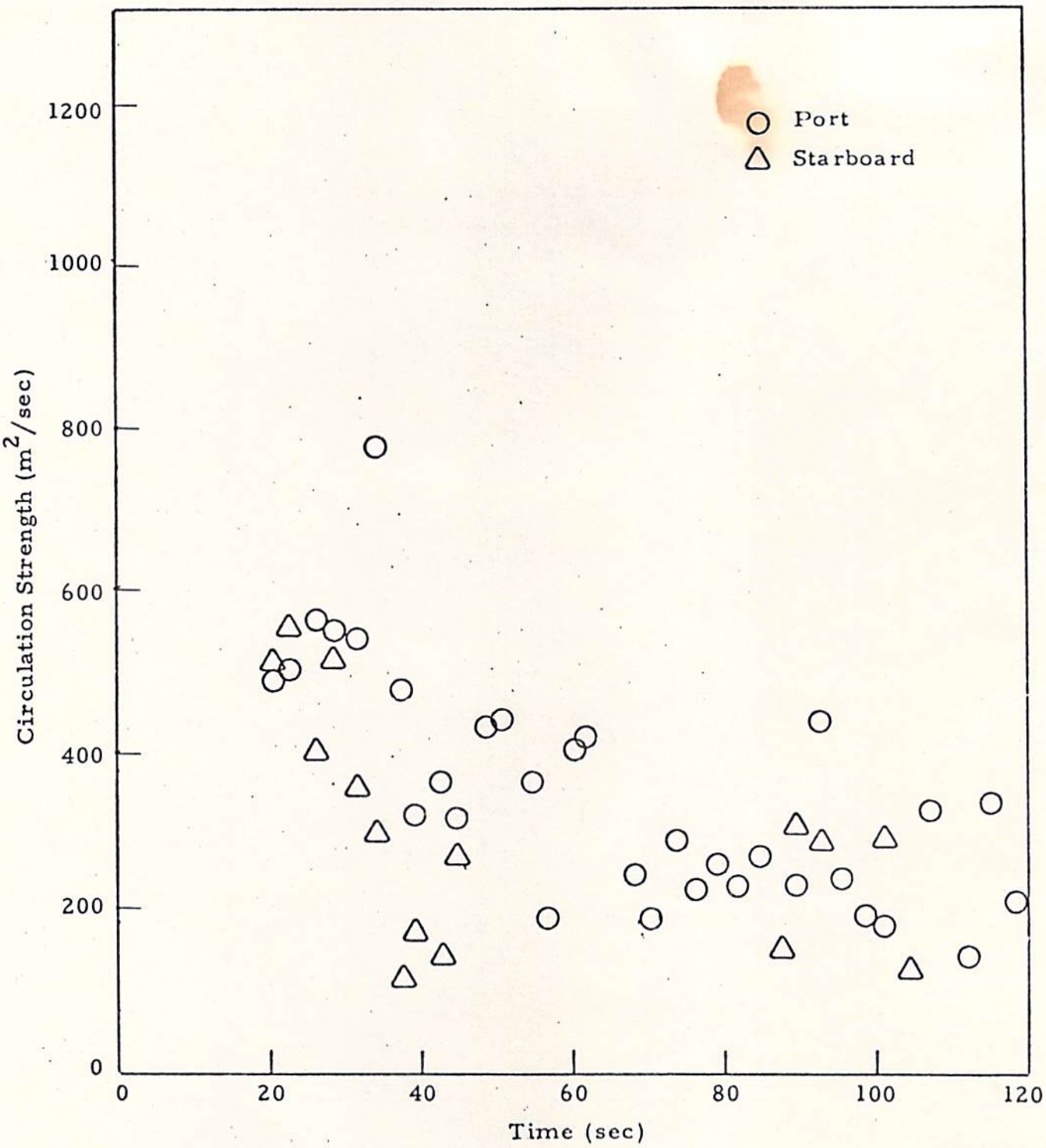

Observed Circulation Time History for Rosamond B-747 Flyby 49

Appendix H
REPORT OF INVENTIONS

In accordance with the objectives of the contract, wake vortex and wind measurements were carried out at the Rosamond, California, test site with a scanning laser Doppler velocimeter system, and the LDV measurements have been processed, reduced and analyzed. The contract objectives have been met and no new invention or discovery or innovation was found.